Renée Dotson

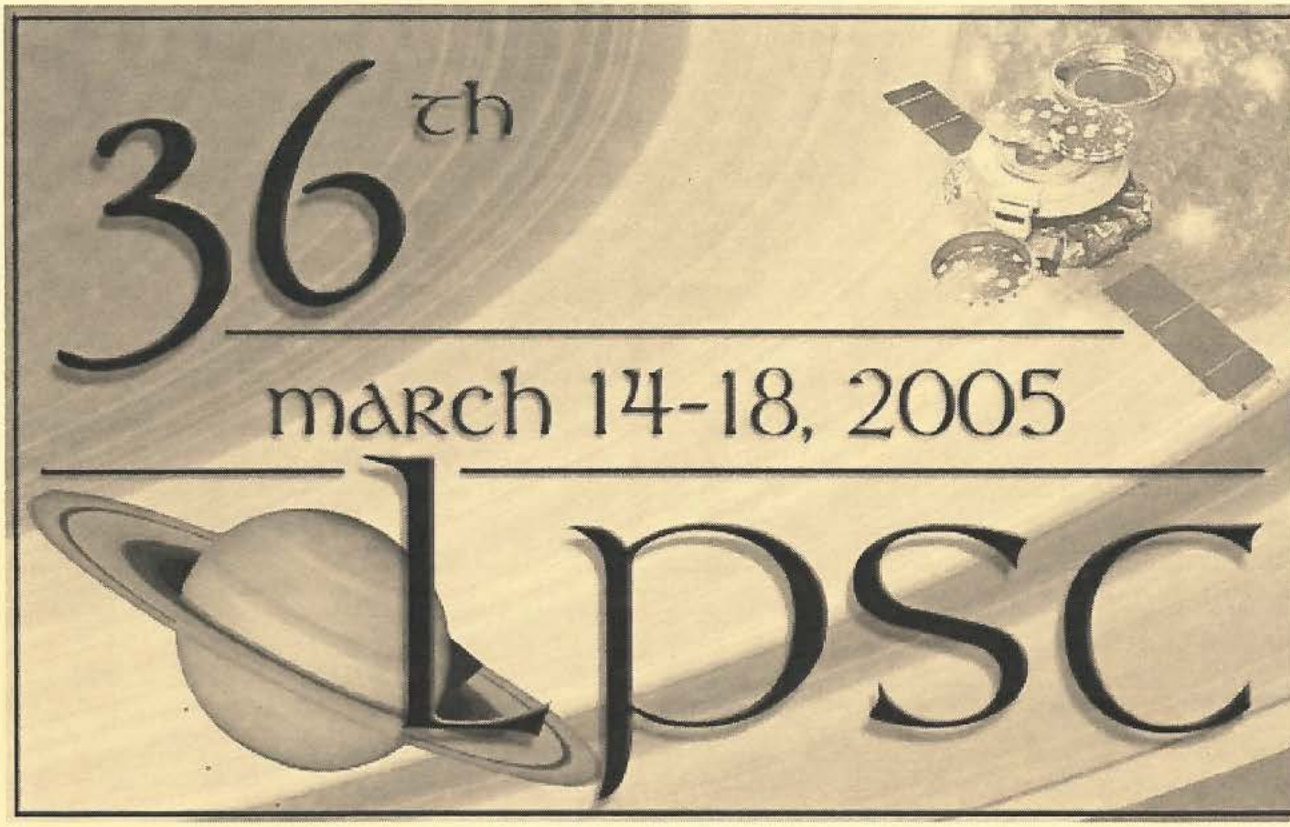

36th Lunar and Planetary Science Conference
Program to Technical Sessions

Sponsored by
Lunar and Planetary Institute
NASA Johnson Space Center

NASA

LPI

Program to Technical Sessions

THIRTY-SIXTH LUNAR AND PLANETARY SCIENCE CONFERENCE

March 14–18, 2005

Sponsored by

Lunar and Planetary Institute
NASA Johnson Space Center

Program Committee

Stephen Mackwell, Co-Chair, *Lunar and Planetary Institute*
Eileen Stansbery, Co-Chair, *NASA Johnson Space Center*
Gretchen Benedix, *Washington University*
Nathan Bridges, *Jet Propulsion Laboratory*
Lauren Browning, *Browning Research*
Barbara Cohen, *University of New Mexico*
Harold Connolly, *Kingsborough College of the City University of New York*
David Draper, *University of New Mexico*
Jeffrey Gillis, *University of Hawai'i*
Keith Holsapple, *University of Washington*
John Jones, *NASA Johnson Space Center*
Amy Jurewicz, *Arizona State University*
Lindsay Keller, *NASA Johnson Space Center*
Walter Kiefer, *Lunar and Planetary Institute*
Julianne Moses, *Lunar and Planetary Institute*
Donald Musselwhite, *Lunar and Planetary Institute*
John Mustard, *Brown University*
Greg Neumann, *Massachusetts Institute of Technology*
Kevin Righter, *NASA Johnson Space Center*
Stephanie Shipp, *Lunar and Planetary Institute*
Linda Spilker, *Jet Propulsion Laboratory*
Tomasz Stepinski, *Lunar and Planetary Institute*
Kathie Thomas-Keprta, *NASA Johnson Space Center*
Timothy Titus, *U.S. Geological Survey*
Elizabeth Turtle, *University of Arizona*
Aileen Yingst, *University of Wisconsin/Green Bay*

South Shore Harbour Resort and Conference Center

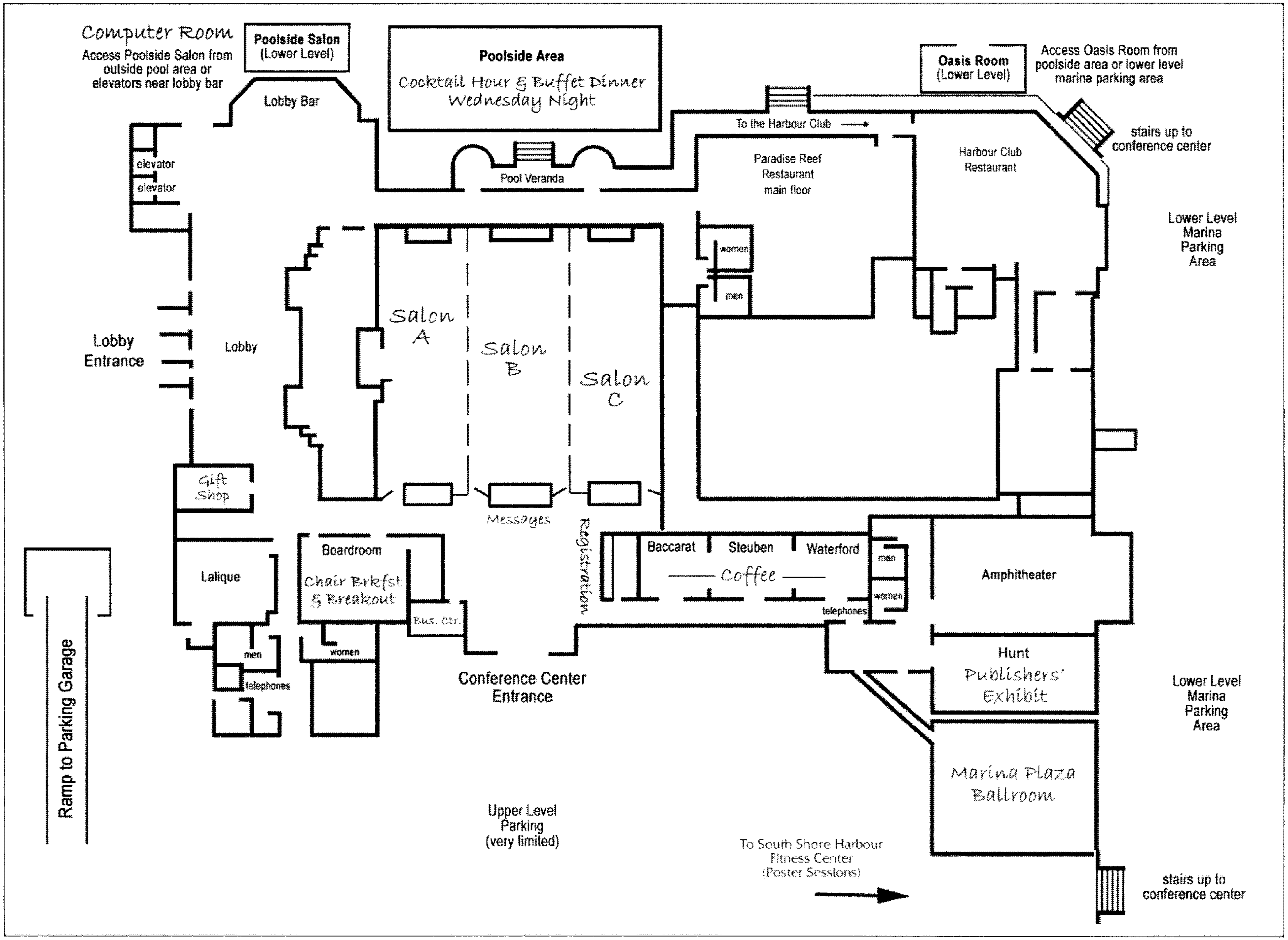

Conference Information

Registration — LPI Open House

A combination Registration/Open House will be held Sunday, March 13, 2005, from 5:00 p.m. until 8:00 p.m. at the Lunar and Planetary Institute. Registration will continue at the South Shore Harbour Resort and Conference Center, Monday through Thursday, 8:00 a.m. to 5:00 p.m., and Friday, 8:00 a.m. to noon. A shuttle bus will be available to transport participants between the LPI and local hotels Sunday evening from 4:45 p.m. to 8:30 p.m.

Business Center

There will no longer be fax or copy service available at the LPSC registration desk. These services are available for a fee at the hotel business center or you may use the LPI facilities (see note about daily shuttle service to the LPI below). Anyone needing to contact attendees during the conference may call 281-334-1000. These messages may be picked up at the LPSC registration desk.

Shuttle Bus Service

A shuttle bus service between the LPI, South Shore Harbour, and various hotels will operate daily. A detailed schedule of the shuttle routes is in your registration packet and is available at the registration desk.

GUIDE TO TECHNICAL SESSIONS AND ACTIVITIES

Sunday Evening, 5:00 p.m.

LPI Hess Room	Registration
LPI Great Room	Reception
LPI Berkner Rooms	Education and Public Outreach Program and Product Demonstrations

Monday Morning, 8:30 a.m.

Salon A	Astrobiology I: Mars, Methane, Minerals, and Missions
Salon B	Mars Express and HRSC I
Salon C	Mars: Interior Processes
Marina Plaza Ballroom	Presolar Grains

Monday Afternoon, 1:30 p.m.

Salon B	PLENARY SESSION: Dwornik Award Presentations followed by Masursky Lecture by Captain John Young

Monday Afternoon, 2:15 p.m.

Salon A	Terrestrial Planet Formation
Salon B	SPECIAL SESSION: Genesis: What We Know, Where We Stand, and the Future
Salon C	Mars Tectonism and Magnetism
Marina Plaza Ballroom	Martian Meteorites: Magmatic Processes

Monday Evening, 5:30 p.m.

Salon B	NASA Headquarters Briefing

Monday Evening, 6:30 p.m.

Marina Plaza Ballroom	Student/Scientist Reception

Tuesday Morning, 8:30 a.m.

Salon A	Martian Impacts: Primary and Secondary
Salon B	SPECIAL SESSION: OMEGA@Mars: New Insights Into Surface Composition
Salon C	Astrobiology II: Microbes, Missions, and Early Terrestrial Life
Marina Plaza Ballroom	Interplanetary Dust

Tuesday Afternoon, 1:30 p.m.

Salon A	Impacts: Ejecta Effects **3:15 p.m.** Venus
Salon B	SPECIAL SESSION: Mars Polar Atmosphere Surface Interactions
Salon C	Nakhlites and Chassignites: New Arrivals and Familiar Friends
Marina Plaza Ballroom	Mars Potpourri: Wet and Dry, Sandy and Dusty

Tuesday Evening, 7:00–9:30 p.m.

Fitness Center — Poster Session I

- *Presolar Grains*
- *Micrometeorites and Interplanetary Dust*
- *Stardust Mission: Aerogel Extraction and Instrumentation*
- *Genesis: Field Recovery, Status of Select Materials, Analytical Methods*
- *Mercury*
- *Lunar Meteorites*
- *Lunar Mission: Past, Present, Future*
- *Martian Meteorites: Magmatic Processes*
- *Nakhlites and Chassignites: New Arrivals and Familiar Friends*
- *Martian Meteorites: ALH 84001*
- *Martian Meteorites: Shocking*
- *Achondrites*
- *Iron and Stony-Iron Meteorites*
- *Refractory Inclusions*
- *Impact Modeling*
- *Impact Experiments*
- *Martian Impacts*
- *OMEGA@Mars: New Insights Into Surface Composition*
- *Mars Express and HRSC II*
- *Mars Polar Atmosphere Surface Interactions*
- *Mars Geophysics*
- *Mars Tectonics*
- *Mars Volcanism*
- *Mars Cratering and Analogs*
- *Dry (?) Mars: Aeolian Processes, Mass Wasting, and Rocks*
- *Mars Ice: Landforms and Processes*
- *Mars Potpourri*
- *Mars: Instruments and Data Interpretation Techniques*
- *Instruments II: Gamma-Ray Through Visible and Fancy Lasers*
- *Venus*
- *Astrobiology*
- *Education and Public Outreach: K–12 Programs, Professional Development, and Informal Education*
- *Education and Public Outreach: Visualization and Data Integration*

Wednesday Morning, 8:30 a.m.

Salon A	Asteroid Spectroscopy and Mineralogy
Salon B	MER Results I
Salon C	Mars Volcanism and Tectonism
Marina Plaza Ballroom	Chondrules and Chondrites

Wednesday Afternoon, 1:30 p.m.

Salon A	Lunar Basalts: A Heap O'KREEP
Salon B	Cassini at Saturn I: Huygens Probe and Titan Results
Salon C	Chondrites
Marina Plaza Ballroom	MER Results II

Wednesday Evening, 5–6:30 p.m.

Marina Plaza Ballroom	Targeting Sites for Observation by the Mars Reconnaissance Orbiter, Part 1: Capabilities and Plans for Community Input

Wednesday Evening, 6:30–9:30 p.m.

Poolside	Cocktail Hour followed by Buffet Dinner

Thursday Morning, 8:30 a.m.

Salon A	Small Bodies: Bumping, Spinning, and Shaking
	10:45 a.m. Impacts: Shock Effects
Salon B	Cassini at Saturn II: Orbiter and Titan Results
Salon C	Lunar Highlands: Impacts and Isotopes
Marina Plaza Ballroom	Refractory Inclusions

Thursday Afternoon, 1:30 p.m.

Salon A	Impacts: Shocks, Structures, and Models
Salon B	Cassini at Saturn III: Titan Surface, Rings, and Icy Satellites
Salon C	Oxygen in the Solar System
Marina Plaza Ballroom	Martian Fluvial Landforms and Processes

Thursday Evening, 7:00–9:30 p.m.

Fitness Center — Poster Session II

Lunar Potpourri
Lunar Impacts
Lunar Regolith: Measurements, Experiments, and Calculations
Lunar Surface Remote Sensing
Lunar Geophysics
Lunar Isotopes
Impacts and Their Effects on Earth and Above
MER and MOC Results
Mars Geochemistry
Wet Mars: Oceans, Gullies, and More
Mars Global Units and Composition
Mars Infrared Spectroscopy
Mars Climate/Atmosphere
Mars: Marscellaneous
Instruments I: Rovers, Robotics, IR, and More
Exploration: The Future
Meteorite Characterization Techniques
Enstatite Chondrites
Organics in Meteorites
Carbonaceous Chondrites
Ordinary Chondrites
Oxygen in the Solar System
Early Solar System Processes and Planet Formation
Asteroids, Comets, and Small Bodies
Cassini at Saturn: Titan, Saturn, Rings, Icy Satellites
Outer Solar System

Friday Morning, 8:30 a.m.

Salon A	Europa (and Triton)
Salon B	Mars: From Hydrogen to Ice and Implications for Climate Change
Salon C	Differentiated Meteorites
Marina Plaza Ballroom	Early Solar System Evolution

Friday Afternoon, 1:30 p.m.

Salon A	Galilean Satellites
Salon B	Mars Geochemistry and Weathering
Salon C	Remote Sensing, Mare Basalts, and Lunar Resource Deposits
Marina Plaza Ballroom	Chronology of a Protoplanetary Disk

Print-only presentations are listed on pages 150 – 159

*** Denotes speaker**

Sunday, March 13, 2005
E/PO PROGRAM AND PRODUCT DEMONSTRATIONS
5:00 p.m. LPI

Lindstrom M. M. Tobola K. W. Stocco K. Henry M. Allen J. S. McReynolds J. Porter T. T. Veile J.
Space Rocks Tell Their Secrets: Space Science Applications of Physics and Chemistry for High School and College Classes — Update **[#1453]**
This education package strives to help teachers get their students closer to the investigation of science. Continued development of and revisions to the original idea and design have created an innovated tool for the chemistry and physics class.

Fauerbach M. Henry D. P. Schmidt D. L.
Project LAUNCH — Bringing Space into Math and Science Classrooms **[#1094]**
Project LAUNCH is a teacher professional development program that has been created in collaboration between the Whitaker Center for Science, Mathematics and Technology Education at Florida Gulf Coast University and the Florida Space Research Institute.

Myers E. Coppin P. Wagner M. Fischer K. Lu L. McCloskey R. Seneker D. Cabrol N. A. Wettergreen D. Waggoner A.
Using Near Real-Time Mission Data for Education and Public Outreach: Strategies from the Life in the Atacama E/PO Effort **[#2322]**
An intimate connection with science operations for the Life in the Atacama 2004 mission allowed the EventScope E/PO team to develop strategies to bring the experience of the mission to the public in near real-time.

Chuang F. C. Pierazzo E. Osinski G.
The Explorer's Guide to Impact Craters **[#2390]**
We propose to create an educational program that integrates a web-based curriculum with planetary exhibits and hands-on student activities to introduce the study of impact craters.

Mészáros I. Hargitai H. Horváth A. Kereszturi A. Sik A. Bérczi Sz.
Second Unusual Guidebook to Terrestrial Field Work Studies: Astronauts with Roving Vehicle, Robotic Rovers on Planetary Surfaces (Seventh Concise Atlas in the Solar System Series of Textbooks at Eötvös University, Hungary) **[#1177]**
Our new concise atlas of Solar System Environmental Studies shows a) Apollo's field works in lunar rock deserts, b) Lunokhod rovers' field works, c) Pathfinder's Sojourner's works around Sagan Station, and d) MER rovers' field works.

Monday, March 14, 2005
ASTROBIOLOGY I: MARS, METHANE, MINERALS, AND MISSIONS
8:30 a.m. Salon A

Chairs: C. C. Allen
J. Parnell

8:30 a.m. Des Marais D. J. * Clark B. C. Crumpler L. S. Farmer J. D. Grotzinger J. P. Haskin L. A. Knoll A. H. Landis G. A. Moersch J. Schröder C. Wdowiak T. Yen A. S. Squyres S. W.
Astrobiology and the Basaltic Plains in Gusev Crater **[#2353]**
Basalts and soils on the plains contain both nutrients and sources of redox energy needed for life as we know it. Liquid water has been scarce recently, however, obliquity-related climate variations perhaps created favorable subsurface conditions.

8:45 a.m. Oehler D. Z. * Allen C. C. McKay D. S.
Impact Metamorphism of Subsurface Organic Matter on Mars: A Potential Source for Methane and Surface Alteration **[#1025]**
Methane generated from Martian kerogen by impact metamorphism may seep to the surface, accounting for some of the methane recently detected in the Martian atmosphere as well as the bright crater rings seen in MOC images from Meridiani Planum.

9:00 a.m. Allen C. C. * Oehler D. Z.
Thinking Like a Wildcatter — Prospecting for Methane in Arabia Terra, Mars **[#1398]**
Enhanced concentrations of methane have been observed over Arabia Terra. We are investigating surface indicators of methane, geological/geophysical indicators of basins and hydrothermal areas, and potential methane release paths to the atmosphere.

9:15 a.m. Thomas-Keprta K. L. * Clemett S. J. Bazylinski D. A. Kirschvink J. L. McKay D. S. Vali H. Gibson E. K. Jr. Romanek C. S.
Focused Ion Beam Microscopy of ALH84001 Carbonate Disks **[#2341]**
Our aim is to understand the mechanism(s) of formation of carbonate assemblages in ALH84001. We present here analyses by transmission electron microscopy (TEM) of carbonate thin sections produced by both focused ion beam (FIB) sectioning and ultramicrotomy.

9:30 a.m. Parnell J. * Osinski G. R. Lee P. Cockell C. S.
Microbial Preservation in Sulfates in the Haughton Impact Structure Suggests Target in Search for Life on Mars **[#1031]**
Microbes occur within transparent gypsum crystals in the Haughton crater. The crystals transmit light for photosynthesis, but protect from dehydration and wind. Sulfates on the Martian surface should be a priority target in the search for life.

9:45 a.m. Stoker C. R. * Stevens T. Amils R. Gómez-Elvira J. Rodriguez N. Gomez F. Gonzales-Torril E. Aguillera A. Fernández-Remolar D. Dunagan S. Lemke L. Zavaleta J. Sanz J. L.
Characteriation of a Subsurface Biosphere in a Massive Sulfide Deposits at Rio Tinto, Spain: Implications for Extant Life on Mars **[#1534]**
This paper describes the first results of geobiological drilling at Rio Tinto Spain which has discovered a subsurface biosphere living in a massive pyrite formation. We focus on the strategy for selecting drilling locations, sample handling, data acquired from cores, and biological results.

10:00 a.m. Schieber J. *
Granular Microbial Habitats Built from Iron Sulfides: Alternative Microbial Lifestyles? **[#1972]**
Concentrically zoned pyrite grains grew as granular microbial colonies. They stayed in the surface layer during long history of reworking and accretion and consist of marcasite and pyrite cortices with sulfide mineralized microbial remains.

10:15 a.m. Bowden S. A. * Parnell J. Cooper J.
The Extraction of Organic Compounds from Sulphate Minerals for Astrobiological Exploration **[#1325]**
We have used sulphate crystals, which were precipitated from a parent solution containing organic molecules of astrobiological interest, to develop a micro-extraction method. The method was successfully applied to a geological sample and will be used as a template for a lab on a chip system.

10:30 a.m. Stivaletta N. * Barbieri R. Marinageli L. Ori G. G Bosco M.
Fossil Endolithic Cyanobacteria in Evaporites: Implications for the Astrobiological Exploration **[#1354]**
The study focuses on the microbial activity in dry and saline conditions of southern Tunisia. We have investigated the preservation potential of endolithic microbes in continental evaporite deposits.

10:45 a.m. Sakon J. J. * Burnap R. L.
A Further Analysis of Potential Photosynthetic Life on Mars **[#2120]**
This project researched the possibility of photosynthetic life on Mars. Antarctic nitrogen-fixing cyanobacteria were used as potential analogs and were subjected to various Martian-simulated conditions.

11:00 a.m. Link L. S. * Jakosky B. M. Thyne G. D.
Potential for Life on Mars from Low-Temperature Aqueous Weathering **[#1477]**
Simple reactions involving water and rock at low temperatures (as low as 0°C) are sources of geochemical energy that are able to support metabolism for potential martian microbes.

11:15 a.m. Maule J. * Toporski J. Wainwright N. Steele A.
An Integrated System for Labeling and Detection of Biological Molecules in Mars Analog Regolith Using an Antibody Microarray **[#1921]**
This study describes an integrated method for the labeling and detection of biological molecules in Mars analog regolith with an antibody microarray, indicating its potential as an *in situ* life detection tool.

11:30 a.m. Weinstein S. Pane D. Ernst L. A. Minkley E. Lanni F. Wettergreen D. S. Wagner M. Heys S. Teza J. Waggoner A. S. *
Fluorescent Imager for Biological Imaging in Daylight **[#1488]**
We have developed an imaging system for detecting fluorescence signals from sparse microorganisms and biofilms during autonomous rover exploration. To overcome significant obstacles, we incorporated a novel approach to accommodate daytime imaging.

Monday, March 14, 2005
MARS EXPRESS AND HRSC I
8:30 a.m. Salon B

Chairs: G. Neukum
D. A. Williams

8:30 a.m. Chicarro A. F. *
The Mars Express Mission — Summary of Scientific Results from Orbit **[#1035]**
After over a year of successful operations around Mars, major breakthroughs have been made by most experiments onboard the Mars Express spacecraft. Abundance of water-ice at the poles and methane in the atmosphere, as well as recent volcanic and glacial processes, are the most relevant.

8:45 a.m. Pinet P. C. * Cord A. Jehl A. Daydou Y. Chevrel S. C. Baratoux D. Greeley R. Williams D. A. Neukum G. Mars Express HRSC Co-Investigator Team
Mars Express Imaging Photometry and Surface Geologic Processes at Mars: What Can be Monitored Within Gusev Crater? **[#1721]**
The MEx/HRSC multiangular observations produced over Gusev floor monitor surface scattering properties and reveal significant photometric variations (surface roughness, phase function parameters) in relation to the investigated geologic surfaces.

9:00 a.m. Neukum G. * Jaumann R. Hoffmann H. Hauber E. Head J. W. III Basilevsky A. T. Ivanov B. A. Werner S. C. van Gasselt S. Murray J. B. McCord T. B. Greeley R. HRSC Co-Investigator Team
Mars: Recent and Episodic Volcanic, Hydrothermal, and Glacial Activity Revealed by the Mars Express High Resolution Stereo Camera (HRSC) **[#2144]**
The analysis of HRSC image data shows that calderas on five major volcanoes in the Tharsis and Elysium regions have undergone repeated activation and resurfacing during the last 20% of Martian history, with caldera floors as young as 100 Ma, and flank eruptions as young as 2 Ma.

9:15 a.m. Greeley R. * Williams D. A. Neukum G. Werner S. C. Zegers T. Foing B. H. van Kan M. Lanagan P. D. Pinet P. Mars Express HRSC Team
Fluid Lava Flows in Gusev Crater, Mars **[#2094]**
Basaltic rocks in Gusev are modeled to have viscosities of 2.3 to 50 Pa•s at the time of eruption and thus were emplaced as very fluid flood lavas, consistent with the morphologies seen in orbiter data, at 3.65 by based on crater counts.

9:30 a.m. Zegers T. E. * van Kan M. Foing B. H. Pischel R. Gwinner K. Scholten F. Werner S. Neukum G. HRSC Co-Investigator Team
Mountainous Units in the Martian Gusev Highland Region: Volcanic, Tectonic, or Impact Related? **[#1651]**
Geological mapping and structural analysis of the highland region of Gusev crater was carried out, combining THEMIS and HRSC image data and HRSC digital terrain models (DTM), based on HRSC stereo capabilities.

9:45 a.m. Werner S. C. * Neukum G. HRSC Co-Investigator Team
Major Volcanic Constructs Seen from Mars Express HRSC — New Insights into Their Evolutionary History **[#1766]**
All major volcanic constructs including many Paterae and Tholi have been covered in the first period of the mission. This provides a new opportunity to better characterize most of the volcanoes in the Tharsis and Elysium region and highland volcanoes geomorphologically and chrono-stratigraphically.

10:00 a.m. Williams D. A. * Greeley R. Zuschneid W. Werner S. Neukum G. Crown D. A. Gregg T. K. P. Raitala J. HRSC Co-Investigator Team
Hadriaca Patera: Volcanic History Derived from HRSC-based Crater Counts **[#1470]**
We discuss the results of HRSC-based crater counts of units on Hadriaca Patera that were constrained by previous mapping. We also discuss the implications of these results for the volcanic history of Hadriaca Patera.

10:15 a.m. Kostama V.-P. * Ivanov M. A. Korteniemi J. Aittola M. Raitala J. Glamoclija M. Marinangeli L. Neukum G. HRSC Co-Investigator Team
Major Episodes of the Hydrologic History of Hesperia Planum, Mars **[#1659]**
Hesperia Planum (HP) hosts an array of landforms suggesting the interaction of volcanic and fluvial processes. We outline the most important features in the region correlating temporally the processes that have led to their formation.

10:30 a.m. Jaumann R. * Reiss D. Frei S. Scholten F. Gwinner K. Roatsch T. Matz K.-D. Hauber E. Mertens V. Hoffmann H. Head J. W. III Hiesinger H. Carr M. H. Neukum G. HRSC Co-Investigator Team
Martian Valley Networks and Associated Fluvial Features as Seen by the Mars Express High Resolution Stereo Camera (HRSC) **[#1765]**
In High Resolution Stereo Camera (HRSC) images of the Mars Express Mission a 130 km long inner channel is Lybia Montes. Based on HRSC stereo information we were able to determine the depth of this inner structure and thus we could estimate the discharge in the inner channel.

10:45 a.m. Masson Ph. Ansan V. * Mangold N. Quantin C. Neukum G. HRSC Co-Investigator Team
HRSC/MEX Analysis of Valley Networks in Echus Chasma Plateau and in Aeolis Region **[#1340]**
HRSC data allows us to study valley networks with high resolution imagery and DTMs. First results in Noachian highlands and Hesperian plateau of Valles Marineris show drainage densities and parameters similar to terrestrial rivers systems.

11:00 a.m. Hauber E. * Gwinner K. Stesky R. Fueten F. Michael G. Reiss D. Zegers T. Hoffmann H. Jaumann R. van Gasselt S. Neukum G. HRSC Co-Investigator Team
Interior Layered Deposits in Valles Marineris, Mars: Insights from 3D-Data Obtained by the High Resolution Stereo Camera (HRSC) **[#1760]**
We use HRSC stereo images to study the Interior Layered Deposits (ILD) in the Valles Marineris on Mars. Our results indicate diverse layering morphologies and geometries. No single scenario seems to be able to explain the formation of all ILD.

11:15 a.m. Raitala J. * Aittola M. Korteniemi J. Kostama V.-P. Hauber E. Kronberg P. Neukum G. HRSC Co-Investigator Team
Claritas Paleolake Studied from the MEX HRSC Data **[#1307]**
Water was transported from the southern Claritas Fossae upland peaks into the Claritas basin. The channel from the paleolake into Icaria Planum displays also sapping, crater lake with delta, and alluvial fan.

11:30 a.m. Baratoux D. Mangold N. * Pinet P. C. Forget F. Masson P. Chevrel S. C. Daydou Y. Jehl A. Greeley R. Neukum G. HRSC Co-Investigator Team
New Insights for the Formation of Slope Streaks on Mars from a Systematic Mapping Using Mars Express HRSC Data: A Dry Granular Avalanche Controlled by Wind-Transported Dust **[#1599]**
We present a mapping of slope streaks using HRSC data at Olympus Mons aureole. We argue from these data that slope streaks are a dry-granular avalanche which can be triggered by the accumulation of dust at hill crests in the downstream side of the wind flow.

Monday, March 14, 2005
MARS: INTERIOR PROCESSES
8:30 a.m. Salon C

Chairs: M. A. Wieczorek
L. T. Elkins-Tanton

8:30 a.m. Monders A. G. * Médard E. Grove T. L.
Primary Martian Basalts at Gusev Crater: Experimental Constraints **[#2069]**
Experimentally determined high-pressure, high-temperature phase relations of the Gusev Crater basalts indicate that the basalts originated from high-degree shallow melting of a primitive Martian mantle and may be part of the primitive Martian crust.

8:45 a.m. Christensen P. R. * McSween H. Y. Jr. Bandfield J. L. Ruff S. W. Rogers A. D. Hamilton V. E. Gorelick N. Wyatt M. B. Jakosky B. M. Kieffer H. H. Malin M. C. Moersch J. E.
The Igneous Diversity of Mars: Evidence for Magmatic Evolution Analogous to Earth **[#1273]**
THEMIS compositional mapping has revealed a diversity of igneous materials, from picritic basalts to dacite and granitoids that rivals the Earth. Olivine basalts are relatively common; local magma evolution has produced dacites and granitoids.

9:00 a.m. Agee C. B. * Draper D. S.
High Pressure Melting of H-Chondrite: A Match for the Martian Basalt Source Mantle **[#1434]**
Experiments on H-chondrite (Mg# = 80) yield liquids that can simply evolve to close matches to potential shergottite parent liquids.

9:15 a.m. Médard E. * Grove T. L.
Early Irreversible Hydrous Melting and Degassing of the Martian Interior: An Experimental Study **[#1744]**
Hydrous experiments on a primitive Martian composition suggest that an early hydrous melting event occurred during the accretion process. This event would have profoundly differentiated the Martian mantle and removed H_2O from the planet's interior.

9:30 a.m. Solomon S. C. * Aharonson O. Hauck S. A. II Jakosky B. M. Phillips R. J. Zuber M. T.
Why the Martian Mantle is (Mostly) "Wet" **[#1689]**
On the basis of a synthesis of geophysical arguments, planetary formation simulations, and information from Martian meteorites, we argue that the bulk of the Martian mantle has been geophysically "wet" for most of Martian history.

9:45 a.m. Elkins-Tanton L. T. * Parmentier E. M.
The Fate of Water in the Martian Magma Ocean and the Formation of an Early Atmosphere **[#1906]**
A chondritic martian magma ocean degasses during solidification to create an initial water atmosphere consistent with the planet's current water content, while the mantle retains sufficient water to reduce viscosity and encourage convection.

10:00 a.m. Parmentier E. M. * Zaranek S. E. Elkins-Tanton L. T.
A Mechanism for the Formation and Evolution of Tharsis as a Consequence of Mantle Overturn: Large Scale Lateral Heterogeneity in a Stably Stratified Mantle **[#1768]**
Tharsis is considered a consequence of melting of a large scale mantle heterogeneity following mantle overturn after fractional magma ocean solidification. Long-lived volcanism does not require a long term heat flux from the core or magnetic field.

10:15 a.m. King S. D. * Redmond H. L.
The Crustal Dichotomy and Edge Driven Convection: A Mechanism for Tharsis Rise Volcanism? **[#1960]**
This work uses numerical modeling and analysis of the Martian areoid to assess the conditions underwhich edge driven convection could form Tharsis rise.

10:30 a.m. Dombard A. J. * Phillips R. J.
Tectonic Evidence for Crustal Underplating of the Tharsis Montes, Mars **[#1878]**
Thermomechanical finite element simulations including an underplate thermal anomaly predict large, sharply peaked stress distributions consistent with graben annuli around these large volcanoes, allowing a more precise estimate of regional heat flow.

10:45 a.m. Lillis R. J. * Manga M. Mitchell D. L. Lin R. P. Acuña M. H.
Evidence for a Second Martian Dynamo from Electron Reflection Magnetometry **[#1578]**
Using high-sensitivity electron reflection magnetometry, we present the magnetic signatures and crater ages of Martian volcanoes as evidence for two separate episodes of dynamo activity on early Mars.

11:00 a.m. Wenzel M. J. * Manga M. Lillis R. J.
Mantle Convection and Two Episodes of Martian Dynamo Activity **[#1584]**
We use a 2D numerical mantle convection model to explore parameter space. We evaluate conditions that might explain two episodes of martian dynamo activity.

11:15 a.m. Wieczorek M. A. * Greff-Lefftz M. Labrosse S. van Thienen P. Rouby H. Besse J. Feldman W. C.
The Case for a Martian Inertial Interchange True Polar Wander Event **[#1679]**
The initial formation of the Tharsis plume and subsequent volcanic construction likely have given rise to ~90° of true polar wander on Mars. We argue that two antipodal hydrogen deposits located at the equator are relicts of ancient polar caps.

Monday, March 14, 2005
PRESOLAR GRAINS
8:30 a.m. Marina Plaza Ballroom

Chairs: L. R. Nittler
T. K. Croat

8:30 a.m. Yada T. * Stadermann F. J. Floss C. Zinner E. Olinger C. T. Graham G. A. Bradley J. P. Dai Z. R. Nakamura T. Noguchi T. Bernas M.
Discovery of Abundant Presolar Silicates in Subgroups of Antarctic Micrometeorites **[#1227]**
Six presolar silicates have been discovered in three Antarctic micrometeorites based on oxygen isotopic analyses with a NanoSIMS. Four of them were classified as Group 1 grains, and two as Group 4 grains.

8:45 a.m. Hoppe P. * Mostefaoui S. Stephan T.
NanoSIMS Oxygen- and Sulfur-Isotope Imaging of Primitive Solar System Materials **[#1301]**
We report results from an O- and S-isotope imaging survey of the Acfer 094 meteorite and of eleven microtome sections from two non-cluster IDPs. Based on large O-isotopic anomalies, 7 presolar grains, silicates and spinel, were found in Acfer 094.

9:00 a.m. Nguyen A. N. * Zinner E. Stroud R. M.
Continued Characterization of Presolar Silicate Grains from the Acfer 094 Carbonaceous Chondrite **[#2196]**
We have identified 11 additional presolar silicates and 8 presolar oxides from the Acfer 094 meteorite. The Si isotopic compositions of ten presolar silicates are reported. TEM study of one grain identified it as an amorphous silicate containing large amounts of Mg and Fe.

9:15 a.m. Stadermann F. J. * Floss C. Bland P. A. Vicenzi E. P. Rost D.
An Oxygen-18 Rich Presolar Silicate Grain from the Acfer 094 Meteorite: A NanoSIMS and ToF-SIMS Study **[#2004]**
Accidental discovery of a presolar Fe-rich olivine in a study of micro-CAIs.

9:30 a.m. Kobayashi S. * Tonotani A. Sakamoto N. Nagashima K. Krot A. N. Yurimoto H.
Presolar Silicate Grains from Primitive Carbonaceous Chondrites Y-81025, ALHA 77307, Adelaide and Acfer 094 **[#1931]**
The abundances of presolar silicates are different among the least metamorphosed and altered chondrites. This may indicate heterogeneous distribution of presolar silicates among chondrite forming regions in the solar nebula.

9:45 a.m. Nittler L. R. * Alexander C. M. O'D. Stadermann F. J. Zinner E. K.
Presolar Al-, Ca-, and Ti-rich Oxide Grains in the Krymka Meteorite **[#2200]**
We report the isotopic data (O, Mg-Al, K, Ca and Ti) for 46 new presolar oxide grains from the Krymka meteorite, including 15 Hibonite and 2 TiO_2 grains. The grains show a wide range of isotopic anomalies including evidence for extinct ^{41}Ca.

10:00 a.m. Bernatowicz T. J. * Akande O. W. Croat T. K. Cowsik R.
Constraints on Grain Formation Around Carbon Stars from Laboratory Studies of Presolar Graphite **[#1509]**
Realistic models of mass outflows from AGB stars (1.1-5 solar masses) show that graphite grains grow over a 2–10 y time interval at radii of 2.3—3.7 A.U. Pressure constraints require that grains form in clumps or jets with enhanced density.

10:15 a.m. Amari S. * Zinner E. Lewis R. S.
Presolar Graphite and Its Noble Gases **[#1867]**
Of four graphite-rich fractions from the Murchison meteorite, the three low-density fractions including KFB1 (2.10–2.15 g/cm^3) contain ^{18}O-rich grains with $20 < {}^{12}C/{}^{13}C < 200$. Populations of grains that carry Kr-S and Ne-G in KFB1 are still uncertain.

10:30 a.m. Jadhav M. Maruoka T. Amari S. Zinner E.
Finally: Presolar Graphite Grains Identified in Orgueil **[#1976]**
We report the successful isolation of presolar graphite grains from Orgueil. Carbon and oxygen isotopic data for these grains are presented, and the isotopic characteristics of Orgueil graphite are found to be similar to those of Murchison graphite.

10:45 a.m. Heck Ph. R. * Marhas K. K. Baur H. Hoppe P. Wieler R.
Presolar He and Ne in Single Circumstellar SiC Grains Extracted from the Murchison and Murray Meteorites **[#1938]**
We present new He and Ne analyses on single presolar SiC grains from the Murchison and Murray carbonaceous chondrites. We find that about a third of all studied grains contain nucleosynthetic ^{4}He and/or ^{22}Ne above our detection limits.

11:00 a.m. Gilmour J. D. * Turner G.
Reconsideration of the Constraints on Nucleosynthetic Sources of Xenon in Presolar Material **[#1630]**
We re-examine the constraints imposed on nucleosynthetic processes by xenon isotopic data from presolar material.

11:15 a.m. Stroud R. M. * Bernatowicz T. J.
Surface and Internal Structure of Pristine Presolar Silicon Carbide **[#2010]**
We report results from transmission electron microcopy studies of the surface and internal structure of two pristine presolar SiC grains, including definitive evidence of an oxide rim on one grain, and the presence of internal TiC and AlN grains.

11:30 a.m. Croat T. K. * Stadermann F. J. Bernatowicz T. J.
Internal Grains Within KFC Graphites: Implications for Their Stellar Source **[#1507]**
TEM and NanoSIMS investigations find high s-process element enrichments in internal carbides, suggesting an AGB origin for most Murchison KFC presolar graphites. Other rare phases (iron phases and metallic osmium) are consistent with a SN origin.

Monday, March 14, 2005
PLENARY SESSION:
DWORNIK AWARD PRESENTATIONS AND MASURSKY LECTURE
1:30 p.m. Salon B

Chairs: S. J. Mackwell
E. K. Stansbery

Presentation of the 2004 GSA Stephen E. Dwornik U.S. Citizen Student Award Winners

Masursky Lecture:

Introduction by Lieutenant General Jefferson D. Howell Jr., Director of the NASA Johnson Space Center

Masursky Lecture by Captain John Young: "The Future of Human Space Exploration and Why"

Monday, March 14, 2005
TERRESTRIAL PLANET FORMATION
2:15 p.m. Salon A

Chairs: T. Rushmer
D. C. Rubie

2:15 p.m. Righter K. * Sutton S. R. Newville M. Le L. Schwandt C. S.
Micro-XANES Measurements on Experimental Spinels and the Oxidation State of Vanadium in Coexisting Spinel and Silicate Melt **[#1140]**
We show that experimental spinels coexisting with silicate melt always have lower valence vanadium, and that spinels typically have 3+, whereas the coexisting melt has 4+ or 5+. Implications of these results for planetary basalts will be discussed.

2:30 p.m. Kegler Ph. * Holzheid A. Rubie D. C. Frost D. Palme H.
New Results of Metal/Silicate Partitioning of Ni and Co at Elevated Pressures and Temperatures **[#2030]**
New experiments of metal silicate partitioning of Ni and Co confirm earlier conclusions that the Ni and Co contents of the Earth's mantle was not established by metal-silicate equilibration in a deep magma ocean.

2:45 p.m. Danielson L. R. * Sharp T. G. Hervig R. L.
Implications for Core Formation of the Earth from High Pressure-Temperature Au Partitioning Experiments **[#1955]**
The results of high P-T Au partitioning experiments and multi-variable modeling are consistent with the equilibrium core formation hypothesis. Metal-silicate equilibrium could have occurred in a magma ocean at pressures of 27 GPa and 2127°C.

3:00 p.m. Humayun M. * Rushmer T. Rankenburg K. Brandon A. D.
A Model for Siderophile Element Distribution in Planetary Differentiation **[#2208]**
Model shows the siderophile element pattern of residual metal in equilibrium with S-rich metallic liquids; ureilites appear to have residual metal from low-degree partial melts.

3:15 p.m. Rushmer T. * Petford N. Humayun M.
Shear-induced Segregation of FeLiquid in Planetsimals: Coupling Core Forming Compositions with Transport Phenomena **[#1320]**
Using a combination of experimental work and numerical modeling, we explore rates of core formation during planetesimal growth. The relationship between liquid metal fraction, HSE concentrations and liquid metal flow rates are addressed.

3:30 p.m. Terasaki H. Rubie D. C. * Mann U. Frost D. Langenhorst F.
The Effects of Oxygen, Sulphur and Silicon on the Dihedral Angles Between Fe-rich Liquid Metal and Olivine, Ringwoodite and Silicate Perovskite: Implications for Planetary Core Formation **[#1129]**
The effects of dissolved O, S, and Si on percolative core formation on Earth and Mars have been studied experimentally. Complete metal-silicate separation by percolation was not possible on either planet, indicating the necessity of a magma ocean.

3:45 p.m. Bell D. R. * Hervig R. L. Buseck P. R.
Li Isotope Studies of Olivine in Mantle Xenolihs by SIMS **[#2178]**
Li isotope heterogeneity is recorded from intra-mineral to regional scales in olivine from terrestrial mantle xenoliths. δ^7Li variations with a range of 25‰ result from magmatic mixing, metasomatic, transport and alteration effects.

4:00 p.m. Marty B. * Yokochi R. Ballentine C. J.
Neon Isotope Heterogeneity in the Terrestrial Mantle: Implication for the Acquisition of Volatile Elements in Terrestrial Planets **[#1865]**
Neon presents a primordial isotope heterogeneity in the terrestrial mantle. Ne coming from the deep mantle is solar-like whereas neon sampled from the convective mantle is typical of Ne trapped in gas-rich meteorites, implying different acquisition processes.

4:15 p.m. Marrocchi Y. * Derenne S. Marty B. Robert F.
On the Sitting of Trapped Noble Gases in Insoluble Organic Matter of Primitive Meteorites **[#1780]**
Solvation experiment was performed on insoluble organic matter of Orgueil (CI). Results suggest that P1 noble gases are sited in the volume of organic matter.

Monday, March 14, 2005
SPECIAL SESSION: GENESIS:
WHAT WE KNOW, WHERE WE STAND, AND THE FUTURE
2:15 p.m. Salon B

Chairs: A. J. G. Jurewicz
E. K. Stansbery

2:15 p.m. Burnett D. B. *
Overview

2:30 p.m. Reisenfeld D. B. * Wiens R. C. Barraclough B. L. Steinberg J. E. DeKoning C. Zurbuchen T. Burnett D. S.
The GENESIS Mission Solar Wind Samples: Collection Times, Estimated Fluences, and Solar-Wind Conditions **[#1278]**
We have correlated the GENESIS sample collection times for the different solar-wind regimes with compositional data from GENESIS/GIM and ACE/SWICS instruments. We discuss GENESIS regime selection and new results in solar-wind elemental fractionation.

2:45 p.m. Stansbery E. K. * Genesis Recovery Processing Team
Genesis Recovery Processing **[#2179]**
After the Genesis hard landing on September 8, 2004, the science canister could not be transported without significant risk of further damage to the collectors. As a result, the decision was made to de-integrate the canister in the cleanroom at UTTR.

3:00 p.m. Allton J. H. * Stansbery E. K. McNamara K. M.
Size Distribution of Genesis Solar Wind Array Collector Fragments **[#2083]**
Genesis array collectors were broken on impact. The initial documentation done in Utah allows an estimate of the number and size of collector fragments. This is useful for planning curation and allocation for solar wind studies.

3:15 p.m. McNamara K. M. Westphal A. Butterworth A. L. Burnett D. B.
Genesis: Sorting Out the Pieces **[#2406]**
Due to failed parachutes during Genesis recovery, significant collector damage and fragment mixing occurred. We discuss generating the detailed information of material, solar wind regime collected, and condition of collector.

3:30 p.m. Burnett D. B. * McNamara K. M. Jurewicz A. J. G. Woolum D.
Molecular Contamination on Anodized Aluminum Components of the Genesis Science Canister **[#2405]**
Some anodized aluminum components recovered from within the Genesis science canister show evidence of discoloration, leading to concerns with respect to material ooutgassing in space. This study attempts to characterize that discoloration.

3:45 p.m. McNamara K. M. * Stansbery E. K.
Analysis of Molecular Contamination on Genesis Collectors Through Spectroscopic Ellipsometry **[#2402]**
Ellipsometry measurements of Genesis collectors.

4:00 p.m. Lauer H. V. * McNamara K. M. Westphal A. Butterworth A. L. Burnett D. B. Jurewicz A. J. G. Woolum D. Allton J. H.
Genesis: Removing Contamination from Sample Collectors **[#2407]**
The impact of the Genesis spacecraft into UTTR soil on September 8, 2004, resulted in the introduction of particulate contamination on collector surfaces. A variety of dust and debris removal techniques are being evaluated by the science team.

4:15 p.m. DISCUSSION ON EARLY SCIENCE AND SAMPLE ALLOCATION

Monday, March 14, 2005
MARS TECTONISM AND MAGNETISM
2:15 p.m. Salon C

Chairs: H. V. Frey
M. E. Purucker

2:15 p.m. Frey H. V. * DeSoto G. E. Lazrus R. M.
Regional Studies of Highland-Lowland Age Differences Across the Mars Crustal Dichotomy Boundary **[#1407]**
Buried lowlands in two regions across the Mars dichotomy boundary have crater retention ages equal to the global average lowlands. Cratered terrain in W Arabia has a similar (not older) age, but elsewhere highlands appear older than the lowlands.

2:30 p.m. Kiefer W. S. *
Gravity Models of the Hemispheric Dichotomy in Eastern Mars: Lithospheric Thickness and Subsurface Structure **[#1192]**
Gravity observations indicate the presence of buried, high-density loads along the dichotomy boundary in much of eastern Mars. This contrasts with the negative gravity anomalies seen along the Arabia Terra portion of the dichotomy boundary.

2:45 p.m. Roberts J. H. * Zhong S.
Crustal Relaxation and Its Implications for the Martian Crustal Dichotomy **[#2170]**
Viscoelastic relaxation calculations show that the crustal dichotomy would have relaxed in less than 1 Gy, given that the early crust was relatively warm. We propose degree-1 mantle convection as a force to maintain the dichotomy early on.

3:00 p.m. Connerney J. E. P. * Acuña M. H. Kletetschka G. Ness N. F. Mitchell D. L. Lin R. P.
Tectonic Implications of Mars Crustal Magnetism **[#1401]**
We present here a new map of the magnetic field of Mars. The Mars crust retains in places the magnetic signature originally imprinted more than 4 billion years ago when it formed by crustal spreading in the presence of a reversing dynamo.

3:15 p.m. Purucker M. E. * Whaler K. A.
A Martian Paleomagnetic Pole Estimate Made Using the Distribution and Intensity of Large Scale Magnetic Features **[#1720]**
Using the the regional distribution of magnetization, we deduce a new paleomagnetic pole associated with the large magnetic features of the Cimmeria region. The pole would suggest that the Tharsis bulge was within 20 degrees of the magnetic equator when the Martian magnetic field was active.

3:30 p.m. Hood L. L. * Harrison K. P.
Are Martian Crustal Magnetic Anomalies and Valley Networks Concentrated at Low Paleolatitudes? **[#1110]**
The mean paleomagnetic equator calculated from an analysis of crustal magnetic anomalies tends to follow the distributions of both valley networks and magnetic fields.

3:45 p.m. Hanna J. C. * Phillips R. J.
Tectonic Pressurization of Aquifers in the Formation of Mangala and Athabasca Valles on Mars **[#2261]**
Several Martian outflow channels emanate from extensional tectonic features, including Mangala and Athabasca Valles. We demonstrate that these floods could have been produced as a direct result of the pressurization of the aquifers by the tectonism.

4:00 p.m. Polit A. T. * Schultz R. A. Soliva R.
A Tale of Two Stratigraphies: From Alba Patera to the Northern Plains **[#2175]**
We use fault population characteristics and measured throw distributions from grabens on Alba Patera and the northern plains to map out distinct boundaries in the Martian crust.

4:15 p.m. Neuffer D. P. * Schultz R. A.
Landslides in Interior Layered Deposits, Valles Marineris, Mars: Effects of Water and Ground Shaking on Slope Stability **[#2076]**
Using slope stability analysis, we assessed the failure mechanisms of landslides in the Interior Layered Deposits of Valles Marineris, Mars. Four landslides could have failed under dry conditions, while one slope failure probably involved water.

Monday, March 14, 2005
MARTIAN METEORITES: MAGMATIC PROCESSES
2:15 p.m. Marina Plaza Ballroom

Chairs: J. H. Jones
H. Y. McSween Jr.

2:15 p.m. Jones J. H. *
Isotopic Constraints on the Petrology of Martian Meteorites **[#1860]**
Chemical fractionations of parent-daughter chronometer systems place constraints on SNC petrology.

2:30 p.m. Warren P. H. * Bridge J. C.
Geochemical Subclassification of Shergottites and the Crustal Assimilation Model **[#2098]**
Shergottites fall into three discrete geochemical classes. Mixing models to form the slightly depleted and moderately depleted shergottites via assimilation of crust by highly depleted shergottitic magmas require a remarkably flat crustal REE pattern.

2:45 p.m. Nekvasil H. * Filiberto J.
The Earth/Mars Dichotomy in Mg/Si and Al/Si Ratios: Is It Real? **[#1413]**
Intra-plate cumulates on Earth have similar Mg/Si, Al/Si ratios to SNC bulk compositions, suggesting that SNC compositions may reflect accumulation of ferromagnesian minerals in terrestrial-like liquids rather than a Fe-rich, Al-poor Martian mantle.

3:00 p.m. Whitaker M. L. * Nekvasil H. Lindsley D. H.
Potential Magmatic Diversity on Mars **[#1440]**
This experimental work has shown that under different conditions of fractionation, terrestrial olivine tholeiite parent liquid can give rise to a wide array of possible Martian magmatic diversity without calling upon plate tectonic processes.

3:15 p.m. Dalton H. A. * Musselwhite D. S. Kiefer W. S. Treiman A. H.
Experimental Petrology of the Basaltic Shergottite Yamato 980459: Implications for the Thermal Structure of the Martian Mantle **[#2142]**
We are conducting crystallization experiments on a synthetic Y98 composition. Results indicate that Y98 is a primary melt with its source at about 100 km depth. This places significant constraints on thermal state of the martian mantle.

3:30 p.m. McSween H. Y. Jr.* Milam K. A.
Comparison of Olivine-rich Martian Basalts and Olivine-Phyric Shergottites **[#1202]**
Olivine-rich basalts at the Spirit landing site have many similarities with olivine-phyric shergottites and olivine determined from orbital thermal emission spectroscopy.

3:45 p.m. Symes S. J. * Borg L. E. Shearer C. K. Asmerom Y. Irving A. J.
Geochronology of NWA 1195 Based on Rb-Sr and Sm-Nd Isotopic Systematics **[#1435]**
We have determined the Rb-Sr and Sm-Nd isotopic systematics of olivine-phyric shergottite NWA 1195. The crystallization age is 348 ± 19 Ma. NWA 1195 is isotopically unlike QUE 94201 and must derive from a less LREE-depleted source region.

4:00 p.m. Boctor N. Z. * Wang J. Alexander C. M. O'D. Hauri E. Irving A. J.
SIMS Analysis of Volatiles and H Isotope Studies of the Nakhlites Yamato 000593 (Y000593) and North West Africa 998 (NWA998) **[#1751]**
First SIMS analysis of the volatiles CO_2, F, Cl, and S in nakhlites are presented together with water abundances and H isotope signatures of melt inclusions and the nominally anhydrous minerals. Volatile loss by degassing seem to have occurred.

4:15 p.m. Chaklader J. * Shearer C. K. Hörz F.
Li, B — Behavior in Lunar Basalts During Shock and Thermal Metamorphism: Implications for H_2O in Martian Magmas **[#1426]**
Li-B depletions in Martian basalts were cited as evidence for significant magmatic water-loss. Similar depletions were observed in completely dry lunar basalts. We examine the effects of crystal chemistry, shock pressure, and thermal metamorphism on the behavior of Li-B in lunar pyroxenes.

Tuesday, March 15, 2005
MARTIAN IMPACTS: PRIMARY AND SECONDARY
8:30 a.m. Salon A

Chairs: J. B. Plescia
A. S. McEwen

8:30 a.m. Barlow N. G. *
Martian Impact Craters as Revealed by MGS and Odyssey **[#1415]**
The revision of the "Catalog of Large Martian Impact Craters" using MGS and Odyssey data is revealing important new information about crater ejecta and interior features and the environmental conditions under which they form.

8:45 a.m. Mouginis-Mark P. J. * Boyce J. M.
The Unique Attributes of Martian Double Layered Ejecta Craters **[#1111]**
We have used all THEMIS VIS images obtained up until October 2004 to study the morphology and distribution of double layered ejecta craters on Mars and find several unique attributes. eighty-nine craters, 7.5–29.0 km in diameter, have been identified.

9:00 a.m. Suzuki A. * Kumagai I. Nagata Y. Kurita K. Barnouin-Jha O. S.
The Formation of Radial Linements on Fluidized Ejecta **[#2331]**
We have conducted laboratory experiments using water and glass beads to see the interaction between a vortex ring and a particle layer. We indicate that even present Martian conditions are sufficient to form surface lineations seen on ejecta of pedestal craters.

9:15 a.m. Abramov O. * Kring D. A.
Impact-induced Hydrothermal Activity on Early Mars **[#1048]**
We present the numerical simulation results of hydrothermal activity in early Martian craters. Duration of hydrothermal activity in a range of craters is estimated, and the system mechanics are discussed. Habitability of these systems is considered.

9:30 a.m. Plescia J. B. *
Small-Diameter Martian Craters: Applicability for Chronology **[#2171]**
Craters in the size range of meters to hundreds of meters can not be reliably used for either relative or absolute chronologies on Mars.

9:45 a.m. Hartmann W. K. *
Adventures (Arrrggghh!) in Crater Counting: Small Crater Controversies **[#1427]**
An invited review is given regarding crater counting techniques.

10:00 a.m. Tanaka K. L. * Skinner J. A. Jr. Barlow N. G.
The Crater Production Function for Mars: A –2 Cumulative Power-Law Slope for Pristine Craters >5 km in Diameter Based on Crater Distributions for Northern Plains Materials **[#2162]**
Based on revised geologic mapping and an improved crater database for the Martian northern plains, we propose that the Mars crater size-frequency crater production function follows closely a –2 power low in the 5 to ~100 km diameter range.

10:15 a.m. McEwen A. S. * Preblich B. Turtle E. Studer D. Artemieva N. A. Golombek M. P. Hurst M. Kirk R. L. Burr D. M.
Distant Secondary Craters and Age Constraints on Young Martian Terrains **[#2111]**
Small martian craters (<300 m) are mostly distant secondaries, not useful for age dating, and the primary production function is "flatter" than previously assumed, which is why much of the Martian surface has well-preserved meter-scale morphologies.

10:30 a.m. Tornabene L. L. * McSween H. Y. Jr. Moersch J. E. Piatek J. L. Milam K. A. Christensen P. R.
Recognition of Rayed Craters on Mars in THEMIS Thermal Infrared Imagery: Implications for Martian Meteorite Source Regions **[#1970]**
Additional discoveries of large martian rayed craters in THEMIS TIR images has interesting implications for possible source regions of the Martain Meteorites. Links between rayed craters as seen in THEMIS TIR, possible source regions and the MM are presented.

10:45 a.m. Bart G. D. * Melosh H. J.
Ejected Boulders: Implications for Secondary Craters and the Age Dating of Surfaces **[#2022]**
We characterized boulders around four craters on the Moon and Mars and compared the results with studies of secondary craters. Our cumulative SFD plot for boulders has a slope of –4, similar to that which was found for secondary craters.

11:00 a.m. Artemieva N. A. *
Small Primaries Versus Large Secondaries on Mars — Numerical Approach **[#1589]**
Using numerical simulations we compare crater strewn fields created by a disrupted and dispersed projectile with distal secondary craters formed by high-velocity ejecta from 10-km-diameter Zunil crater.

11:15 a.m. Bottke W. F. * Nesvorny D. Durda D. D.
Are Most Small Craters Primaries or Secondaries: Insights from Asteroid Collisional/Dynamical Evolution Models **[#1489]**
We determined the main belt and NEA size distributions (SD) for D > 10 cm bodies over the last 4.6 Gy. The slope of our NEA SD at small sizes is shallower than the lunar/martian crater SD. Because crater scaling laws cannot explain the difference, most small craters must be secondaries.

11:30 a.m. Bierhaus E. B. * Merline W. J. Chapman C. R.
Variation in Size-Distributions Between Adjacent and Distant Secondary Craters **[#2386]**
We find that on Europa adjacent secondary craters exhibit steeper size-distributions than the distant secondary craters.

11:45 a.m. DISCUSSION ON PRIMARY VS. SECONDARY CRATERING

Tuesday, March 15, 2005
SPECIAL SESSION: OMEGA@MARS:
NEW INSIGHTS INTO SURFACE COMPOSITION
8:30 a.m. Salon B

Chairs: J. F. Mustard
J.-P. Bibring

8:30 a.m. Cruikshank D. P.
Introduction to Special Session

8:35 a.m. Bibring J.-P. * Langevin Y. OMEGA Team
Mars Surface Diversity as Observed by the OMEGA/Mars Express Investigation **[#2035]**
The OMEGA/Mars Express VIS-NIR hyperspectral imager is providing a comprehensive compositional coverage of Mars at a km to sub-km resolution. Major results will be summarized, and tentative interpretations discussed, in terms of Mars evolution.

9:00 a.m. Mustard J. F. * Poulet F. Gendrin A. Head J. W. III Mangold N. Bibring J.-P. Langevin Y. Gondet B. Sotin C. Le Mouélic S. Pinet P. OMEGA Science Team
Crustal Formation, Volcanism, and Alteration in the Syrtis Major Region Revealed by OMEGA Data **[#1341]**
Deposits of mafic iron-bearing silicates (pyroxene and olivine) and hydrated silicates are observed in the Syrtis Major region. Distinct evidence for the interaction of volcanism and volatile-rich substrates suggests hydrothermal alteration.

9:15 a.m. Sotin C. Le Mouélic S. * Combe J.-P. Quesnel Y. Langlais B. Mustard J. Ladai A. Bibring J.-P. Langevin Y. Gendrin A. Erard S. Gondet B. OMEGA Science Team
Mineralogy of the Magnetic Anomaly Site South of Syrtis Derived from OMEGA/Mars Express Hyperspectral Data **[#1696]**
This paper analyses hyperspectral data obtained by OMEGA/Mars Express and compared the mineral maps to magnetic anomalies in the Syrtis Major area. There is no obvious correlation between the magnetic anomaly map and the map of the major constituants.

9:30 a.m. Gendrin A. * Mangold N. Bibring J.-P. Langevin Y. Gondet B. Poulet F. Bonnello G. Quantin C. Mustard J. Arvidson R. E. Le Mouélic S. OMEGA team
Sulfates on Mars Layered Terrains: OMEGA High Resolution Campaign Confirms Low Resolutions Identifications **[#1363]**
We compare sulfate rich areas identified by OMEGA observed at higher and lower resolution.

9:45 a.m. Langevin Y. Poulet F. * Bibring J.-P. Gondet B.
Observations of Calcium Sulfate Deposits at High Latitudes by OMEGA/Mex at Km/Pixel Resolutions **[#1652]**
In December 2004, The OMEGA Vis/NIR imaging spectrometer on board Mars Express has imaged at km/pixel resolutions a region dominated by calcium sulfates observed at lower resolutions in September.

10:00 a.m. Mangold N. * Gendrin A. Quantin C. Gondet B. Langevin Y. Bibring J.-P. OMEGA Co-Investigator Team
Analysis of Candor Chasma Interior Layered Deposits from OMEGA/MEX Spectra **[#1330]**
The thick layered deposits of Candor Chasma exhibit signatures of sulfates on OMEGA spectra. This association highlights the role of water in the formation or alteration of layered deposits.

10:15 a.m. Arvidson R. E. * Poulet F. Bibring J.-P. Wolff M. Gendrin A. Morris R. V. Freeman J. J. Mangold N. Bellucci G. OMEGA Science Team
Mars Express OMEGA Observations over Terra Meridiani **[#1934]**
Surface reflectance spectra from Mars Express OMEGA data near the Opportunity landing site in Terra Meridiani are analyzed. Results are compared to Opportunity rover analyses in Eagle and Endurance craters.

10:30 a.m. Pelkey S. M. * Gendrin A. Mustard J. F. Mangold N. Bibring J.-P. Langevin Y. Gondet B. OMEGA Science Team
An Integrated Study of OMEGA-Identified Mineral Deposits in Eastern Hebes Chasma, Mars **[#1891]**
Incorporation of multiple remote-sensing data sets allows us to better understand sulfate deposits in eastern Hebes Chasma identified from Mars Express OMEGA data.

10:45 a.m. Milliken R. E. * Mustard J. F.
A Laboratory-based Model for Estimating Absolute H_2O Content of Minerals Using VIS-NIR Spectroscopy **[#1368]**
We propose a model for estimating absolute water content of minerals based on VIS-NIR data. The model is independent of composition and based on laboratory measurements.

11:00 a.m. Poulet F. * Langevin Y. Bibring J.-P. Gondet B. Arvidson R. E. OMEGA Team
Mineralogy of the Northern High Latitude Regions of Mars **[#1828]**
We have used OMEGA data to analyze the surface composition of the regions located between 50°N and the permanent polar cap.

11:15 a.m. Schmitt B. * Douté S. Langevin Y. Forget F. Bibring J.-P. Gondet B. OMEGA Team
Northern Seasonal Condensates on Mars by OMEGA/Mars Express **[#2326]**
The northern seasonal condensates on Mars have been monitored by the OMEGA imaging spectrometer (Mars Express) from Ls 330° to 90°. We report the evolution of their physical state (sublimation sequence of CO_2 ice, then H_2O ice), their spatial distribution and their temporal evolution.

11:30 a.m. Drossart P. Forget F. * Encrenaz T. Melchiorri R. Fouchet T. Vinatier S. Bézard B. Combes M. Bibring J.-P. Langevin Y. Gondet B. Ignatiev N. Zasova L. Lopez-Valverde M. A. Garcia-Comas N. OMEGA Team
Atmospheric Studies with OMEGA/Mars Express **[#1737]**
Atmospheric studies with OMEGA/Mars Express have been made in several domains concerning the Martian atmosphere structure and dynamics: pressure variations for wave activity search, limb observations for dust and cloud vertical structure retrieval as well as non-LTE gas emissions.

Tuesday, March 15, 2005
ASTROBIOLOGY II:
MICROBES, MISSIONS, AND EARLY TERRESTRIAL LIFE
8:30 a.m. Salon C

Chairs: **N. A. Cabrol**
J. F. Lindsey

8:30 a.m. Chafetz H. S. *
Microbially Induced Precipitates: Examples from CO_3, Si-, Mn- and Fe-rich Deposits **[#1084]**
Microbially induced precipitates associated with terrestrial spring deposits from geographically widely distributed sites and different element compositions provide insights with regard to the search for extraterrestial life.

8:45 a.m. Xu H. F. * Chen T.
Nano-structured Minerals as Signature of Microbial Activity **[#1897]**
The nanoporous magnetite and nano-fibrous calcite with unusual shape from both modern and paleosols are directly related to microbial activity. The study provides us useful information about possible bacterial activities on the Mars.

9:00 a.m. Ciftcioglu N. * McKay D. S.
Overview of Biomineralization and Nanobacteria **[#1205]**
Biomineralizing unique microorganism, Nanobacteria might be a good model for understanding the environmental, physical, chemical and even immunological effects on biomineralization mechanism.

9:15 a.m. Willis M. J. * Ahrens T. J. Bertani L. E. Nash C. Z.
Survival Limits of Bacteria During Shock Compression: Application to the Early Earth **[#1903]**
We describe experiments in which shock recovery is performed on live E.coli bacteria in liquid. Shocked samples are analyzed to find survival rate and damage, and results are extrapolated to impacts on early Earth. We find 1% survival at 2.4 GPa.

9:30 a.m. Schuerger A. C. * Nicholson W. L.
Synergistic Effects of Low Pressure, Low Temperature, and CO_2 Atmospheres Inhibit the Growth of Terrestrial Bacteria Under Simulated Martian Conditions **[#1366]**
Thirteen species of spore-forming and non-spore forming mesophilic bacteria that are common spacecraft contaminants were tested under simulated Mars conditions. All bacteria were unable to grow at 15 mb of CO_2 or lower, but Escherichia coli was able to grow at 25 mb.

9:45 a.m. Fernández-Remolar D. C. * Prieto-Ballesteros O. Rodríguez N. Dávila F. Stevens T. Amils R. Gómez-Elvira J. Stoker C.
Río Tinto Faulted Volcanosedimentary Deposits as Analog Habitats for Extant Subsurface Biospheres on Mars: A Synthesis of the MARTE Drilling Project Geobiology Results **[#1360]**
Reconstruction of the probable habitats hosting the detected microbial communities through the integration of the geobiological data obtained from the MARTE drilling campaigns, TEM sounding and field surface geological survey.

10:00 a.m. Mahaney W. C. * Milner M. W. Dohm J. M. Baker V. R. Netoff D. Malloch D. Miyamoto H. Hare T. M. Komatsu G.
Piping Structures on Earth and Possibly Mars: Astrobiological Implications **[#1149]**
Terrestrial environments with variable compositions of microorganisms are similar to water-rich environments on Mars that may contain fossilized or extant microbial life in similar surface or subsurface settings.

10:15 a.m. Cabrol N. A. * Wettergreen D. S. Whittaker R. Grin E. A. Moersch J. E. Chong-Diaz G. Cockell C. S. Coppin P. Dohm J. M. Fisher G. Hock A. N. Marinangeli L. Minkley N. Ori G. G. Piatek J. Waggoner A. Warren-Rhodes K. Weinstein S. Wyatt M. Apostolopoulos D. Smith T. Wagner M. Stubbs K. Thomas G. Glasgow J.
Searching for Life with Rovers: Exploration Methods & Science Results from the 2004 Field Campaign of the "Life in the Atacama" Project and Applications to Future Mars Missions **[#1244]**
LITA develops and field tests a long-range automated rover and a science payload to search for microbial life in the Atacama. The Atacama's evolution provides a unique training ground for designing and testing exploration strategies and life detection methods for the search for life on Mars.

10:30 a.m. Rouzaud J. N. * Skrzypczak A. Bonal L. Derenne S. Quirico E. Robert F.
The High Resolution Transmission Electron Microscopy: A Powerful Tool for Studying the Organization of Terrestrial and Extra-Terrestrial Carbons **[#1322]**
High Resolution Transmission Electron Microscopy (HRTEM) makes possible the imaging of the profile of the polyaromatic layers, allowing a knowledge of carbons, such as disordered natural carbons from meteorites and from Precambrian metasediments.

10:45 a.m. Robert F. * Selo S. Hillion F. Skrzypczak A.
NanoSims Images of Precambrian Fossil Cells **[#1314]**
First NanoSims Images (carbon, nitrogen, sulfur) of 4 micron fossil cells from the Gunflint Iron Formation (2 Ga. old).

11:00 a.m. De Gregorio B. T. * Sharp T. G. Flynn G. J.
A Comparison of the Structure and Bonding of Carbon in Apex Chert Kerogenous Material and Fischer-Tropsch-Type Carbons **[#1866]**
Both materials are completely amorphous and show similar C=C peaks in EELS and XANES spectra, but there is an overabundance of C=O bonds in FTT carbon. It is feasible that microbial-like features in the Apex chert could be abiotic.

11:15 a.m. Skrzypczak A. * Derenne S. Binet L. Gourier D. Robert F.
Characterization of a 3.5 Billion Year Old Organic Matter: Electron Paramagnetic Resonance and Pyrolysis GC-MS, Tools to Assess Syngeneity and Biogenecity **[#1351]**
The combination of spectroscopic and analytical techniques applied to the kerogen of the Warrawoona chert (3.5 Byr) leads to new information on the controversial question of the origin of life especially the syngeneity of the archean organic matter.

11:30 a.m. Lindsey J. F. * Brasier M. D. Green O. R.
Does the Planet Drive the Biosphere? Steps Towards a Universal Biology **[#1001]**
Carbon isotope data from carbonates in Archean and Paleoproterozoic basin of Western Australia suggest that there is a link between the biosphere and the supercontinent cycle.

Tuesday, March 15, 2005
INTERPLANETARY DUST
8:30 a.m. Marina Plaza Ballroom

Chairs: S. Messenger
M. J. Genge

8:30 a.m. Westphal A. J. * Bradley J. P.
Synthesis of GEMS from Shock-accelerated Crystalline Dust in Superbubbles: Model and Predictions **[#1904]**
We have recently proposed a model of GEMS formation from shock-accelerated crystalline dust in superbubbles. Here we briefly review the main points of the model, and suggest tests that will either prove or rule out this hypothesis.

8:45 a.m. Keller L. P. * Messenger S. Christoffersen R.
GEMS Revealed: Spectrum Imaging of Aggregate Grains in Interplanetary Dust **[#2088]**
Spectrum imaging of GEMS grains reveals that most are aggregates of smaller subgrains with diverse compositions that formed in the early solar nebula.

9:00 a.m. Brownlee D. E. * Joswiak D. J. Bradley J. P. Matrajt G. Wooden D. H.
Cooked GEMS – Insights into the Hot Origins of Crystalline Silicates in Circumstellar Disks and the Cold Origins of GEMS **[#2391]**
GEMS were heated to provide insight into the thermal formation to crystalline silicates from primitive amorphous silicate materials. The sub-solidus transformation of amorphous material in GEMS provides insight into the origin of GEMS as well as crystalline silicates around other stars.

9:15 a.m. Messenger S. * Keller L. P.
Association of Presolar Grains with Molecular Cloud Material in IDPs **[#1846]**
We have identified two presolar silicate grains associated with interstellar molecular cloud material in IDPs. Most of the grains associated with the D hotspot are high temperature crystalline components that likely formed in the solar system.

9:30 a.m. Floss C. * Stadermann F. J.
NanoSIMS D/H Imaging of Isotopically Primitive Interplanetary Dust Particles **[#1423]**
Hydrogen isotopic imaging of isotopically primitive IDPs shows that D anomalies occur both as small discrete hotspots and as larger micron-sized regions, perhaps suggesting different carrier phases. No correlation of H and N anomalies was found.

9:45 a.m. Flynn G. J. * Lanzirotti A. Sutton S. R.
Chemical and Mineralogical Analyses of Particles from the Stratospheric Collections Coinciding with the 2002 Leonid Storm and the 2003 Comet Grigg-Skjellerup Trail Passage **[#1148]**
Eight stratospheric particles collected coincident with Earth's passage through the dust trail of comet Grigg-Skjellerup, analyzed by synchrotron X-ray fluorescence and diffraction, show a wide diversity of chemical and mineralogical compositions.

10:00 a.m. Genge M. J. *
Multiple Chondrule Populations Within Micrometeorites **[#1306]**
Composite particles, containing igneous objects and fine-grained matrix, strongly suggest that at least two chondrule populations are sampled by micrometeorites — a carbonaceous chondrite-like and an ordinary chondrite-like population.

10:15 a.m. Joswiak D. J. * Matrajt G. Brownlee D. E.
Electron Energy Loss Spectroscopy Measurements of Ferric Iron in Cronstedtite from a Hydrated IDP: Comparison to Ferric Iron Contents in Cronstedtite in CM Chondrites **[#2340]**
EELs measurements of ferric iron in cronstedtite in a hydrated IDP show a large range in ferric/ferrous ratios. This contrasts with a narrow range observed in cronstedtite in CM chondrites and may imply oxidation changes after equilibration.

10:30 a.m. Nakamura K. * Messenger S. Keller L. P.
TEM and NanoSIMS Study of Hydrated/Anhydrous Phase Mixed IDPs: Cometary or Asteroidal Origin? **[#1824]**
We report a combined mineralogical and isotopic study of an unusual anhydrous IDP that contains minor hydrous phases. This IDP was found to have ^{15}N enrichments that reach +900‰. These observations suggest that some minor aqueous processing may have occurred in Kuiper belt objects.

10:45 a.m. Toppani A. * Robert F. Libourel G. de Donato P. Barrès O. d'Hendecourt L. Ghanbaja J.
Experimental Evidence for Condensation of 'Astrophysical' Carbonate **[#1894]**
We have experimentally shown that carbonates can be formed by non-equilibrium condensation using only gas phase species. Such scenario can explain their presence in planetary nebulae and in protostellar environments free of large parent bodies.

11:00 a.m. Dai Z. R. * Bradley J. P. Erni R. Browning N.
High-Resolution Electron Energy-Loss Spectroscopy (HREELS) Using a Monochromated TEM/STEM **[#2110]**
The NASA SRLIDAP funded monochromated TEM/STEM is now operational at LLNL. Preliminary data is shown for the analysis of individual interplanetary dust particles.

11:15 a.m. Rietmeijer F. J. M. * Borg J. Rotundi A.
Revisiting C_{60} Fullerene in Carbonaceous Chondrites and Interplanetary Dust Particles: HRTEM and Raman Microspectroscopy **[#1225]**
HRTEM and microRaman spectroscopy can detect minute amounts of C_{60} fullerene in cometary IDPs and carbonaceous chondrites prior to destruction by interactions with the atmosphere. Stardust samples must be protected to avoid fullerene deterioration.

11:30 a.m. Clemett S. J. * McKay D. S.
Ultra-Fast Laser Desorption/Laser Ionization Mass Spectrometry for the Organic Analysis of Stardust Sample Return **[#2295]**
We have developed a new generation ultra-fast laser desorption/laser ionization mass spectrometer, recently completed at NASA Johnson Space Center, capable of performing *in situ* organic analysis of Stardust samples at the ppm detection level.

Tuesday, March 15, 2005
IMPACTS: EJECTA EFFECTS
1:30 p.m. Salon A

Chairs: O. S. Barnouin-Jha
F. T. Kyte

1:30 p.m. Barnouin-Jha O. S. * Cintala M. J. Crawford D. A.
Impact into Coarse Grained Spheres **[#1585]**
In this study, we use experimental techniques to report on how coarse grained targets might influence ejecta excavation and crater shape.

1:45 p.m. Yamamoto S. * Okabe N. Kadono T. Sugita S. Matsui T.
Measurements of Ejecta Velocity Distribution by a High-Speed Video Camera **[#1600]**
We performed impact experiments into glass sphere targets in order to measure the velocity distribution of ejecta with velocities ranging from a few to tens of m/s.

2:00 p.m. Schönian F. * Tagle R. Stöffler D. Kenkmann T.
Geology of Southern Quintana Roo (Mexico) and the Chicxulub Ejecta Blanket **[#2389]**
In southern Quintana Roo (Mexico) the Chicxulub ejecta blanket is discontinuously filling a karstified pre-KT land surface. This suggests a completely new scenario for the geological evolution of the southern Yucatán Peninsula.

2:15 p.m. Kring D. A. * Showman A. P. Durda D. D.
Global Winds and Aerosol Updrafts Created by the Chicxulub Impact Event **[#1544]**
Impact-generated thermal contrasts in the atmosphere may have generated high-velocity winds aloft and at the Earth's surface.

2:30 p.m. Kyte F. T. * Gersonde R. Kuhn G.
Detailed Results on Analyses of Deposits of the Eltanin Impact, Recovered in Sediment Cores from Polarstern Expedition ANT-XVIII/5a **[#2129]**
An expedition by the RV Polarstern in 2001 explored 80,000 km^2 of ocean floor and recovered 16 sediment cores containing ejecta deposits from the Eltanin impact. Details of this deep-ocean impact and the most meteorite-rich locality on Earth are discussed.

2:45 p.m. Ohno S. * Sugita S. Kadono T. Ishibashi K. Igarashi G. Matsui T.
An Experimental Method to Estimate the Chemical Reaction Rate in Vapor Clouds: An Application to the K/T Impact **[#1794]**
We propose a new experimental method to estimate the chemical reaction rate in vapor clouds. We also apply the method to the redox reactions of sulfur oxides and discuss the implication of the results to the K/T event.

3:00 p.m. Sheffer A. * Melosh H. J.
Why Moldavites are Reduced **[#1468]**
We use an isentropic cooling path to model the formation and oxygen reduction of moldavite tektites. The cooling path is inherently reducing, so no reducing agents are necessary.

Tuesday, March 15, 2005
VENUS
3:15 p.m. Salon A

Chairs: V. L. Hansen
S. E. Smrekar

3:15 p.m. Hansen V. L. *
Crustal Plateaus as Ancient Large Impact Features: A Hypothesis **[#2251]**
An alternate hypothesis of crustal plateau formation through deformation and progressive crystallization of a huge lava pond, that results from massive melting of the mantle due to bolide impact with ancient thin Venus lithosphere is presented.

3:30 p.m. Martin P. * Stofan E. R. Glaze L. S.
Analysis of Coronae in the Parga Chasma Region, Venus **[#1617]**
Parga Chasma is a 10,000 km long fracture and trough system in the southern hemisphere of Venus. We perform a statistical analysis of the spatial distribution of coronae in this region, and examine the variations in volcanism and relative timing of corona formation with respect to local rifting.

3:45 p.m. Smrekar S. E. * Stofan E. R. Buck W. R. Martin P.
Parga Chasma: Coronae and Rifting on Venus **[#2324]**
Do coronae occur along rifts due to regional extension or do coronae cause extension? We estimate trough widths, elastic thickness and crustal thickness for segments of Parga Chasma and compare them with models of regional uniform rifting.

4:00 p.m. Basilevsky A. T. * Head J. W. III
Venus: Geologic Mapping and History of the Beta Regio Structure **[#1050]**
Geologic mapping of V17 Beta Regio complemented with other studies of this area and the geophysical modelling showed that the Beta tectonic uplift started close to the time T (mean surface age of Venus) and still continued after 0.5T.

4:15 p.m. Grindrod P. M. * Nimmo F. Stofan E. R. Guest J. E.
Strain as an Indicator of Multiple Episodes of Uplift and Extrusion at Radially-fractured Centers on Venus **[#1304]**
We have measured the strain recorded at four radially-fractured centers on Venus, and modeled it in terms of uplift caused by the inflation of a spherical magma body at depth.

4:30 p.m. Ivanov M. A. * Head J. W. III
Abundance, Geological Settings, and Areal Distribution of Young Small Shield Volcanoes on Venus **[#1046]**
Analysis of the stratigraphic position of small shields shows that ~10% of the total population of these structures postdates emplacement and deformation of regional plains, which is poorly consistent with the nondirectional model of Venus history.

Tuesday, March 15, 2005
SPECIAL SESSION
MARS POLAR ATMOSPHERE SURFACE INTERACTIONS
1:30 p.m. Salon B

Chairs: T. N. Titus
T. H. Prettyman

1:30 p.m. Barnes J. R. *
Planetary Eddies in the MGS TES Data and Winter Argon Transports **[#1267]**
Meridional transports of Ar are implied by Odyssey GRS observations during southern winter. Variations in weather system activity determined from MGS TES data suggest that the transports are produced primarily by these systems.

1:45 p.m. Sprague A. L. * Boynton W. V. Kerry K. Nelli S. M. Murphy J. R. Reedy R. C. Metzger A. E. Hunten D. M. Janes K. D. Crombie K.
Distribution and Abundance of Mars' Atmospheric Argon **[#2085]**
One and one half Mars years (MY 26 and 27) of atmospheric argon measurements are described and studied in the context of understanding how argon, a minor constituent of Mars atmosphere that does not condense at Mars temperatures, can be used to study martian circulation and dynamics.

2:00 p.m. Tyler D. Jr.* Barnes J. R.
Mesoscale Simulations of Polar Circulations: Late Spring to Late Summer **[#2193]**
Using the OSU Mars MM5 we have performed numerous simulations from late spring through late summer. These simulations have been performed at high resolution over the northern polar region and utilize realistic representations of the surface.

2:15 p.m. Levrard B. * Forget F. Laskar J. Montmessin F.
A GCM Recent History of Northern Martian Polar Layered Deposits: Contribution from Past Equatorial Ice Reservoirs **[#1783]**
3D-LMD GCM simulations of the martian water cycle have been performed to determine the rates of exchange of surface ice between the northern cap and tropical areas for a wide range of obliquity and orbital parameters values and to reconstruct an history of the northern cap over the last 10 Ma.

2:30 p.m. Bonev B. P. * Bjorkman J. E. Hansen G. B. James P. B. Wolff M. J.
Effects of Atmospheric Dust on Residual South Polar Cap Stability **[#1101]**
We model the response of the Residual South Polar Cap to atmospheric dust in order to study its interannual stability. We use measurements of the visible albedo of the cap obtained by HST in 2003 to help constrain models for the surface frost.

2:45 p.m. Douté S. * Schmitt B. Bibring J.-P. Langevin Y. Altieri F. Bellucci G. Gondet B. MEX OMEGA Team
Nature and Composition of the Icy Terrains of the South Pole of Mars from MEX OMEGA Observations **[#1734]**
From OMEGA observations, we first determine the modes of coexistence between H_2O, CO_2 ices and dust and then give an estimate of the relatives abundances of the previous compounds at the surface of the South polar region of Mars in late summer.

3:00 p.m. Sanin A. B. * Mitrofanov I. G. Litvak M. L. Kozyrev A. S. Parshukov A. V.
Exploration of Martian Polar Residual Caps from HEND/ODYSSEY Data **[#1674]**
The given presentation is devoted to the detalied study of composition (water ice/CO_2 frost) of martian polar residual caps based on neutron spectrometry data from HEND/ODYSSEY.

3:15 p.m. Aharonson O. * Schorghofer N.
Distribution, Exchange, and Topographic Control of Subsurface Ice on Mars **[#2217]**
We consider the effect of surface slope and slope distribution on the Martian ground ice distribution and find that depending on the length-scale, these slopes may have profound implications for the equilibrium ice table.

3:30 p.m. Boynton W. V. * Kim K. J. Drake D. Reedy R. Janes D. Kerry K. Williams R. Crombie K. GRS Science Team
Determination of Both Depth and Ice Content of Sub-Surface Ice in the Polar Regions **[#2154]**
The GRS determined fluxes of gamma rays from Si and H are used to determine both the H_2O content and burial depth of the sub-surface ice in the polar regions. We find an H_2O content of about 50% in the north and 75% in the south.

3:45 p.m. Colaprete A. * Barnes J. R. Haberle R. M. Holligsworth J. L. Kieffer H. H. Titus T. N.
Nature of the South Pole on Mars Determined by Topographic Forcing of Atmosphere Dynamics **[#2055]**
Using observations and simulations we demonstrate that the nature of the south pole on Mars is determined by mid-latitude, large scale topography.

4:00 p.m. Ivanov A. B. * Wagstaff K. L. Titus T. N.
Tracking Retreat of the North Seasonal Ice Cap on Mars: Results from the THEMIS Investigation **[#2156]**
We validated and tested two algorithms to track retreat of seasonal ice caps on Mars. One of the algorithms is proposed for onboard implementation to start an interannual ice cap monitoring program using THEMIS instrument.

4:15 p.m. Prettyman T. H. * Elphic R. C. Feldman W. C. Murphy J. R. Nelli S. Titus T. N. Tokar R. L.
Spatial Deconvolution of Mars Odyssey Neutron Spectroscopy Data: Analysis of Mars Southern Seasonal Cap **[#1384]**
We show that spatial deconvolution of neutron spectroscopy data is required for an accurate analysis of the south polar seasonal cap and atmosphere during recession. Analysis of regional features and comparisons to GCM calculations are presented.

4:30 p.m. Forget F. * Levrard B. Montmessin F. Schmitt B. Douté S. Langevin Y. Bibring J.-P.
Mars Water Ice and Carbon Dioxide Seasonal Polar Caps: GCM Modeling and Comparison with Mars Express OMEGA Observations **[#1605]**
Numerical simulations of the Martian climate/CO_2 cycle/water cycle and Mars Express OMEGA observations are analysed and compare to better understand the seasonal polar caps.

Tuesday, March 15, 2005
NAKHLITES AND CHASSIGNITES:
NEW ARRIVALS AND FAMILIAR FRIENDS
1:30 p.m. Salon C

Chairs: G. McKay
R. P. Harvey

1:30 p.m. Mikouchi T. * Monkawa A. Koizumi E. Chokai J. Miyamoto M.
MIL03346 Nakhlite and NWA2737 "Diderot" Chassignite: Two New Martian Cumulate Rocks from Hot and Cold Deserts **[#1944]**
MIL03346 and "Diderot" are new nakhlite and chassignite, respectively. Their mineralogy and petrology show that MIL03346 is very similar to NWA817, but Diderot is clearly different from Chassigny in several respects.

1:45 p.m. McKay G. * Schwandt C.
Mineralogy and Petrology of New Antarctic Nakhlite MIL 03346 **[#2351]**
MIL 03346 appears to be a new end member in the continuum of nakhlite textures and zoning patterns. It has the most highly zoned olivines and the most Fe-enriched pyroxenes of any nakhlite. These characteristics suggest that MIL is the fastest-cooled and thus the shallowest of all nakhlites.

2:00 p.m. Rutherford M. J. * Calvin C. Nicholis M. McCanta M. C.
Petrology and Melt Compositions in Nakhlite MIL 00346: Significance of Data from Natural Sample and from Experimentally Fused Groundmass and M.I.'s **[#2233]**
Textural and compositional analyses of Mil-03346 phenocrysts and refused groundmass indicate magmatic conditions and environment of crystallization for this new nakhlite.

2:15 p.m. Hammer J. E. * Rutherford M. J.
Experimental Crystallization of Fe-rich Basalt: Application to Cooling Rate and Oxygen Fugacity of Nakhlite MIL-03346 **[#1999]**
A series of experiments on synthetic basalt over a range of constant-rate cooling conditions and fO_2's (IW-MNO) suggest crystallization of the natural intercumulus liquid in response to mean cooling at 6°C/h, near the NNO buffer.

2:30 p.m. Stopar J. D. * Lawrence S. J. Lentz R. C. F. Taylor G. J.
Preliminary Analysis of Nakhlite MIL 03346, with a Focus on Secondary Alteration **[#1547]**
MIL 03346 has the largest grains and most mesostasis of any nakhlite. It contains an assortment of aqueous products including gypsum. Fluids containing Ca, K, and S may have deposited evaporite minerals. Olivine is at various stages of alteration.

2:45 p.m. Murty S. V. S. * Mahajan R. R. Goswami J. N. Sinha N.
Noble Gases and Nuclear Tracks in the Nakhlite MIL 03346 **[#1280]**
Noble gases and nuclear track data give an exposure age of 10 Ma and a pre-atmospheric radius of ~6 cm for MIL 03346. Noble gas elemental ratios indicate a more severe elemental fractionation for the Mars atmospheric component in MIL 03346, as compared to other nakhlites.

3:00 p.m. Mohapatra R. K. * Crowther S. Gilmour J. D.
Xenon in Yamato 000593 & NWA 817- Nakhlites from Two Diverse Terrestrial Environments **[#1757]**
We have analysed mineral separates from two newly discovered martian meteorites Yamato 000593 and NWA 817 for their xenon isotopes by RELAX to understand the nature of volatile components, and present here preliminary data and results from the study.

3:15 p.m. Misawa K. * Shih C.-Y. Reese Y. Nyquist L. E.
Crystallization Age and Source Signature of Chassigny **[#1698]**
We present the new Sm-Nd isotopic data for Chassigny and discuss the nature of its source materials. Eight data points define a linear array corresponding to a Sm-Nd age of 1.36 ± 0.03 Ga with an initial ε^{143}Nd = +16.6 ± 0.2.

3:30 p.m. Harvey R. P. * Hamilton V. E.
Syrtis Major as the Source Region of the Nakhlite/Chassigny Group of Martian Meteorites: Implications for the Geological History of Mars **[#1019]**
The observed geology and spectroscopy of Syrtis Major is a compelling match to the mineralogy and hypothesized setting of the nakhlite/Chassigny group of martian meteorites. If this connection is real, it solves many interesting timescale-based problems in martian geology.

3:45 p.m. Weiss B. P. * Shuster D. L.
Martian Surface Paleotemperatures from Thermochronometry of Meteorites **[#1156]**
Noble gas thermochronometry of Martian meteorites places quantitative constraints on their shock history and constrains climatic evolution. Our calculations suggest that for the last 4 Gyr, the near-surface has not been significantly warmer than the present cold conditions.

4:00 p.m. Rost D. * Vicenzi E. P. Pauli E. C.
Halite, Sulfate, and Clay Assemblages in the Nakhla Martian Meteorite **[#2306]**
Analysis of clays found in Nakhla mineral assemblages indicate different sources for minor and trace elements: local chemistry is probably responsible for varying Na, K, Al, Ti, Cr contents whereas other elements may stem from the involved fluid.

4:15 p.m. Rao M. N. Sutton S. R. * McKay D. S.
Evaporative Evolution of Martian Brines Based on Halogens in Nakhlites and MER Samples **[#1358]**
Comparison of Cl and Br from Nakhla veins to MER samples suggests two kinds of brine solutions existed on Mars, one early and one late in the evaporation sequence. These solutions precipitated the secondary salts at the Meridiani and Gusev sites.

4:30 p.m. Bridges J. C. * James R. H. Pearson V. K. Baker L. Verchovsky A. B. Wright I. P.
Lithium and Carbon Isotopic Fractionations Between the Alteration Assemblages of Nakhla and Lafayette **[#1758]**
Nakhla and Lafayette δ^7Li values for samples and extracts (4.1–14.2‰) are consistent with brine evaporation. Relatively ^{13}C-poor siderite in Lafayette suggests more than one carbon source was sampled.

Tuesday, March 15, 2005
MARS POTPOURRI: WET AND DRY, SANDY AND DUSTY
1:30 p.m. Marina Plaza Ballroom

Chairs: L. K. Fenton
K. K. Williams

1:30 p.m. Williams K. K. * Grant J. A. Fortezzo C. M.
New Insights into the Geologic History of Margaritifer Sinus and Discovery of a Phreatomagmatic Event During Late-Stage Fluvial Activity **[#1439]**
MGS and MO data have been used to study the geologic history of the Margaritifer basin area beyond what was possible with Viking images. A new discovery is a likely phreatomagmatic edifice that formed at the confluence of two major valley systems.

1:45 p.m. Irwin R. P. III* Maxwell T. A. Howard A. D. Craddock R. A. Moore J. M.
A Noachian/Hesperian Hiatus and Erosive Reactivation of Martian Valley Networks **[#2221]**
Fan and delta morphology, channel hydrology, late exit breaches of closed basins, and base level changes suggest a hiatus in valley network activity while fretted terrain developed, followed by an erosive Early Hesperian reactivation of valleys.

2:00 p.m. McMenamin D. S. * McGill G. E.
Processes Involved in the Formation of Martian Fan-shaped Deposits **[#1732]**
We use martian delta morphology to re-evaluate the processes involved in delta formation, identify various types of deltas and fan-shaped deposits observed in high-resolution imagery, and predict the existence of certain kinds of deltas.

2:15 p.m. Soukhovitskaya V. * Manga M.
Martian Landslides in Valles Marineris: Wet or Dry? **[#1093]**
We analyze the geometric properties of landslides on Earth and compare these with landslides in Valles Marineris to learn about the dynamics of Martian landslides and to determine whether liquid water played a significant role in forming them.

2:30 p.m. Kraal E. R. * Moore J. M. Howard A. D. Asphaug E.
Alluvial Fans on Mars **[#1558]**
We present a comprehensive survey of Martian alluvial fans in craters from 0°–30°S, examine the apparent clustering of fans, and to address the issue of gravity scaling in a quantitative manner.

2:45 p.m. Bourke M. C. *
Alluvial Fans on Dunes in Kaiser Crater Suggest Niveo-Aeolian and Denivation Processes on Mars **[#2373]**
Alluvial fans on large barchan dunes in Kaiser Crater suggest denivation triggers for fluvial flow.

3:00 p.m. Grant J. A. * Golombek M. P. Haldemann A. F. C. Crumpler L. S. Li R. Athena Science Team
Crater Gradation in Gusev Crater, Meridiani Planum, and on the Earth **[#1472]**
Crater gradation in Meridiani and Gusev does not involve water, thereby enabling processes subordinate on Earth to dominate. Craters at Meridiani are more modified, but gradation at both locations is dominated by eolian and mass-wasting processes.

3:15 p.m. Balme M. R. * Bourke M. C.
Preliminary Results from a New Study of Transverse Aeolian Ridges (TARs) on Mars **[#1892]**
We present preliminary results from a study of Transverse Aeolian Ridges (TARs) on Mars. We have found similarities in morphology between TARs and large dark dunes and that TARs and large dark dunes have distinctive thermal signatures.

3:30 p.m. Fenton L. K. *
Seasonal Movement of Material on Dunes in Proctor Crater, Mars: Possible Present-Day Sand Saltation **[#2169]**
Investigation of MOC NA images of an intercrater dune field has led to the discovery of possible evidence for limited dune activity and sand saltation during the MGS mission.

3:45 p.m. Szwast M. A. * Richardson M. I. Vasavada A. R.
Surface Dust Redistribution on Mars as Observed by the Mars Global Surveyor **[#2191]**
A study of MGS TES albedo data set as a proxy for dust cover was performed focusing around the 2001 global dust storm. We found widespread surface dust redistribution caused by the storm, and recovery since implying a multi-year cyclical nature.

4:00 p.m. Bulmer M. H. * Glaze L. S. Anderson S.
Distinguishing Between Primary and Secondary Emplacement Events of Blocky Volcanic Deposits Using Rock Size Distributions **[#1676]**
The objective of this field study was to quantitatively characterize the surface block size distributions collected at multiple locations and to develop a technique that could easily be applied to remote sensing images of blocky planetary flows.

4:15 p.m. Viles H. A. * Brearley A. J. Bourke M. C. Holmlund J.
What Processes Have Shaped Basalt Boulders on Earth and Mars? Studies of Feature Persistence Using Facet Mapping and Fractal Analysis **[#2237]**
Facet mapping at Ephrata Fan suggest a potentially high persistence of fluvially-created features on basalt boulders on Earth. The absence of any such features at Gusev Crater imply that fluvial processes have not affected the boulders there.

4:30 p.m. Shockey K. M. * Zimbelman J. R.
The Medusae Fossae Formation: Mapping the Origins **[#1799]**
To better understand the origins of the Medusae Fossae Formation, we are mapping the Gordii Dorsum escarpment and surrounding areas.

Tuesday, March 15, 2005
POSTER SESSION I
7:00 p.m. Fitness Center

Presolar Grains

Marhas K. K. Hoppe P. Ott U.
Continued Study of Ba Isotopic Compositions of Presolar Silicon Carbide Grains from Supernovae **[#1855]**
Ba isotopic compositions in Type X SiC grain show lower than solar $^{135}Ba/^{136}Ba$ and $^{137}Ba/^{136}Ba$ and higher than solar $^{138}Ba/^{136}Ba$. This can be explained by mixing of s-processed matter with r-processed/n-burst processed matter in SN.

Savina M. R. Paul M. Ofan A. Barzyk J. G. Pellin M. J.
A Search for Live ^{244}Pu in Deep-Sea Sediments: Preliminary Results of Method Development **[#2350]**
We report on the initial stages of a search for live ^{244}Pu in deep-sea sediments. We propose to use Resonant Ionization Mass Spectrometry to improve sensitivity over existing methods.

Chen C. Taylor S. Sharma M.
Iron and Osmium Isotopes from Stony Micrometeorites and Implications for the Os Budget of the Ocean **[#2134]**
Five micrometeorites were analyzed for Os and Fe concentrations and/or isotopes. >99.5% of Os and up to 90% of Fe has been lost. We interpret this to mean that Fe and Os are being lost as nanoparticles contributing to dissolved Os in the ocean.

Zinner E. * Amari S. Jennings C. Mertz A. F. Nguyen A. N. Nittler L. R. Hoppe P. Gallino R. Lugaro M.
Al and Ti Isotopic Ratios of Presolar SiC Grains of Type Z **[#1691]**
Al and Ti isotopic ratios were measured in type Z SiC grains. The Al ratios are in the range of those in mainstream grains and are much smaller than those in presolar oxide grains. The Ti ratios confirm the grains' origin in low-metallicity AGB stars.

Tizard J. Lyon I. C. Henkel T.
Elemental Abundance in Presolar SiC: Comparing Grains Separated by Acid Residue and Gentle Separation Procedures **[#2115]**
We present a comparison of elemental abundances, by TOFSIMS analysis, in presolar silicon carbide grains including grains separated by acid dissolution and grains separated by a new gentle separation method to look for artificial anomalies.

Yoshida T. Umeda H. Nomoto K.
Silicon Isotopic Ratios of Presolar Grains from Supernovae **[#1556]**
We investigate Si isotopic ratios of mixtures of supernova ejecta using 3.3, 4, 6, and 8 M He star models. The isotopic signature $\delta^{29}Si/^{28}Si > \delta^{30}Si/^{28}Si$ of supernova grains is better reproduced by the supernova mixtures of less massive stars.

Stephan T. Weber I. Hoppe P.
TOF-SIMS, NanoSIMS, and TEM Analysis of Interplanetary Dust Particle Sections **[#1645]**
Three IDPs were selected for TOF-SIMS, NanoSIMS, and TEM analysis. This suite of analytical techniques allows to obtain information on the elemental, isotopic, and mineralogical composition of IDPs on a sub-micrometer scale.

Floss C. Stadermann F. J.
Presolar (Circumstellar and Interstellar) Phases in Renazzo: The Effects of Parent Body Processing **[#1390]**
Although aqueous alteration probably destroyed or equilibrated most presolar silicates in matrix material from Renazzo, this meteorite contains high abundances of SiC, and has N isotopic micro-distributions that are similar to those in IDPs.

Nagashima K. Sakamoto N. Yurimoto H.
Destruction of Presolar Silicates by Aqueous Alteration Observed in Murchison CM2 Chondrite **[#1671]**
Four presolar silicates and 14 presolar carbonaceous grains were found in Murchison. The lower abundance of presolar silicates than that of presolar carbonaceous grains suggests preferential destruction of presolar silicates by aqueous alteration.

Verchovsky A. B. Fisenko A. V. Semjonova L. F. Wright I. P.
Nanometer-sized Diamonds from AGB Stars **[#2285]**
We obtained some evidence that a small fraction of presolar diamonds could come from AGB stars.

Fisenko A. V. Verchovsky A. B. Semjonova L. F. Wright I. P.
A Model for Multiple Populations of Presolar Diamonds **[#2304]**
We developed a three-population model which is able to explain variations of nitrogen concentration and isotopic composition observed during stepped combustion of presolar diamonds.

Micrometeorites and Interplanetary Dust

Lever J. H. Habermehl M. Fiolitakis A. Taylor S.
Collecting Time-sequenced Records of Micrometeorites from Polar Ice Caps **[#1105]**
Our goal is to design, build and calibrate a collector that can obtain time-sequenced records of micrometeorites and terrestrial dust during hot-water drilling operations into polar ice caps.

Duprat J. Engrand C. Maurette M. Gounelle M. Kurat G. Leroux H.
Friable Micrometeorites from Central Antarctica Snow **[#1678]**
We recovered micrometeorites trapped in central Antarctica surface snow. The CONCORDIA-Collection is characterized by minimal terrestrial weathering and friable fine-grained micrometeorites. Size distributions are reported.

Gattacceca J. Rochette P. Folco L. Perchiazzi N.
A New Micrometeorite Collection from Antarctica and Its Preliminary Characterization by Microobservation, Microanalysis and Magnetic Methods **[#1315]**
Thousands of micrometeorites were collected in aeolian deposits in Antarctica during the XIX PNRA expedition. Such large and well preserved population offers a good opportunity to test and develop a magnetic classification procedure, in parallel to mineralogical and geochemical characterization.

Smith J. B. Dai Z. R. Weber P. K. Graham G. A. Hutcheon I. D. Bajt S. Ishii H. A. Bradley J. P.
Nitrogen Isotopic Anamolies in a Hydrous Interplanetary Dust Particle **[#1003]**
The discovery of an ^{15}N-enrichment in a serpentine-rich IDP is reported. This isotopic anomaly within an amorphous carbon grain may be inherited from the cold molecular cloud.

Matrajt G. Brownlee D. E. Joswiak D. J. Taylor S.
Atmospheric Entry Heating Effects on Organic Carbonaceous Phases of IDPs and Polar Micrometeorites: An EELS Study **[#1553]**
Energy Electron Loss Spectroscopy (EELS) was combined to high resolution imaging to differentiate the thermally processed carbon from the pristine carbon in IDPs and micrometeorites.

Quirico E. Rouzaud J.-N. Bonal L. Montagnac G.
Maturation Grade of Coal Samples as Revealed by Raman Spectroscopy **[#1657]**
Raman spectroscopy is a useful tool for studying organic matter in cometary grains and pristine chondrites. This study focused on the definition of optimized experimental parameters, and revealed sample photoinstability under laser irradiation.

Reedy R. C.
Recent Solar-Proton Fluxes **[#2184]**
The event-integrated fluences of solar protons up to 2004 have been determined and compared to previous data. The current solar cycle has been very active, and very large fluxes of solar protons have affected spacecraft and meteorites.

Bajt S. Baragiola R. A. Bringa E. M. Bradley J. P. Dai Z. R. Dukes C. A. Felter T. Graham G. A. Kucheyev S. O. Loeffler M. J. Martin M. C. Tielens A. Torres D. van Breugel W.
Amorphization of Forsterite Grains Due to High Energy Heavy Ion Irradiation – Implications for Grain Processing in ISM **[#2342]**
The absence of crystalline silicates in diffuse ISM is intriguing and not well understood. Our irradiation experiments on forsterite single crystals support the hypothesis that high energy heavy cosmic rays can efficiently amorphize silicate grains in the ISM.

Ipatov S. I. Kutyrev A. S. Madsen G. J. Mather J. C. Moseley S. H. Reynolds R. J.
Dynamical Zodiacal Cloud Models Constrained by High Resolution Spectroscopy of the Zodiacal Light **[#1266]**
Using dynamical models of the zodiacal cloud, we investigated how the solar spectrum is changed by scattering by dust particles and compared the results with the observations.

Marov M. Ya. Ipatov S. I.
Migration of Dust Particles and Volatiles Delivery to the Inner Planets **[#1268]**
Model of collision probabilities of dust debris with Earth and Venus was developed. Dust particles could be most efficient in the organic matter inventory surviving atmospheric entry, rather than significantly contribute to the accretion of the inner planets.

Morlok A. Menzies O. N. Koehler M. Bland P. A. Cressey G. Grady M. M.
Mid-Infrared Spectroscopy of CAI and AOA from the Allende CV3.2 Chondrite **[#1644]**
Mid-infrared spectra of bulk CAI from the CV3.2 chondrite Allende are presented and compared with astronomical spectra of cometary dust, zodiacal light, the circumstellar disk of beta Pictoris and dust around the red supergiant PR Per.

Morlok A. Koehler M. Grady M. M.
Infrared Spectroscopy of Extraterrestrial Material: Comparison with Astronomical Spectra of Dust **[#1646]**
Infrared spectra of components (CAI, matrix etc.) from type 3 carbonacous chondrites (Allende, Ornans, Vigarano) are compared with infrared spectra from astronomical objects (comets, zodiacal light, circumstellar disks and others).

Aerogel Extraction and Instrumentation

Ott U. Sudek Ch. Maul J. Bernhard P. Elmers H. J. Schönhense G.
Nano-ESCA: A Valuable Tool for Studying Presolar Grains (and Other Extraterrestrial Materials) **[#1294]**
Nano-ESCA is a surface science technique with ~0.1 eV energy and ~100 nm lateral resolution. It may be a valuable tool for characterizing elemental distributions and binding states in small grains.

Chen C.-Y. Shen J. J. Lee T. Calaway W. Veryovkin I. Moore J. Pellin M.
Developing SNMS for Full-Spectrum High-Sensitivity In-Situ Isotopic Analysis of Individual Comet Grains Collected by Stardust? **[#1373]**
In anticipation of the return of comet dust grains by the Stardust mission in mid-January next year, Academia Sinica and Argonne National Laboratory have entered into a collaboration to develop instrument and method for the isotopic analysis of these samples.

Henkel T. Tizard J. Lyon I. C.
IDLE: (Interstellar Dust Laser Explorer), a New Instrument for Submicron Analyses of Stardust — Quantification in SIMS and Laser SNMS **[#1759]**
We have developed a new TOFSIMS/laser-SNMS instrument for the analysis of interstellar grains using laser secondary neutral mass spectrometry to improve sensitivity and quantification over SIMS analysis for the heavier elements of the periodic table.

Ishii H. A. Brennan S. Luening K. Pianetta P. Bradley J. P. Snead C. J. Westphal A. J.
Hard X-Ray Spectro-Microscopy Techniques at SSRL for Astromaterials Analysis **[#1393]**
We describe micro-focus X-ray techniques for the study of elemental and chemical state distributions in IDPs, micrometeoroids and Stardust particles.

Ishii H. A. Graham G. A. Kearsley A. T. Grant P. G. Snead C. J. Bradley J. P.
Ultrasonic Micro-Blades for the Rapid Extraction of Impact Tracks from Aerogel **[#1387]**
Sample recovery from silica aerogel collectors is critical for Stardust science return. We report a rapid and simple approach for extracting particle impact tracks from aerogel.

Kearsley A. T. Burchell M. J. Graham G. A. Cole M. J. Wallis D.
Interpreting Micrometeoroid Residues on Metallic Spacecraft Surfaces: Clues from Low Earth Orbit, the Laboratory and to Come from Stardust? **[#1670]**
Micrometeoroid impacts leave residue. Laboratory light gas gun shots provide a good velocity analogue for impacts on metal components of Stardust; the residues may help to identify cometary residues on metallic spacecraft surfaces in low Earth orbit.

Dominguez G. Westphal A. J.
Modeling Large Interstellar Dust Grain Impacts in Sample Return Missions **[#2286]**
We present results of our modeling of large interstellar dust grain impacts onto the surfaces of current (Genesis, Stardust) and future (XPC) sample return missions. These results include the number, size, velocity, and impact angle distributions.

Okudaira K. Yano H. Noguchi T. Nakamura T. Burchell M. J. Cole M. J.
Are They Really Intact? — Evaluation of Captured Micrometeoroid Analogs by Aerogel at the Flyby Speed of Stardust **[#1832]**
We simulate hypervelocity capturing (6 km/s) analog particles by aerogel (0.03 g/cc) for Stardust mission. The extracted particles (lizardite and cronstedtite) lost their volumes and original surface morphologies and had vesiculated textures.

Graham G. A. Sheffield-Parker J. Bradley J. P. Kearsley A. T. Dai Z. R. Mayo S. C. Teslich N. Snead C. Westphal A. J. Ishii H. A.
Electron Beam Analysis of Micrometeoroids Captured in Aerogel as Stardust Analogues **[#2078]**
This paper discusses the use of X-ray phase contrast ultramicroscopy and analytical scanning electron microscopy for the analysis micrometeoroids embedded in aerogel.

Snead C. J. Butterworth A. L. Westphal A. J. Grant P. G.
Extracting Hypervelocity Impact Track Events in Aerogel in Cross-section Wafers **[#2370]**
Material deposited on the walls of hypervelocity impact tracks in aerogel extracted in 30 μm thick aerogel cross-sections.

Westphal A. J. Butterworth A. L. Snead C. J. Craig N. Anderson D. Jones S. M. Brownlee D. E. Farnsworth R. Zolensky M. E.
Stardust@home: A Massively Distributed Public Search for Interstellar Dust in the Stardust Interstellar Dust Collector **[#1908]**
We are developing a project to recruit the public in the search for interstellar dust in the Stardust IS dust collector, based in part on the wildly popular SETI@home project, which has five million subscribers. We call the project Stardust@home.

Genesis: Field Recovery, Status of Select Materials, Analytical Methods

Mao P. H. Kunihiro T. McKeegan K. D. Coath C. D. Jarzebinski G. Burnett D. S.
Preliminary Evaluation of the Secondary Ion/Accelerator Mass Spectrometer, MegaSIMS **[#2259]**
We present progress on the development of MegaSIMS, a hybrid SIMS/AMS designed to measure the O and N isotopic abundance ratios from one of the Genesis SiC concentrator samples.

Stansbery E. K. McNamara K. M.
Genesis Preliminary Examination — Ellipsometry Overview **[#2145]**
Spectroscopic Ellipsometry is a measurement technique using polarized light to characterize thin films, surfaces, and material microstructure. We will explain this technique as it pertains to preliminary examination of Genesis collector materials.

McNamara K. M.
Genesis Field Recovery **[#2403]**
This details the recovery of the Genesis spacecraft and payload from the impact site at UTTR on Sept. 8–9, 2004.

Nishiizumi K. Allton J. H. Burnett D. S. Butterworth A. L. Caffee M. W. Clark B. C. Jurewicz A. J. G. Komura K. Westphal A. J. Welten K. C. Woolum D. S.
Status of Genesis Mo-Pt Foils **[#2266]**
Mo-coated Pt foils were exposed to solar wind by the Genesis mission. Solar wind ions were captured in the Mo. Objective is the measurement of radionuclides from the sun. The hard landing of the SRC has resulted in contaminated and crumpled foils. We present a status report and revised plan.

Allton J. H. Stansbery E. K. McNamara K. M. Meshik A. See T. H. Bastien R.
Initial Subdivision of Genesis Early Science Polished Aluminum Collector **[#1806]**
The polished aluminum collector, part of the Genesis Mission Early Science Return, was extracted from the damaged canister intact, but bent and with a few mud spatters. Pre- and post-flight curation handling and subdivision of the collector by sawing is described.

Grimberg A. Bühler F. Bochsler P. Heber V. Baur H. Wieler R.
Trapping and Release Data of Artificially Implanted Noble Gases into Metals — Tests for Genesis Targets **[#1355]**
Two noble gas irradiation experiments were carried out to determine mass discrimination for different Genesis target materials and to demonstrate the depth resolution of closed-system stepwise etching on the metallic glass Ax1.

Marty B. Burnard P. Zimmermann L. Robert P.
Nitrogen-Noble Gas Static Mass Sepectrometry of Genesis Collector Materials **[#1686]**
Gases (N, Ne, Ar) are extracted from Au-coated sapphire and diamond-like carbon collectors using an F2 excimer laser, without blank contributions the substrate. N is purified using a low blank CuO/Cu cycle prior to analysis by high resolution multicollector mass spectrometer.

Mercury

Barkin Yu. V. Ferrandiz J. M.
Mercury: Libration, Gravitational Field and Its Variations **[#1075]**
Mercury librations in longitude and variations of its gravitational field have been studied on the base of plane model about the motion of non-spherical celestial (rigid or elastic) body with a liquid core in the gravitational field of the Sun.

Redmond H. L. King S. D.
Thermal History Calculations Versus Full Convection Models: Application to the Thermal Evolution of Mercury **[#1905]**
We present a suite of convection calculations with a constant viscosity and dry, olivine rheology. By comparing our convective models with previous calculations, we hope to resolve the inconsistencies in previous thermal history models of Mercury.

Yseboodt M. Margot J. L.
Evolution of Mercury's Obliquity **[#2336]**
We investigate whether planetary perturbations cause variations in the obliquity of Mercury. Such variations would affect the determination of the planet's internal structure with the scheme proposed by *Peale* (1976).

Stanley S. Zuber M. T. Bloxham J. Hutchison W. E.
Using Future Observations to Determine Whether the Source of Mercury's Magnetic Field is an Active Dynamo **[#1953]**
We use numerical dynamo models that are consistent with Mercury's weak observed magnetic field to examine what future observations of Mercury's magnetic field by the MESSENGER and Bepi-Colombo missions could determine whether the source of the field is an active dynamo.

d'Uston C. Thocaven J. J. Hasebe N. Klingelhöfer G. Gellert R. Chernenko A. Leleux P. Gasnault O. Maurice S. Pirard B. Mandrou P. Baratoux D. Poitrasson F. Brückner J. Lawrence D. J. Dunkin S. Grande M. Kobayashi M. Fujii M. Miyachi T. Shibamura E. Sugihara T. Kato M. Okada T.
MANGA, a Gamma-Ray and Neutron Spectrometer for the Bepi Colombo Mission **[#1873]**
MANGA, is a high performance combination of neutron and gamma-ray spectrometers. Being among the pre-selected instruments on the Mercury Planetary Orbiter of the BepiColombo mission, it is intended to characterize Mercury's origin and history.

Helbert J. Jessberger E. Benkhoff J. Arnold G. Banaszkiewicz M. Bischoff A. Blecka M. Calcutt S. Coangeli L. Coradini A. Erard S. Fonti S. Killen R. Knollenberg J. Kührt E. Mann I. Mall U. Moroz L. Peter G. Rataj M. Robinson M. Spohn T. Sprague A. Stöffler D. Taylor F. Warrell J.
MERTIS — A Thermal Infrared Imaging Spectrometer for the Bepi-Colombo Mission **[#1753]**
MERTIS is part of the payload of the Bepi-Colombo mission, focused on studying the surface of Mercury, identify rock-forming minerals and map the mineralogy globally with a resolution of 500 m.

André S. L. Watters T. R. Robinson M. S.
A Topographic Analysis of Beethoven Basin, Mercury **[#1871]**
We present an analysis of the long wavelength topography of the Beethoven basin of Mercury.

Hargitai H.
Bilingual Map of Mercury **[#1583]**
As part of the Multilingual Map Series of the Terrestrial Planets and their Moons, the latest of the series, the Map of Mercury was published in 2004.

Donaldson Hanna K. L. Sprague A. L. Kozlowski R. W. H.
Mercury: First Spectra from 8 to 25 μm Using MIRSI **[#1460]**
Spectral measurements from 8 to 25 μm of Mercury's surface were taken using MIRSI (Mid-InfraRed Spectrometer and Imager) mounted on the NASA Infrared Telescope Facility (IRTF) on Mauna Kea, Hawaii.

Watters T. R. Nimmo F. Robinson M. S.
The Origin of Polygonal Troughs in the Caloris Basin of Mercury **[#1449]**
The imaged portion of the Caloris basin on Mercury is characterized by smooth plains deformed by complex extensional troughs that form giant polygons. We suggest that the polygonal troughs are caused by lateral crustal flow into the basin.

Burbine T. H. Trombka J. I. Bergstrom P. M. Jr. Christon S. P.
Calculating the X-Ray Fluorescence from the Planet Mercury Due to High-Energy Electrons **[#1416]**
Modeling has been done to determine if X-ray fluorescence resulting from the impact of high-energy electrons accelerated in Mercury's magnetosphere can be detected by Messenger.

Lunar Meteorites

Neal C. R Shearer C. K. Kramer G. Y.
Are the Apollo 14 High-Al Basalts Really Impact Melts? **[#1665]**
Ion microprobe analyses of olivines from Apollo 14 basalts and olivine vitrophyres show the high-Al basalts are not impact melts.

Day J. M. D. Taylor L. A. Patchen A. D. Schnare D. W. Pearson D. G.
Comparative Petrology and Geochemistry of the LaPaz Mare Basalt Meteorites **[#1419]**
We present a detailed study of the LaPaz mare basalt meteorites, demonstrating that they are paired and have similarities to Apollo 12 basalts.

Collins S. J. Righter K. Brandon A. D.
Mineralogy, Petrology and Oxygen Fugacity of the LaPaz Icefield Lunar Basaltic Meteorites and the Origin of Evolved Lunar Basalts **[#1141]**
The LaPaz basaltic meteorites represent an evolved basaltic liquid that is more fractionated than most meteorites and Apollo samples. We will discuss the mineralogy, petrology, temperature of equilibration, oxygen pressure, and ideas for their origin.

Joy K. H. Crawford I. A. Russell S. S. Kearsley A. T.
LAP 02205, LAP 02224 and LAP 02226 — Lunar Mare Basaltic Meteorites. Part 1: Petrography and Mineral Chemistry **[#1697]**
We present a petrological and mineralogical investigation into the LAP 02205, 02224 and 02226 lunar mare basalt meteorites to discuss their pairing relationship.

Joy K. H. Crawford I. A. Russell S. S. Kearsley A. T.
LAP 02205, LAP 02224 and LAP 02226 — Lunar Mare Basaltic Meteorites. Part 2: Geochemistry and Crystallisation **[#1701]**
We present bulk rock chemical data and mineral trace element data, and discuss crystallisation trends in the lunar mare basaltic meteorites LAP 02205, 02224 and 02226.

Taylor L. A. Day J. M. D.
FeNi Metal Grains in LaPaz Mare Basalt Meteorites and Apollo 12 Basalts **[#1417]**
FeNi metal grains in LaPaz and Apollo 12 basalts extend a similar, extreme range in Co and Ni abundances. Order of crysallization of these metals varies in thier respective basalts due to relative incompatibility of Co and Ni.

Schnare D. W. Taylor L. A. Day J. M. D. Patchen A. D.
Petrography and Mineral Charecterization of Lunar Mare Basalt Meteorite LAP 02-224 **[#1428]**
We present a detailed study of lunar mare basalt meteorite LAP02-224. As well as demonstrating a lunar origin for this meteorite, we highlight some unique mineralogic and petrologic characteristics.

Patchen A. D. Taylor L. A. Day J. M. D.
Mineralogy and Petrography of Lunar Mare Regolith Breccia Meteorite MET 01-210 **[#1411]**
We present results for lunar regolith breccia MET 01-210 which demonstrate it is composed of material with lunar mare affinities, and is not an anorthositic regolith breccia, as was previously thought.

Huber H. Warren P. H.
MET01210: Another Lunar Mare Meteorite (Regolith Breccia) with Extensive Pyroxene Exsolution, and Not Part of the YQ Launch Pair **[#2401]**
The MET01210 lunar meteorite is a mainly mare regolith breccia. Like several other mare lunaites, it has pyroxenes with remarkably extensive exsolution. Pairing with "YQ" appears unlikely on both mineralogical and bulk-compositional grounds.

Korotev R. L. Irving A. J.
Compositions of Three Lunar Meteorites: Meteorite Hills 01210, Northeast Africa 001, and Northwest Africa 3136 **[#1220]**
MET 01210 and NWA 3136 are breccias dominated by mare basalt; NEA 001 is a feldspathic breccia similar to other feldspathic lunar meteorites. There is no compositional evidence that any of the three is terrestrially or source-crater paired with another lunar meteorite.

Kuehner S. M. Irving A. J. Rumble D. III Hupé A. C. Hupé G. M.
Mineralogy and Petrology of Lunar Meteorite NWA 3136: A Glass-welded Mare Regolith Breccia of Mixed Heritage **[#1228]**
NWA 3136 is a well consolidated, polymict lunar regolith breccia consisting of mineral and lithic clasts derived predominantly from VLT and high-Ti mare basalts, but with a smaller proportion (~20%) of highlands lithologies.

Haloda J. Irving A. J. Tycova P.
Lunar Meteorite Northeast Africa 001: An Anorthositic Regolith Breccia with Mixed Highland/Mare Components **[#1487]**
Lunar meteorite Northeast Africa 001 is a clast-rich anorthositic regolith breccia with minor mare basalt component, representing independent fall. The possible source area for NEA 001 is a terrain of highlands rich in ferroan lithologies.

Ranen M. C. Jacobsen S. B.
Trace Element Analysis of Lunar Soils by ICP-MS **[#2029]**
Trace element data on a suite of 14 samples from the Apollo 14 and Apollo 16 missions are reported here. With the latest ICP-MS quadrupole instruments a comprehensive concentration profile can be measured on only 200 μg of sample.

Riner M. A. Robinson M. S. Tangeman J. A. Elphic R. C.
Is Ilmenite Always the Dominant Carrier of Titanium in Lunar Mare Basalts? **[#1943]**
This work examines spectral differences between plausible lunar analog opaque mineral powders and their respective quenched glasses to investigate discrepancies between independent methods of lunar surface titanium abundance estimation.

Fernandes V. A. Morris A. Burgess R.
New Ar-Ar Age Determinations for the Lunar Mare Basalts Asuka 881757 and Yamato 793169 **[#1002]**
New Ar-Ar ages were determined for lunar mare meteorites A881757 (3.69 ± 0.07 Ga), and Y793169 (3.71 ± 0.11 Ga) and disturbed at 430 Ma. Possible source regions: SW rim of Mare Humorum or Mare Australe; or Lake Endymion. CRE-ages are Y = 1.1 Ma and A = 0.9 Ma.

Lunar Missions: Past, Present, Future

Foing B. H. Racca G. D. Grande M. Huovelin J. Josset J. L. Keller H. U. Nathues A. Malkki A. Heather D. Koschny D. Almeida M. Frew D. Lumb R. Volp J. Zender J.
ESA's SMART-1 Mission at the Moon: First Results, Status and Next Steps **[#2404]**
ESA's SMART-1 is at the Moon! Launched by Ariane-5 in Sept. 2003, it used primary solar electric propulsion to reach lunar capture on 17 November 2004, and to spiral down to lunar science orbit. First data and results from the cruise approach and lunar commissioning will be presented.

Mitrofanov I. G. Sanin A. B. Kozyrev A. S. Litvak M. L. Mokrousov M. I. Tretyakov V. I.
Lunar Exploration Neutron Detector for NASA Lunar Reconnaissance Orbiter **[#1879]**
The Lunar Exploration Neutron Detector instrument will operate onboard the NASA Lunar Reconnaissance Orbiter. The LEND is designed to find hydrogen and water resources on the Moon and to measure the radiation environment for future human missions.

Robinson M. S. Eliason E. M. Hiesinger H. Jolliff B. L. McEwen A. S. Malin M. C. Ravine M. A. Roberts D. Thomas P. C. Turtle E. P.
LROC — Lunar Reconnaissance Orbiter Camera **[#1576]**
The Lunar Reconnaissance Orbiter Camera (LROC) consists of two narrow-angle components to provide 0.5-m/p scale BW images over a 5-km swath, and a wide-angle component to provide images at a scale of 100 m/p in seven bands over a 100-km swath to address two of the prime LRO measurement requirements.

Clark P. E. Curtis S. A. Rilee M. L. Floyd S. R.
ALI (Autonomous Lunar Investigator): Revolutionary Approach to Exploring the Moon with Addressable Reconfigurable Technology **[#1217]**
Addressable Reconfigurable Technology (ART), conceived for future ANTS (Autonomous Nanotechnology Swarm) Architectures, is now implemented as Autonomous Lunar Investigator (ALI) rovers, a mission concept allowing autonomous exploration of the lunar farside and poles within 10 years.

Spudis P. D. Bussey D. B. J. Lichtenberg C. Marinelli B. Nozette S.
Mini-SAR: An Imaging Radar for the Chandrayaan-1 Mission to the Moon **[#1153]**
We will fly a small imaging radar on the Indian Chandrayaan mission to the Moon, to be launched in September, 2007. Mini-SAR will map the scattering properties of the lunar poles, determining the presence and extent of polar ice.

Okada T. Shirai K. Yamamoto Y. Arai T. Ogawa K. Hosono K. Kato M.
Lunar X-Ray Fluorescence Spectrometry from SELENE Lunar Polar Orbiter **[#1174]**
We have been developing an X-ray fluorescence spectrometer, XRS, for SELENE mission to map major elemental composition of lunar surface. The scientific objectives as well as current status of the instrumental development is also described.

Arai T. Yamamoto Y. Okada T. Shirai K. Ogawa K. Hosono K. Kato M.
Onboard Software Analysis of SELENE XRS **[#1631]**
An X-ray fluorescence spectrometer (XRS) onboard SELELE spacecraft will quantitatively determine major elemental compositions of the lunar surface. In this study, we introduce observation data analysis by using software process of onboard computer.

Hasebe N. Yamashita N. Kobayashi M.-N. Miyachi T. Miyajima M. Okudaira O. Kobayashi S. Hosojima T. Pushkin K. N. Tezuka C. Doke T. Shibamura E.
Planetary Gamma-Ray Imager Using High Pressure Xenon Time Projection Chamber **[#1861]**
Gamma-ray imaging camera is considered for planetary science. The high pressure Xe time projection chamber (HPXe-TPC) is introduced, which is estimated to have a spatial resolution of 5 to 40 km at the altitude of 100 km.

Kobayashi M.-N. Berezhnoy A. A. d'Uston C. Fujii M. Hasebe N. Hiroishi T. Kaneko H. Miyachi T. Mori K. Maurice S. Nakazawa M. Narasaki K. Okudaira O. Shibamura E. Takashima T. Yamashita N.
Global Mapping of Elemental Abundance on Lunar Surface by SELENE Gamma-Ray Spectrometer **[#2092]**
Elemental composition on the surface of a planet is very important information. Gamma-ray spectrometer (GRS) will be on board SELENE and will provide global mapping of lunar surface material composition.

Ohtake M. Arai T. Takeda H.
Study of the Apollo16 Landing Site: Re-Visit as a Standard Site for the SELENE Multiband Imager **[#1637]**
Purpose of this study is to re-evaluate optical properties of Apollo 16 landing site by studying correlation between their mineralogy and reflectance spectra and select a best standard area for the Multiband Imager for the SELENE mission.

Yamada R. Yamada I. Kobayashi N. Takeuchi N. Shiraishi H. Tanaka S. Fujimura A.
Mizutani H. LUNAR-A Penetrator Science Team
Characteristics of a Seismometer for the LUNAR-A Penetrator **[#1715]**
We examined the dynamic response of the LUNAR-A seismometer at Inuyama Seismic Observatory after the impact tests, which simulate the impacts condition of the penetrator on the lunar surface. We confirmed that its dynamic response was similar to that of STS-2 in the range 0.2 Hz to 6.0 Hz.

Head J. N. Hoppa G. V. Gardner T. G. Seybold K. S. Svitek T.
Autonomous Low Cost Precision Lander for Lunar Exploration **[#1471]**
A planetary vehicle derived from mature DOD technologies with 10-meter landing precision has been designed. Such precision enables exploration of high-value, hard-to-reach targets. Applications include the Moon, Europa, Mars, and small bodies.

Keller J. W. Zurbuchen T. H. Baragiola R. A. Cassidy T. A. Chornay D. J. Collier M. R. Hartle R. E. Johnson R. E.
Killen R. M. Koehn P. Ogilvie K. W. Scherer S. Stubbs T.
Pickup Ion Mass Spectrometry for Surface Bounded Exospheres and Composition Mapping of Lunar and Planetary Surfaces **[#1801]**
We discuss the study of surface bounded exospheres such as those found on the Moon and Mercury through pickup ion mass spectrometry and mapping the surface compositions of these objects.

Becker T. Weller L. Gaddis L. R. Soltesz D. Cook D. Archinal B. A Bennett A. McDaniel T.
Redding B. Richie J.
Lunar Orbiter Revived: Update on Final Stages of Scanning, Archiving, and Cartographic Processing at USGS **[#1836]**
U. S. Geological Survey Astrogeology Program reports on the status of their effort to scan and process Lunar Orbiter film-strip data. The ultimate product will be a global, cartographically accurate digital mosaic of the Moon.

Martian Meteorites: Magmatic Processes

Irving A. J. Bunch T. E. Wittke J. H. Kuehner S. M.
Olivine-Orthopyroxene-Phyric Shergottites NWA 2626 and DaG 476: The Tharsis Connection **[#1229]**
Yet another primitive shergottite was found in Northwest Africa in 2004, and orthopyroxene phenocrysts have been recognized in olivine-phyric shergottite DaG 476. Could most shergottites be samples from Tharsis volcanoes?

Shearer C. K. Borg L. E. Papike J. J. Chaklader J. Symes S. J. Irving A. J. Herd C. D. K.
Do Early Liquidus Phases in Olivine-Phyric Martian Basalts Reflect the Characteristics of Their Mantle Sources? Insights from NWA 1110, NWA 1195, and NWA 2046 **[#1193]**
Olivine in martian meteorites NWA 1110, NWA 1195, NWA 2046 reflect both the f_{O_2} conditions and incompatible element nature of the sources for olivine-phyric martian basalts.

Filiberto J. Nekvasil H. Lindsley D. H.
An Experimental Crystallization Study of a Proposed High-Fe, Low-Al Martian Parental Liquid at Elevated Pressure **[#1359]**
We have conducted experiments at 4.3 kbar (~35 km depth on Mars) and at 9.3 kbar (~70 km depth on Mars) in order to assess phase relations of high-Fe, low-Al magmas at elevated pressures.

Koizumi E. Mikouchi T. Chokai J. Miyamoto M.
Crystallization Experiment of Los Angeles Basaltic Shergottite: Implication for the Crystallization of Los Angeles and Dhofar 378 **[#2015]**
We performed a crystallization experiment using the LA bulk composition to investigate the crystallization history, and compared LA mineralogy with that of Dhofar 378 and applied the experimental result to compare LA with Dhofar 378.

Calvin C. Rutherford M.
ALH77005: The Magmatic History from Rehomogenized Melt Inclusions **[#1895]**
The liquid line of descent for ALH77005 has been outlined from rehomogenized melt inclusions. Chromite composition, sulfur saturation, and chlorine content are also discussed with respect to ALH77005's petrogenetic history.

McCubbin F. M. Whitaker M. L. Lindsley D. H. Nekvasil H.
Kaersutite (Ti-rich Amphibole) in the SNC Meteorites: Can It Crystallize at Low Pressure? **[#1967]**
An experimental study was conducted to investigate the possibility of low-pressure stability (0–2 kbar and 700°–900°C) of fluor-kaersutite in SNC meteorites.

Anand M. Russell S. S. Mullane E. Grady M. M.
Fe Isotopic Composition of Martian Meteorites **[#1859]**
In the present work, we have measured iron isotope compositions of a group of Martian meteorites to establish a baseline Fe-isotope fractionation pattern in the case of high-temperature igneous rocks from Mars.

Weidner E. Frey F. Pedersen B. Burghammer M. Schmidbauer E.
Cation Distribution in Pyroxene from Martian Meteorite **[#1409]**
Clinopyroxenes from the martian meteorite NWA856 were studied by means of single crystal diffractometry and Mössbauer spectroscopy. A structure refinement with Bragg data from martian pyroxene single crystals was performed and the cation distribution determined.

Nakhlites and Chassignites: New Arrivals and Familiar Friends

McBride K. M. Righter K. Satterwhite C. E. Schwarz C. Robinson P.
Curation and Allocation of the New Antarctic Nakhlite, MIL03346 **[#1499]**
We will provide a full summary of the curation and allocation of the new Antarctic nakhlite, MIL03346, which was discovered in 2003 in the Miller Range of the Transantarctic Mountains.

Kinman W. S. Neal C. R.
Petrology of Nakhlite MIL 03346 **[#1660]**
We will present mineralogical and whole-rock elemental data for new nakhlite MIL-03346.

Anand M. Williams C. T. Russell S. S. Jones G. James S. Grady M. M.
Petrology and Geochemistry of Nakhlite MIL 03346: A New Martian Meteorite from Antarctica **[#1639]**
MIL 03346 is the first nakhlite in the US Antarctic collection. We have performed detailed mineralogical and bulk-geochemical investigations to compare petrogenesis of this Martian meteorite with other nakhlites.

Dyar M. D. Pieters C. M. Hiroi T. Lane M. D. Marchand G. J.
Integrated Spectroscopic Studies of MIL03346 **[#1261]**
Mossbauer, thermal emittance, mid-IR, near-IR, and visible region spectra are reported for whole rock and cpx separate of MIL03346. Results confirm the absence of olivine, and suggest that MIL03346 is the most oxidized of all SNCs studied by us to date.

Beck P. Barrat J.-A. Gillet P. Franchi I. A. Greenwood R. C. Van de Moortele B. Reynard B. Bohn M. Cotten J.
The Diderot Meteorite: The Second Chassignite **[#1326]**
The Diderot meteorite is a dunite discovered in Sahara. The martian origin is unambiguous and Diderot shares strong petrographical similarities with Chassigny.

Terada K. Sano Y.
U-Pb Systematics of Phosphates in Nakhlites **[#1178]**
U-Pb systematics of phosphate grains from Martian meteorites, Lafayette and Yamato-000593/000749, were measured using an ion microprobe.

Garrison D. H. Bogard D. D.
Ar-Ar Ages of Nakhlites Y000593, NWA998, and Nakhla and CRE Ages of NWA998 **[#1137]**
New Ar-Ar ages of nakhlites NWA-998, Y-000593, and Nakhla indicate a common formation time, a likely common Mars ejection time, and variable amounts of trapped Martian radiogenic ^{40}Ar.

Musselwhite D. S. Treiman A. H. Shearer C.
Light Lithophile Element Trends in Nakhlite NWA 817 Pyroxenes: Implications for Water on Mars **[#1230]**
Abundances of LLE are strongly zoned in augites of the NWA 817 nakhlite. Be and B increase to grain rims, consistent with their geochemical behavior as incompatible elements. Oddly, Li increases outward in some rims, but decreases in others.

Chevrier V. Lorand J. P.
Sulfide Mineralogy, Redox Conditions and Alteration Effects in Some SNC Meteorites **[#2067]**
Sulfides mineralogy and compositions have been studied in some SNC meteorites. Results show the presence of preterrestrial hydrothermal alteration, while compositions of unaltered sulfides are in accordance with published redox conditions of SNC's.

Martian Meteorites: ALH 84001

Niles P. B. Leshin L. A. Golden D. C. Socki R. A. Guan Y. Ming D. W.
Modeling Chemical and Isotopic Variations in Lab Formed Hydrothermal Carbonates **[#2046]**
Most martian secondary minerals have likely not experienced significant diagenesis. Thus lab-formed carbonates provide an empirical view of kinetic processes important during carbonate precipitation and of the scales at which those processes operate.

Treiman A. H.
Olivine and Carbonate Globules in ALH84001: A Terrestrial Analog, and Implications for Water on Mars **[#1107]**
Low-temperature carbonate globules in ALH84001 are found near olivine grains that equilibrated at T > 800° C. Terrestrial analogs from Spitsbergen (Norway) suggest an explanation of this association; the carbonate globules may have been deposited in cavities where olivine had been dissolved out.

Bell M. S. Golden D. C. Zolensky M. E.
Experimental Shock Decomposition of Siderite to Magnetite **[#1851]**
Magnetite was created in closed system siderite shock experiments at 49 GPa. Shock metamorphism is a likely mechanism for magnetite formation in Martian meteorite ALH84001.

Min K. Reiners P. W.
Low-Temperature Thermal History of Martian Meteorite ALH84001 from (U-Th)/He Thermochronometry **[#2214]**
Single grain (U-Th)/He ages from ALH84001 are interpreted either by (1) a single intense (maximum temperature of ~430° C) shock event at 15 Ma, or (2) stronger shock at sometime between (0.3 01500.7) Ga and 15 Ma, followed by a minor shock at 15 Ma.

Martian Meteorites: Shocking

Schwenzer S. P. Herrmann S. Ott U.
Noble Gases in Mineral Separates from Shergotty and Zagami **[#1310]**
He, Ne, Ar, Kr, and Xe data on mineral separates provide information on gases of different origin, Martian and terrestrial. Further processes of signature formation, e.g. He loss due to shock effects, are discussed.

Beck P. Gillet P. El Goresy A. Mostefaoui S.
Timescales of Shock Processes and the Size of Martian Meteorites Source Craters, Constrained from Shock Metamorphism **[#1333]**
Mineralogical transformations and chemical exchanges occuring during the shock metamorphism are used to constrain the shock duration.

Frey F. Weidner E. Burghammer M. Paulmann C.
Martian and Lunar Pyroxene Microstructures Studied by Single-Crystal X-Ray Diffraction **[#1403]**
Microstructures of extraterrestrial pyroxenes bear information about prior thermal history, shock history, if any, and radiation damage.

Rochette P. Gattacceca J. Chevrier V. Hoffmann V. Lorand J. P. Funaki M. Hochleitner R.
A Synthesis on the Magnetic Properties of Martian Meteorites **[#1614]**
Detailed magnetic data is presently available on all Martian meteorites known today, except Yamato 793605, 980459 and 1075, GRV99027, NWA 1950 and 3171, i.e., 26 over 32 unpaired SNCs. We also include original paleomagnetic data on MIL03346.

Achondrites

Spivak-Birndorf L. Wadhwa M. Janney P. E. Foley C. N.
Al-Mg Isotopic Systematics in the Angrite Sahara 99555 and the Primitive Achondrite Brachina **[#2201]**
We report high precision Mg isotopic systematics in Sahara 99555 and Brachina. ^{26}Al-^{26}Mg systematics in Sahara 99555 give a ^{27}Al/^{26}Al ratio of $(5.8 \pm 1.9) \times 10^{-7}$ at the time of its formation, and are concordant with previously determined ^{53}Mn-^{53}Cr systematics.

Yanai K. Noda M.
Petrological Comparison of Mongolian Jalanash Ureilite and Twelve Antarctic Ureilites **[#1028]**
Only one Mongolian Jalanash ureilite has been compared petrologically with twelve Antarctic ureilites for their texture, mineral compositions and bulk chemical compositions.

Cohen B. A. Swindle T. D. Olson E. K.
Geochronology of Clasts in Polymict Ureilite Dar Al Gani 665 **[#1704]**
We dated three clasts representing different feldspathic lithologies from the ureilite parent body (UPB). One clast, a basaltic product of UPB partial melting, is ~4.5 Ga. Two other clasts are ~3.1 Ga and may date impact processes on the UPB.

Bjonnes E. E. Delaney J. S.
Comparison of the Lithologies on the Surface of the Asteroid 4 Vesta Based on the Petrology of 91 & 92 Series Antarctic Achondrites **[#1344]**
Detailed chemical analysis of the 91–92 series Antarctic achondrites provides further insight into the petrographic differences that exist on the surface of the asteroid 4 Vesta. Compositional variations between several meteorite samples are described and discussed.

Domanik K. J. Sideras L. C. Drake M. J.
Olivine and Ca-Phosphate in the Diogenites Manegaon and Roda **[#2128]**
This abstract describes igneous contacts in Manegaon and Roda that involve olivine and orthopyroxene (plus other phases), as well as contacts involving orthopyroxene and Ca-phosphate minerals (both F-apatite and REE-bearing whitlockite).

Irving A. J. Kuehner S. M. Carlson R. W. Rumble D. III Hupé A. C. Hupé G. M.
Petrology and Multi-Isotopic Composition of Olivine Diogenite NWA 1877: A Mantle Peridotite in the Proposed HEDO Group of Meteorites **[#2188]**
The HEDO group is proposed to include the five known olivine diogenites. Plagioclase-free, Cr-rich harzburgite NWA 1877 may be a sample of the infertile mantle of 4Vesta or a larger predecessor planetary body.

Lowe J. J. Hill D. H. Domanik K. J. Lauretta D. S. Drake M. J. Killgore M.
NWA 2736: An Unusual New Graphite-bearing Aubrite **[#1913]**
Mineral compositions are reported for NWA 2736, an unusual new graphite-bearing aubrite. It is related to known aubrites and EL enstatite chondrites.

Mullane E. Russell S. S. Gounelle M.
Aubrites: An Iron and Zinc Isotope Study **[#1251]**
Both iron and zinc isotopes are fractionated in aubrites and we explore the reasons for fractionation.

Iron and Stony-Iron Meteorites

Grokhovsky V. I. Ustyugov V. F. Badyukov D. D. Nazarov M. A.
Dronino: An Ancient Iron Meteorite Shower in Russia **[#1692]**
Dronino is a huge iron meteorite shower recovered in Russia. In trace elements Dronino is anomalous. Sections show duplex structure (kamacite and martensite). This structure could be formed by reheating of intital octahedral texture.

Grokhovsky V. I. Oshtrakh M. I. Milder O. B. Semionkin V. A. Kadushnikov R. M. Glazkova S. A.
Structural Studies of Iron Meteorite Dronino **[#1980]**
Study of metal and sulphide nodules of meteorite Dronino was made using microhardness, digital microscopy with image analysis platform SIMAGIS, electron probe microanalysis using scanning electron microscope Philips 30XL with EDS, Mössbauer spectroscopy and X-ray powder diffraction.

Watson H. C. Watson E. B. McDonough W. F. Ash R. D.
Siderophile Element Profile Measurements in Iron Meteorites Using Laser Ablation ICP-MS **[#2141]**
Laser ablation ICP-MS was used to measure concentration profiles of siderophile elements Cu, Ga, Ge, Mo, Ru, Rh, Pd, Re, Os, Ir, Pt, and Au in iron meteorites. Preliminary values for equilibrium partition coefficients are also reported.

Yang J. Goldstein J. I. Scott E. R. D.
Metallographic Cooling Rate of IVA Irons Revisited **[#1347]**
We revisited cooling rate of IVA irons based on updated parameters and an explanation of varying cooling rate in low Ni end of the IVA has been given.

Ruzicka A. Hutson M.
Filter-Press Differentiation: A Newly-Recognized Fractionation Mechanism for Silicate Inclusions in Sombrerete and Possibly in Other Iron Meteorites **[#1169]**
A novel crystal/liquid fractionation mechanism, which we term "filter-press differentiation", best accounts for chemical heterogeneity of silicate inclusions in the Sombrerete iron meteorite. A similar process may have affected other silicated irons.

Bogard D. D. Garrison D. H. Takeda H.
Ar-Ar and I-Xe Ages of Caddo County and Thermal History of IAB Iron Meteorites **[#1132]**
New Ar-Ar and I-Xe ages of silicate from the Caddo County IAB iron, along with literature data on IABs, appear inconsistent and may suggest a complex parent body history.

Kalinina G. V. Kashkarov L. L. Ivliev A. I. Skripnik A. Ya.
Radiation and Shock-Thermal Parameters of Pallasites: Resulting from Different Compaction History? **[#1708]**
Olivine crystals from the Brenham, Eagle Station, Marjalahti and Omolon were examined by the track and thermoluminescence (TL) methods.

Tomiyama T. Huss G. R.
Minor Element Behavior of Pallasite Olivine: Understanding Pallasite Thermal History and Chronology **[#2071]**
We investigated chemical zoning and Mn-Cr isotopic sytematics of olivine in some pallasites and disscussed the possible influence of chemical diffusion on Mn-Cr dating.

Petaev M. I. Jacobsen S. B.
LA-ICP-MS Study of Trace Elements in the Chaunskij Metal **[#1740]**
We report new LA-ICP-MS data for 19 elements in the metal grains from the Chaunskij silicate inclusions. The metal of silicate inclusions is different from the host metal of Chaunskij as well as from metal nodules of common mesosiderites.

Emami M. H. Monsef R.
Petrological and Geochemical Consideration on the Tuserkanite Meteorite **[#1241]**
On June 27, 1985, a light gray meteorite with dark vein system in 5.7 kg weight fell from the sky that its landing in Esmaeel Abad. According to our studies, this sample could be derived from high fractionate rhyolite composition which is similar to lunar residual rhyolitic rocks.

Refractory Inclusions

Cosarinsky M. McKeegan K. D. Hutcheon I. D. Weber P. Fallon S.
Magnesium and Oxygen Isotopic Study of the Wark-Lovering Rim Around a Fluffy Type-A Inclusion from Allende **[#2105]**
We present a combined Mg and O isotopic study of Wark-Lovering rim phases in an Allende CAI using both high-precision and high spatial resolution ion microprobe techniques.

Friedrich J. M. Ebel D. S. Weisberg M. K. Birdsell J.
The Crucible: An Unusual Matrix-enclosing Igneous CAI in NWA 2364 (CV3) **[#1756]**
We describe the structure, mineralogy and petrology of a large, deformed Ca-, Al-rich inclusion in NWA 2364 (CV3). This remarkable 18-mm CAI appears cup-shaped (hence "the crucible"), and envelops a portion of the host chondrite.

Varela M. E. Kurat G. Zinner E.
Can Glasses Help Us to Unravel the Origin of Barred Olivine Chondrules? **[#1436]**
Barred olivine (BO) chondrules are one of the most striking objects in chondrites. Here we report on detailed studies of two BO chondrules and elaborate the prominent role liquids played in their origin.

Wark D. A. Shelley J. M. G. O'Neill H.
The First Step in CAI Rim Formation: Flash Heating or Subsolidus Evaporation? **[#1643]**
We show that the first step in CAI rim formation was not intense flash heating but rather slower subsolidus heating since the subrim zone was not melted, an unlikely outcome if flash heating occurred.

Impact Modeling

Baldwin E. C. Vocadlo L. Crawford I. A.
Validation of AUTODYN in Replicating Large-Scale Planetary Impact Events **[#1380]**
AUTODYN is shown to be proficient in replicating planetary impact events. Future work is proposed to combine numerical modelling with remotely sensed data from SMART-1.

Wünnemann K. Collins G. S. Melosh H. J.
A Novel Porosity Model for Use in Hydrocode Simulations **[#1508]**
As an alternative to existing porosity models, like the P-α model, we present a novel approach for dealing with compaction of porosity in hydrocode calculations. In addition to the model description we provide a comparison with experimental data.

Bray V. J. Collins G. S. Morgan J. V.
Determination of the Acoustic Fluidization Parameters as Applied to Impacts on the Icy Satellites **[#1889]**
We report on numerical modeling that aims to better constrain the impact process on the icy satellites and the effect of rheologic target variations on crater depth and morphology.

Ong L. Gisler G. Weaver R. Gittings M.
Numerical Simulations of Impactor Penetration into Ice-Over-Water Targets **[#2400]**
Two-dimensional vertical impacts of ice projectiles into ice-over-water targets were modeled using the continuous adaptive mesh Eulerian code RAGE. Simulations were of both laboratory- and Europa-scale impacts, and are compared to experimental results of impacts into ice-on-water targets.

Wada K. Senshu H. Matsui T.
Numerical Simulation of Impact Cratering on Adhesive Granular Material **[#1596]**
We conduct numerical simulation of impact cratering on granular target with various adhesion. Our result shows that the adhesion becomes important when the size of target particles is smaller than about 0.1 mm on Earth, and 1 mm on Eros.

Ivanov B. A. Stöffler D.
The Steinheim Impact Crater, Germany: Modeling of a Complex Crater with Central Uplift **[#1443]**
Numerical modeling of the Steinheim impact crater formation is presented. The model reproduce the complex crater morphology.

Ishimaru R. Senshu H. Sugita S. Matsui T.
Numerical Simulation of Chemical Reactions Within a Vapor Plume Induced by Cometary Impact **[#1601]**
We develop a new numerical code to simulate a gas-phase reaction network within an impact vapor plume formed by a cometary impact and conduct numerical simulations for various impact conditions (e. g., a radius of comet and an impact velocity).

Pierazzo E. Artemieva N. A.
Atmospheric Fragmentation of the Canyon Diablo Meteoroid **[#2325]**
We present initial estimates of the motion in the atmosphere of an iron projectile similar to Canyon Diablo, to constrain the initial conditions of the impact event that generated Meteor Crater.

Impact Experiments

Eberhardy C. A. Schultz P. H.
Source and Evolution of Vapor Due to Impacts into Layered Carbonates and Silicates **[#1484]**
Enhanced impact vaporization is observed for experimental impacts into targets with a thin layer of dolomite overlying sand relative to dolomite only targets. Two possible processes to increase vapor production are discussed.

Anderson J. L. B. Schultz P. H.
The Effect of Projectile Density and Disruption on the Crater Excavation Flow-Field **[#1773]**
Ejection parameters are used to examine the effect of projectile properties on excavation flow-fields during experimental impacts. Implications include using ejection angles as a measure of projectile to target density ratios and penetration depth.

Ernst C. M. Schultz P. H.
Investigations of the Luminous Energy and Luminous Efficiency of Experimental Impacts into Particulate Targets **[#1475]**
Light emitted by experimental impacts into nonvolatile particulate targets is of much longer duration than for comparable impacts into solid targets due to a strong thermal signal. Up to 60% of the luminous energy is emitted after the intensity peak.

Takagi Y. Hasegawa S. Teramoto K. Yano H. Yamamoto S. Sugita S. Abe M.
Impact Cratering Experiments in Microgravity Environment **[#1627]**
We performed impact cratering experiments in microgravity and vacuum environment and obtained data on diameter of crater. The result shows that the diameter of crater formed in the glass-sphere layer does not have the gravity dependence.

Martian Impacts

Louzada K. L. Stewart S. T. Weiss B. P.
Shock Demagnetization of Pyrrhotite **[#1134]**
We present new data from shock recovery experiments on pyrrhotite at pressures between 1 and 4 GPa. The results indicate that pyrrhotite demagnetizes due to shock in the pressure range inferred from large impact basins on Mars.

Ivanov B. A.
Shock Melting of Permafrost on Mars: Water Ice Multiphase Equation of State for Numerical Modeling and Its Testing **[#1232]**
We present here the new ANEOS-based multiphase equation of state for water/ice constructed for usage in hydrocodes and first numerical experiments on Martian permafrost shock melting.

Newsom H. E. Nelson M. J. Shearer C. K. Misra S. Narasimham V.
Hydrothermal Alteration at Lonar Crater, India and Elemental Variations in Impact Crater Clays **[#1143]**
The importance of craters as small as the Lonar crater (1.8 km diam.) to the surface of Mars and other bodies is indicated by new evidence for aqueous or hydrothermal alteration in the ejecta blanket and beneath the crater floor.

Meresse S.   Costard F.   Mangold N.
Evidence for Removal Episode on Northern Plains from the Martian Fluidized Ejecta Volume **[#1748]**
The measurement of the lobate ejecta volume provide new data about the morphometry and the characteristics of Martian craters. It also constitutes a good method for the observation and the quantification of the surface modifications.

Ghent R. R.   Carter L. M.   Leverington D. W.   Campbell B. A.
A Comparison of Impact-related Deposits Surrounding Craters on the Moon, Venus, and Mars **[#2070]**
This work explores the distribution and properties of surficial impact-related deposits on the Moon, Mars, and Venus, using previous results for lunar craters as a framework for exploration of potentially similar deposits on Venus and Mars.

Plesko C. S.   Brumby S. P.   Asphaug E.
A Comparison of Automated and Manual Surveys of Small Craters in Elysium Planitia **[#1971]**
In this study we compare automated crater counts against expert manual counts in MOC images of Elysium Planitia. We find that the accuracy of our automated crater counts are comparable to expert manual counts, and are useful in culling large datasets for images that merit expert examination.

Preblich B.   McEwen A. S.   Studer D.
Mapping Rays and Secondary Craters from Zunil, Mars **[#2112]**
Daytime and nighttime THEMIS IR mosaics were created of a 1600-km radius area around a 10.1-km diameter crater named Zunil located in the Cerberus Plains of Mars to map its asymmetric rays and associated secondary craters.

Block K. M.   Barlow N. G.
Secondary Cratering Rates on the Basaltic Plains of Mars and the Moon **[#1816]**
The pupose of this study is to determine if there exists a statistical difference between secondary cratering rates on the lunar maria and Martian volcanic plains. A difference in these rates will impact the age estimates of Martian terrain units.

Hillman E.   Barlow N. G.
Martian Central Pit Craters **[#1418]**
MOC and THEMIS image analysis is revealing large numbers of craters with central pits. Craters are between 20 and 80 km diameter and display a range of preservation states.

Öhman T.   Aittola M.   Kostama V.-P.   Hyvärinen M.   Raitala J.
Preliminary Study of Polygonal Impact Craters in Argyre Region, Mars **[#1731]**
Polygonal impact crater rim strikes around Argyre basin, Mars, reveal regional fracture patterns, genetically linked to Valles Marineris, as well as radial fracturing emanating from Argyre. Fracturing caused by the Tharsis bulge may also be present.

Arkani-Hamed J.
Giant Impact Basins Trace the Ancient Equator of Mars **[#2177]**
The rotation axis of Mars is determined from the location of 5 giant impact basins. It is shown that the basins are located on a great circle, suggesting that the circle was the equator of Mars at the time of impacts, about 4 Gyr. ago.

OMEGA@Mars: New Insights Into Surface Composition

Bonello G.   Berthet P.   d'Hendecourt L.
Identification of Magnesium Sulfate Hydration State Derived from NIR Reflectance Spectroscopy **[#1996]**
The present work is a first step in making a comprehensive analysis of NIR reflectance spectral features related to hydration state (water content) of magnesium sulfates which is essential for remote sensing analysis of such materials at the surface of Mars.

Cloutis E. A.
Diagnostic Absorption Features in Sulfate Reflectance Spectra Across OMEGA Wavelength Range **[#1323]**
Sulfates exhibit a number of diagnostic spectral properties across the 0.3 to 5.2 µm wavelength range. These features allow sulfate minerals to be detected and individual species uniquely identified even in the presence of accessory phases.

Milliken R. E.   Mustard J. F.   Poulet F.   Bibring J.-P.   Langevin Y.   Gondet B.   Pelkey S.   Mars Express OMEGA Team
Mapping the Water Content of the Martian Surface Using Mars Express OMEGA Data **[#1370]**
A laboratory-based model is applied to the 3 µm water band present in MEX-OMEGA data to estimate absolute water content of the surface.

Bishop J. L.   Schiffman P.   Lane M. D.   Dyar M. D.
Solfataric Alteration in Hawaii as a Mechanism for Formation of the Sulfates Observed on Mars by OMEGA and the MER Instruments **[#1456]**
Solfataric alteration in the Kilauea caldera, HI, forms sulfates and hydrated phases from volcanic ash. Spectral analyses are presented for detection of these minerals/phases on Mars by OMEGA and for groundtruthing the OMEGA spectra with MER data.

Langevin Y. Poulet F. Bibring J.-P. Schmitt B. Douté S. Gondet B.
Observations of the North Permanent Cap of Mars in Mid-Summer by OMEGA/MEX at km per Pixel Resolutions **[#1650]**
The OMEGA VIS/IR imaging spectrometer on board Mars Express performed observations of permanent surface ice at high northern latitudes at resolutions of 1 km/pixel or less in December 2004.

Gendrin A. Bibring J.-P. Mustard J. F. Mangold N. Quantin C. Gondet B. Langevin Y. Poulet F. Sotin C. Le Mouélic S. Combe J.-P. Hutchison L. OMEGA Team
Identification of Predominant Ferric Signatures in Association to the Martian Sulfate Deposits **[#1378]**
We identify predominant ferric signatures in association to the sulfate deposits mapped by OMEGA. These signatures could suggest that geological processes similar to what happened in Terra Meridiani could have taken place in Valles Marineris as well.

Ansan V. Mangold N. Lucas A. Gendrin A. Le Mouélic S. Poulet F. Bibring J.-P. OMEGA Co-Investigator Team
Analysis of Layered Deposits in Terby Crater (Hellas Region, Mars) Using Multiple Datasets MOC, THEMIS and OMEGA/MEX Data **[#1324]**
Terby crater displays thick layered deposits with interesting characteristics such as unconformities visible on MOC images and hydrated minerals detected on OMEGA/MEX spectral data.

Quantin C. Gendrin A. Mangold N. Bibring J.-P. Poulet F. Allemand P. OMEGA Team
Sulfate Deposits Identified by OMEGA in Melas Chasma **[#1789]**
The study of the distribution of sulfate signatures detected by OMEGA in Melas Chasma reveals that the signatures are correlated to layered deposits over widespread area in space and in elevation.

Hutchison L. Mustard J. F. Gendrin A. Bibring J.-P. Langevin Y. Gondet B. Mangold N. OMEGA Science Team
Mafic Polyhydrated Sulfates and Kieserite in Capri Chasma **[#1404]**
OMEGA spectra of interior layered deposits in Capri-Eos Chasma show signatures consistent with kieserite and polyhydrated sulfates. OMEGA parameter maps identifying sulfates in Capri Chasma will be shown together with spectra from Rio Tinto, Spain.

Mustard J. F. Poulet F. Gendrin A. Mangold N. Bibring J.-P. Langevin Y. Gondet B. Belluci G. Altiere F. OMEGA Science Team
Compositional Diversity of the Martian Crust from OMEGA Observations **[#1316]**
OMEGA data of exposed crust identify low-Ca pyroxene rich regions in Noachian-aged terrain, high-Ca pyroxene-rich regions in more recent volcanics and dune deposits, and olivine in ancient rocks through to recent volcanic and crater floor deposits.

Kanner L. C. Mustard J. F. Bibring J.-P. Gendrin A. Langevin Y. Gondet B. Pelkey S. OMEGA Science Team
Analysis of Martian Pyroxene Compositions in Syrtis Major: Full MGM Application to OMEGA **[#1730]**
Spectra from the OMEGA spectrometer of the Syrtis Major region of Mars are analyzed for pyroxene compositions. MGM results indicate the presence of two pyroxenes and a compositional variation between the Noachian terrain and Hesperian volcanics.

Pelkey S. M. Mustard J. F. Bibring J.-P. Milliken R. E. Langevin Y. Gondet B. Gendrin A. Poulet F. Erard S. Murchie S. Arvidson R. E. OMEGA Science Team CRISM Team
Global Spectral and Compositional Diversity of Mars: A Test of CRISM Global Mapping with Mars Express OMEGA Data **[#1458]**
The OMEGA data set provides us with an ideal opportunity to evaluate and refine the multispectral mapping strategy set forth for CRISM operations.

Poulet F. Mangold N. Mustard J. Bibring J.-P. Gendrin A. Langevin Y. Gondet B. Masson Ph. Head J. W. III Neukum G. OMEGA Team HRSC Team
Spectral and Morphologic Properties of Nili Fossae **[#1819]**
OMEGA-MEx has detected the largest and the highest concentration of olivine on Mars in Nili Fossae. Of specific interest is the presence of hydrated minerals in this very rich olivine-bearing region. We examine the geomorphology of this complex region with HRSC image.

Pinet P. C. Daydou Y. Cord A. Chevrel S. C. Poulet F. Erard S. Bibring J.-P. Langevin Y. Melchiorri R. Bellucci G. Altieri F. Arvidson R. E. OMEGA Co-Investigator Team
Derivation of Mars Surface Scattering Properties from OMEGA Spot Pointing Observations **[#1694]**
OMEGA emission phase function (EPF) observation shows that one may access from orbit to geology-driven surface scattering properties such as surface roughness. It has implications for spectroscopic interpretation and for CRISM observations to come.

Combe J.-P. Sotin C. Le Mouélic S. Launeau P. Mustard J. F. Gendrin A. Bibring J.-P. Gondet B. Langevin Y. OMEGA Science Team
Methodology of Hyperspectral Reflectance Data Analysis for Mineralogical Mapping of Planetary Surfaces : Application to OMEGA/Mars-Express Images **[#1633]**
Methodology of hyperspectral data analysis is investigated to interpret OMEGA/Mars-Express images. Results of the Modified Gaussian Model (MGM) and a recursive linear unmixing algorithm are compared with previous detection of minerals like hematite.

Mars Express and HRSC II

Koehler U. Neukum G. van Gasselt S. Jaumann R. Roatsch Th. Hoffmann H. Zender J. Acton C. Drigani F. HRSC Co-Investigator Team
Public Outreach and Archiving of Data from the High Resolution Stereo Camera Onboard Mars Express: 2004 — The First Year **[#2202]**
During 2004, the HRSC imaging experiment onboard Mars Express recorded 23 Gigabyte of raw data. Every six months these HRSC 'Level 2' data are fed into ESA's Planetary Science Archive (PSA) that sends all data also to the Planetary Data System (PDS).

Shean D. E. Head J. W. III Marchant D. R. Neukum G. HRSC Co-Investigator Team
Arsia Mons Fan-shaped Deposit: Spatial and Temporal Relationships Among Cold-based Glaical Facies from HRSC Data **[#2190]**
New high-resolution HRSC images reveal details of a fan-shaped deposit on the flanks of Arsia Mons interpreted to be a cold-based, tropical mountain glacier, showing evidence for superposed moraines, debris-covered alpine and piedmont glacial deposits, and candidate subglacial eruptions.

Hiesinger H. Head J. W. III Neukum G. Jaumann R. Hauber E. Carr M. H. Masson Ph. Foing B. H.
Evidence for Snow and Ice Accumulation Aiding Debris Flow and Glacial Flow at Mid- to Low-Latitudes on Mars **[#1988]**
HRSC image data show debris aprons suggesting extremely ice-rich glacier-like viscous flow and sublimation, and ice-rich debris-covered glaciers suggesting geologically recurring glacial activity in low- and mid-latitude regions.

Dickson J. L. Head J. W. III Parsons R. L. Neukum G. HRSC Co-Investigator Team
Arsia Mons Flank Pit Craters and Valleys: Modification by Downslope Movement Processes **[#1790]**
We use new HRSC image data to document pit crater and linear valley modification processes at the southern margin and flank of the summit of Arsia Mons. Candidates include mass wasting, slumping, gelifluction, solifluction, and glaciation.

Reiss D. Michael G. G. Hauber E. van Gasselt S. Jaumann R. Neukum G. HRSC Co-Investigator Team
Ages of Rampart Craters in the Xanthe Terra Region and Southern Chryse Planitia, Mars: Implications for the Distribution of Ground Ice in Equatorial Regions **[#1725]**
We determined the absolute ages of rampart craters in two near equatorial regions on Mars by measuring the ejecta blankets superposed crater frequencies in Mars Express High Resolution Stereo Camera (HRSC) imagery.

Lahtela H. Korteniemi J. Kostama V.-P. Raitala J. Neukum G. HRSC Co-Investigator Team
The Ancient Lakes in Hellas Basin Region as Seen Through the First Year of Mars Express HRSC-Camera **[#1683]**
This study concentrates on mapping and describing the paleolakes on Hellas Basin region using the Mars Express HRSC images. The camera has imaged the area with enough good coverage to to give preliminary view of paleolake distribution there.

Korteniemi J. Kostama V.-P. Aittola M. Öhman T. Törmänen T. Lahtela H. Raitala J. Neukum G. HRSC Co-Investigator Team
Mars Express HRSC Analysis of Two Impact Craters in Terra Tyrrhena, Mars **[#1680]**
Two craters in Terra Tyrrhena north of Hellas basin exhibit anomalous floors. Here we present the geological history of the area.

Korteniemi J. Lahtela H. Raitala J. Neukum G. HRSC Co-Investigator Team
Anomalous Depressions on the Circum-Hellas Crater Floors as Seen in the First Year MEX HRSC Images **[#1669]**
The Hellas rim and basin region exhibit a multitude of anomalous pits, collapses and depressions on the crater floors. We use the new HRSC images to identify and categorize these features and find that they are mostly erosion- and volatile-related.

Aittola M. Kostama V.-P. Raitala J. Korteniemi J. Greeley R. Williams D. Hauber E. Neukum G. HRSC Co-Investigator Team
Amphitrites Patera Studied from the Mars Express HRSC Data **[#1664]**
The multi-channel data of the HRSC reveals several surface units with different properties within the Amphitrites Patera, as well as evidences of small scale volcanic activity postdating the formation of the patera.

Mangold N. Masson Ph. Ansan V. Quantin C. Neukum G. HRSC Co-Investigator Team
Analysis of Valley Networks on Valles Marineris Plateau Using HRSC/MEX Data **[#1336]**
Dense dendritic networks of valleys likely formed by surface run off are observed close to Echus Chasma attesting of late fluvial episodes in that region. Inverted channels near Juventae Chasma suggests this process was not restricted in one location.

McColley S. M. Head J. W. III Neukum G. HRSC Team
The Medusae Fossae Formation: Geological Characteristics and Topographic and Stratigraphic Relationships of the Lower Member Along Southeastern Elysium Planitia **[#1184]**
A detailed geologic assessment of the lower member (Aml) of the Medusae Fossae Formation along southeastern Elysium Planitia.

Thompson T. W. Horttor R. L. Acton C. H. Jr. Zamani P. Johnson W. T. K. Plaut J. J. Holmes D. P. No S. Asmar S. W. Goltz G.
The Mars Express/NASA Project at JPL **[#1088]**
ESA's Mars Express Mission, which has been in orbit since December 2003, is supported by a number of U.S. contributions described in this report.

Spiegel M. Schmidt R. Stilla U. Baumgartner A. Neukum G. HRSC Co-Investigator Team
Registering HRSC Imagery of the Mars Express Mission to Mars Observer Laser Altimeter Data **[#1761]**
The goal is to register the HRSC data of Mars Express Mission to the Mars Observer Laser Altimeter data (MOLA). The concept and results of the bundle adjustment with and without MOLA data as control information is described.

Schmidt R. Spiegel M. Heipke C. Oberst J. Neukum G. HRSC Co-Investigator Team
Automatic Tie Point Generation for the Processing of HRSC Imagery of the Mars Express Mission **[#1769]**
The automatic determination of tie points for the improvement of the exterior orientation of the spacecraft is carried out at Institute of Photogrammetry and GeoInformation (IPI) of Universität Hannover and is presented in this abstract.

Werner S. C. Ivanov B. A. Neukum G. van Kan M. Zegers T. E. Foing B. H. Greeley R. Williams D. HRSC Co-Investigator Team
Evolutionary History of Gusev — The MER Landing Site — Seen by MEX-HRSC **[#1777]**
The evolutionary history of Gusev and its vicinity is discussed. Comparing Gusev-sized impact craters the level of infill of Gusev is about 1–1.5 km more than for others, possibly due to the contribution of fluvial activity of Ma'adim Vallis.

Raitala J. Basilevsky A. T. Neukum G. Werner S. C. Denk T. McCord T. B. HRSC C-Investigator Team
Mars Express HRSC Colors of White Rock, Arabia, Mars **[#1710]**
The MEX HRSC spectral data suggest (but not prove) that White Rock may be evaporite deposit resembling the Opportunity sulfate deposits.

Hauber E. Gwinner K. Reiss D. Scholten F. Michael G. G. Jaumann R. Ori G. G. Marinangeli L. Neukum G. HRSC Co-Investigator Team
Delta-like Deposits in Xanthe Terra, Mars, as Seen with the High Resolution Stereo Camera (HRSC) **[#1661]**
HRSC images show delta-like deposits in impact craters in Xanthe Terra on Mars. The morphology and topography of the deposits suggest a formation as Gilbert-type deltas and are in agreement with clastic sedimentation in a lacustrine environment.

Pischel R. Zegers T. Hoffmann H. Hauber E. Mertens V. Roatsch T. Jaumann R. Matz K.-D. Companys V. Lauer M. Denis M. Moorhouse A. Rabenau E. Ricketts M.
Targeting Mars — The Mars Express Science Planning and Operations **[#1017]**
Since the ESA Mars Express mission arrived at Mars more than 600 orbits have been used for observations. The paper describes the complex process of planning the science operations for Mars Express with emphasis on the accuracy of observations.

Komatsu G. Ori G. G. Di Lorenzo S. Rossi A. P. Neukum G. HRSC Co-Investigator Team
Morphology and Morphometry of Fluidized Ejecta Blankets: New Results from the Mars Express High Resolution Stereo Camera **[#1379]**
The morphology and morphometric properties of fluidized Martian impact crater ejecta blankets were studied using the HRSC stereo data set. The results indicate their origin as water-related ejecta emplacement and liquefaction/fluidization.

van Gasselt S. Hauber E. Reiss D. Scholten F. Neukum G. HRSC Co-Investigator Team
Slope Morphologies of the Hellas Mensae Constructs, Eastern Hellas Planitia, Mars **[#2090]**
Lobate debris aprons of the Eastern Hellas region show a variety of adjacent landforms that contributed to their formation. Through time, varying amounts of available water or ice caused retreat and movement of surficial deposits with varying rheologic behaviours.

Martin P. D. Cord A. Foing B. H. Zegers T. van Kan M. Pinet P. Daydou Y. Hoffmann H. Hauber E. Jaumann R. Neukum G. HRSC Co-Investgator Team
Photometric and Compositional Surface Properties of the Gusev Crater Region, Mars, as Derived from Multi-Angle, Multi-Spectral Investigation of Mars Express HRSC Data **[#1687]**
The focus of this investigation is to use the potential of the HRSC multi-angular and multi-spectral data sets for identifying photometric, color and compositional units and their heterogeneity.

Basilevsky A. T. Neukum G. Ivanov B. A. Werner S. C. van Gasselt S. Head J. W. III
Hauber E. HRSC Co-Investigator Team
Mars Express HRSC View of Western Olympus Mons: Evidence for Ice-bearing Deposit and High-Altitude Glaciation **[#1060]**
The analysis of the HRSC images for the western Olympus Mons provides evidence of the presence of an ice-bearing deposit composing part of the Olympus Mons construct as well as evidence of the high-altitude glaciations in the geologic past.

Mars Polar Atmosphere-Surface Interactions

Nelli S. M. Murphy J. R. Sprague A. L. Boynton W. V. Prettyman T. H.
Dissecting the Polar Asymmetry in the Non-Condensable Gas Enhancement on Mars: A Numerical Modeling Study **[#2132]**
Using the NASA Ames General Circulation Model (GCM), we modeled the Martian argon cycle. The model produced a North/South Polar asymmetry, similar to that seen in the observed data.

Levrard B. Forget F. Montmessin F. Schmitt B. Douté S. Langevin Y. Poulet F. Bibring J.-P. Gondet B.
High LMD GCM Resolution Modeling of the Seasonal Evolution of the Martian Northern Permanent Cap: Comparisons with Mars Express OMEGA Observations **[#1882]**
A high resolution modelling of the northern cap ($1° \times 1°$) has been performed in the 3-D LMD GCM to investigate the seasonal evolution of the permanent water ice cap (ice thickness, temperature...). Comparisons will be made with unprecedently resolved MEX/OMEGA observations (MArs Express).

Wrobel K. E. Schultz P. H. Crawford D. A.
Formation of High-Latitude Pedestal Craters **[#1221]**
Computational models demonstrate the effects of a blast wave and temperature pulse due to direct energy coupling to the atmosphere during crater formation. Results present a new formation hypothesis for high-latitude pedestal craters.

Kreslavsky M. A. Head J. W. III
Permanent CO_2 Deposits on Mars at Low Obliquity: The Role of Surface Topography **[#1234]**
During long low obliquity epochs, massive solid CO_2 deposits would form on steep pole-facing topographic slopes at moderately high latitudes rather than at the poles. Such deposits could survive short obliquity peaks and leave observable traces.

Russell P. S. Head J. W. III
Circum-Polar Craters with Interior Deposits on Mars: Polar Region Geologic, Volatile, and Climate History with Implications for Ground Ice Signature in Arabia Terra **[#1541]**
Morphological variety and distribution of ice-rich crater-interior deposits suggest emplacement originally contiguous with PLD, as ice stability shifted from lower to higher latitudes with decreasing obliquity. Similar deposits in Arabia are consistent with this model.

van Gasselt S. Reiss D. Thorpe A. Neukum G.
Development of Polygonal Thermal Contraction Patterns in a South Polar Trough, Mars — 3 Years of Observations **[#2059]**
Multi-temporal MOC image coverage of a south polar trough show polygonal contraction-crack patterns that have changed significantly during two seasons. It is shown that formation can be explained by a three-layer model.

Langsdorf E. L. Britt D. T.
Classification and Distribution of Patterned Ground in the Southern Hemisphere of Mars **[#2140]**
We have mapped the occurrence of polygonal terrain on Mars from –60° S to –90° S. Several different types of polygons were found: small scale, large scale polygonal nets on level terrain, and large scale polygonal nets in craters.

Wagstaff K. L. Castaño R. Chien S. Ivanov A. B. Titus T. N.
Towards Onboard Orbital Tracking of Seasonal Polar Volatiles on Mars **[#1582]**
We present an automated method, BIT, to perform orbital tracking of the Mars polar caps onboard Mars Odyssey. Evaluated on 476 archived THEMIS images, BIT shows excellent agreement with a model derived from manual TES annotations.

Titus T. N.
Mars Polar Cap Edges Tracked over 3 Full Mars Years **[#1993]**
In this study, we use 3 Mars years of TES IR and VIS data to characterize the seasonal cap edges as a function of season and longitude, which aid in the detection of inter-annual changes and longitudinal asymmetries in both the seasonal caps advance and retreat.

Schorghofer N. Edgett K. S.
Seasonal Surface Frost at Low Latitudes on Mars **[#1569]**
Seasonal surface frost is observed in MOC images on pole facing slopes at latitudes as low as 35 degrees south. We conclude the frost consists of CO_2 and is probably preceded by H_2O deposition.

Hecht M. H.
The Influence of Local Geometric Effects on Mars Polar Processes **[#2281]**
Perforated textures are likely to result from the formation of seasonal CO_2 deposits by condensation, resulting in erroneous measurements of density, transparency, and underlying surface structures. For similar reasons, ablation from contoured ice scarps may be a dominant process in polar evolution.

Zent A. P. Sutter B.
Melting in Martian Snowbanks **[#2374]**
A mass and energy balance model of snowbanks on Mars is under development. Results will be presented for evolution under different climatic regimes.

Mischna M. A. Richardson M. I.
GCM Simulations of the Tropical Hydrogen Distribution Observed by Mars Odyssey **[#1518]**
We use the GFDL Mars GCM with a fully coupled atmosphere-regolith water cycle to understand the age of the hydrogen deposits observed by Mars Odyssey. Trends in subsurface ice evolution are observed during various obliquity and polar cap conditions.

Chamberlain M. A. Boynton W. V.
Effect of Ground Ice on Apparent Thermal Inertia on Mars **[#1566]**
Ground ice in the martian polar regions can lower or raise the ground temperature and apparent thermal inertia observed by spacecraft, depending on the depth of ice and season of observation.

Sizemore H. G. Mellon M. T.
Effects of Rocks on Martian Ground Ice and Neutron Flux **[#1774]**
We present numerical simulations of the three-dimensional distribution of ground ice in a heterogeneous martian soil and discuss the implications of our results for the interpretation of Mars Odyssey Gamma Ray Spectrometer data.

Moores J. E. Brown R. H. Lauretta D. S. Smith P. H.
Preliminary Results of Sublimation Fractionation in Dusty Disaggregated Samples **[#1973]**
Using a cryostat, the behavior of dusty ice as an analogue for polar regolith is investigated. A 25 wt% mixture of 1–2 μm TiO_2 dust in a 5 vol% D_2O/H_2O solution was used based upon a precipitation origin and exhibited increasing fractionation with time.

Milkovich S. M. Head J. W. III
Stratigraphic Analysis of the North Polar Cap of Mars: Recent Climate History **[#1079]**
Analysis of the north polar layered deposits with FFT and curve matching algorithms reveals distinct patterns within the layer stratigraphy that can be correlated with polar climate history and compared with initial results from the south PLD.

Milkovich S. M. Head J. W. III Marchant D. R.
Evidence for Internal Deformation and Flow in the Northern Polar Cap of Mars **[#1080]**
Several layers exposed at the base of troughs near the margin of the north polar cap display features consistent with brittle deformation, implying that at least part of the cap experienced flow at one time.

Fishbaugh K. E.
Characterization of Martian North Polar Geologic Units Using Mars Odyssey THEMIS Data **[#1335]**
We present the results of a preliminary analysis of martian north polar region THEMIS data. Our goal is to better understand the composition and thermal properties of the polar geologic units.

Plaut J. J.
An Inventory of Impact Craters on the Martian South Polar Layered Deposits **[#2319]**
A new inventory of impact craters on the martian south polar layered deposits is obtained from Mars Odyssey THEMIS visible images. The crater abundance, consistent with earlier counts, yields an age of tens of My for the upper surface of the deposit.

Tanaka K. L. Kolb E. J. Skinner J. A. Jr. Rodriguez J. A. P.
Climate History of the Polar Regions of Mars Deduced from Geologic Mapping Results **[#1911]**
We propose a climate history for the polar regions of Mars, based on our new geologic mapping results combined with previous crater chronology studies and orbitally driven climate models.

Kolb E. J.   Tanaka K. L.
Chasmata of Planum Australe, Mars: Are Their Formation and Location Structurally Controlled? **[#2298]**
This abstract details results of our 1:1.5M-scale geologic mapping of Mars' polar ice caps. We show that the location and formation of the south pole chasma of Planum Australe are structurally controlled by substrate and SPLD paleosurface topography.

Rodriguez J. A. P.   Sasaki S.   Fairén A. G, Miyamoto H.   Schulze-Makuch D.
Basement Topographic Control on the Chasmata Initial Growth and Distribution in the Martian Southern Polar Cap **[#1795]**
We examine the geomorphic and topographic characteristics of the chasmata in the southern polar cap and discuss how the irregular topography of the underlying basement may have played a significant role in their initiation and growth.

Mars Geophysics

Draper D. S.   Borg L. E.   Agee C. B.
Crystallization of a Martian Magma Ocean and the Formation of Shergottite Source Regions: A Less Fe-rich Mars? **[#1429]**
Modeling a martian magma ocean having a composition slightly less Fe-rich than previously thought yields good matches to compositions of proposed shergottite parent melts.

Sohl F.   Schubert G.   Spohn T.
Geophysical Constraints on the Composition and Structure of the Martian Interior **[#2147]**
Models of the Martian interior based on the most recent value of the moment of inertia (MoI) are compared to previous models. We consider consequences a lower MoI may have for the planet's bulk chemistry and find that the Martian mantle is likely to be more Earth-like than previously thought.

Roberts J. H.   Zhong S.
Degree-1 Mantle Convection and the Origin of the Martian Hemispheric Dichotomy **[#1399]**
We present a model in which viscosity layering in the Martian mantle leads to degree-1 convection in under 100 Myr. We propose degree-1 mantle convection as a mechanism for producing the crustal dichotomy early in Martian history and maintaining it.

Reese C. C.   Solomatov V. S.
Subduction Initiation by Stagnant Lid Convection in Spherical Shell Geometry: Implications for Mars **[#1974]**
Scaling laws developed for spherical shell geometry indicate that initiation of subduction in the stagnant lid regime requires a very weak lithosphere as was found in two-dimensional simulations.

van Thienen P.   Lognonné P.
Formation of Martian Volcanic Provinces by Lower Mantle Flushing? **[#1277]**
We present results of numerical mantle convection experiments in which we try to ascertain whether the flushing of the martian lower mantle (if present) could provide a mechanism for the generation of a small number of plume-like features, showing localized upwelling of hot material.

Guest A.   Smrekar S. E.
Constraints on Thermal Evolution of Mars from Relaxation Models of Crustal and Topographic Dichotomy **[#1880]**
We constrain the early thermal evolution of Mars by testing the effect of temperature evolution in the mantle and lithosphere on the relaxation of the martian dichotomy. Thermo-magmatic stagnant lid model allows for the preservation of the martian dichotomy.

Belleguic V.   Wieczorek M.   Lognonné P.
Modeling of Surface and Subsurface Loads Associated with the Major Martian Volcanoes **[#1909]**
Localized spectral admittances of the large martian volcanoes are modeled by assuming that surface and subsurface loads are elastically supported by the lithosphere.

Milbury C. A.   Raymond C. A.   Jewell J. B.   Smrekar S. E.   Schubert G.
Joint Inversion and Forward Modeling of Gravity and Magnetic Data in the Ismenius Region of Mars **[#2075]**
Gravity and magnetic field anomalies may be correlated in the Ismenius area, which would permit detailed interpretation of the crustal history. We test this hypothesis by carrying out a series of joint inversions of gravity and magnetic field data.

Mitchell D. L.   Lillis R. J.   Lin R. P.   Connerney J. E. P.   Acuña M. H.
A Global Map of Mars' Crustal Magnetic Field Based on Electron Reflectometry **[#2366]**
We present a global map of the amplitude of Mars' crustal magnetic field at 170 km altitude based on electron reflectometry, using data from the MAG/ER experiment onboard Mars Global Surveyor.

Jurdy D. M. Stefanick M. J.
Vertical Extrapolation of Mars Magnetic Streamline Function to Surface **[#1864]**
We model Mars' magnetic field using the streamline function at the surface with vertical dipoles to determine the depths and magnitudes of sources.

Artemieva N. A. Hood L. L. Ivanov B. A.
Impact Demagnetization of the Martian Crust: Primaries Versus Secondaries **[#1112]**
Outside the transient cavity, demagnetization by secondary impacts is at least comparable with demagnetization in a direct shock wave. If magnetic minerals are in the upper crust, then shock by secondaries will be important.

Biswas S. Ravat D.
Why Meaningful Paleopoles Can't be Determined Without Special Assumptions from Mars Global Surveyor Data? **[#2192]**
In this paper we explore the non-uniqueness in the magnetization vectors used for determining paleopoles on Mars.

Ravat D.
Deconstructing a Few Myths in the Interpretation of Satellite-Altitude Crustal Magnetic Field: Examples from Mars Global Surveyor **[#2114]**
In this paper, I justify modeling of satellite-altitude magnetic field anomalies using the equivalent source method with radially-polarized and other dipole orientations and the source location interpretation using the Analytic Signal field.

Voorhies C. V.
More on Magnetic Spectra from Correlated Crustal Sources on Mars **[#1490]**
Theoretical magnetic spectra for laterally correlated sources in Mars's crust are described in the context of previous work. Preliminary results from applications to observational spectra, extracted from MGS MAG/ER data, are to be presented and discussed.

Urquhart M. L.
Impact of Low Thermal Conductivity Layers on the Bulk Conductivity of a Martian Crustal Column **[#2337]**
The impact of low and high thermal conductivity layers in the Martian crust on column averaged thermal conductivity and geothermal gradients are investigated, along with the implications for calculations of the depth to melting for ground ice.

Karatekin O. Dehant V. de Viron O. Van Hoolst T.
Atmospheric Excitation of Mars Polar Motion **[#1803]**
The rotation of Mars is not constant and present irregularities with time. Those are mostly associated with the atmosphere, and the condensation/sublimation of the icecaps. We have estimated the amplitudes of the two polar motion normal modes, i.e., the Chandler wobble and the Inner Core wobble.

Matsuyama I. Mitrovica J. X. Perron J. T. Manga M. Richards M. A.
Rotational Stability of Dynamic Planets with Lithospheres **[#2230]**
We investigate the long term rotational stability of terrestrial planets subject to surface mass and internal (convectively driven) loading. The stability theory extends work by *Willemann* [1984] and is illustrated with several case studies.

Mars Tectonics

Hynek B. M. Phillips R. J.
The Etched Terrain in Arabia Terra, Mars, is Tilted **[#1222]**
The horizons of etched terrain layers in Meridiani are tilted and most follow the model topography of Tharsis-induced loading with a contribution from the pole-to-pole slope. This may indicate a very ancient age for rocks in this region of Mars.

Beyer R. A. McEwen A. S.
Constraints on the Origin of Fine Layers in Ganges Mensa and Hebes Mensa, Mars **[#1070]**
These mensae have been proposed to have steeply dipping layers. The dip angle and direction of these layers can be constrained with MOC and MOLA data. We find no evidence that steep layers are present, most are much shallower than thirty degrees.

Fueten F. Stesky R. MacKinnon P. Zegers T. Hauber E. Foing B. H. Pischel R. Gwinner K. Scholten F. Neukem G. HRSC Co-Investigator Team
Attitude Determination of Geological Layers Using HRSC Data and Orion Software **[#1498]**
Attitude of ILD layering in Valles Marineris, Mars, is measured using HRSC data and Orion software.

Okubo C. H. Schultz R. A.
Evidence of Tharsis-Radial Dike Intrusion in Southeast Alba Patera from MOLA-based Topography of Pit Crater Chains **[#1007]**
Pit crater chains in southeast Alba Patera are found to have local cross-strike topographies that are consistent with a mixed-mode of causative dike intrusion and normal faulting, with the causative tendencies changing with position along strike of each pit crater chain.

Wyrick D. Y. Ferrill D. A. Morris A. P. Sims D. W. Franklin N. M.
Quantifying Fault Networks on Alba Patera, Mars **[#2279]**
Newly developed terrestrial approaches were applied to martian fault networks to quantify the extent and degree of fault network connectivity. These techniques will provide key constraints for martian hydrological models.

Lucchitta B. K.
Light Layer and Sinuous Ridges on Plateau Near Juventae Chasma, Mars **[#1500]**
The layer is associated with ridges topped by channels, indicating inverted relief. Dark flows overlap the light layer, suggesting interbedding with lavas, and strengthening the idea that light, incompetent layers occur in the walls of the Valles Marineris.

Dimitrova L. L. Holt W. E. Haines A. J.
Constraining Lithospheric Stress and Strain on Mars from Mars Global Surveyor (MGS) Topography, Gravity and Crustal Thickness: I. Viscous Rheology Solutions **[#2039]**
We calculate the vertically integrated deviatoric horizontal stresses associated with horizontal gradients of gravitational potential energy on Mars for viscous rheologies. We compare our results with grabens and wrinkle ridges in and around Tharsis.

Dimitrova L. L. Holt W. E. Haines A. J.
Constraining Lithospheric Stress and Strain on Mars from Mars Global Surveyor (MGS) Topography, Gravity and Crustal Thickness: II. Elastic Rheology Solutions **[#2051]**
We calculate the vertically integrated deviatoric horizontal stresses associated with horizontal gradients of gravitational potential energy on Mars for elastic rheologies. We obtained an improved fit to structures in and around Tharsis.

Mars Volcanism

Hughes S. S. Sakimoto S. E. H. Gregg T. K. P. Brady S. M.
Petrologic Evidence for Multiple, Chemically Evolved Magma Batches and Implications for Plains Volcanism on Earth and Mars **[#2396]**
Geochemical models of magma evolution, oxygen fugacity determinations, and variable eruptive temperatures of plains-style basalts suggest an extensive system of small mafic intrusions beneath the volcanic plains.

Brady S. M. Hughes S. S. Sakimoto S. E. H. Gregg T. K. P.
Exploring the Link Between Geochemistry and Volcano Morphology on the Eastern Snake River Plain, a Planetary Analog to Mars Volcanism **[#2359]**
This study shows a positive correlation between a strong diktytaxitic texture and increased summit steepness among ESRP basaltic shield volcanoes.

Ori G. G. Pacifici A. Komatsu G. Neukum G. HRSC Science Team
A Probable Fluid Lava Flow in the Hebes Mensa (Mars) Studied by HRSC Images **[#1648]**
A dark rills and pond features on the northern slope of the Hebes Mensa could be formed by fluid lava flows. Mud and debris flows can be taken into account, but the stability of the feature (observed during Viking time) support a volcanic origin.

Shockey K. M. Zimbelman J. R.
A Long Lava Flow in the Tharsis Region of Mars as Mapped Using THEMIS Data **[#1937]**
A long lava flow to the west of Ascraeus Mons, was previously examined using MOLA data. The same flow is now being mapped using THEMIS data.

Rampey M. L. Milam K. A. McSween H. Y. Jr. Moersch J. E. Christensen P. R.
Lava and Flows of the Arcadia Region of Mars **[#1834]**
This study examines morphological and spectral data sets from a region in the northern plains of Mars informally known as the Tyndall Dome Field (TDF) for evidence of silicic volcanism.

Miyamoto H. Crown D. A. Haruyama J. Kobayashi T. Nishibori T. Okada T. Rodriguez J. A. Rokugawa S. Tokunaga T. Suzuki K. Masumoto K.
Emplacement of Pahoehoe Lobes: A Simplified Two-Component Model and Field Measurements by Ground Penetrating Radar **[#1619]**
We present a simple two-component model as a possible theoretical explanation of the self-confinement mechanism of the lateral spreading of an isolated lobe. The model also explains why the cross section of a flow has a parabolic shape.

Jaeger W. L. Keszthelyi L. P. Burr D. M. Emery J. P. Baker V. R. McEwen A. S. Miyamoto H.
Basaltic Ring Structures as an Analog for Ring Features in Athabasca Valles, Mars **[#1886]**
Ring structures on the floor of Athabasca Valles, Mars are similar in morphology and geologic context to terrestrial basaltic ring structures in the Channeled Scabland, which formed by phreato-volcanism in actively-inflating basaltic sheet flows.

Mitchell K. L. Wilson L.
Recent and Future Volcanism on Dormant Mars **[#1933]**
We suggest that Mars is dormant rather than extinct, in a cycle characterised by ~100 Ma epochs of inactivity, punctuated with ~1 Ma, single-centre, eruptive epochs. We then estimate when the next eruption will occur, and its likely duration.

Milazzo M. P. McEwen A. S.
Endogenic Thermal Activity at Cerberus Fossae, Mars? **[#1998]**
Cerberus Fossae: Compare spring, autumn brightness. Is Mars still alive?

Crown D. A. Berman D. C. Bleamaster L. F. III Chuang F. C. Hartmann W. K.
Martian Highland Paterae: Studies of Volcanic and Degradation Histories from High-Resolution Images and Impact Crater Populations **[#1476]**
Crater size-frequency distributions from MOC, THEMIS, and Viking images and small-scale morphologic characteristics are used to provide new assessments of the volcanic and degradation histories of Martian highland paterae.

Mars Cratering and Analogs

Buczkowski D. L. Frey H. V. McGill G. E.
Effect of Cover Thickness on the Relationship of Surface Relief to Diameter of Northern Lowland QCDs on Mars **[#1106]**
Analytical analysis of QCDs predicts that the relationship of surface relief to diameter varies depending on the thickness of the cover material. Comparison to actual QCDs in Utopia, Isidis and Acidalia implies that this prediction is accurate.

Buczkowski D. L. Frey H. V. McGill G. E.
Geographic Distribution of QCDs Around the Northern Plains Basins of Mars and the Relationship to Lowland Materials **[#1215]**
We explore the geographic distribution of QCDs around the Utopia, Isidis and Acidalia basins and compare their location to geologic units and materials. We also compare evidence for relative thickness of cover material at the three basins.

Howenstine J. B. Kiefer W. S.
Morphometry of Large Martian Impact Craters **[#1742]**
We have measured crater depths and rim heights for large craters on Mars. The results constrain fill thickness on crater floors and will support forth-coming gravity modeling. Gusev crater has between 0.8 and 2.2 km of post-impact fill on its floor.

Jaret S. J. Albin E. F.
Crater Count Chronology and Timing of Ridged Plains Emplacement at Schiaparelli Basin, Mars **[#1922]**
Found in eastern portion of the Terra Meridiani region of Mars is Schiaparelli, a 470-km diameter impact structure. Our investigation seeks to compare the age of ridged plains material, interpreted as volcanic lava flows, within and adjacently exterior to the basin rim.

Morris A. R. Mouginis-Mark P. J.
Thermally Distinct CratersNnear Hrad Vallis, Mars **[#1493]**
In this study we examine the characteristics and possible formation mechanisms of thermally distinct craters near Hrad Vallis, Mars, using MOC, THEMIS and MOLA data.

Ackerman E. S.
Volumetric Analysis of Martian Rampart Craters **[#2151]**
Viking images and MOLA data were used to calculate ejecta volumes and transient cavity volumes for Martian rampart craters. Comparing these volumes may indicate whether there is a volatile component being added to the ejecta flow.

Matias A. Jurdy D. M.
Study of a 15 km Crater with Diverse Morphology, Elysium Planitia, Mars **[#1163]**
We examine the nature of the 14.9 km diameter crater (28.3 N, 116.7 E) with an unusual lobe on its southwestern rim, part of an assessment of rampart craters on northwestern Elysium Planitia.

Fagents S. A. Baloga S. M. Mouginis-Mark P. J.
Boundary Conditions on the Formation of Ramparts on Fluidized Ejecta Deposits Around Martian Impact Craters **[#2127]**
We present a model for the formation of rampart deposits and explore various source boundary conditions. We find that only modest initial velocities (<40 m/s) and source flow depths (<30 m) are required to reproduce observed morphologies.

Mest S. C.   Crown D. A.
Impact Crater Deposits in the Martian Highlands **[#1785]**
Impact craters in the martian highlands preserve long and complex histories of degradation, and contain interior deposits that may be sedimentary, mass wasting, (and) or volcanic in origin. Crater morphologies, geologies and ages are being determined.

Peet V. M.   Ramsey M. S.   Crown D. A.
Comparison of Terrestrial Morphology, Ejecta, and Sediment Transport of Small Craters: Volcanic and Impact Analogs to Mars **[#2080]**
Two terrestrial craters are examined as a Mars analog for formation and sediment transport processes. It is hypothesized that an analog for formational and surface processes on Mars pertaining to small craters can be developed that distinguishes one crater type from the other.

Farr T. G.
Visible-Near Infrared Imaging Spectrometer Data of Explosion Craters **[#2365]**
New high resolution visible-near infrared imaging spectrometer data of explosion craters at the Nevada Test Site will allow study of ejecta patterns, compositional modifications due to the explosions, and the role of craters as subsurface probes.

Dry (?) Mars: Aeolian Processes, Mass Wasting, and Rocks

Mullins K. F.   Hayward R. K.   Titus T. N.   Bourke M. C.   Fenton L. K.
Mars Digital Dune Database: A Quantitative Look at the Geographic Distribution of Dunes on Mars **[#1986]**
Initial steps in developing a digital dune database in a global geographic context for Mars have been completed. This database currently contains information delineating the dune fields between ±65 degrees latitude.

Banks M.   Bridges N. T.   Benzit M.
Measurements of the Coefficient of Restitution of Quartz Sand on Basalt: Implications for Abrasion Rates on Earth and Mars **[#2116]**
Using high speed video to assess grain-rock interactions, it was found that the KE lost on impact is generally proportional to incoming velocity and impact angle, but that only a fraction of this energy goes into direct abrasion of the rock surface.

Neakrase L. D. V.   Greeley R.   Williams D. A.   Reiss D.   Michaels T. I.   Rafkin S. C. R.   Neukum G.   HRSC Team
Hecates Tholus, Mars: Nighttime Aeolian Activity Suggested by Thermal Images and Mesoscale Atmospheric Model Simulations **[#1898]**
Previously unidentified wind streaks identified on nighttime IR images on Hecates Tholus volcano on Mars agree with predictions of nighttime patterns by an atmospheric model, suggesting that nighttime winds are responsible for modifying the surface in contrast to afternoon winds.

Neakrase L. D. V.   Greeley R.   Iversen J. D.   Balme M. R.   Foley D. J.   Eddlemon E. E.
Dust Devils on Mars: Effects of Surface Roughness on Particle Threshold **[#1857]**
The aim of this study is to determine experimentally the effects of non-erodable roughness elements on vortex particle threshold through laboratory simulations of natural surfaces pertaining to dust devils on Earth and Mars.

Schneider R. D.   Hamilton V. E.
Variations Among Dark-toned Intracrater Deposits in Amazonis Planitia **[#1543]**
We have performed an analysis with THEMIS data that indicates there are visible and spectral variations among 21 dark-toned intracrater deposits in Amazonis Planitia. We explore the reasons for spectral differences among the three types of deposits.

Foley D. J.   Whelley P. L.   Greeley R.   Neakrase L. D. V.
Dust Devil Tracks on Mars: Observation and Analysis from Orbit and the Surface **[#1162]**
The Mars Exploration Rover Spirit traversed a dust devil track. Analysis of dust and fine particles present inside, on the contact, and outside of the track support the hypothesis that dust devils can remove dust and fine particles from the surface.

Gibbons A.   Yang F.   Mlsna P.   Geissler P. E.
Automated Procedures for Detecting Martian Dust Devils **[#2005]**
We have begun to explore the application of numerical pattern recognition techniques to the problem of identifying Martian dust devils in orbital imagery.

Scott A. G.   Williams W. J. W.   Mazumder M. K.   Biris A.   Srirama P. K.
Bridging a High School Science Fair Experience with First Year Undergraduate Research: Using the E-SPART Analyzer to Determine Electrostatic Charge Properties of Compositionally Varied Rock Dust Particles as Terrestrial Analogues to Mars Materials **[#2284]**
More is known about Mars from data collected in 2004. We present particle size and electrostatic data for particles derived from various terrestrial materials to provide analogue studies for what also appears to be present: sedimentary compositions.

Chojnacki M. Jakosky B. M. Hynek B. M.
Surficial Properties of Landslide Units in Ophir Chasma, Mars, from Remote-sensing Data **[#2323]**
We mapped the surface layers of the Ophir Chasma region of Valles Marineris using observations made by the MGS's TES and the MO's THEMIS. We found the landslide units of Ophir's north wall to have a diverse range of characteristics.

Barnouin-Jha O. S. Wada K. Matsui T. Sugita S.
The Flow Dynamics of Long Run-Out Landslides on Mars from 3-D Granular Flow Models **[#1588]**
We use 3-D granular flow models to constrain morhological and topographic attributes of long run-out landslides on Mars.

Pierre N. M. Yingst R. A. Johnson J. R.
Classification of Mars Pathfinder Rocks Using Multispectral Data **[#1948]**
This study represents the first attempt at a systematic spectral classification of a significant percentage of rocks at the Mars Pathfinder landing site, and is part of a larger effort to correlate quantitative rock morphology with spectral data.

Yingst R. A. Biedermann K. L. Pierre N. M. Haldemann A. F. C. Johnson J. R.
Correlation of Rock Spectra with Quantitative Morphologic Indices: Evidence for a Single Rock Type at the Mars Pathfinder Landing Site **[#1896]**
We compare multispectral data with quantitative indices of morphologic characteristics to determine the number of unique rock mineralogies — as opposed to purely external or surface materials — at the Mars Pathfinder landing site.

Mars Ice: Landforms and Processes

Head J. W. III Marchant D. R. Fastook J. L.
Regional Mid-Latitude Glaciation on Mars: Evidence for Marginal Glacial Deposits Adjacent to Lineated Valley Fill **[#1257]**
Deposits on plateaus adjacent to mid-latitude lineated valley fill on Mars are interpreted to be moraines and sublimation tills resulting from valley filling with glacial ice and overflow during periods of extensive Amazonian glaciation.

Chapman M. G. Soderblom L. A. Cushing G.
Evidence of Very Young Glacial Processes in Central Candor Chasma, Mars **[#1850]**
Apparently, ice-formed features occur on the floor of Valles Marineris. The observation that they are associated with dark floor material indicates that the glacier(s?) was relatively young — suggesting late-stage surface ice in equatorial Mars.

Parsons R. L. Head J. W. III
Ascraeus Mons Fan-shaped Deposit, Mars: Geological History and Volcano-Ice Interactions of a Cold-based Glacier **[#1139]**
The work presented here is a re-examination of the Ascraeus Mons fan-shaped deposit using higher resolution data than has previously been available in order to assess the plausibility of a cold-based glacial origin for the deposit.

Chuang F. C. Crown D. A.
Martian Debris Aprons: Morphometric Comparisons of the Eastern Hellas and Tempe/Mareotis Populations **[#1519]**
Here we report on a revised compilation of eastern Hellas apron morphometries using MGS and MO data and comparisons to the Tempe/Mareotis apron population.

Nussbaumer J. W.
Extent and Further Characteristics of Former Glaciated Terrain in Elysium Planitia, Mars **[#1949]**
Here is presented the hypothesis that ice sheets from a retreating and sublimating frozen lake changed the planet's surface in southeastern Elysium Planitia, Mars. This hypothesis is based on observed morphologies, that are similar to morphologies in terrestrial formerly glaciated environments.

Soare R. J. Burr D. M. Wan Bun Tseung J. M. Peloquin C.
Possible Pingos and Periglacial Landscapes in Northwest Utopia Planitia, Mars (II) **[#1102]**
The pingo-like mounds and associated crater-floor landforms identified by us in MOC-EO300299 and MOC-EO500113 may be commonplace in northwest Utopia Planitia. If so, this could point to periglacial processes actively having shaped the landscape, as recently as the last episode of high obliquity.

Soare R. J. Wan Bun Tsueng J. M. Peloquin C.
Possible Thermokarst and Alas Formation in Utopia Planitia, Mars **[#1103]**
Our research evaluates the plausibility of thermokarst formation in an area of Utopia Planitia where thermokarst-like features are highly concentrated: 260–281 degrees longitude and 40–50 degrees latitude.

Levy J. S. Head J. W. III Marchant D. R.
The Origin and Evolution of Oriented-Network Polygonally Patterned Ground: The Antarctic Dry Valleys as Mars Analogue **[#1334]**
We have examined oriented networks of polygonally patterned ground in Mullins Valley and Beacon Valley, Antarctica, which may provide a time-series of polygon initiation and evolution under Mars-like climate conditions.

Lefort A.   Russell P.   Thomas N.
Ice Sublimation Landforms in Peneus and Amphitrites Patera **[#1626]**
The Amphitrites-Peneus patera complex exhibits surficial features possibly formed by ice sublimation. We use a combination of MOLA, MOC and Themis data to map this region and study the formation and evolution of these terrains.

Russell P. S.   Lefort A.   Thomas N.
Modeling Ice Stability with Topography on a Local Scale, Mars **[#1554]**
We model ice stability on a local scale, examining 1) the relative importance of four energy-balance factors introduced by topography, 2) the resulting spatial variation in ice stability, and 3) the resulting cycle in which changes in surface shape depend on shape itself.

Mars Potpourri

Farrell W. M.   Delory G. T.   Atreya S. K.   Wong A.-S.   Renno N. O.   Sentmann D. D.   Marshall J. G.   Cummer S. A.   Rafkin S.   Catling D.
Mars Atmospheric Chemistry in Electrified Dust Devils and Storms **[#1104]**
Martian dust devils and storms generate electricity, and this electricity alters the local chemistry to produce oxidants.

Brandenburg J. E.
On the Possibility of a Persistent Greenhouse Regime on Mars **[#1763]**
A model of a persistent greenhouse regime on Mars is presented. A conventional CO_2 greenhouse is stabilized against short term pressure instabilities by paleo-ocean to provide pressure and temperature buffering and by oxygen formd acids against long term chemical instability.

Johnson J. R.   Staid M. I.
Thermal Infrared Spectral Deconvolution of Experimentally Shocked Basaltic Rocks Using Experimentally Shocked Plagioclase Endmembers **[#1848]**
Thermal infrared laboratory spectra of shocked bytownite feldspars were combined with standard mineral libraries to deconvolve spectra of shocked basaltic rocks to determine the accuracy with which pressures can be estimated in shocked basalts.

Maturilli A.   Witzke A.   Helbert J.   Moroz L.   Arnold G.   Wagner C.
Emissivity Spectral Measurements of Particulate Planetary Analog Materials **[#1770]**
Emission spectra of planetary surfaces contain extensive information on the surface properties and in particular on mineralogical composition. We present here a device built at DLR (Berlin) that enables us to measure emissivity spectra of analog materials in the mid-infrared wavelength region.

Cushing G.   Titus T. N.
Thermal Inertia of the Arsia Mons Caldera: A Site for Nightly CO_2 Condensation **[#2135]**
In this study of the Arsia Mons caldera, we compare MGS TES temperature observations with various thermal models. Homogeneous models are not adequate to explain the observations. Results from multi-layered cases are presented.

McDowell M. L.   Hamilton V. E.
Characteristics of Intracrater Thermal Anomalies in Southwestern Margaritifer Terra **[#1548]**
We use thermophysical properties, albedo, short wavelength emissivity, composition, and geomorphology to understand the formation of anomalously warm intracrater deposits in southwestern Margaritifer Terra.

Glotch T. D.   Rogers D.   Christensen P. R.
A Newly Discovered Hematite-rich Unit in Aureum Chaos: Comparison of Hematite and Associated Units with Those in Aram Chaos **[#2159]**
A new hematite-rich deposit in Aureum Chaos has been discovered with data from the Thermal Emission Spectrometer. Additionally, a caprock unit resembling that in Aram Chaos is seen. A comparison of the units in Aram and Aureum Chaos is presented.

Baratoux D.   Mangold N.   Arnald O.   Gregoire M.   Ceuleneer G.   Van Ginneken M.   Platevoët B.   Bardinzeff J. M.   Chevrier V.   Pinet P.   Mathé P. E.
Origins and Transport of Volcanic Sands in Iceland and Implications for the Evolution of Volcanic Material on Mars **[#1603]**
The objective of this study is to know if we can obtain the nature of volcanic rocks for the hyperspectral observations of volcanic sands on Mars. We present a chemical and mineralogical analysis of volcanic material in Iceland as analogs of Martian volcanic sands.

Lee P. Boucher M. Desportes C. Glass B. J. Lim D. McKay C. P. Osinski G. R. Parnell J. Schutt J. W.
Mars, Always Cold, Sometimes Wet: New Constraints on Mars Denudation Rates and Climate Evolution from Analog Studies at Haughton Crater, Devon Island, High Arctic **[#2270]**
Analysis of crater modification on Mars and at Haughton Crater, Devon Island, High Arctic, recently found to be of Eocene age [1], suggest that Mars was never climatically wet and warm for geological lengths of time during or since the Late Noachian.

Boyce J. M. Mouginis-Mark P. J. Garbeil H. Soderblom L. A.
History of Major Degradational Events in the Highlands of Mars: Preliminary Results from Crater Depth/Diameter Measurements **[#1055]**
We use depth/diameter data for 1,692 impact craters (diam. 6 to >100 km) to study the degradational history of the Martian highlands. We recognize a fluvial erosional event in the Late Noachian and subsequent eolian and infilling and erosion.

DeSoto G. E. Frey H. V.
Relative Ages of the Highlands, Lowlands, and Transition Zone Along a Portion of the Mars Crustal Dichotomy from Densities of Visible and Buried Impact Craters **[#2383]**
Using MOLA data, the relative ages of three types of terrains along a portion of the Mars crustal dichotomy were found with densities of buried and visible craters.

Wilson S. A. Howard A. D.
Geomorphic and Stratigraphic Analysis of Layered Deposits in Terby Crater, Mars **[#2060]**
The diversity of landforms in Terby Crater including ridges, layered deposits, mantled ramps, fans and viscous flow features are indicative of a dynamic geologic history, making this locality ideal for studying landform-climate relationships on Mars.

Moore J. M. Howard A. D.
Layered Deposits and Pitted Terrain in the Circum Hellas Region **[#1512]**
On the highlands surrounding Hellas are a number of craters with irregular depressions on their floor. This abstract describes these features and presents several working hypotheses for their origin.

Skinner J. A. Jr. Tanaka K. L. Rodriguez J. A. P. Kargel J. S.
The Southern Utopia Highland-Lowland Boundary: Basin Structural Controls on Aquifer Development and Volatile-driven Resurfacing **[#2119]**
We propose that the southern Utopia HLB plains units derived from sedimentary volcanism and aquifer collapse within a structurally isolated, sedimentary sequence related to the Utopia multi-ring impact structure.

Mars: Instruments and Data Interpretation Techniques

Bue B. D. Stepinski T. F.
Automated Classification of Landforms in Terra Cimmeria, Mars **[#1195]**
We present an automated method for identification of landforms on Mars. Application to the Terra Cimmeria region yields 20 landform types whose spatial distribution is shown using a thematic map. Future application includes automated crater counting.

Blair M. W. Kalchgruber R. Deo S. McKeever S. W. S.
Developing OSL Geological Dating Techniques for Use on Future Missions to Mars **[#1317]**
The basic principles of OSL dating are outlined and some of the challenges to developing OSL dating for use on Mars are addressed.

Cord A. Martin P. Foing B. H. Jaumann R. Hauber E. Hoffman H. Neukum G. HRSC Co-Investigator Team
Macroscopic Texture of the Martian Surface: Application of a Filtering Method Using Mars Express HRSC Data **[#1615]**
We quantify the texture of Martian surface at the scale of a few pixels using images from HRSC (Mars Express). This can be linked with the relative thickness of dust deposit and then with some geological and geomorphological properties of the surface.

Glotch T. D. Bandfield J. L. Christensen P. R.
Factor Analysis and Target Transformation of Mini-TES Spectra: Recovery of Scene Endmembers at Meridiani Planum **[#2174]**
Factor analysis and target transformation techniques have been applied to Mini-TES data at Meridiani Planum. Four spectral components are present in the scene, including hematite, basalt, dust, and a sulfate and silica-rich rock.

Seshadri S. Buehler M. G. Anderson R. C. Kuhlman G. Keymeulen D. Cheung I. W. Schaap M. G.
Applicability of Electrical and Electroanalytical Techniques to Detect Water and Characterize the Geochemistry of Undisturbed Planetary Soils **[#2195]**
Electrical and electroanalytical measurements performed directly in undisturbed soils to identify water-bearing soils and to investigate aqueous soil geochemistry are shown to be feasible in soils with moisture levels expected on Mars.

Lee J. B. Sahai S. K. Paxton S. T. Hadaway S.
Ground Penetrating Radar in Sedimentary Rocks **[#1057]**
This abstract is about how Ground Penetrating Radar (GPR) works, the difficulties in using GPR, and the possibilities of which GPR can be used for.

Burt D. M.
Using an Inexpensive Digital Camera to Photograph Mars-Analog Materials at the Scale of the MER Microscopic Imager, and at Other Scales **[#1705]**
Using the right techniques, many consumer-level digital cameras can be used to take photos analogous to those sent back from Mars by the MER Microscopic Imager.

Instruments I: Gamma-Ray Through Visible and Fancy Lasers

Sklute E. C. Rothstein Y. Dyar M. D. Schaefer M. W. Menzies O. N. Bland P. A. Berry F. J.
Temperature Dependence and Recoil-free Fraction Effects in Olivines Across the Mg-Fe Solid Solution **[#1888]**
Measurements of temperature dependence of synthetic olivines with compositions across the Mg-Fe solid solution are used to calculate recoil-free fractions.

Agresti D. G. Dyar M. D. Schaefer M. W.
MERView: A New Computer Program for Easy Display of MER-acquired Mössbauer Data **[#1941]**
MER Mössbauer data in the PDS are in a form unfamiliar to most spectroscopists, with time and effort required to convert to a more user-friendly form. A new Windows-based computer program, MERView, does this conversion quickly and conveniently.

Rothstein Y. Sklute E. C. Dyar M. D. Schaefer M. W.
Effects of Variable Temperature on Mossbauer Data Acquisition: Laboratory-based and MER a Results **[#2216]**
The effects of variable temperature and short duration run times on Mossbauer spectra are considered, both on the basis of laboratory data and of released MER A results.

Pirard B. d'Uston C. Maurice S. Gasnault O.
Performance Limits of New Generation Scintillators for Planetary Gamma-Ray Spectroscopy **[#2187]**
Performances of new scintillators such as $LaBr_3$:Ce are evaluated in terms of spectral resolution for use in planetary gamma-ray spectroscopy.

Wiens R. Maurice S. Bridges N. Clark B. C. Cremers D. A. Herkenhoff K. E. Kirkland L. E. Mangold N. Manhés G. Mauchien P. McKay C. P. Newsom H. Poitrasson F. Sautter V. d'Uston C. Vaniman D. Shipp S.
ChemCam Science Objectives for the Mars Science Laboratory (MSL) Rover **[#1580]**
ChemCam consists of two remote sensing instruments for the 2009 MSL rover. The LIBS instrument provides elemental composition data on samples within 13 m of the rover. The Remote Micro-Imager provides the highest resolution images 2 m to infinity.

Harris R. D. Cremers D. A. Khoo C. Benelli K.
LIBS-based Detection of Geological Samples at Low Pressures (<0.0001 torr) for Moon and Asteroid Exploration **[#1796]**
LIBS was studied for the analysis of geological samples at pressures ~0.0003 torr to simulate the Moon and asteroids. Analytical lines, calibration curves, and detection limits were determined for *in situ* and stand-off analysis at 5.3 meters.

Radziemski L. J. Cremers D. A. Benelli K. Khoo C. Harris R. D.
LIBS-based Detection of As, Br, C, Cl, P, and S in the VUV Spectral Region in a Mars Atmosphere **[#1747]**
LIBS was studied for the detection of As, Br, C, Cl, P, S using the vacuum ultraviolet spectral region. Analytical lines, calibration curves, and detection limits were determined and the effect of Mars atm. CO_2 on the analysis was determined.

Wiens R. C. Thompson J. Sharma S. Misra A. K. Barefield J. Clegg S. Steele S. Newsom H. Sallé B. Maurice S.
Remote LIBS Analyses of Zagami and DAG 476 Martian Meteorites **[#2209]**
We investigate the ability of Laser Induced Breakdown Spectroscopy, recently selected for the 2009 MSL rover, to remotely determine differences between basaltic rock types on Mars by analyzing two different shergottite meteorites from Mars.

Sallé B. Mauchien P. Lacour J.-L. Maurice S. Wiens R. C.
Laser-induced Breakdown Spectroscopy: A New Method for Stand-Off Quantitative Analysis of Samples on Mars **[#1693]**
ChemCam (Laser-Induced Breakdown Spectroscopy + Micro-Imaging) is an instrument selected for the MSL rover scheduled for launch in 2009. We present the capabilities of the LIBS method for standoff analysis of geological samples in Martian conditions.

Thompson J. Wiens R. C. Sharma S. Lucey P. G. Misra A. K.
Combined Remote LIBS and Raman Spectroscopy Measurements **[#1517]**
Presentation of a combined data set of remote LIBS and Raman Spectroscopy (RS) measurements, showing how the two techniques complement each other. Research toward a combined remote LIBS/RS instrument.

Sridhar N. Dunn D. S. Price K. T. Miller M. A. Pabalan R. T. Abrajano T. A.
Development of a Surface Enhanced Raman Spectroscopy Technique for Identification of Biomarkers on Mars **[#1133]**
The paper describes a new Surface Enhanced Raman Spectroscopy technique for identification of biomarkers on Mars. The technique will enable the identification of femotomolar levels of biomarker molecules in either mineral assemblage or soil.

Misra A. K. Sharma S. K. Lucey P. G.
Single Pulse Remote Raman Detection of Minerals and Organics Under Illuminated Condition from 10 Meters Distance **[#1546]**
A directly coupled portable remote Raman instrument developed by the University of Hawaii has been shown here to identify several minerals, chemicals and organics from a distance of 10 m using a single laser pulse in a well illuminated background.

Kuebler K. Jolliff B. L. Wang A. Haskin L. A.
Extracting Olivine (Fo-Fa) Compositions from Raman Spectral Peak Positions **[#2086]**
This improved olivine calibration builds on our ability to extract petrologic information from a suite of Raman spectra. An ability to extract petrologic data from samples at a landing site will greatly improve our geologic understanding of the site.

Sharma S. K. Wang A. Haskin L. A.
Remote Raman Measurements of Minerals with Mars Microbeam Raman Spectrometer (MMRS) **[#1524]**
We have measured remote Raman spectra of various minerals with a remote Raman receiver interfaced to a miniaturized Mars microbeam Raman spectrometer (MMRS). Our data show that remote Raman measurements can be made with a miniaturized Raman spectrometer such as MMRS.

Pollock H. R. Haring R. E. Sutin B. Mustard J. Boardman J.
Wide Field Imaging Spectrometer (WFIS) — Instrument Design and First Field Tests **[#2310]**
WFIS is a new instrument concept that provides hyperspectral images with a compact system. A flight-like opto-mechanical WFIS engineering model was constructed and has been used to demonstrate data collection techniques and to provide representative data for simulations for future applications.

Edgett K. S. Bell J. F. III Herkenhoff K. E. Heydari E. Kah L. C. Minitti M. E. Olson T. S. Rowland S. K. Schieber J. Sullivan R. J. Yingst R. A. Ravine M. A. Caplinger M. A. Maki J. N.
The MArs Hand Lens Imager (MAHLI) for the 2009 Mars Science Laboratory **[#1170]**
The MArs Hand Lens Imager (MAHLI) will acquire color, high resolution views of martian surface material during the Mars Science Laboratory (MSL) mission, launching in 2009.

Malin M. C. Bell J. F. III Cameron J. Dietrich W. E. Edgett K. S. Hallet B. Herkenhoff K. E. Lemmon M. T. Parker T. J. Sullivan R. J. Sumner D. Y. Thomas P. C. Wohl E. E. Ravine M. A. Caplinger M. A. Maki J. N.
The Mast Cameras and Mars Descent Imager (MARDI) for the 2009 Mars Science Laboratory **[#1214]**
The MastCam and MARDI will be used to explore the geology and geomorphology of the MSL landing site. MastCam and MARDI are both capable of high-definition video.

Mungas G. S. Beegle L. W. Boynton J. Sepulveda C. A. Fisher T. A. Balzer M. A. Sobel H. R. Deans M. Lee P.
CHAMP — Camera, Handlens, and Microscope Probe **[#2045]**
CHAMP (Camera, Handlens And Microscope Probe) is a novel field microscope capable of color imaging with continuously variable spatial resolution from infinity imaging down to diffraction-limited microscopy (3 μm/pixel).

Farrand W. H. Merényi E. Murchie S. Barnouin-Jha O. S.
Spectral Class Distinctions Observed in the MPF IMP SuperPan Using a Self Organizing Map **[#2009]**
Examination of the Imager for Mars Pathfinder (IMP) SuperPan with a Self Organizing Map ANN indicates spectral variability within previously identified physical classes and new insights into class distribution in the near and far field.

Maurice S. Wiens R. Manhès G. Cremers D. A. Barraclough B. L. Bernardin J. Bouyé M. Cros A. Dubois B. Durand E. Hahn S. Kouach D. Lacour J.-L. Landis D. Moore T. Parès L. Platzer J. Saccoccio M. Sallé B. Whitaker R.
ChemCam Instrument for the Mars Science Laboratory (MSL) Rover **[#1735]**
ChemCam is an active remote sensing instrument selected for the MSL project to investigate details of the Martian geochemistry.

Crowther S. A. Mohapatra R. K. Turner G. Blagburn D. J. Gilmour J. D.
Characteristics and Applications of RELAX, an Ultrasensitive, Resonance Ionization Mass Spectrometer for Xenon **[#1723]**
We report the features and characteristics of RELAX — Refrigeration Enhanced Laser Analyser for Xenon — the most sensitive resonance ionisation mass spectrometer currently available for determination of xenon isotope ratios.

Anderson F. S. Whitaker T. Miller G. Young D. Mahoney J. Norman M. French L.
A LASER RIMS Instrument to Date Igneous Rocks Using Rb-Sr and Measure Elemental Chemistry **[#1843]**
We are developing a laser ablation (LA) resonance ionization (RI) mass spectrometer (MS) under PIDDP to make *in situ* measurements of rock age and geochemistry on bodies with rocky surfaces.

Venus

Elkins-Tanton L. T. Hess P. C. Smrekar S. E. Parmentier E. M.
Volcanism and Volatile Recycling on Venus from Lithospheric Delamination **[#1893]**
Lithospheric delamination on Venus can produce low- and high-viscosity lavas, consistent with surface observations, and can refertilize the mantle. Delamination reduces the mantle melting temperature with time and encourages catastrophic resurfacing.

Grosfils E. B. Drury D. E. Hurwitz D. M. Kastl B. Long S. M. Richards J. W. Venechuk E. M.
Geological Evolution of the Ganiki Planitia Quadrangle (V14) on Venus **[#1030]**
Here we summarize our ongoing analysis of the complex material unit stratigraphy in V14 and some of the major implications for the formation and evolution of this part of Venus.

Venechuk E. M. Hurwitz D. M. Drury D. E. Long S. M. Grosfils E. B.
Analysis of the Tectonic Lineaments in the Ganiki Planitia (V14) Quadrangle, Venus **[#1047]**
We analyzed compressive and extensional tectonic lineaments from the Ganiki Planitia (V14) Quadrangle, Venus to determine relative trends regarding orientation and length. We compared the trends to synthesize a stress history of the quadrangle.

Richards J. Hardin J. Grosfils E. B.
Classification of Geological Material Units in the Ganiki Planitia Quadrangle (V14) of Venus Using Statistical Clustering Methods **[#1115]**
Using mixture models and the expectation-maximization (EM) algorithm, we perform statistical clustering with the numerical data of radar backscatter and four physical property data sets to analyze an existing geologic map of the V14 quadrangle of Venus.

Ivanov M. A. Head J. W. III
Geological Mapping of Quadrangles V-3, V-7, and V-57, Venus: Preliminary Results **[#1062]**
Preliminary results of geological mapping in three quadrangles (V-3, V-7, V-57) are presented.

McColley S. M. Head J. W. III
Venus Geologic Mapping: Insights into Crustal Evolution on Local, Regional, and Global Scales **[#1405]**
A discussion of high resolution mapping results from within the Lada Terra quadrangle and the connection between geologic observations and geodynamic models.

Oshigami S. Namiki N.
Cross-Sectional Profile of Baltis Vallis Channel on Venus: Reconstruction from Magellan SAR Brightness Data **[#1555]**
We develop a new method to reconstruct small scale topography from brightness of SAR images, and reconstruct cross-sectional profiles of Baltis Vallis. The results indicate that Baltis Vallis have been formed by mechanical erosion in general.

Carter L. M. Campbell D. B. Campbell B. A.
Physical Properties of Volcanic Deposits on Venus from Radar Polarimetry **[#1745]**
Arecibo dual-polarization maps are compared to Magellan images and emissivity data to investigate the physical properties of volcanic deposits in shield fields and highland areas.

Lang N. P. Hansen V. L.
Venusian Channel Formation as a Subsurface Process **[#2320]**
We propose the alternative hypothesis that some channels form as the result of a subsurface fluid eroding overlying material.

Hansen V. L.
New Observations of Crustal Plateau Surface Histories, Venus: Implications for Crustal Plateau Hypotheses **[#2000]**
Geohistories documented for four crustal plateaus surface presents challenges to both downwelling and plume hypotheses of plateau formation, and lead to a third hypothesis, plateau formation involving crystallization of a huge lava pond.

McDaniel K.   Hansen V. L.
Circular Lows, a Genetically Distinct Subset of Coronae? **[#2367]**
We mapped several circular lows, coronae marked by amphitheater-like depressions to evaluate models of formation. These features are not easily accommodated by a diapiric model and suggest that coronae may form by more than one mechanism.

Hoogenboom T.   Martin P.   Houseman G. A.
Elastic Thickness Estimates for Coronae Associated with Chasmata on Venus **[#1923]**
We investigate the relationship between the local elastic lithospheric thickness and the relative ages of coronae on Venus in an attempt to further understand corona and chasmata formation/evolution.

Smrekar S. E.   Anderson F. S.
Global Admittance Estimates of Elastic and Crustal Thickness of Venus: Results from Top, Hot Spot, and Bottom Loading Models **[#1804]**
A global admittance map is classified into 35 admittances classes and used to estimate crustal and elastic thickness from top and bottom loading models, providing a map of lithospheric properties. Small scale (~1000 km) variations are abundant.

Törmänen T.   Aittola M.   Kostama V.-P.   Raitala J.
Distribution and Classification of Multiple Coronae on Venus **[#1640]**
We have conducted a new survey of multiple coronae on Venus from Magellan images and topographic data. We identified 70 multiple coronae. Results from study of distribution, topographic setting and morphological characteristics are presented.

Stoddard P. R.   Jurdy D. M.
Comparing Topographic Profiles on Venus and Earth **[#2247]**
We compare topographic profiles from Venus chasmata and regions with terrestrial profiles of rift systems and hotspots. Long-wavelength correlations can be made, indicating probable similarities in deep-rooted thermal processes.

Leitner J. J.   Firneis M. G.
Why Earth-like Plate-Recycling Cannot Operate on Venus at Present: A Theoretical Estimation of Trench Pull and Ridge Push **[#1058]**
The theoretical power of trench pull and ridge push forces on Venus has been estimated from a 2D model and resulted in an explanation for the lack of recent plate-recycling processes during the last 500 million years.

Purdie P.   Petford N.
Addams Crater, Venus: Outflow Analogous with a Submarine Debris Flow? **[#1044]**
The extraordinary outflow length and morphology of Addams crater deposits are compared with the Saharan submarine debris flow off Northwest Africa. Vapor cloud modelling and comparison of sonar data with radar images suggest a possible similar origin for the Addams crater outflow deposits.

Bondarenko N. V.   Kreslavsky M. A.   Head J. W. III
North-South Roughness Anisotropy on Venus: Magellan Altimeter Data Revisited **[#1236]**
Shift of the strongest radar altimeter echo from nadir is used to map north-south small-scale slope asymmetry. We compare the asymmetry features with geology. The asymmetry map is useful for studies of surficial deposits and their evolution.

Kreslavsky M. A.   Ford P. G.   Pettengill G. H.   Head J. W. III
New Results from the Magellan Bistatic Radar Experiment **[#1568]**
Polarization of bistatic radar echo gives unambiguous information about electromagnetic properties of the surface material. We report on new results from 1993 Magellan bistatic radar experiment on Venus.

Long S. M.   Grosfils E. B.
Quantitative Analysis of Venus Radar Backscatter Data in ArcGIS **[#1032]**
Here we present methods for performing quantitative analysis of Magellan radar backscatter data from the Ganiki Plantia (V14) quadrangle using ArcGIS 9. This allows for rigorous comparison of mapped units, and yields insight into geologic processes.

Morgan P.   Reyes C.   Smrekar S. E.
A Prototype Flux-Plate Heat-Flow Sensor for Venus Surface Heat-Flow Determinations **[#1454]**
Episodic resurfacing of Venus predicts high heat loss followed by decreasing heat flow. At present, several hundred Ma since the last resurfacing, heat flow should be low. A thermal flux-plate sensor has been designed to test this prediction.

Lognonné P.   Occhipinti G.   Garcia R.
Seismic Interior/Atmospheric Coupling on Venus **[#2274]**
A large coupling between the interior and the atmosphere is shown, leading to an escape of 15% of the energy of seismic surface waves in the atmosphere. Such coupling can be used to detect seismic signals from future Venus orbiter and must also be taken into account in Venus' spin evolution theories.

Johnson N. M. Fegley B. Jr.
Phlogopite Decomposition, Water, and Venus **[#1992]**
We present our initial results on the decomposition rate of phlogopite mica and the implications it holds for Venus.

Astrobiology

Archer D. Jr. Smith P.
Searching for the Missing Martian Organics with the Mars Phoenix Scout Mission **[#1598]**
Recent theories have called into question the conclusion that there are no surface organics on Mars. It is now believed that simple organics could be formed during the oxidative decay of more complex organics. The Phoenix lander has the ability to detect these molecules, if present.

Mahaffy P. R. Brinckerhoff W. B. Buch A. Cabane M. Coll P. Demick J. Glavin D. P. Navarro-Gonzalez R.
Measurement Protocols for In Situ Analysis of Organic Compounds at Mars and Comets **[#2224]**
We explore *in situ* techniques for the determination of the abundance and chemical and isotopic composition of organic molecules in comets and those that might be found in protected environments at Mars as a first step toward understanding prebiotic chemistries on these solar system bodies.

Skelley A. M. Scherer J. R. Aubrey A. D. Grover W. H. Ivester R. H. C. Ehrenfreund P. Grunthaner F. J. Bada J. L. Mathies R. A.
Sensitive Amino Acid Composition and Chirality Analysis with the Mars Organic Analyzer (MOA) **[#1109]**
The Mars Organic Analyzer (MOA) is a portable system for amino acid analysis that consists of a compact instrument and a novel multi-layer CE microchip. The MOA has been successfully field tested on representative soil samples.

Glavin D. P. Aubrey A. Dworkin J. P. Botta O. Bada J. L.
Amino Acids in the Antarctic Martian Meteorite MIL03346 **[#1920]**
Investigations of the Antarctic martian meteorite MIL03346 using high performance liquid chromatography and liquid chromatography time of flight mass spectrometry revealed that trace levels of amino acids are present.

Suzuki A. Kebukawa Y. Nakashima S. Keller L. P. Zolensky M. E. Nakamura T.
Infrared Micro-Spectroscopy of Organic and Hydrous Components in Some Antarctic Micrometeorites **[#1176]**
IR micro-spectroscopy of aliphatic and hydrous components of AMMs suggests that this type of study can be a possible classification method for micrometeorites. Some AMMs show distinct characteristics for these components.

Bonal L. Quirico E. Montagnac G. Reynard B.
Laser-induced Fluorescence: Potential Interests for Immature Organic Matter Characterization **[#1858]**
Preliminary results of Laser Induced Fluorescence on chondrites, kerogens and tholins show that the signal is sensitive to the composition and to the structure of the material.

Court R. W. Sephton M. A. Parnell J. Gilmour I.
The Combustion Characteristics and Stable Carbon Isotopic Compositions of Irradiated Organic Matter: Implications for Terrestrial and Extraterrestrial Sample Analysis **[#1845]**
Exposure to ionizing radiation causes the mean combustion temperature of naturally occurring, solid, terrestrial organic matter, derived from the radiation-induced polymerization of methane, to increase.

Kebukawa Y. Nakashima S. Zolensky M. E.
In-Situ Heating Decrease Kinetics of Aliphatic Hydrocarbons in Tagish Lake Meteorite by Micro-FTIR **[#1146]**
Kinetic heating experiments of organic material in the Tagish Lake chondrite were conducted *in situ* under a micro-FTIR. Two types of aliphatic C-H groups were revealed, one thermally fragile and the other being significantly more refractory.

Gerasimov M. V. Safonova E. N.
Impacts of Large Meteorites as a Possible Source of Complex Organic Species on Titan **[#1066]**
Experimental modeling proves that hypervelocity impacts of large meteorites on Titan's surface produce complex organic species (up to C_{30}).

Brinckerhoff W. B. Managadze G. G. Chumikov A. E. Managadze N. G.
Processing and Synthesis of Pre-Biotic Chemicals in Hypervelocity Impacts **[#1377]**
We describe recent studies of the possible synthesis and processing of pre-biotic chemicals in hypervelocity dust impacts using pulsed laser based simulations of the impact plasma and reflectron time-of-flight mass spectrometry.

Nuth J. A. III Johnson N. M.
Protostars are Nature's Chemical Factories **[#1849]**
Many grain types act to promote the surface mediated conversion of molecular hydrogen, nitrogen and CO into organic molecules. Recent work demonstrating that inner nebular materials can flow back into the outer nebula ensure that some fraction of this product is incorporated into planetesimals.

Saha C. P. Bryson C. E. Sarrazin P. Blake D. F.
PoDS: A Powder Delivery System for Mars In-Situ Organic, Mineralogic and Isotopic Analysis Instruments **[#1575]**
PoDS is a Powder Delivery System intended to satisfy the collection, processing and distribution requirements of powder samples for Mars *in situ* mineralogic, organic and isotopic measurement instruments.

Martín-Gago J. A. Mateo-Martí E. Prieto-Ballesteros O. Atienza C. Sobrado J. M. Gómez-Elvira J.
A New Simulation Chamber for Studying Planetary Environments **[#1625]**
We present a versatile planetary simulation chamber able to reproduce atmosphere and sample temperature for most of the planets. It has been especially developed to make feasible *in situ* irradiation and characterization of the sample.

Mateo-Marti E. Martín-Gago J. A. Prieto-Ballesteros O. Atienza C. Sobrado J. M. Gómez-Elvira J.
An Experimental Set-Up for Studying the Chemical Effect of Irradiation on Different Planets **[#1624]**
We present an overview of the technical capabilities of a recently build experimental system for simulating the environment of different planetary bodies and the chemical effect of irradiation from different sources.

Hurowitz J. A. Tosca N. J. McLennan S. M. Schoonen M. A. A.
Mechanically Produced Radical Species at Silicate Surfaces and the Oxidant in Martian Soils **[#1991]**
The silicate minerals present in basalt are shown to produce oxidizing species in solution after crushing. These results may provide an explanation for the reactive, oxidizing nature of the Martian soils as observed by the Viking Labeled Release and Gas Exchange experiments.

Duong T. A. Kanik I.
Classification of Ion Mobility Data Using the Neural Network Approach **[#2231]**
In this work, the ion mobility spectral data, obtained from electrospray ionization ion mobility spectrometer system, are used as input data for CEP neural network code to learn and validate.

Weinstein S. Pane D. Warren-Rhodes K. Cockell C. Ernst L. A. Minkley E. Fisher G. Emani S. Wettergreen D. S. Wagner M. Cabrol N. A. Waggoner A. S.
Use of a Novel Rover-mounted Fluorescence Imager and Fluorescent Probes to Detect Biological Material in the Atacama Desert in Daylight **[#1494]**
We deployed our fluorescence imaging system which detects fluorescence signals from sparse microorganisms and biofilms on Carnegie Mellon University's autonomous rover Zoë. The results of the 2004 Atacama Desert field season, in Chile, are discussed.

Piatek J. L. Moersch J. E. Wyatt M. Rampey M. Cabrol N. A. Wettergreen D. S. Whittaker R. Grin E. A. Chong Diaz G. Cockell C. Coppin P. Dohm J. M. Fisher G. Hock A. N. Marinangeli L. Minkley N. Ori G. G. Waggoner A. Warren-Rhodes K. Weinstein S. Apostolopoulos D. Smith T. Wagner M. Stubb K. Thomas G. Glasgow J.
Spectroscopic Results from the Life in the Atacama (LITA) Project 2004 Field Season **[#1563]**
Analysis of spectroscopy datasets from rover field tests in the Atacama Desert (Chile), focusing on the composition of the surface and identification of potential habitats for life.

Wettergreen D. Cabrol N. A. Whittaker W. Chong-Diaz G. Calderón F. Heys S. Jonak D. Lüders A. Moersch J. E. Pane D. Smith M. Stubbs K. Teza J. Tompkins P. Villa D. Williams C. Wagner M. Waggoner A. Weinstein S. Wyatt M.
Robotic Technologies for Surveying Habitats and Seeking Evidence of Life: Results from the 2004 Field Experiments of the "Life in the Atacama" Project **[#2316]**
The Life in the Atacama project is surveying habitats and mapping the distribution of life in regions of the Atacama Desert. The project seeks to develop robotic technologies and exploration methods that are necessary for the long-distance traverse essential to the investigation.

Dohm J. M. Cabrol N. A. Grin E. A. Moersch J. E. Chong Diaz G. Cockell C. Coppin P. Fisher G. Hock A. N. Marinangeli L. Minkley N. Ori G. G. Piatek J. L. Warren-Rhodes K. Weinstein S. Wyatt M. Smith T. Wagner M. Stubb K. Thomas G. Glasgow J.
Life in the Atacama — Year 2: Geologic Reconnaissance Through Long-Range Roving and Implications on the Search for Life **[#1579]**
The Life in the Atacama-2004 project, which included geological, morphological, and mineralogical mapping through combined satellite, field-based, and microscopic perspectives and long-range roving, led to the localization of potential habitats.

Battler M. Stoker C.
Searching for Life Underground: An Analysis of Remote Sensing Observations of a Drill Core from Rio Tinto, Spain for Mineralogical Indications of Biological Activity **[#2392]**
A subsurface chemoautotrophic biosphere has been identified in Spain, and a similar one may exist on Mars. This project attempted to identify biosignatures in a Rio Tinto drill core, using only remote sensing data.

Stoker C. R. Lemke L. G. Cannon H. Glass B. J. Dunagan S. Zavaleta J. Miller D. Gómez-Elvira J.
Field Simulation of a Drilling Mission to Mars to Search for Subsurface Life **[#1537]**
We describe a simulation of a Mars drilling mission using a robotic drill and sample handling system, and a science payload including surface and downhole remote sensing and life detection instruments that takes place in Fall 2005.

Sharma S. K. Misra A. K. Lucey P. G. McKay C. P.
A Compact Instrument for Remote Raman and Fluorescence Measurements to a Radial Distance of 100 M **[#2058]**
We have developed a combined remote inelastic scattering (Raman) and laser-induced fluorescence emission (LIFE) compact instrument capable of providing accurate information about minerals, organic and biogenic materials to a radial distance of 100 m.

Stone W. C. Greenberg R. J. Durda D. D. Franke E. A.
The DEPTHX Project: Pioneering Technologies for Exploration of Extraterrestrial Aqueous Channels **[#2206]**
This project is developing an autonomous vehicle for underwater exploration of confined channels, with sensors for life detection, in preparation for eventual missions to extraterrestrial aqueous environments, e.g., suboceanic hydrothermal vents or crustal cracks on Europa.

Shirley J. H. Carlson R. W. Zimmerman W. F. Rivellini T. P. Sabahi D.
To Land on Europa **[#2197]**
Scientific and technical issues arising for a JIMO Europa lander include questions of surface contamination by propellant residues, lander survival in rough terrains, and the problem of subsurface sample acquisition to depths of ~1 m.

Parnell J. Baron M. Cockell C. S.
Endolithic Colonization of Fluid Inclusion Trails in Mineral Grains **[#1285]**
Many scenarios for the colonization of planetary surfaces by microbial life involve endoliths. This study records microbial mass along fluid inclusion trails (healed microfractures) in quartz grains.

Brown I. I. Mummey D. Cooksey K. E. McKay D. S.
Iron-tolerant Cyanobacteria as a Tool to Study Terrestrial and Extraterrestrial Iron Deposition **[#1159]**
A new genus of cyanobacteria exhibiting elevated dissolved iron tolerance and the ability to precipitate hematite on its exopolymeric sheath is described in this study as a tool to study terrestrial and extraterrestrial iron deposition.

Blackhurst R. L. Roberts D. Jadbubansa P. Genge M. J. Grady M. M.
Cryptoendolith Colonization of Diverse Substrates (1): Cultivation and Characterization **[#1067]**
We are investigating whether cryptoendolithic microorganisms are able to colonize diverse substrates through biogenic weathering. This first part of the study involves the cultivation and characterization of microbial consortia from Antarctic sandstone habitats.

Mendez C. Garza E. Gulati P. Morris P. A. Allen C. C.
Isolation and Identification of Microorganisms in JSC Mars-1 Simulant Soil **[#2360]**
JSC Mars-1 was assayed for the presence of bacteria. Molecular analysis of the soil revealed several species of bacteria.

Schulze-Makuch D. Irwin L. N. Lipps J. H. LeMone D. Dohm J. M.
Scenarios for the Evolution of Life on Mars **[#1728]**
Here, we relate the possible evolution of life on Mars to the Martian environmental history; and conclude on strategies for survival ranging from psychrophilic life to lifestyles that may use alternating cycles between dormant and active life forms.

Fairén A. G. Amils R.
Martian Acidic Environments Through Time: Opportunities for Life **[#1085]**
Hemispheric acidic oceans on Mars represent a localized stage in the Noachian. Shallow surface acidic water have also been flowing recurrently on several martian locations during the Hesperian and the Amazonian. Life may have gained a foothold in these environments.

Fisk M. R. Storrie-Lombardi M. C. Joseph J.
Elemental Abundance Distributions in Basalt Clays and Meteorites: Is It a Biosignature? **[#2275]**
Bayesian classification algorithms distinguishes biotic and abiotic alteration in sub-oceanic basalts using elemental abundance data. The data address the more general question of utilizing elemental abundance distribution in clays as a valid biosignature for analysis of meteorites.

Brunner B.   Coleman M. L.
$\Delta^{17}O$ of Martian Sulfate: Assessment as a Tool to Recognize the Impact of Biological Sulfur Cycling on Mars **[#1932]**
Martian sulfate deposits are an archive of past or present biotic processes even in the absence of traces of extraterrestrial life. We assess the analysis of mass independent isotope fractionation of oxygen in sulfate as a biosignature.

Lauer H. V. Jr.   Ming D. W.   Golden D. C.
Thermal Characterization of Fe_3O_4 Nanoparticles Formed from Poorly Crystalline Siderite **[#2153]**
In this study, we describe the synthesis or a suite of sub micron (<200 nm) magnetite particles. We then analyze them thermally using scanning differential calorimetry and crystal phase-wise by X-ray diffraction.

Bjonnes E. E.   Lindsay J. F.
The Depositional Setting of the Earth's Earliest Sedimentary Rocks **[#1821]**
Some of the oldest sedimentary rocks come from the Australian Coucal Formation. We investigate the composition and texture of the basalt and chert layers within this formation and discuss their implications for their depositional setting.

Trail D.   Mojzsis S. J.   Harrison T. M.
Hadean Crustal Processes Revealed from Oxygen Isotopes and U-Th-Pb Depth Profiling of Pre-4.0 Ga Detrital Zircons from Western Australia **[#2223]**
Identification of zircons up to 4.37 Ga, U-Th-Pb zircon depth profiling, and oxygen isotopes on >3.8 Ga zircons.

Lerman L.
Could Martian Strawberries Be? — Prebiotic Chemical Evolution on an Early Wet Mars **[#2317]**
The universality of chemical physics dictates the ubiquity of bubbles, aerosols, and droplets on planets with water and simple amphiphiles. Their ability to functionally support prebiotic chemical evolution seems critical: on the early Earth and Mars, and quite likely for Titan and Europa.

Lerman L.
Do Martian Blueberries Have Pits? — Artifacts of an Early Wet Mars **[#2210]**
Early Martian weather cycles would have supported organic chemical self-organization, the assumed predecessor to an independent "origin" of Martian life. Artifacts of these processes are discussed, including the possibility that Martian blueberries nucleated around organic cores.

Smythe W. D.   Lopes R. M.   Pieri D. C.   Hall J. L.
An Approach to In-Situ Observations of Volcanic Plumes **[#2296]**
Aerobots enable *in situ* measurement of volcanic plumes — which play a profound role in the evolution of life. Plume measurements are vital for understanding how volcanos work and mitigating volcanic hazards. Plume aerobots can prototype platforms for Titan exploration.

Education and Public Outreach: K–12 Programs, Professional Development, and Informal Education

Urquhart M. L.   Bober K. M.
Impacting Classroom Teachers Through Long-Term Professional Development **[#1480]**
Comparisons between the impact on teachers and their classrooms of our short-term teacher workshops (a common form of E/PO) and our long-term professional development for teachers that integrate space science E/PO into content-rich courses.

Higbie M. A.   Treiman A. H.   Kiefer W. S.   Shipp S. S.
Using a Field Experience to Build Understanding of Planetary Geology **[#2377]**
The Lunar and Planetary Institute hosts yearly field-based workshops using Earth analogs to build understanding of planetary geology for educators.

Milford C. R.   Marek M.
Mars ROCKS! in North Dakota, Solar System Ambassador Program in North Dakota **[#2302]**
Activities and programs of the North Dakota NASA/JPL Solar System Ambassador outreach project.

Grier J. A.   Reinfeld E. L.   Dussault M. E.   Steel S. J.   Gould R.
The Solar System in Its Universal Context: Ideas, Misconceptions, Strategies and Programs to Enhance Learning **[#1954]**
Preliminary analysis of our data relevant to learning about the solar system relating to its context within the larger universe. Presentation of educational strategies, products and experiences that enhance this learning.

Bowman C. D.   Aubin B.   Bebak M.   Smith C.   Stocco K.
Students and Teachers Help Scientists on Mars **[#2113]**
During the Mars Exploration Rover mission, thirteen teams of high school students and teachers from around the country paired with MER science team members to help explore Mars through NASA's Athena Student Interns Program.

Aubele J. C. Stanley J. A. Aragon J. Grochowski A. Jones K. L. Crumpler L. S.
Increasing Science Literacy and Public Support for Planetary Science: MER Museum Exhibits, Educational Programming and Public Outreach at the NM Museum of Natural History & Science and Lodestar Astronomy Center **[#2343]**
The New Mexico Museum of Natural History and Science and LodeStar Astronomy Center created and provided a complete range of MER-related outreach and educational programs targeted to teachers, students, families, and the general public.

Klug S. L. Christensen P. R. Rogers L. Gorelick N. Rogers D. Jones B. Brindley T. Ki J. Rogers T. Staley L. Scanlan K. Daub G.
Rock Around the World: Extending a Global Reach to Involve Students in Science Using Infrared Research at Mars **[#2371]**
The Rock Around the World Program has coupled the excitement of learning about Earth and Mars with helping to contribute to this knowledge on a personal basis. This is a world-wide program.

Peterson C. A. Smith G. A. Hawke B. R.
The Aristarchus Plateau: The Next Step in Human Exploration of the Moon **[#1673]**
The Aristarchus plateau is a good location for a lunar base. We have developed a poster that can be used for education about the next steps in lunar exploration, distributed as an electronic file, and printed as a series of 8 1/2 × 11 inch pages.

Education and Public Outreach: Visualization and Data Integration

Roark J. H. Masuoka C. M. Frey H. V. Keller J. Williams S.
Topography Analysis and Visualization Software Supports a Guided Comparative Planetology Education Exhibit at the Smithsonian's Air and Space Museum **[#1838]**
The Planetary Geodynamics Laboratory designed, produced and recently delivered a "museum-friendly" version of GRIDVIEW, a grid visualization and analysis application, to the Smithsonian's National Air and Space Museum.

Bleamaster L. F. III Bhartia V. V. Crown D. A.
Visualization of Mars Data Sets: Views from Hellas Basin **[#2164]**
A comprehensive Geographical Information Systems database and software package provides the opportunity to produce new 3-D perspective views of geologic relationships for use in our Mapping Planetary Surfaces (MAPS) education and public outreach project.

Uno J. Mikouchi A. K.
Virtual Reality Technology as a Tool to Enhance Collaboration Between Space Exploration and Public Outreach: The Case Using the Mars Exploration Rover Images **[#2152]**
We present computer-based outreach material developed by the virtual reality (VR) team at JAXA. It shows that VR technology for human space flight can be a strong tool to produce a unique material for the public to personalize space exploration.

Cull S. C. Condit C. D.
A Dynamic Digital Map of Mars **[#1383]**
The Dynamic Digital Map of Mars incorporates hundreds of maps, images, and articles with interactive tours, exercises, movies, animations, and class activities. It is designed as a teaching tool for undergraduate science classes.

Meyer B. S.
Online Tools for Astronomy and Cosmochemistry **[#1457]**
We have developed a number of interactive Web-based tools for astronomy and nuclear astrophysics that may be of interest to professional scientists, students, and the general public. These tools are located at http://nucleo.ces.clemson.edu.

Reddy V. Dyvig R. R. Heathcote B. D. Pravec P.
Rotational Studies of Asteroids with Small Telescopes **[#1394]**
Small telescopes (< 1.0 m) can play an important role in minor planet research. We present the results of rotational studies of 1459 Magnya, and Apollo-type PHA 2004 VW14 as examples of research that can be conducted using small telescopes.

Eichhorn G. Accomazzi A. Grant C. S. Henneken E. A. Kurtz M. J. Thompson D. M. Murray S. S.
New Features in the ADS Abstract Service **[#1207]**
The ADS provides free online access to over 4 million abstracts and over 3 million scanned pages of the astronomical, planetary and physics literature, including full text searching and personalized notification (myADS) at http://ads.harvard.edu.

Wednesday, March 16, 2005
ASTEROID SPECTROSCOPY AND MINERALOGY
8:30 a.m. Salon A

Chairs: S. Erard
L. A. McFadden

8:30 a.m. Gaffey M. J. *
The Critical Importance of Data Reduction Calibrations in the Interpretability of S-type Asteroid Spectra **[#1916]**
S-asteroid spectra are especially sensitive to distortion during the reduction of raw data to calibrated spectra. This can lead to major errors in mineralogical interpretations. Two major problems and the procedures to ameliorate them are discussed.

8:45 a.m. Sunshine J. M. * Bus S. J. Burbine T. H. McCoy T. J.
Tracing Oxygen Fugacity in Asteroids and Meteorites Through Olivine Composition **[#1203]**
We present new spectra of well-characterized olivine-rich meteorites and show that olivine Fa# can be accurately inferred from spectra. Using the same approach, new asteroid data are examined to infer the oxygen fugacity of olivine-rich asteroids.

9:00 a.m. Trigo-Rodríguez J. M. * Castro-Tirado A. J. Llorca J.
Evidence of Hydrated 109P/Swift-Tuttle Meteoroids from Meteor Spectroscopy **[#1485]**
Evidence for the possible presence of water in meteoroids released from comet 109P/Swift-Tuttle is presented. A Perseid fireball spectrum obtained during the 2004 campaign shows O and H lines, consistent with the presence of water in the mineral components of the meteoroid.

9:15 a.m. Emery J. P. * Cruikshank D. P. Van Cleve J. Stansberry J. A.
Mineralogy of Asteroids from Observations with the Spitzer Space Telescope **[#2072]**
Thermal emission measurements of the low-albedo Trojan asteroid 624 Hektor indicate a surface mineralogy of fine-grained silicates. We present the data and analysis leading to this conclusion and compare with similar data of Main Belt asteroids.

9:30 a.m. Reddy V. * Hardersen P. S. Gaffey M. J. Abell P. A.
Mineralogy and Temperature-induced Spectral Investigations of A-type Asteroids 246 Asporina and 446 Aeternitas **[#1375]**
We investigated temperature-induced spectral effects on A-asteroid 446 Aeternitas by observing at different heliocentric distances and did not find any change in the olivine feature. Mineralogy of 446 Aeternitas and 246 Asporina is also estimated.

9:45 a.m. Abell P. A. * Gaffey M. J. Landis R. R. Jarvis K. S.
Compositional Investigation of Binary Near-Earth Asteroid 66063 (1998 RO_1): A Potentially Undifferentiated Assemblage **[#2283]**
Near-IR spectra of binary near-Earth asteroid 1998 RO_1 indicate this object may be an undifferentiated assemblage similar to an L-ordinary chondrite, or an assemblage that experienced low partial melting and thus similar to a primitive achondrite.

10:00 a.m. Hardersen P. S. * Gaffey M. J. Abell P. A.
Detailed Mineralogical Characterizations of Four S-Asteroids: 138 Tolosa, 306 Unitas, 346 Hermentaria, and 480 Hansa **[#1240]**
Near-IR spectra were obtained for S-asteroids 138 Tolosa, 306 Unitas, 346 Hermentaria, and 480 Hansa. Spectral band parameters and the resulting mineralogical characterizations suggest that all four asteroids are thermally-evolved and non-chondritic.

10:15 a.m. McFadden L. A. * Goldman N. J. Gaffey M. J. Izenberg N. R.
Evidence for Partial Melting in Reflectance Spectra of 433 Eros **[#1561]**
Near-IR spectra of asteroid 433 Eros analyzed using MGM fitting results compositions indicating partial melting consistent with results from XGRS flown on NEAR. Partial melting had to occur before it was fragmented to its current state and size.

10:30 a.m. Erard S. * Forni O. Ollivier M. Dotto E. Roush T. Poulet F. Müller T.
The 2004 Opposition of Ceres Observed with Adaptive Optics on the VLT **[#1388]**
Ceres has been observed with NACO on the VLT. Imaging and spectroscopy were performed in the 1.1–4.1 μm range with spatial resolution up to 50 km. The aim is 1) to provide the first IR map of Ceres 2) to map compositional variations at the surface.

10:45 a.m. Li J.-Y. * McFadden L. A. Parker J. Wm. Young E. F. Thomas P. C. Russell C. T. Stern S. A. Sykes M. V.
HST Photometry and Surface Mapping of Asteroid 1 Ceres **[#1345]**
The first spatially resolved, photometrically calibrated surface albedo maps of Ceres are constructed from HST observations at a spatial resolution of 60 km, showing a very uniform surface with a mean V-band SSA of 0.07 ± 2%.

11:00 a.m. Lawrence S. J. * Lucey P. G. Taylor G. J.
Asteroid Modal Mineralogy Using Hapke Mixing Models: Testing the Utility of Spectral Lookup Tables **[#2362]**
The effectiveness of a Hapke-based spectral mixing model used in conjunction with a spectral lookup table is discussed.

11:15 a.m. Foley C. N. * Nittler L. R. Brown M. R. M. McCoy T. J. Lim L. F.
Chromium on Eros: Further Evidence of Ordinary Chondrite Composition **[#2017]**
We have obtained the first determination of an asteroidal Cr abundance by remote-sensing X-ray spectroscopy of Eros. The values determined provide further support for a link between S(IV) asteroids and ordinary chondrite meteorites.

11:30 a.m. Rivkin A. S. * McFadden L. A. Binzel R. P. Sykes M.
Rotationally Resolved Spectroscopy of Vesta in the 2–3 μm Region **[#1811]**
We present spectra from 2001–2004, and show that the northern and southern hemispheres of Vesta are distinct. The northern hemisphere shows evidence of a ~1% band at 3 μm, while the southern hemisphere does not. We suggest the band is due to contamination from carbonaceous impactors.

11:45 a.m. Klima R. L. * Pieters C. M. Dyar M. D.
Pyroxene Spectroscopy: Effects of Major Element Composition on Near, Mid and Far-Infrared Spectra **[#1462]**
Pyroxene composition is used extensively in characterizing the igneous evolution of planets. We present an analysis of a comprehensive set of synthetic pyroxenes from 0.5 to 50 μm to address fundamental constraints of crystal structure on absorption.

Wednesday, March 16, 2005
MER RESULTS I
8:30 a.m. Salon B

Chairs: J. R. Johnson
R. E. Arvidson

8:30 a.m. Squyres S. W. * Athena Science Team
Recent Results from the Spirit Mars Exploration Rover Mission **[#1918]**
This abstract is one of two overview abstracts describing recent results from the Mars Exploration Rover mission. The focus of this abstract is Spirit's exploration of the Columbia Hills.

8:45 a.m. Arvidson R. E. * Squyres S. W. Malin M. C. Poulet F. Bibring J.-P. Langevin Y. Gondet B. Athena Science Teams OMEGA Science Team
Recent Results from the Opportunity Mars Exploration Rover Mission **[#1958]**
The Opportunity rover undertook an extensive campaign of observations at the site of the heat shield impact, both to characterize the shield itself and to examine the shallow subsurface materials excavated by the impact.

9:00 a.m. Bell J. F. III* Arneson H. M. Farrand W. H. Goetz W. Hayes A. G. Herkenhoff K. E. Johnson M. J. Johnson J. R. Joseph J. Kinch K. M. Lemmon M. T. Madsen M. B. McCartney E. Morris R. V. Proton J. Savransky D. Seelos F. Soderblom J. Sohl-Dickstein J. N. Sullivan R. J. Wolff M. J. Athena Science Team
Large Multispectral and Albedo Panoramas Acquired by the Pancam Instruments on the Mars Exploration Rovers Spirit and Opportunity **[#1337]**
The Mars Exploration Rover Pancam instruments have acquired dozens of very large color and "albedo" panoramas during their missions. This abstract summarizes these data products and briefly describes their scientific utility.

9:15 a.m. Christensen P. R. * Wyatt M. B. Glotch T. D. Rogers A. D. Anwar S. Arvidson R. E. Bandfield J. L. Blaney D. L. Budney C. Calvin W. M. Fallacaro A. Fergason R. L. Gorelick N. Graff T. Hamilton V. E. Hayes A. G. Johnson J. R. Knudson A. T. McSween H. Y. Jr. Mehall G. L. Mehall L. K. Moersch J. E. Morris R. V. Smith M. D. Squyres S. W. Ruff S. W. Wolff M. J.
Mineral Composition and Abundance of the Rocks and Soils at Gusev and Meridiani from the Mars Exploration Rover Mini-TES Instruments **[#1276]**
Mini-TES has identified Mg and Ca sulfates and high-silica minerals in the Meridiani outcrops. Spherules are dominantly hematite. Plagioclase/pyroxene/olivine sands occur at both sites. Bounce Rock is a pyroxene-dominated basalt similar to EET79001.

9:30 a.m. Herkenhoff K. E. * Squyres S. Arvidson R. E. Bass D. Bell J. F. III Bertelsen P. Cabrol N. A. Ehlmann B. L. Farrand W. H. Gaddis L. R. Greeley R. Grotzinger J. P. Hayes A. Hviid S. F. Johnson J. R. Jolliff B. L. Kinch K. M. Knoll A. H. Lemmon M. T. Madsen M. Maki J. N. McLennan S. M. Ming D. W. Morris R. Rice J. Richter L. Sims M. Smith P. Soderblom L. Spanovich N. Sullivan R. Weitz C.
Overview of Athena Microscopic Imager Results **[#1778]**
The Athena Microscopic Imagers on the Mars Exploration Rovers continue to obtain excellent data.

9:45 a.m. Gellert R. * Zipfel J. Brückner J. Dreibus G. Lugmair G. W. Rieder R. Wänke H. Klingelhöfer G. Clark B. C. Ming D. W. Yen A. Squyres S. Athena Science Team
Results of the Alpha-Particle-X-Ray Spectrometer on Board of the Mars Exploration Rovers **[#1997]**
We report results of APXS analyses acquired during the MER missions. The chemical compositions of soils, rocks and outcrops provide evidence for evaporate rich sediments and alteration of igneous rocks under aqueous conditions.

10:00 a.m. Klingelhöfer G. * Rodionov D. S. Morris R. V. Schröder C. de Souza P. A. Jr. Ming D. W. Yen A. S. Bernhardt B. Renz F. Fleischer I. Wdowiak T. Squyres S. W. Athena Science Team
MIMOS II on MER — One Year of Mössbauer Spectroscopy on the Surface of Mars: From Jarosite at Meridiani Planum to Goethite at Gusev Crater **[#2349]**
The miniaturized Mössbauer spectrometer MIMOS II is part of payload of the Mars Exploration Rovers Spirit and Opportunity, performing successfully during first year of operation. A summary of the results will be given.

10:15 a.m. Madsen M. B. * Arneson H. M. Bertelsen P. Bell J. F. III Binau C. S. Gellert R. Goetz W. Gunnlaugsson H. P. Herkenhoff K. E. Hviid S. F. Johnson J. R. Johnson M. J. Kinch K. M. Klingelhöfer G. Knudsen J. M. Leer K. Madsen D. E. McCartney E. Merrison J. Ming D. W. Morris R. V. Olsen M. Proton J. B. Rodionov D. Sims M. Squyres S. W. Wdowiak T. Yen A. S.
An Update on Results from the Magnetic Properties Experiments on the Mars Exploration Rovers, Spirit and Opportunity **[#2379]**
We show how the magnetic properties experiments on Spirit and Opportunity provide information on the distribution of magnetic minerals in the dust on Mars, with emphasis on results from Opportunity.

10:30 a.m. Bartlett P. W. * Carlson L. E. Chu P. C. Davis K. R. Gorevan S. Kusack A. G. Myrick T. M. Wilson J. J.
Summary of Rock Abrasion Tool (RAT) Results Pertinent to the Mars Exploration Rover Science Data Set **[#2292]**
The Rock Abrasion Tool (RAT) serves as the sample preparation device on the Mars Exploration Rover payload, grinding a circular spot on the order of millimeters deep into a rock face to remove surface layers, preparing the rock for observation.

10:45 a.m. Farrand W. H. * Bell J. F. III Johnson J. R. Clark B. C. Joliff B. L.
Visible/Near Infrared Spectral Characterization of In Situ Rock Outcrops at Meridiani Planum as Observed by the Mars Exploration Rover Opportunity **[#2082]**
Multispectral observations by the Mars Exploration Rover Opportunity's Pancam are used to characterize spectral variability among the layered rock outcrops examined by the rover. The use of this VNIR spectral data to aid in stratigraphic analysis of the rock outcrops is also described.

11:00 a.m. Johnson J. R. * Arvidson R. E. Bell J. F. III Farrand W. H. Guinness E. A. Johnson M. J. Herkenhoff K. E. Lemmon M. T. Morris R. V. Seelos F. IV Soderblom J. Soderblom L. Squyres S. Wolff M. Athena Science Team
Photometric Observations of Soils and Rocks at the Mars Exploration Rover Landing Sites **[#1815]**
The MER Pancams have acquired multispectral reflectance observations of rocks and soils at different incidence, emission, and phase angles that will be used for photometric modeling of surface materials.

11:15 a.m. Clark B. C. * McLennan S. M. Morris R. V. Gellert R. Jolliff B. L. Knoll A. H. Lowenstein T. K. Ming D. W. Tosca N. J. Christensen P. R. Yen A. Brückner J. Calvin W. M. Farrand W. H. Zipfel J. Gorevan S. Squyres S. W.
Results and Implications of Mineralogical Models for Chemical Sediments at Meridiani Planum **[#1446]**
Outcrops of salt-rich silicic sediments at Meridiani Planum were analyzed using sample preparation via grinding to reveal rock interiors. X-ray fluorescence and Mössbauer analysis are combined with IR spectroscopy to infer mineral composition.

11:30 a.m. Morris R. V. * Ming D. W. Clark B. C. Klingelhöfer G. Gellert R. Rodionov D. Schroeder C. de Souza P. A. Yen A. Athena Science Team
Abundance and Speciation of Water and Sulfate at Gusev Crater and Meridiani Planum **[#2239]**
Combined Mössbauer and APXS data have been used to determine the abundance and speciation of water and sulfate at Gusev crater and Meridiani Planum. The Meridiani outcrop is estimated to have about 7 wt% water equivalent.

Wednesday, March 16, 2005
MARS VOLCANISM AND TECTONISM
8:30 a.m. Salon C

Chairs: H. Hiesinger
L. P. Keszthelyi

8:30 a.m. Bleacher J. E. * Greeley R. Williams D. A. Bentley M. Neukum G. Hauber E. HRSC Co-Investigation Team
Olympus Mons: Inferred Changes in Late Stage Effusive Activity Based on Lava Flow Mapping of Mars Express High Resolution Stereo Camera Data **[#1364]**
Olympus Mons mapping, to estimate the percent of flows emplaced by lava tubes or channels, indicates that late stage activity was typified by channel-forming eruptions with older tube-forming eruptions being more important on the north flank.

8:45 a.m. McGovern P. J. * Morgan J. K.
Spreading of the Olympus Mons Volcanic Edifice, Mars **[#2258]**
Topographic profiles of the Olympus Mons volcanic edifice on Mars suggest that the flanks have spread outward to accommodate growth. We compare models of the volcanic spreading process to observed profiles in order to infer the structure of the edifice.

9:00 a.m. Enevoldsen A. A. * Sakimoto S. E. H. Cooley C. R.
Elevation-dependent Flow Rates on Olympus Mons **[#1595]**
Using MOLA and THEMIS data, we determine the flow rates of small lava flows on Olympus Mons and quantify the differences in flow rates of low- and high-elevation flows. The lowest flow rate we found thus far is 40 m^3/s and the highest is 5800 m^3/s.

9:15 a.m. Hiesinger H. * Head J. W. III Neukum G. HRSC Co-Investigator Team
Rheological Properties of Late-Stage Lava Flows on Ascraeus Mons: New Evidence from HRSC **[#1727]**
We report on estimates of the rheological properties of late-stage lava flows on the eastern flank of Ascraeus Mons, Mars, using HRSC data; we conclude that the lava flows investigated are likely to be basaltic to andesitic in composition.

9:30 a.m. Wilson L. * Shean D. E. Head J. W. III
Subglacial Dike Emplacement on Mars: Radial Ridges Associated with the Pavonis Mons Fan-shaped Deposit **[#1189]**
Ridges radial to Pavonis Mons and underlying the fan-shaped deposit on its NW flank are interpreted to be the remnants of dikes emplaced beneath a cold-based tropical mountain glacier.

9:45 a.m. Murray J. B. * van Wyk de Vries B. Muller J.-P. Neukum G. Page D.
Late Stage Water Eruptions on the Flanks of Large Martian Volcanic Constructs **[#1717]**
Evidence is presented for water eruption at the foot of giant Martian volcanoes, a result of edifice sinking into an icy, incompetent substratum. Analogies with Mt. Haddington, Antarctica, are striking.

10:00 a.m. Garry W. B. * Gregg T. K. P.
Analysis of Downstream Transitions in Morphology and Structure of Lava Channels on Mars **[#2019]**
An analysis of stable, transitional, and dispersed flow zones in Martian lava channels. These zones have been observed in terrestrial lava channels and simulated channels. We present a comparative study of terrestrial, PEG, and Martian channels.

10:15 a.m. Gregg T. K. P. * Crown D. A.
What is Hesperia Planum, Mars? An Examination of Multiple Working Hypotheses **[#1962]**
Hesperia Planum is the type locale for "Hesperian ridged plains" on Mars, and is commonly believed to be composed of flood lavas. However, its surface may not be entirely Hesperian, nor composed of a single material unit. We present alternative interpretations for Hesperia Planum.

10:30 a.m. Keszthelyi L. P. *
Some Simple Models for Rootless Cone Formation on Mars **[#1914]**
Simple calculations and observations of terrestrial analogs suggest that rootless cones on Mars require intimate mixing of liquid lava and water.

10:45 a.m. Okubo C. H. * Schultz R. A.
Evidence of Normal Faulting and Dike Intrusion at Valles Marineris from Pit Crater Topography **[#1008]**
Pit crater chain topography is found to be consistent with causative normal faulting and dike intrusion to the north of the Ius–Melas–Coprates chasmata, while causative normal faulting is the sole process identified to the south of this chasmata.

11:00 a.m. Megé D. * Peulvast J.-P. Masson Ph.
A Planetary Example of Tectonic Inversion: Folding and Thrusting in the Valles Marineris Graben System on Mars **[#1772]**
We describe folding and thrusting in Valles Marineris and propose that they result from sackung.

11:15 a.m. Vidal A. * Mueller K. M. Golombek M. P.
Geometry of Thrust Faults Beneath Amenthes Rupes, Mars **[#2333]**
Amenthes Rupes is a large lobate scarp which deforms a crater at the dichotomy boundary. Shortening estimates from this crater are made and combined with axial surface mapping and mechanical modeling to constrain fault depth.

11:30 a.m. Artita K. S. * Schultz R. A.
Significance of Deformation Band-like Strike-Slip Faults on Mars **[#2225]**
We present new MOLA-, MDIM-, and THEMIS-based observations of strike-slip faults in East Coprates Planum (–19°S to –31°S, 300° to 310°). Our results indicate that strike-slip faults in the southern region behave like deformation bands, structures commonly found in porous, granular materials.

Wednesday, March 16, 2005
CHONDRULES AND CHONDRITES
8:30 a.m. Marina Plaza Ballroom

Chairs: H. C. Connolly Jr.
A. E. Rubin

8:30 a.m. Alexander C. M. O'D. *
Re-Examining the Role of Chondrules in Producing the Elemental Fractionations in Chondrites **[#1348]**
A CI-like component dominates chondrite matrices and carries the most volatile elements. Chondrules are responsible for the elemental fractionations in OCs. Loss of type IA chondrules, and gain of type IA evaporates can explain the compositions of bulk OCs, and type IIA and type B chondrules.

8:45 a.m. Scott E. R. D. * Krot A. N.
Thermal Processing and Accretion of Silicate Dust into Chondrites and Comets **[#2007]**
Matrices of primitive chondrites resemble crystalline and amorphous silicates in IDPs and probably condensed in chondrule-forming regions. This favors shock formation at 2–3 AU and rim accretion after matrix silicates were mixed with sticky organics.

9:00 a.m. Connolly H. C. Jr.* Jones R. H.
Understanding the Cooling Rates Experienced by Type II Porphyritic Chondrules **[#1881]**
We review how the cooling rates of chondrules are determined, what the rates are for type IIA chondrules, and discuss the implications and limitation of the different rates that have been determined.

9:15 a.m. Libourel G. * Krot A. N. Tissandier L.
Gas-Melt Interaction During Chondrule Formation **[#1877]**
The mineralogy, chemistry and isotopic compositions of chondrules in primitive chondrites are inconsistent with their closed-system crystallization and suggest instead that gas-melt interaction played a major role in evolution of chondrule melts.

9:30 a.m. Cohen B. A. Levasseur S. Zanda B. Hewins R. H. * Halliday A. N.
Isotopic Mass Fractionation of Iron in Chondrules, Evaporation or Reduction? **[#1690]**
The nature of Fe-isotopic mass fractionation measured in chondrules is controversial. Reduction experiments of fayalite yielded a strongly fractionated glass along side metal lacking mass fractionation. We argue for a diffusion-controlled fractionation to explain the data.

9:45 a.m. Fedkin A. V. * Grossman L. Ghiorso M. S.
Vapor Pressures and Evaporation Coefficients of Fe, Na and K over Chondrule Composition Melts **[#2273]**
We applied MELTS to published evaporation data on chondrule liquids to get vapor pressures and evaporation coefficients for Na, K and Fe. This approach explains the persistence for many hours of Fe metal and significant FeO in the *Cohen and Hewins* (2004) experiments.

10:00 a.m. Tachibana S. * Huss G. R. Kita N. T. Shimoda H. Morishita Y.
The Abundances of Iron-60 in Pyroxene Chondrules from Unequilibrated Ordinary Chondrites **[#1529]**
Excesses of ^{60}Ni, which correlate with Fe/Ni ratios, have been found in four pyroxene-rich chondrules from unequilibrated ordinary chondrites, Semarkona and Bishunpur. The inferred $(^{60}Fe/^{56}Fe)_0$ for the chondrules range from 2×10^{-7} to 5×10^{-7}.

10:15 a.m. Nakamoto T. * Hayashi M. R. Kita N. T. Tachibana S.
Generation of Chondrule Forming Shock Waves in Solar Nebula by X-Ray Flares **[#1256]**
Our Magneto-Hydrodynamics numerical simulations show that chondrule forming shock waves, which are appropriate for chondrule formation, are generated in the upper region of the solar nebula by X-ray flares and expanding magnetic bubbles.

10:30 a.m. Miura H. * Nakamoto T.
Appropriate Shock Waves for Chondrule Formation: Heating Rate and Cooling Rate Constraints **[#1248]**
In order to produce chondrules, the heating mechanism should satisfy at least two constraints; the rapid heating and the appropriate cooling rate. Shock waves generated by the X-ray flares seem to satisfy both constraints.

10:45 a.m. Zolotov M. Yu. * Mironenko M. V. Shock E. L.
Aqueous Alteration and Hydrogen Generation on Parent Bodies of Unequilibrated Ordinary Chondrites: Thermodynamic Modeling for the Semarkona Composition **[#2271]**
Aqueous alteration is modeled in conjunction with changes in volumes and pressure along with reaction progress. The results are consistent with redox and hydration/dehydration pathways in chondrites.

11:00 a.m. Brandon A. D. * Puchtel I. S. Humayun M. Zolensky M.
Osmium Isotope Evidence for an S-Process Carrier in Primitive Chondrites **[#1396]**
Depletions in ^{186}Os, ^{188}Os and ^{190}Os in Tagish Lake, Ornans, Parnellee, and Indarch relative to H-Group ordinary chondrites is likely the result of an undigested s-process carrier for Os. Alternatively, these systematics may result from nebular heterogeneity.

11:15 a.m. Rubin A. E. *
Relationships Among Oxidation State, Bulk Chemistry, Oxygen-Isotopic Composition, Petrologic Type and Chondrule Size in Ordinary Chondrites **[#1226]**
Each ordinary-chondrite group comprises chondrites of different petrologic types and exhibits a narrow range in oxidation state, bulk chemical composition, O-isotopic composition and chondrule size. Relationships among these properties reflect both nebular and asteroidal processes.

Wednesday, March 16, 2005
LUNAR BASALTS: A HEAP O'KREEP
1:30 p.m. Salon A

Chairs: B. L. Jolliff
C. R. Neal

1:30 p.m. Lucey P. G. * Gillis J. J. Cahill J. T.
Quantitative Mineralogy of South Pole-Aitken Basin **[#1520]**
Mineral maps of South Pole-Aitken reveal extensive exposures of basaltic material.

1:45 p.m. Campbell B. A. * Hawke B. R.
Cryptomare Deposits Revealed by 70-cm Radar **[#1381]**
We use new 70-cm lunar radar images to map deeply buried cryptomare deposits.

2:00 p.m. Hawke B. R. * Gillis J. J. Giguere T. A. Blewett D. T. Lawrence D. J. Lucey P. G. Peterson C. A. Smith G. A. Spudis P. D. Taylor G. J.
The Earliest Mare Basalts **[#1642]**
The early mare basalts associated with lunar cryptomaria are dominated by VLT and low-TiO_2 basalts. No high-TiO_2 basalts were identified. At least some of the buried mare units in three cryptomaria may be high-alumina mare basalts.

2:15 p.m. Gaffney A. M. * Borg L. E. Asmerom Y.
^{238}U-^{206}Pb Age and Uranium-Lead Isotope Systematics of Mare Basalt 10017 **[#1478]**
We have determined a ^{238}U-^{206}Pb age for mare basalt 10017 that is concordant with previously-determined Rb-Sr ages for this sample. The high-μ and high-Ti nature of this basalt indicates that it probably originates from an ilmenite-rich source.

2:30 p.m. Borg L. E. * Shearer C. K. Asmerom Y. Papike J. J.
Geochemical and Isotopic Systematics of the Youngest Dated Lunar Igneous Rock, Northwest Africa 773 **[#1026]**
A crystallization age of 2.865 ± 0.031 Ga, an initial ε_{Nd} of -7.84 ± 0.22, and an initial $^{87}Sr/^{86}Sr$ ratio of 0.703568 ± 0.000032 has been determined for an olivine-rich clast in the lunar meteorite Northwest Africa 773. This is the youngest lunar sample yet dated.

2:45 p.m. Shearer C. K. * Borg L. E. Papike J. J.
A View of KREEP-rich Lunar Basaltic Magmatism Through the Eyes of NWA 773 **[#1191]**
Lunar meteorite NWA 773 provides valuable insights into the duration of lunar magmatism and important magmatic processes.

3:00 p.m. Jolliff B. L. * Zeigler R. A. Korotev R. L. Barra F. Swindle T. D.
A Thorium-rich Mare Basalt Rock Fragment from the Apollo 12 Regolith: A Sample from a Young Procellarum Flow? **[#2357]**
Basaltic rock fragment 12032,366-18, found in the Apollo 12 regolith, is a new, Th-rich mare basalt type, potentially representing basalts so far indicated only by remote sensing. Ar-Ar results suggest a crystallization age <3 Ga.

3:15 p.m. Hackwill T. * Guest J. E. Spudis P.
Basalts in Mare Humorum and S.E. Procellarum **[#1649]**
Crater depths are used to suggest the volume of basalt in Mare Humorum. Clementine data is used to investigate the spatial distribution of basaltic units in Mare Humorum and S.E. Procellarum in terms of FeO and TiO_2 wt%.

3:30 p.m. Kramer G. Y. * Neal C. R.
Investigating the Sources of the Apollo 14 High-Al Mare Basalts **[#1957]**
Incompatible trace element ratios and Rb-Sr isotopic data require three distinct sources and eruption events to produce the Apollo 14 high-Al mare basalts. We determine the composition and mineralogy of these sources using cumulates from the crystallized lunar magma ocean.

3:45 p.m. Liang Y. * Morgan Z. T. Hess P. C.
On the Physical and Chemical Consequences of Lunar Picritic Magma-Anorthosite Reaction **[#1706]**
Melting and dissolution of anorthosite in lunar picritic magmas produce a thermo-chemical boundary layer that plays a crucial role in determining the CaO and Al_2O_3 abundance of the assimilated melts, and possibly the production of high-Al basalts.

4:00 p.m. Dwarzski R. E. * Draper D. S. Shearer C. K. Agee C. B.
High Pressure Phase Relations and Trace Element Partitioning in Apollo 14 Black Glass **[#1450]**
The high pressure phase equilibria and trace element partitioning of Apollo 14 black glass are used to assess whether garnet was retained in its source region.

4:15 p.m. Neal C. R. * Shearer C. K. Kramer G. Y.
Garnet in the Lunar Mantle: Further Evidence from Volcanic Glass Beads **[#1755]**
Trace element signatures from Apollo 12 and Apollo 14 high-Ti volcanic glass beads are consistent with garnet being retained in the source.

4:30 p.m. Khan A. * Maclennan J. Taylor S. R. Mosegaard K. Gagnepain-Beyneix J. Lognonné P.
Selenelogical Tomography — Inferring the Composition of the Moon from the Apollo Lunar Seismic Data, Mass and Moment of Inertia **[#1121]**
We have inverted the Apollo lunar seismic data, mass and moment of inertia to infer the composition of the Moon. Our results indicate a pyroxenite upper mantle and lower mantle consisting of olivine and garnet cumulates. Also, lunar bulk composition and Mg# are different to the Earth's upper mantle.

Wednesday, March 16, 2005
SPECIAL SESSION
CASSINI AT SATURN I: HUYGENS PROBE AND TITAN RESULTS
1:30 p.m. Salon B

Chairs: J.-P. Lebreton
M. G. Tomasko

1:30 p.m. Matson D. L. * Lebreton J. P. Spilker L. J.
Cassini-Huygens in Orbit Around Saturn **[#1514]**
The Cassini-Huygens orbiter instruments have been very active since early 2004. Highlights of the orbiter discoveries made so far are presented and placed in the context of what we know about the Saturnian system.

1:45 p.m. Lebreton J. P. * Matson D. L. Huygens Team
The Huygens Mission at Titan: Results Highlights **[#2024]**
Huygens descent in Titan's atmosphere is planned on January 14, 2005. This paper will give an overview of the Huygens mission. Highlights of the observations will be presented.

2:00 p.m. Tomasko M. G. * Doose L. R. Rizk B. Smith P. See C. Bushroe M. McFarlane L. Engel S. Eibl A. Karkoschka E. Prout M. Dafoe L. E. West R. Soderblom L. Archinal B. A. Keller U. Schroeder S. Kuppers M. Bézard B. Lellouch E. Coustenis A. deBergh C. Combes M. Schmitt B. Douté S. Thomas N. Gliem F. Lemmon M. T.
First Results from the Descent Imager/Spectral Radiometer (DISR) Experiment on the Huygens Entry Probe of Titan **[#2194]**
We will present the first results of the Descent Imager/Spectral Radiometer (DISR) experiment on the Huygens Entry Probe of Titan.

2:30 p.m. Zarnecki J. C. *
First Results from the Huygens Surface Science Package **[#1295]**
The Surface Science Package (SSP) is one of the six scientific instruments carried by ESA's Huygens probe. First results from the Huygens descent to Titan on January 14, 2005, will be presented, both from the perspective of instrument performance and scientific results.

2:45 p.m. Niemann H. B. * GCMS Experiment Team
Cassini-Huygens Probe Gas Chromatograph Mass Spectrometer (GCMS) Experiment — First Results **[#1663]**
GCMS results of the chemical composition measurement of the Titan atmosphere obtained during the Cassini-Huygens Probe entry will be presented.

3:00 p.m. Israel G. M. * Niemann H. B. ACP Experiment Team
Cassini-Huygens Aerosol Collector Pyrolyser (ACP) Experiment **[#2409]**
A preliminary estimation of the chemical composition of the matter collected by the ACP instrument (both the phochemical aerosols particles and the condensed organics) will be given. ACP prylysates are sent to the GCMS probe instrument and GCMS data products relevant to ACP are provided to the ACP Team for analysis.

3:15 p.m. Fulchignoni M. * Angrilli F. BarNun A. Barucci M. A. Bianchini G. Borouki W. Coradini M. Coustenis A. Falkner P. Ferri F. Flamini E. Grard R. Hamelin M. Harri A.-M. Leppelmeier G. Lopez-Moreno J. McDonnell A. McKay C. Neubauer F. Pedersen A. Picardi G. Pirronello V. Rodrigo R. Schwingenschuh K. Svedhem H. Zarnecki J.
Physical Characterization of Titan Atmosphere by the Huygens Atmospheric Structure Instrument (HASI) **[#2104]**
Presentation of results obtained after the Huygens descent.

3:30 p.m. Bird M. K. * Dutta-Roy R. Allison M. D. Asmar S. W. Atkinson D. H. Edenhofer P. Plettemeier D. Tyler G. L.
The Cassini/Huygens Doppler Wind Experiment: Results from the Titan Descent **[#1620]**
The Huygens Doppler Wind Experiment (DWE) determined the height profile of the zonal winds during the Titan descent, commencing with parachute deployment at an altitude of ca. 150 km down to impact on the surface.

3:45 p.m. Smith P. H. * Tomasko M. G. Doose L. R. Rizk B. Moores J. E.
The Atmospheric View from the Side Window of Huygens Probe **[#1771]**
As the Huygen Probe's descends through Titan's atmosphere, the DISR instrument will compress side-looking images into vertical strips every few kilometers. High signal-to-noise ratios and a near horizontal viewing geometry make them sensitive to thin hazes and other subtle features.

4:00 p.m. Elachi C. Wall S. D. Allison M. D. Anderson Y. Boehmer R. Callahan P. Encrenaz P. Flamini E. Francescetti G. Gim Y. Hamilton G. Hensley S. Janssen M. A. Johnson W. T. K. Kelleher K. Kirk R. L. * Lopes R. M. Lorenz R. D. Lunine J. Muhleman D. O. Ostro S. J. Paganelli F. Picardi G. Posa F. Roth L. E. Seu R. Shaffer S. Soderblom L. A. Stiles B. Stofan E. Vetrella S. West R. Wood C. A. Wye L. Zebker H. A.
Cassini RADAR's First Look at Titan **[#2294]**
The first Cassini RADAR observations of Titan reveal a geologically complex, rather smooth and radar-bright surface. Features include multiple types that may be cryovolcanic, and radar-dark possible organic deposits, but few candidate impact craters.

4:15 p.m. McEwen A. S. * Turtle E. Perry J. Fussner S. Porco C. West R. Johnson T. V. Collins G. C. Del Genio T. Barbara J. Cassini ISS Team
Cassini Imaging Results at Titan **[#1968]**
Cassini ISS has measured wind speeds and haze properties and mapped much of Titan's surface at 938 nm. We will present multiple hypotheses for the complex albedo patterns.

4:30 p.m. Waite J. H. Jr.* Niemann H. Yelle R. V. Kasprzak W. Cravens T. Luhmann J. McNutt R. Ip W.-H. Gell D. Muller-Wordag I. C. F. Ledvina S. Magee B. Borggren N. Fletcher G. Walter E. Miller R. Xu J. Block B. Arnett K.
Ion Neutral Mass Spectrometer Measurements from Titan **[#2057]**
In its first flyby of Titan, Cassini/INMS has found that the upper atmospheric structure remains virtually unchanged since the Voyager flyby 20 years ago. The data also provides isotopic clues about the evolution of the atmosphere.

Wednesday, March 16, 2005
CHONDRITES
1:30 p.m. Salon C

Chairs: D. S. Lauretta
R. H. Jones

1:30 p.m. Bland P. A. * Rost D. Vicenzi E. P. Stadermann F. J. Floss C. Fries M. Steele A. Benedix G. K. Lee M. R. Watt L. E. Kearsley A. T.
Trace Element Carrier Phases in Primitive Chondrite Matrix: Implications for Volatile Element Fractionation in the Inner Solar System **[#1841]**
We are attempting to characterise the trace element carrier phases within Acfer 094 matrix using a combination of ToF-SIMS, NanoSIMS, Raman and EDS, in order to discriminate between models for volatile element depletion.

1:45 p.m. Wasson J. T. * Trigo-Rodriguez J. M. Rubin A. E.
Dark Mantles Around CM Chondrules are not Accretionary Rims **[#2314]**
Fine dark mantles around some CM chondrules consist of nebular materials but porosities are low, inconsistent with nebular formation. We suggest that the mantles resulted from asteroidal impact compaction that predated aqueous alteration.

2:00 p.m. Zega T. J. * Garvie L. A. J. Dódony I. Stroud R. M. Buseck P. R.
Polyhedral Serpentine Grains in CM Chondrites **[#2087]**
We expand on previous efforts to characterize serpentines in CM chondrites and report results on a polyhedral form.

2:15 p.m. Brearley A. J. * Chizmadia L. J.
On the Behavior of Phosphorus During the Aqueous Alteration of CM2 Carbonaceous Chondrites **[#2176]**
X-ray mapping of chondrules in CM2 chondrites Y791198, Mighei and ALH81002 shows that Ca and P, leached from chondrule mesostasis are precipitated as Ca-phosphate in fine-grained rims supporting parent body alteration.

2:30 p.m. Amelin Y. * Krot A. N.
Young Pb-Isotopic Ages of Chondrules in CB Carbonaceous Chondrites **[#1247]**
CB carbonaceous chondrites Gujba and Hammadah al Hamra 237 have Pb-isotopic ages of 4562.7 ± 0.5 Ma and 4562.8 ± 0.9 Ma, respectively.

2:45 p.m. Lauretta D. S. * Guan Y. Leshin L. A.
Hydrogen Abundances in Metal Grains from the Hammadah Al Hamra (HaH) 237 Metal-rich Chondrite: A Test of the Nebular-Formation Theory **[#1839]**
We have measured the abundance of H in metal grains from HaH 237. The results confirm a nebular origin for these grains and constrain the partial pressure of H_2 present during their formation.

3:00 p.m. Schoenbeck T. W. * Palme H. Huss G. R.
SIMS Analysis of Moderately Lithophile Elements in CR and CB Chondrite Metal— - Characteristic Properties of Pristine and Processed Metal **[#2130]**
We present SIMS analyses for moderately lithophile elements in HaH 27 (CB chondrite) and Acfer 209 (CR chondrite). The data provides distiguishing features between condensed metal and processed metal.

3:15 p.m. Burger P. V. * Brearley A. J.
Localized Chemical Redistribution During Aqueous Alteration in CR2 Carbonaceous Chondrites EET 87770 and EET 92105 **[#2288]**
Elemental exchange and chemical redistribution between chondrules and matrices is examined in CR2 carbonaceous chondrites EET 87770 and EET 92105. Results are used to place constraints on aqueous alteration reactions on meteorite parent bodies.

3:30 p.m. Abreu N. M. * Brearley A. J.
HRTEM and EFTEM Studies of Phyllosilicate-Organic Matter Associations in Matrix and Dark Inclusions in the EET92042 CR2 Carbonaceous Chondrite **[#1826]**
HRTEM and EFTEM have been used to characterize the associations of phyllosilicates and organic matter in fine-grained matrix and dark inclusions in the EET 92042 CR chondrite.

3:45 p.m. Jones R. H. * Guan Y. Leshin L. A. Larsen T. Sharp Z. D.
Oxygen Isotope Distribution in NWA 739, a CH Chondrite with Affinities to Acfer 182 **[#1813]**
We report the bulk oxygen isotope composition of NWA739, and SIMS oxygen isotope measurements on individual silicate grains. There appear to be two groups of silicates: one distributed along CCAM, and one distributed along the CR mixing line.

4:00 p.m. Goldstein J. I. * Jones R. H. Kotula P. G. Michael J. R.
Microstructure and Thermal History of Metal Particles in CH Chondrites **[#1391]**
This paper provides detailed microstructural and microchemical information at the nm to μm scale (SEM, EPMA, TEM, EBSD) for a select suite of metal particles in four CH chondrites, ALH 85085, PAT 91546, Acfer 214, NWA 739.

4:15 p.m. Weisberg M. K. * Kimura M. McCoy T. J. Lin Y.
Olivine and the Thermal History of the E Chondrite Parent Body **[#1420]**
The Cr content of olivine has potential as an indicator of petrologic subtype and for identifying the most primitive E chondrites. Of the five E chondrites studied so far, ALH85119, EET83322 and MAC88136 are less equilibrated than LEW87234 and Y691.

4:30 p.m. McCoy T. J. * Brown M. R. M. Nittler L. R. Rost D.
Metal-Sulfide-cemented Agglutinates: What's Really Happening with Sulfur on Asteroidal Surfaces? **[#1412]**
Metal-sulfide particles with included silicates in the dark portions of ordinary chondrite regolith breccias are possible asteroidal agglutinates formed by micrometeorite bombardment.

Wednesday, March 16, 2005
MER RESULTS II
1:30 p.m. Marina Plaza Ballroom

Chairs: M. P. Golombek
S. M. McLennan

1:30 p.m. Brückner J. * Dreibus G. Jagoutz E. Gellert R. Lugmair G. W. Rieder R. Wänke H. Zipfel J. Klingelhöfer G. Clark B. C. Ming D. W. Yen A. Herkenhoff K. E. Athena Science Team
Hematite on the Surface of Meridiani Planum and Gusev Crater **[#1767]**
Instruments of the two Mars Exploration Rovers collected data on different hematite bearing samples, as soils, rocks, outcrops, spherules, and fragments. Combining these data, different occurrences of hematite on the martian surface are discussed.

1:45 p.m. Wang A. * Haskin L. A. Squyres S. W. Arvidson R. E. Crumpler L. S. Gellert R. Hurowitz J. A. Schröder C. Tosca N. Herkenhoff K. E. Jolliff B. L. Athena Science Team
Sulfate Deposition in Regolith Exposed in Trenches on the Plains Between the Spirit Landing Site and Columbia Hills in Gusev Crater, Mars, **[#2236]**
Sulfates (mainly Mg-sulfates) were identified in the subsurface regolith exposed by trenches in the Gusev plains between the Spirit landing site and the Columbia Hills. Evidences and hypotheses will be discussed.

2:00 p.m. McLennan S. M. * Bell J. F. III Calvin W. M. Christensen P. R. Clark B. C. de Souza P. A. Farrand W. H. Fike D. Gellert R. Ghosh A. Glotch T. D. Grotzinger J. P. Hahn B. C. Herkenhoff K. E. Hurowitz J. A. Johnson J. R. Johnson S. S. Jolliff B. L. Klingelhöfer G. Knoll A. H. Learner Z. Malin M. C. McSween H. Y. Jr. Pocock J. Ruff S. W. Squyres S. W. Tosca N. J. Watters W. Wyatt M. B. Yen A. Athena Science Team
Provenance and Diagenesis of Impure Evaporitic Sedimentary Rocks on Meridiani Planum, Mars **[#1884]**
Impure evaporitic sedimentary rocks preserved on Meridiani Planum preserve textural, mineralogical and geochemical evidence for a protracted and complex history of syndepositional through burial diagenesis dominated by phreatic meteoric conditions.

2:15 p.m. Yen A. S. * Ming D. W. Gellert R. Clark B. C. Morris R. V. Rodionov D. Schröder C. Klingelhöfer G.
Subsurface Weathering of Rocks and Soils at Gusev Crater **[#1571]**
Data collected from Spirit at Gusev Crater suggest that enhanced weathering of rocks and soils occurs beneath the immediate surface. We believe that this alteration is a result of diurnal condensation of thin-films of water on subsurface materials.

2:30 p.m. Schröder C. * Klingelhöfer G. Morris R. V. Rodionov D. S. de Souza P. A. Ming D. W. Yen A. S. Gellert R. Bell J. F. III
Weathering of Basaltic Rocks from the Gusev Plains up into the Columbia Hills from the Perspective of the MER Mössbauer Spectrometer **[#2309]**
Mössbauer spectra of rocks at the foot of the Columbia Hills show a decrease in olivine accompanied by an increase in the Fe-oxides magnetite, hematite, and nanophase Fe^{3+}-oxides, suggesting that chemical weathering processes in the presence of water have altered these rocks and outcrops.

2:45 p.m. Ming D. W. * Morris R. V. Gellert R. Yen A. Bell J. F. III Blaney D. L. Christensen P. R. Crumpler L. S. Chu P. C. Farrand W. H. Gorevan S. Herkenhoff K. E. Klingelhöfer G. Rieder R. Rodionov D. S. Ruff S. W. Schröder C. Squyres S. W. Athena Science Team
Geochemical and Mineralogical Indicators for Aqueous Processes on the West Spur of the Columbia Hills in Gusev Crater **[#2125]**
The Athena Science Instrument payload onboard the Spirit rover in Gusev crater is providing datasets that suggest the outcrops and rocks on the West Spur of the Columbia Hills are altered by water.

3:00 p.m. Parker T. J. * Haldemann A. F. C. Athena Science Team
A Marine Origin for the Meridiani Planum Landing Site? **[#2363]**
A marine origin for the Opportunity site is discussed, which we feel provides a better 'fit' to the local-scale results identified by Opportunity, and the regional-scale characteristics of Meridiani Planum provided by data from orbiting spacecraft, when considered together.

3:15 p.m. Golombek M. P. * Grant J. A. Crumpler L. S. Greeley R. Arvidson R. E. Athena Science Team
Climate Change from the Mars Exploration Rover Landing Sites: From Wet in the Noachian to Dry and Desiccating Since the Hesperian **[#1539]**
The salt water sedimentary evaporites in Meridiani Planum document a warmer and wetter environment in the Noachian. In contrast, the gradation history of the Gusev plains argues for a dry and desiccating environment since the Late Hesperian.

3:30 p.m. Crumpler L. S. * Athena Science Team
MER Field Observations and Analysis of Vesicles in the Gusev Plains: Significance as Records of Emplacement Environment **[#2122]**
Analysis of the occurrences, size, and shape distribution of vesicles from MER field data provide some preliminary estimates of the volatile content, lava emplacement style, and atmospheric conditions (pressure) at the time that the Gusev basalts were erupted.

3:45 p.m. Sullivan R. * Bell J. F. III Calvin W. M. Fike D. Golombek M. P. Greeley R. Grotzinger J. P. Herkenhoff K. E. Jerolmack D. Malin M. C. Ming D. Soderblom L. A. Squyres S. W. Thompson S. Watters W. A. Weitz C. Yen A.
Aeolian Processes at the Mars Exploration Rover Opportunity Landing Site **[#1942]**
Wind at the MER Meridiani Planum landing site has created drifts, dunes, and ubiquitous ripples, sorted grains, formed bright wind streaks downwind from craters seen from orbit, and eroded rock with abrading, wind-blown material.

4:00 p.m. Chan M. A. * Beitler B. Parry W. T. Ormö J. Komatsu G.
Utah Marbles and Mars Blueberries: Comparitive Terrestrial Analogs for Hematite Concretions on Mars **[#1402]**
Compelling comparisons show why Utah iron oxide-cemented "marbles" are a good analog for Mars hematite "blueberries". Terrestrial examples offer valuable models for interpreting the diagenetic history and importance of water on Mars.

4:15 p.m. Coleman M. L. *
Processes of Formation of Spheroidal Concretions and Inferences for "Blueberries" in Meridiani Planum Sediments **[#2148]**
Formation of spheroidal concretions on Earth results generally from reactions of organic matter in oxidized sediments. Had organic matter been present in Merididani Planum it could have produced a reduced iron mineral phase later oxidized to hematite.

4:30 p.m. Burt D. M. * Knauth L. P. Wohletz K. H.
Origin of Layered Rocks, Salts, and Spherules at the Opportunity Landing Site or Mars: No Flowing or Standing Water Evident or Required **[#1527]**
Layered rocks at Meridiani Planum may be distal base surge deposits related to meteorite impact into an ice, brine, and salt-rich regolith, rather than evaporites of an acid sea.

Thursday, March 17, 2005
SMALL BODIES: BUMPING, SPINNING, AND SHAKING
8:30 a.m. Salon A

Chairs: K. A. Holsapple
D. G. Korycansky

8:30 a.m. Schultz P. H. * Anderson J. L. B.
Alternative Cratering Scenarios for the Deep Impact Collision **[#1926]**
We don't know exactly what to expect during the Deep Impact collision in 2005 but laboratory experiments provide constraints and strategies for interpreting the nature of the upper 20 m of comet 9P/Tempel 1.

8:45 a.m. Wünnemann K. * Collins G. S. Melosh H. J.
Numerical Modelling of the Deep Impact Mission Experiment **[#1837]**
The Deep Impact Mission will provide insights of the comet Tempel 1 by shooting a projectile onto the surface of the comets nucleus. We present hydrocode calculations to estimate the size of the resulting crater.

9:00 a.m. Thomas P. C. * Robinson M. S.
Seismic Shaking Removal of Craters 0.2–0.5 km in Diameter on Asteroid 433 Eros **[#1695]**
Crater density distribution on asteroid Eros indicate removal of 0.2 to 0.5 km diameter craters by seismic effects from formation of the 7.6 km crater Shoemaker.

9:15 a.m. Richardson J. E. * Melosh H. J. Greenberg R. J.
A Stochastic Cratering Model for Asteroid Surfaces **[#2032]**
The observed cratering records on asteroid surfaces provide us with important clues to their past bombardment histories. We present results from a stochastic cratering simulation specifically designed for modeling crat populations on asteroids.

9:30 a.m. Cheng A. F. *
Asteroid Collisional Evolution: Implications for Internal Structure **[#1506]**
A new model of asteroid collisional evolution is constrained by a size distribution inferred from crater size distributions on the Moon, Mercury and Mars. The asteroid size distribution is constrained to evolve over 3.! to the present day state.

9:45 a.m. Dawe W. Murray M. Burchell M. J. *
Catastrophic Disruption of Porous and Solid Ice Bodies **[#1096]**
We report on a programme of 19 laboratory impacts onto ice targets (porous and solid) at speeds of 1 to 7 km/. We determine the energy density for catastrophic disruption and show that it differs significantly for porous vs. solid ice bodies. This is contrary to results at lower impact speeds.

10:00 a.m. Korycansky D. G. * Asphaug E.
Polyhedron Modeling of Rubble-Pile Asteroids **[#1400]**
We report on our progress in modeling asteroid rubble pile structure and dynamics using polyhedral models.

10:15 a.m. Holsapple K. A. *
Asteroid Spin Data: No Evidence of Rubble-Pile Structures **[#2329]**
New analyses of spin limits for cohesive ellipsoidal asteroids dispel the idea that the data strongly suggests rubble-pile structures. Instead the data, including some new data from the main belt, is entirely consistent with limits for large cohesive bodies with strength.

10:30 a.m. Scheeres D. J. *
Solar Radiation Pressure and Transient Flows on Asteroid Surfaces **[#1919]**
The effect of solar radiation pressure (SRP) on small regolith particles is discussed. SRP can play a major role in the surface migration of dust particles, whether or not electromagnetic levitation or seismic shaking is present.

Thursday, March 17, 2005
IMPACTS: SHOCK EFFECTS
10:45 a.m. Salon A

Chairs: J. F. McHone

10:45 a.m. Xie Z. * Sharp T. G. DeCarli P.
Pressure Histories from Thin and Thick Shock-induced Melt Veins in Meteorites **[#1216]**
The crystallization history of shock vein depend on vein thickness (quench rate) and timing of vein formation. Thin-vein assemblages generally imply lower crystallization pressures. Three explanations were discussed: injection; multiple shock events; and quench rate.

11:00 a.m. Gucsik A. * Nishido H. Ninagawa K. Toyoda S. Bidló A. Brezsnyánszky K. Tsuchiyama A.
Cathodoluminescence Spectral Studies of the Experimentally Shock-deformed Plagioclase: A Possible Explanation of CL Peak Shifts **[#1239]**
CL spectral changes (i.e., peak shifts) in the shocked plagioclase samples are related to distance changes between coordinated $-O^{-}$ and Mn^{2+} activator ion, and changes of distance between electron traps in band gap between the conduction and valance bands.

11:15 a.m. Miura Y. *
Shocked Data of Silica-rich Breccias and X-Ray CT Images of Buried Craters at Takamatsu-Kagawa District in Japan **[#2394]**
Three types of rocks in Takamarsu-Kagawa district are found as original impact rocks, melt brecciated rocks with hydrothermal alteration and volcanic rocks. Three types of shocked quartz with PDFs are found in this district.

11:30 a.m. Harris R. S. * Schultz P. H. Bunch T. E.
Accessory Phases in Argentine Impact Breccias: Implications for Shock History, Emplacement Dynamics, Vapor Composition and Target Lithologies **[#1952]**
Petrographic and SEM analyses of accessory phases (ilmenite, Fe metal, FeS, etc.) in Centinela del Mar (450 ka) and Mar del Plata (3.3 Ma) glasses reveal important information about the dynamic events that produced these melt breccias.

Thursday, March 17, 2005
SPECIAL SESSION
CASSINI AT SATURN II: ORBITER AND TITAN RESULTS
8:30 a.m. Salon B

Chairs: D. L. Matson
L. A. Soderblom

8:30 a.m. Brown R. H. * Baines K. H. Bellucci G. Buratti B. J. Capaccioni F. Cerroni P. Clark R. N. Coradini A. Cruikshank D. P. Drossart P. Formisano V. Jaumann R. Matson D. L. McCord T. B. Mennella V. Nelson R. Nicolson P. Sicardy B. Sotin C.
Cassini VIMS at Saturn: The First 6 Months **[#1166]**
The Cassini Visual and Infrared Mapping Spectrometer (VIMS) has completed its first 6 months in orbit around Saturn and a summary of results will be presented.

8:45 a.m. Flasar F. M. * Cassini CIRS Investigation Team
Early Results on the Saturn System from the Composite Infrared Spectrometer **[#1444]**
We present early results from CIRS spectra on the temperatures, dynamics, and composition of Saturn, its rings, and its moons, Phoebe, Iapetus, and Titan.

9:00 a.m. Esposito L. W. Hansen C. J. * Colwell J. Hendrix A. R. McClintock W. E. Shemansky D. E. Stewart A. I. F. Hallett J. West R. A.
The Saturn System as Observed by Cassini's Ultraviolet Imaging Spectrograph **[#1586]**
Results from the Cassini Ultraviolet Imaging Spectrograph (UVIS) will be presented, focusing on recent observations of Titan and Saturn's icy satellites.

9:15 a.m. Gurnett D. A. * Kurth W. S. Hospodarsky G. B. Persoon A. M. Averkamp T. F. Cecconi B. Lecacheux A. Zarka P. Canu P. Cornilleau-Wehrlin N. Galopeau P. Roux A. Harvey C. Louarn P. Bostrom R. Gustafsson G. Wahlund J.-E. Desch M. D. Farrell W. M. Kaiser M. L. Goetz K. Kellogg P. J. Fischer G. Ladreiter H.-P. Rucker H. O. Alleyne H. Pedersen A.
Cassini Radio and Plasma Wave Observations at Saturn **[#1108]**
Results are presented from the Cassini radio and plasma wave instrument during the approach and first few orbits around Saturn.

9:30 a.m. Reisenfeld D. B. * Baragiola R. A. Crary F. J. Coates A. J. Goldstein R. Hill T. W. Johnson R. E. McComas D. J. Sittler E. C. Shappirio M. D. Steinberg J. T. Smith H. T. Szego K. Thomsen M. F. Tokar R. L. Young D. T.
Ion Composition in Saturn's Plasma Environment: Early Results from the Cassini Plasma Spectrometer **[#1887]**
We report preliminary ion composition findings made by the Cassini Plasma Spectrometer during the first two Cassini orbits, including the closest approach to Saturn and the rings during the tour, and a close flyby of Titan.

9:45 a.m. Dougherty M. K. * Cassini Magnetometer Team
Cassini Magnetometer Observations at Saturn **[#1677]**
This work describes magnetometer observations obtained during the first 6 months of Cassini's orbital tour at Saturn.

10:00 a.m. Krimigis S. M. * Mitchell D. G. Hamilton D. C. Krupp N. Livi S. Roelof E. C. Dandouras J. Mauk B. H. Brandt J. P. Paranicas C. Saur J. Armsrong T. P. Bolton S. Cheng A. F. Gloeckler G. Hsieh K. C. Ip W.-H. Lagg A. Lanzerotti L. J. McEntire R. W. Williams D. J.
Overview of Results from the Cassini Magnetospheric Imaging Instrument (MIMI) During the First Year of Operations **[#1361]**
A high-level overview of MIMI results includes corotation of the magnetosphere, overwhelming presence of water-product ions, identification of a radiation belt inside the D-ring, and inferred presence of neutral gas absorbing ions and electrons inward of Dione's orbit.

10:15 a.m. Doose L. R. * Engel S. Tomasko M. G. Dafoe L. E. West R. Lemmon M. T.
Aerosol and Cloud Properties at the Huygens Entry Site as Derived from the Descent Imager/Spectral **[#2222]**
The size, shape, and number density of Titan aerosols and clouds at the Huygens entry site vs. altitude is presented. The wavelength dependence of the optical properties is also described.

10:30 a.m. Lorenz R. D. * Elachi C. Stiles B. West R. Janssen M. A. Lopes R. M. Stofan E. Paganelli F. Wood C. Kirk R. L. Lunine J. Wall S.
Titan's Elusive Lakes? Properties and Context of Dark Spots in Cassini TA Radar Data **[#1682]**
RADAR shows dark spots; σ_0 seems like asphalt. Titan's ethane lakes?

10:45 a.m. Turtle E. P. * Dawson D. D. Fussner S. Hardegree-Ullman E. McEwen A. S. Perry J. Porco C. C. West R. A. Cassini ISS Team
Liquid Hydrocarbons on Titan's Surface? How Cassini ISS Observations Fit into the Story (So Far) **[#2311]**
Atmosphere desires; radar, but not eyes, implies; hydrocarbon seas.

11:00 a.m. Soderblom L. A. * Brown R. H. Cassini VIMS Team
Deconvolution of Cassini VIMS Titan Cubes into Atmospheric Spectral Scattering, Surface Topographic, and Surface Spectroscopic Components **[#1869]**
Methods are developed to deconvolve Cassini VIMS near-IR spectra of Titan into atmospheric scattering (diffuse radiance scattered to the S/C and downward to the surface), surface topographic signatures, and normalized spectral reflectance variations among surface units.

11:15 a.m. Nelson R. M. * Brown R. H. Hapke B. W. Smythe W. D. Kamp L. Boryta M. Baines K. H. Bellucci G. Biebring J. P. Buratti B. J. Capaccioni F. Cerroni P. Clark R. N. Coradini A. Cruikshank D. P. Drossart P. Formisano V. Jaumann R. Langevin Y. Matson D. L. McCord T. B. Mennella V. Nicholson P. D. Sicardy B. Sotin C.
Cassini VIMS Preliminary Exploration of Titan's Surface Hemispheric Albedo Dichotomy **[#2139]**
Photometric Analysis of Cassini VIMS Images of Titan suggests a hemispheric albedo dichotemy. The reflectance of the surface units is $0.05 < r < 0.2$. Large circular features may be palimpsests.

11:30 a.m. Rodriguez S. * Le Mouélic S. Sotin C. Buratti B. J. Brown R. H.
VIMS Observations of Titan During the First Two Close Flybys by the Cassini-Huygens Mission **[#1939]**
This paper describes VIMS observations of Titan's surface including the the high resolution images (2 km/pixel) that provide new clues on its geology.

Thursday, March 17, 2005
LUNAR HIGHLANDS: IMPACTS AND ISOTOPES
8:30 a.m. Salon C

Chairs: L. E. Nyquist
B. A. Cohen

8:30 a.m. Le Feuvre M. * Wieczorek M. A.
The Asymmetric Cratering History of the Moon **[#2043]**
As a result of the Earth's gravitational field, more impacts occur on the nearside of the Moon than on its farside. This asymmetry may lead to dramatic errors in the dating of planetary surfaces by the crater counting method.

8:45 a.m. Petro N. E. * Pieters C. M.
The Lunar-wide Effects of the Formation of Basins on the Megaregolith **[#1209]**
The role of basins in forming the megaregolith is modeled. The nearside has 10× the basin ejecta and 5× the depth of the mixed zone than the farside. The FHT (*Jolliff et al.*, 2000) is likely a direct consequence of this early regolith history.

9:00 a.m. Mohit P. S. * Phillips R. J.
Viscoelastic Evolution of Lunar Multi-Ring Basins **[#2063]**
Most of the oldest lunar multi-ring basins are highly degraded and have retained little topographic expression. Using a spherical, self-gravitating viscoelastic model, we explore the role of viscous relaxation in the evolution of these basins.

9:15 a.m. Cahill J. T. * Lucey P. G. Steutel D. Gillis J. J.
Analysis of the Lunar Surface with Global Mineral and Mg-Number Maps **[#2186]**
Mg-number (Mg#) is an important petrologic discriminator when evaluating lunar rocks. Here we present a new data set of Mg# for the lunar surface that can be used to analyze crustal materials and modeling in greater spatial and geochemical detail.

9:30 a.m. Warren P. H. * Tonui E. Young E. D.
Magnesium Isotopes in Lunar Rocks and Glasses and Implications for Origin of the Moon **[#2143]**
We have measured Mg isotopes in a highland breccia, four Ap-12 mare basalts, mare volcanic spheroids (Ap-15 green and Ap-17 black) and highland regolith spheroids. The Ap-15 green spheroids are significantly heavier than the Ap-17 black spheroids.

9:45 a.m. Kleine T. Mezger K. * Palme H.
The Hf-W Age of the Lunar Magma Ocean **[#1940]**
We present W isotope data for lunar metals that preserved the indigenous W isotope composition of their host rocks and reveal W isotope heterogeneities in the lunar mantle, indicating that the final crystallization of the lunar magma ocean occurred 42±4 Myr after the start of the solar system.

10:00 a.m. Norman M. D. * Taylor L. A.
Testing the Lunar Cataclysm: Identification of Lunar Impact Melts Possibly Older than Nectaris **[#1570]**
Several lines of evidence favor a cataclysmic bombardment of the Moon at 3.9 Ga. We have identified lunar impact melt breccias that may be older the major nearside basins. Crystallization ages of these pre-Nectarian impact melts may provide a further test of the cataclysm hypothesis.

10:15 a.m. Zellner N. E. B. Swindle T. D. Barra F. Delano J. W. * Tibbetts N. Whittet D. C. B. Spudis P. D.
Chemical and Isotopic Analyses of Apollo 16 Glasses: An Integrated Approach **[#1199]**
An exotic, compositional group of Apollo 16 impact glasses has been found to have an age of ~3770 Ma.

10:30 a.m. Shih C.-Y. * Nyquist L. E. Reese Y. Yamaguchi A. Takeda H.
Rb-Sr and Sm-Nd Isotopic Studies of Lunar Highland Meteorite Y86032 and Lunar Ferroan Anorthosites 60025 and 67075 **[#1433]**
Rb-Sr and Sm-Nd isotopic results for lithologies in lunar highland breccia Y86032 indicate that they were anorthosites produced by plagioclase accumulation from the LMO with $^{147}Sm/^{144}Nd$ = ~0.18 about 4.55 Ga ago.

10:45 a.m. Edmunson J. * Borg L. E. Nyquist L. E. Asmerom Y.
Three-System Isotopic Study of Lunar Norite 78238: Rb-Sr Results **[#1473]**
Rubidium-strontium isotopic systematics of extremely pure mineral fractions from lunar Mg-suite norite 78238 yield a crystallization age of 4366±53 Ma and a metamorphic age of 4003±95 Ma.

11:00 a.m. Day J. M. D. * Pearson D. G. Taylor L. A.
^{187}Re-^{187}Os Isotope Disturbance in LaPaz Mare Basalt Meteorites **[#1424]**
We present new Re-Os isotope data for the LaPaz lunar mare basalt meteorites. This data demonstrates isotopic disturbance of the Re-Os isotope system, possibly due to impact-related shock.

11:15 a.m. Nyquist L. E. * Shih C.-Y. Reese Y. Bogard D. D.
Age of Lunar Meteorite LAP02205 and Implications for Impact-Sampling of Planetary Surfaces **[#1374]**
Ar-Ar and Rb-Sr ages of LAP02205 are ~3.0 Ga. Lunar meteorite ages range within ~2.8–3.8 Ga, and reliably reflect mare surface ages, in contrast to apparently unrepresentative impact-sampling of the Martian surface by Martian meteorites.

11:30 a.m. Cohen B. A. * Swindle T. D. Kring D. A. Olson E. K.
Geochemistry and ^{40}Ar-^{39}Ar Geochronology of Impact-melt Clasts in Lunar Meteorites Dar Al Gani 262 and Calcalong Creek **[#1481]**
Impact-melt clasts in these meteorites are feldspathic and have ages from 1.0 to 3.8 Ga. Of 57 lunar meteorite impact-melt clasts now dated, all were formed after the nearside basins, probably representing later, local impacts.

Thursday, March 17, 2005
REFRACTORY INCLUSIONS
8:30 a.m. Marina Plaza Ballroom

Chairs: K. D. McKeegan
F. M. Richter

8:30 a.m. McKeegan K. D. * Davis A. M. Taylor D. J. MacPherson G. J.
In Situ Investigation of Mg Isotope Compositions in a FUN Inclusion **[#2077]**
The Mg isotopic composition of a forsterite-rich FUN inclusion is investigated by high-precision multiple collector ion microprobe analysis. The CAI is found to have contained live ^{26}Al when it crystallized.

8:45 a.m. Simon S. B. * Grossman L. Hutcheon I. D. Phinney D. L.
Bulk Chemical and Isotopic Compositions of Spinel-, Hibonite-rich Spherules: Clues to Their Origin **[#2211]**
Calculations predict condensation of melilite after hibonite and before spinel, yet in CMs hib-sp inclusions are much more common than hib-mel inclusions. Did hib-sp inclusions originally contain mel and lose Si and Ca by evaporation?

9:00 a.m. Petaev M. I. * Krot A. N. Wood J. A.
Nebular Condensation Under Incomplete Equilibrium: Implications for the Fine-grained Spinel-rich CAIs **[#1238]**
The fine-grained spinel-rich CAIs could have formed by incomplete condensation of a gas of solar composition at low pressures, when the cooling rate of a parcel of gas is higher than the growth rate of the mineral condensing from this gas.

9:15 a.m. Paque J. M. * Burnett D. S. Beckett J. R.
CAI Thermal History Constraints from Spinel: Ti Zoning Profiles and Melilite Boundary Clinopyroxenes **[#1809]**
Two models, subsolidus diffusion and crystallization from melt inclusions, are presented as possible explanations for the observed profiles of Ti in the Type B1 CAI TS 34.

9:30 a.m. Ash R. D. * Lipella M. McDonough W. F. Rudnick R. L.
Nb-Ta Ratios in the Allende CV Chondrite; The Relationships Between Calcium-Aluminium-rich Inclusions, Chondrules and Matrix **[#2168]**
Nb/Ta fractionation in Allende CAIs explains the low ratios observed in CV chondrites. Chondrules from Allende also show low Nb/Ta ratios, which may be the result of inheritance from CAIs. This is not observed in chondrules from other meteorites.

9:45 a.m. Friedrich J. M. * Jochum K. P. Ebel D. S.
First Results of a Physicochemical Survey of CV3 Calcium-Aluminum-rich Inclusions: The Refractory Trace Elements Sr, Y, Zr, Nb, Ba, Hf, Ta **[#1985]**
We have physically, mineralogically, and chemically characterized 20 CV3 CAIs. We investigate the Zr/Hf and Nb/Ta ratios and their relationships with other refractory trace elements within our suite of CAIs and among the minerals contained in them.

10:00 a.m. Yoshitake M. * Yurimoto H.
Long Formation Period of Single CAI: Combination of O and Mg Isotope Distribution **[#1577]**
O and Mg isotope distribution of a CAI suggests that the CAI formation took place over a time of at least 2.6 Myr.

10:15 a.m. Richter F. M. * Janney P. E. Mendybaev R. A. Davis A. M. Wadhwa M.
On the Temperature Dependence of the Kinetic Isotope Fractionation of Type B CAI-like Melts During Evaporation **[#2124]**
The kinetic isotope fractionation factor for Mg evaporating from CAI-like melts is significantly different from the commonly assumed value of $\sqrt{24/25}$. It varies with temperature and for typical natural conditions, 5‰ per amu implies 36%, not 22% Mg loss.

10:30 a.m. Janney P. E. * Richter F. M. Davis A. M. Mendybaev R. A. Wadhwa M.
Silicon Isotope Ratio Variations in CAI Evaporation Residues Measured by Laser Ablation Multicollector ICPMS **[#2123]**
Si isotope data, obtained by laser ablation-MC-ICPMS, are reported for a set of vacuum-evaporated melts with Type-B CAI-like compositions. These data are consistent with previously reported Mg isotope data and are explained by Rayleigh fractionation.

10:45 a.m. Ryerson F. J. * Brenan J. M. Phinney D. L.
Experimental Determination of Li, Be and B Partitioning During CAI Crystallization **[#1532]**
The partitioning of Li, Be, and B has been determined for clinopyroxene, anorthite, melilite, spinel and melt for compositions relavent to the crystallization of CAIs allowing the range of Be/B and Be/Li generated during liquid crystal fractionation to be simulated.

11:00 a.m. Taylor D. J. * McKeegan K. D. Krot A. N.
High Resolution ^{26}Al Chronology: Resolved Time Interval Between Rim and Interior of a Highly Fractionated Compact Type a CAI from Efremovka **[#2121]**
Separate Al-Mg isochrons have been obtained for the interior and rim of E44L, a type A CAI from Efremovka. This resolves a time interval of 300,000 years between the last heating event affecting the interior of the CAI and event resulting in the formation of the Wark-Lovering rim.

11:15 a.m. Dyl K. A. * Simon J. I. Russell S. S. Young E. D.
Rapidly Changing Oxygen Fugacity in the Early Solar Nebula Recorded by CAI Rims **[#1531]**
We present estimates of Ti^{3+}/Ti^{4+} in Al-Ti-rich diopsides from CAI rims showing that CAIs experienced a shift from ~solar to ~chondritic f_{O_2} in less than 300,000 years.

11:30 a.m. Cuzzi J. N. * Petaev M. Ciesla F. J. Krot A. N. Scott E. R. D.
Nebula Models of Non-Equilibrium Mineralogy: Wark-Lovering Rims **[#2095]**
Non-equilibrium minerals in CAIs and AOAs can survive if the alteration time, plausibly the time for atoms to diffuse into the mineral at the local temperature, exceeds their evolution time to cooler regions, plausibly due to turbulent diffusion.

Thursday, March 17, 2005
IMPACTS: SHOCKS, STRUCTURES, AND MODELS
1:30 p.m. Salon A

Chairs: G. R. Osinski
E. Pierazzo

1:30 p.m. Tschauner O. * Willis M. J. Asimow P. D. Ahrens T. J.
Effective Liquid Metal-Silicate Mixing Upon Shock by Power-Law Droplet Size Scaling in Richtmyer-Meshkov Like Perturbations **[#1802]**
A shock recovery experiment with a molten metal/molten silicate interface led to a power-law size distribution of spherical droplets by Richtmeyer-Meshkov instability, a mechanism for efficiently mixing impactor cores with the mantle of proto-Earth.

1:45 p.m. Ai H. A. * Ahrens T. J.
Shock-induced Damage Beneath Normal and Oblique Impact Craters **[#1243]**
Recent experimental study indicates that the large scale impact-induced P-wave velocity reductions beneath the impact craters provide useful and unique constraints for impact history.

2:00 p.m. Osinski G. R. *
Shock-metamorphosed and Shock-melted $CaCO_3$-bearing Sandstones from the Haughton Impact Structure, Canada: Melting of Calcite at ~10–20 GPa **[#2038]**
Calcite-bearing sandstones from the Haughton impact structure, Canada, have been studied in order to better constrain the behaviour of calcite during hypervelocity impact. This study reveals that calcite melts at ~10–20 GPa in porous sedimentary rocks.

2:15 p.m. Hanova J. * Lawton D. C. Visser J. Hildebrand A. R. Ferrierre L.
3D Structural Interpretation of the Eagle Butte Impact Structure, Alberta, Canada **[#2355]**
The Eagle Butte Impact Structure is located in the Cypress Hills of Southeastern Alberta, Canada. This complex impact structure measures ~14 km in diameter, and contains an extensive fault network that displaces strata within the structure.

2:30 p.m. Niccoli M. * Hildebrand A. R. Lawton D. C.
Seismic Velocity Study of the Rim Uplift of the Steen River Impact Crater **[#2356]**
The structure of the rim uplift at the 25 km diameter Steen River has been explored by 2D and 3D seismic reflection and refraction techniques, constrained by downhole well surveys. A complicated deformation history is revealed.

2:45 p.m. Kenkmann T. * Ivanov B. A.
Thin-Skin Delamination of Target Rocks Around the Ries Crater: The Effect of Spallation and Ejecta Drag **[#1039]**
Near-surface detachment faulting is observed at the Ries crater at 10–20 km distance from the center. Our structural data and numerical modeling suggest that surface-parallel decoupling is caused by spallation and subsequent ejecta curtain drag

3:00 p.m. Plescia J. B. *
Haughton: A Peaked Ring Impact Structure **[#1303]**
Analysis of the gravity field of the Haughton structure suggests that it is a peak ring structure.

3:15 p.m. Koeberl C. * Milkereit B. Overpeck J. T. Scholz C. A. Peck J. King J.
The 2004 ICDP Bosumtwi Impact Crater, Ghana, West Africa, Drilling Project: A First Report **[#1830]**
The Bosumtwi impact crater was drilled from July to October 2004. 16 different cores were drilled at six locations within the lake, to a maximum depth of 540 m. A total of about 2.2 km of core material was obtained.

3:30 p.m. Nycz J. C. * Hildebrand A. R.
The Peripheral Peak Ring: A Complex Impact Crater Morphologic Feature Probably Related to Crater Rim Collapse **[#2167]**
The Peripheral Peak Ring is a new complex impact morphology likely caused by collapse of the crater rim at or near the end of modification. Occurring in a fraction of craters indicate varying crustal properties influence final crater morphology.

3:45 p.m. Goldin T. J. * Wünnemann K. Melosh H. J. Collins G. S.
Hydrocode Modeling of the Sierra Madera Impact Structure **[#1071]**
We present hydrocode simulations of the Sierra Madera impact structure. We discuss implications for the final crater diameter, which may be larger than previously reported.

4:00 p.m. Collins G. S. * Wünnemann K.
How Big Was the Chesapeake Bay Impact? Insight from Numerical Modeling **[#1736]**
We suggest that the morphology of the CBIC was strongly affected by the strength and rheology of the target rocks, and that the transient cavity formed during the development of the final crater was smaller (~25 km) than previous estimates.

4:15 p.m. Korycansky D. G. * Lynett P. J.
Offshore Breaking of Impact Tsunami: Van Dorn was Right **[#1160]**
We have calculated the progression of trains of large water waves as they approach the shore for different bathymetric profiles. Large waves (~10–100 m waveheight) of wavelengths up to 10 km should break and dissipate up to tens of km offshore.

4:30 p.m. Pierazzo E. *
Assessing Atmospheric Water Injection from Oceanic Impacts **[#1987]**
The injection of large amounts of water from oceanic impacts will be addressed, with attention to potential long term environmental effects.

Thursday, March 17, 2005
SPECIAL SESSION
CASSINI AT SATURN III: TITAN SURFACE, RINGS, AND ICY SATELLITES
1:30 p.m. Salon B

Chairs: L. J. Spilker
T. V. Johnson

1:30 p.m. Stofan E. R. * Elachi C. Lopes R. M. Lorenz R. D. Kirk R. L. Paganelli F. Wood C. A. Wall S. D. Lunine J. Soderblom L. A. RADAR Science Team
Mapping of Titan: First Results from the Cassini RADAR **[#1714]**
The first Synthetic Aperture Radar swath across the surface of Titan has revealed a surprisingly complex surface.

1:45 p.m. Lopes R. M. * Elachi C. Stofan E. Paganelli F. Wood C. Kirk R. L. Lorenz R. D. Fortes A. D. Lunine J. Wall S. D. Cassini RADAR Team
Cryovolcanic Features on Titan's Surface as Revealed by the Cassini RADAR **[#1885]**
The Cassini RADAR obtained SAR images of about 1.1% of Titan's surface during the spacecraft's fly-by on October 26, 2004. These revealed surface features that are interpreted as the result of cryovolcanism, including extensive flows. New results from the T3 flyby will also be discussed.

2:00 p.m. Paganelli F. * Elachi C. Lopes R. M. West R. Stiles B. Janssen M. A. Stofan E. R. Wood C. A. Lorenz R. D. Lunine J. Kirk R. L. Roth L. E. Wall S. D. Soderblom L. A. Cassini RADAR Science Team
Channels and Fan-like Features on Titan Surface Imaged by the Cassini RADAR **[#2150]**
Cassini's SAR data of Titan's surface show fan and flow features, sinuous and linear channels. SAR-bright return suggests surface roughness at the scale and bigger than Ku-band, and possible volume scattering. Correlation of SAR-bright and radiometric cold regions has been observed.

2:15 p.m. Wood C. A. * Lopes R. M. Stofan E. R. Paganelli F. Elachi C.
Impact Craters on Titan? Cassini RADAR View **[#1117]**
The first Cassini RADAR image of Titan has revealed no certain impact craters, implying a very young surface. However, a 100-km scale possible two-ring impact basin, if real, suggests differential preservation of large features.

2:30 p.m. Lanagan P. D. * Smith P. H. Tomasko M. G. Doose L. R. Rizk B.
DISR Observations of Craters at Titan at the Huygens Landing Site: Insights Anticipated **[#2065]**
Observations of Titan's impact craters near the Huygens landing site as observed by DISR and their implications for Titan will be discussed.

2:45 p.m. Spilker L. J. * Pilorz S. H. Wallis B. D. Brooks S. M. Edgington S. G. Flasar F. M. Pearl J. C. Showalter M. R. Ferrari C. Achterberg R. K. Nixon C. A. Romani P. N. Cassini CIRS Team
Cassini CIRS Observations of Saturn's Rings **[#1912]**
The Cassini Composite Infrared Spectrometer (CIRS) acquired thermal spectra of Saturn's rings. CIRS retrieved temperatures for the lit and unlit sides of the rings from 7 μm to 1 mm, including measurements across the ring shadow boundaries.

3:00 p.m. Denk T. * Neukum G. Roatsch T. McEwen A. S. Turtle E. P. Thomas P. C. Helfenstein P. Wagner R. J. Porco C. C. Perry J. E. Giese B. Johnson T. V. Veverka J. Cassini ISS Team
First Imaging Results from the Iapetus B/C Flyby of the Cassini Spacecraft **[#2268]**
Cassini had a relatively close flyby at Iapetus on New Year's Eve 2005. The 288 ISS images set various constraints on the origin theories of the dark/bright dichotomy, as revealed multiple surface structures at up to 740 m/pxl size.

3:15 p.m. Spencer J. R. * Pearl J. C. Segura M. Cassini CIRS Team
Cassini CIRS Observations of Iapetus' Thermal Emission **[#2305]**
We describe the observations of Iapetus' thermal emission obtained by the Cassini Composite Infrared Spectrometer (CIRS) during its December 31st 2004 Iapetus flyby. Temperatures range from 130 K near the subsolar point to less than 40 K at high latitudes at night.

3:30 p.m. Hendrix A. R. * Hansen C. J.
Iapetus and Phoebe as Measured by the Cassini UVIS **[#2272]**
We present results from the Cassini Ultraviolet Imaging Spectrograph covering observations of Iapetus and Phoebe.

3:45 p.m. Helfenstein P. * Thomas P. Veverka J. Denk T. Neukum G. West R. A. Knowles B. Porco C. Cassini Imaging Team
A Cassini ISS Search for Regolith-Texture Variations on Tethys **[#2399]**
We search for texture variations on Tethys using ISS NAC polarization images obtained in October 2004. We find no evidence for textural variations on size scales comparable to those of impact craters, but we discover diffuse, possibly exogenic, banded polarization feature.

4:00 p.m. Hansen C. J. * Hendrix A. R.
Ultraviolet Views of Enceladus, Tethys, and Dione **[#1594]**
Cassini's Ultraviolet Imaging Spectrograph (UVIS) has observed many of Saturn's icy satellites. Recent results from Enceladus, Tethys and Dione will be reported.

4:15 p.m. Johnson T. V. * Lunine J.
Saturn Satellite Densities and the C/O Chemistry of the Solar Nebula **[#1410]**
New values for the solar abundances of carbon and oxygen result in a significant increase in the expected density of condensates from a solar composition nebula. The consequences for densities of Saturn satellites are discussed.

4:30 p.m. Neukum G. * Wagner R. Denk T. Porco C. C. Cassini ISS Team
The Cratering Record of the Saturnian Satellites Phoebe, Tethys, Dione and Iapetus in Comparison: First Results from Analysis of the Cassini ISS Imaging Data **[#2034]**
In this paper, we will present results of measurements of the crater size-frequency distributions on Cassini ISS high-resolution images of the Saturnian satellites Phoebe, Tethys, Dione and Iapetus.

Thursday, March 17, 2005
OXYGEN IN THE SOLAR SYSTEM
1:30 p.m. Salon C

Chairs: T. R. Ireland
J. W. Delano

1:30 p.m. Clayton R. N. *
Disequilibrium Oxygen Chemistry in the Solar Nebula **[#1711]**
Oxygen isotopic disequilibrium in chondrules and CAIs implies oxygen chemical disequilibrium as well. Reaction with photochemically-produced oxygen atoms may lead to the observed oxidation states of primitive materials, without resort to special mechanisms, such as dust/gas enrichment.

1:45 p.m. Lyons J. R. *
The $\delta^{17}O/\delta^{18}O$ Ratio Associated with CO Photodissociation in the Solar Nebula **[#2037]**
Photodissociation of CO produces nebular water with a $\delta^{17}O/\delta^{18}O$ slope comparable to the measured slope in CAIs if H_2 abosprtion effects during CO are accounted for during CO self-shielding.

2:00 p.m. Ireland T. R. * Holden P. Norman M. D.
The Oxygen Isotopic Composition of the Sun and Implications for Oxygen Processing in Molecular Clouds, Star-forming Regions, and the Solar Nebula **[#1572]**
The solar oxygen isotopic composition is depleted in ^{16}O by 54‰ relative to terrestrial. This composition can be explained by molecular cloud predissociation and gas-solid fractionation during formation of the accretion disk.

2:15 p.m. Chakraborty S. * Thiemens M. H.
Evaluation of CO Self-Shielding as a Possible Mechanism for Anomalous Oxygen Isotopic Composition of Early Solar System Materials **[#1113]**
CO self-shielding is likely a very modest process. Preliminary experiments show large mass independent effect in the photochemistry of CO at around 150 nm thus excited state chemistry of CO may play an important role in the early solar system process.

2:30 p.m. Aléon J. * Robert F. Duprat J. Derenne S.
Extreme Oxygen Isotopic Anomalies from Irradiation in the Early Solar System **[#1890]**
We have discovered SiO_2-rich grains in the Murchison meteorite with ^{17}O and ^{18}O excesses of about two orders of magnitude, which we attribute to spallation in the gas by ^3He-rich impulsive solar flare type particles emitted by the young Sun.

2:45 p.m. Pahlevan K. * Stevenson D. J.
The Oxygen Isotope Similarity of the Earth and Moon: Source Region or Formation Process? **[#2382]**
We propose that the similar oxygen isotope composition between the Earth and Moon is likely to reflect post-impact processes that would tend to homogenize the terrestrial and proto-lunar material.

3:00 p.m. Akaki T. * Nakamura T
Oxygen Isotope Microanalysis of Enveloping Compound Chondrules in CV3 and LL3 Chondrites **[#1559]**
SIMS data for enveloping compound chondrules in CV3 and LL3 chondrites indicate that they were formed by multiple heating events during which the O-isotope compositions of chondrules and nebular gas reservoirs have not changed significantly.

3:15 p.m. Guan Y. * Lin Y. Leshin L. A.
Oxygen Isotope Distribution in Anorthite-Spinel-rich Inclusions from the Ningqiang Carbonaceous Chondrite **[#2027]**
We report oxygen isotope heterogeneity among individual mineral components in anorthite-spinel-rich inclusions from the Ningqiang carbonaceous chondrites, with emphasis on the observation and discussion of ^{16}O -poor perovskite in CAIs.

3:30 p.m. Delano J. W. *
Apollo 14 High-Ti Picritic Glass: Oxidation/Reduction by Condensation of Alkali Metals **[#1081]**
Volcanic fire-fountaining was the setting for extreme alkali enrichment and FeO reduction during the eruption of a high-Ti picritic magma in the region of the Apollo 14 landing site.

3:45 p.m. McCanta M. C. *
Potential Effects of Melt Composition on Redox Ratio: Implications for Oxygen Fugacity Measurements **[#1754]**
An experimental comparison of the effects of oxygen fugacity and composition on melt redox ratio is presented. Although melt composition does influence the redox ratio in some cases, oxygen fugacity is shown to have a substantially greater effect.

4:00 p.m. Sutton S. R. * Newville M.
Vanadium K XANES of Synthetic Olivine: Valence Determinations and Crystal Orientation Effects **[#2133]**
We report vanadium K XANES measurements on synthetic olivine grains and glass and describe inferred vanadium valences. The variations due to crystal orientation are shown to be subtle.

4:15 p.m. Delaney J. S. * Dyar M. D. Gunter M. E. Sutton S. R. Lanzirotti A.
Broad Spectrum Characterization of Returned Samples: Orientation Constraints of Small Samples on X-Ray and Other Spectroscopies **[#1130]**
Orientation effects present significant analytical challenges for spectroscopic techniques that assess multivalent cations. Here, we quantify errors associated with using synchrotron microXANES to study anisotropic pyroxenes.

4:30 p.m. Keefner J. W. * Mackwell S. J. Kohlstedt D. L.
Dunite Viscosity Dependence on Oxygen Fugacity **[#1915]**
Deformation experiments were performed on Åheim dunite over ranges of temperature, stress, and solid state buffer to investigate the dependence of viscosity on oxygen fugacity. The strength difference between experiments demonstrates a power law exponent of 0.19.

Thursday, March 17, 2005
MARTIAN FLUVIAL LANDFORMS AND PROCESSES
1:30 p.m. Marina Plaza Ballroom

Chairs: K. P. Harrison
J. L. Heldmann

1:30 p.m. Williams R. M. E. * Malin M. C. Edgett K. S.
Remnants of the Courses of Fine-Scale, Precipitation-Fed Runoff Streams Preserved in the Martian Rock Record **[#1173]**
Remnants of precipitation-fed streams, similar in scale and topology to terrestrial creeks (and including first-order tributaries), are preserved in the martian rock record and exposed by erosion around the Valles Marineris.

1:45 p.m. Fassett C. I. * Head J. W. III
New Evidence for Fluvial Sedimentary Deposits on Mars: Deltas Formed in a Crater Lake in the Nili Fossae Region **[#1098]**
We present new observations of distributary fan deposits in a 40-km crater. We then analyze the formation of these deposits, which we argue was in a lacustrine environment, and discuss the implications of these findings for Martian climate history.

2:00 p.m. Cull S. C. * McGovern P. J.
Evidence for Extensive Fluvial Erosion Around Olympus Mons: A Multi-Resolution Survey **[#1154]**
This survey supports the hypothesis that an extensive groundwater system exists beneath Olympus Mons, and that its interactions with tectonism have produced much of the fluvial activity observed around the volcano.

2:15 p.m. Stepinski T. F. * Stepinski A. P.
Inferring Early Mars Climate from Comparison of Drainage Basins' Morphologies on Mars and Earth **[#1392]**
A similarity map constructed for 94 Martian and terrestrial drainage basins reveals a systematic difference between the two planets. This difference is explained by climatic differences with Martian basins developing in extremely dry climate.

2:30 p.m. Zimbelman J. R. * Williams S. H. Irwin R. P. III Rivera E. J. Graves L. Ghatan G.
Shorelines in the Western United States as Analogs for Hypothesized Shoreline Features on Mars **[#1733]**
Differential Global Positioning System surveys of shorelines in the western United States reveal distinctive topographic attributes that should aid in evaluating hypothesized shoreline features on Mars.

2:45 p.m. Quantin C. * Allemand P. Mangold N. Dromart G. Delacourt C.
Evidences for Fluvial and Lacustrine Activity on Interior Layered Deposits of Valles Marineris **[#1356]**
We report evidences for a fluvio-lacustrine system supplied by atmospheric precipitations located on Interior Layered Deposits (ILD) of Valles Marineris. Liquid water could have played a role in the erosion of the ILD.

3:00 p.m. Heldmann J. L. * Toon O. B. Pollard W. H. Mellon M. T. Pitlick J. McKay C. P. Andersen D. T.
Formation of Martian Gullies by the Action of Liquid Water Flowing Under Current Martian Environmental Conditions **[#1270]**
We examine the flow of water on Mars to determine what conditions are consistent with the observed gully features. Gully formation is consistent with the action of relatively pure liquid water flowing under current Martian environmental conditions.

3:15 p.m. Bridges N. T. * Lackner C. N.
Age-Orientation Relationships of Northern Hemisphere Martian Gullies and "Pasted-On" Mantling Unit: Implications for Near-Surface Water Migration in Mars' Recent History **[#1764]**
We have evaluated characteristics of northern hemisphere Martian gullies and compared them to predictions for an origin by snowpack melting. We find that the characteristics are consistent with a snowpack model that is driven by recent obliquity cycling.

3:30 p.m. Bleamaster L. F. III* Crown D. A.
Morphologic Characterization of Wall Slopes Along Dao and Harmakhis Valles, Mars: Mantle and Gully Associations **[#1469]**
Dao and Harmakhis Valles provide a unique opportunity to evaluate gully features with respect to latitude, elevation, slope orientation, and geologic unit in a single, distinct geologic setting.

3:45 p.m. Berman D. C. * Hartmann W. K. Crown D. A. Baker V. R.
Arcuate Ridges and Gullies in Martian Craters: Dependence on Orientation and Latitude **[#1213]**
Arcuate ridges and gullies are commonly found in 2 30 km diameter craters in the Phaethontis Quadrangle. The majority of them have pole-facing orientations, however at latitudes higher than 44°S, equator-facing orientations are more prevalent.

4:00 p.m. Treiman A. H. *
Martian Gullies and Groundwater: A Series of Unfortunate Exceptions **[#1713]**
For groundwater to participate in gully formation, it must be available at gully sites. Also, the bedrock must contain impermeable layers that do not tilt away from the gullies. Lamentably, nearly all gully sites fail these requirements.

4:15 p.m. Sears D. * Roe L. Moore S.
Stability of Water and Gully Formation on Mars **[#1496]**
Experimental work, theory, the size and frequency of gullies and sand dune characteristics in a region of Nirgal Vallis, suggests that the major factor in determining the stability of water on Mars is the presence of wind.

4:30 p.m. Harrison K. P. * Grimm R. E.
Tharsis Recharge and the Martian Outflow Channels: Observations and Recent Modeling **[#1211]**
Improved simulations of martian groundwater flow demonstrate the effects of Tharsis recharge on circum-Chryse outflow channel discharge for different initial conditions and aquifer properties, and are supported by observational evidence.

Thursday, March 17, 2005
POSTER SESSION II
7:00 p.m. Fitness Center

Lunar Potpourri

Lowman P. D. Jr.
Origin of the Lunar Highland Crust **[#2215]**
Surface photographs, remote sensing data, and returned sample analyses indicate that the lunar highland crust was formed by eruptions of high aluminum hypersthene basalt.

Gaddis L. R. Skinner J. A. Hare T. M. Tanaka K. Hawke B. R. Spudis P. Bussey D. B. J. Pieters C. Lawrence D. J.
Lunar Geologic Mapping: Preliminary Mapping of Copernicus Quad **[#2021]**
We describe prelimary 1:2.5 M scale geologic map results of the Copernicus quad as part of a new pilot program for systematic, global lunar geologic mapping.

Matsumoto N. Asada N. Demura H.
Automatic Crater Recognition on Digital Terrain Model **[#1995]**
This goal is a software development to detect craters automatically with following parameters; diameter, coordinates, depth, and direction of incidence. Verifications with ideal ellipsoids showed that this tool detected them exactly in diverse cases.

Archinal B. A. Rosiek M. R. Redding B. L.
Unified Lunar Control Network 2005 and Topographic Model **[#2106]**
We describe our effort to merge the existing Unified Lunar Control Network and the Clementine Lunar Control Network to form a new improved global lunar network, including a true 3-D lunar topographic model, the Unified Lunar Control Network 2005.

Anderson R. C. Buehler M. Seshadri S. Kuhlman G. Schaap M.
Dielectric Constant Measurements for Characterizing Lunar Soils **[#1969]**
The return to the Moon has ignited the need to characterize the lunar regoliths using fast, reliable *in situ* methods. Determining the dielectric constant of lunar materials can be very important in characterizing surface deposits, especially those that contain titanium, iron, and water.

Ebel D. S. Fogel R. A. Rivers M. L.
Tomographic Location of Potential Melt-bearing Phenocrysts in Lunar Glass Spherules **[#1505]**
Apollo 17 orange glass spherules contain olivine phenocrysts with melt inclusions from depth. Tomography (<2 μm/pxl) of >200 spherules located 1 phenocryst. We will try to find melt inclusions and obtain original magma volatiles and compositions.

Bérczi Sz. Cech V. Józsa S. Szakmány Gy. Fabriczy A. Földi T. Varga T.
How We Used NASA Lunar Set in Planetary Material Science Analog Studies on Lunar Basalts and Breccias with Industrial Materials of Steels and Ceramics **[#1282]**
Two main rock types of NASA Lunar Set were used in analog studies of processes and textures with selected industrial material samples: for breccias and basalts on the lunar side, ceramics and steels were analogs on the industrial side.

Kim K. J. Reedy R. C. Gasnault O.
Calculations of the Fluxes of 10–250 keV Lunar Leakage Gamma Rays **[#1900]**
The fluxes of 10–250 keV gamma rays from the Moon were calculated for a range of compositions and shown to be useful for some lunar studies. The shapes of the continuum <100 keV and its magnitude >100 keV vary systematically with composition.

Honda C. Fujimura A.
Formation Process of Lunar Sinuous Rilles by Thermal Erosion of Basaltic Lava Flow **[#1562]**
We examined the thermal erosion mechanism of basaltic lava flow for explaining the formation of sinuous rilles on the Moon. Appropriate conditions of candidate basaltic lavas enable us to interpret the formation condition of lunar sinuous rilles.

Skinner J. A. Jr. Gaddis L. R. Keszthelyi L. P. Hare T. M. Howington-Kraus E. Rosiek M.
Alphonsus-type Dark-Halo Craters — Morphometry and Volume Reassessments and Implications for Eruptive Style **[#2344]**
We use digital reproductions and analysis of past topographic datasets to update geomorphic and volumetric measurements for the Alpohonsus-type dark-halo craters.

Lunar Impacts

Zellner N. E. B. Delano J. W. Swindle T. D. Barra F. Olsen E. Whittet D. C. B. Spudis P. D.
Earth-Moon Impacts at ~300 Ma and ~500 Ma Ago **[#1204]**
Impact glasses from Apollo 16 regolith sample 66041,127 have been geochemically analyzed and a subset has been dated by the $^{40}Ar/^{39}Ar$ method. New results, with ages consistent with two break-ups in the Asteroid Belt, are presented here.

Dikov Yu. P. Gerasimov M. V. Yakovlev O. I.
Siderophile Behavior of P in Impact Processes **[#1125]**
Simulation of impact-related vaporization shows an efficient correlated reduction of iron and phosphorous. The reduction of Fe and P is only the effect of high temperature.

Tagle R.
LL-Ordinary Chondrite Impact on the Moon: Results from the 3.9 Ga Impact Melt at the Landing Site of Apollo 17 **[#2008]**
The re-interpretation of chemical data on Apollo 17 impact melt samples shows the possibility of the identification of Moon impactors by using PGE, Ni and Au elemental ratios.

Tagle R. Hecht L.
Evaluation of Chemical Methods for Projectile Identification in Terrestrial and Lunar Impactites **[#1927]**
This paper evaluates the capability of the main currently applied chemical methods to identify and characterize extraterrestrial material in lunar and terrestrial impactites.

Kletetschka G. Freund F. Wasilewski P. J. Mikula V. Kohout T.
Antipodal Magnetic Anomalies on the Moon, Contributions from Impact Induced Currents Due to Positive Holes and Flexoelectric Phenomina and Dynamo **[#1854]**
Lunar antipodal magnetic anomalies are related to impact energy. Factors are magnetic fields from impact plasma, currents from positive holes in rocks, flexoelectric effect, Thermal and/or chemical remanence acquired in the presence of lunar dynamo.

Miura Y.
Crater Variety With and Without Volcanic Rocks Bewteen the Moon and Earth **[#2287]**
Lunar crater of Maria type is different type of volcanic rocks and lava flow on crater on the Earth. Crater structure at Takamatsu-Kagawa district in Japan is similar with mare crater of the Moon with volcanic intrusion along crater structure.

Byrne C. J.
Size Distribution of Lunar Basins **[#1260]**
The distribution by size of the Moon's multi-ringed basins shows a significant difference between basins on the near side and those on the far side. Nearly all large multi-ringed basins (500 km or greater) are confined to a specific region.

Puchtel I. S. Walker R. J. James O. B.
$^{187}Os/^{188}Os$ and Highly Siderophile Element Systematics of Apollo 17 Aphanitic Melt Rocks **[#1707]**
Highly siderophile elements and Os isotopic systematics of Apollo 17 aphanitic melt rocks were studied. The data are consistent with the impactor having HSE characteristics similar to those of some enstatite chondrites.

Lunar Regolith: Measurements, Experiments, and Calculations

Noble S. K. Pieters C. M. Hiroi T.
Extracting Quantitative Data from Lunar Soil Spectra **[#1255]**
Using the LSCC suite of lunar soils, we found that the modified Gaussian modal can be utilized to extract quantitative data from high quality spectra. The model is sensitive to pyx abundance and even the relative portion of high-Ca and low-Ca pyx.

Gunderson K. Whitby J. Thomas N.
Visible and NIR BRDF Measurements of Lunar Soil Simulant **[#1781]**
We present visible and NIR BRDF measurements of JSC-1 lunar soil simulant under normal illumination and at near-zero phase angles for emission angles of 0° to 85°.

Wentworth S. J. Robinson G. A. McKay D. S.
Space Weathering of Intermediate-Size Soil Grains in Immature Apollo 17 Soil 71061 **[#2301]**
We are beginning a new study of space weathering of intermediate-size individual mineral grains from lunar soils. A major goal is to correlate the evidence for space weathering observed in studies of the surfaces of samples with evidence at higher resolution (TEM) using cross-sections.

Buono A. Brophy J. Schieber J. Basu A.
Experimental Production of Pure Iron Globules from Melts of Lunar Soil-Compositions **[#2066]**
Experimental melting of lunar soil compositions in a hydrogen atmosphere reduces the melt and produces submicron sized immiscible globules of pure iron. It is unnecessary to invoke vapor deposition to explain pure iron globules in lunar agglutinates.

Starukhina L. V.
Adhesion Forces Between Regolith Particles: Constraints on the Conditions of Electrostatic Lofting of Dust **[#1343]**
Sticking forces between regolith particles are the main obstacle for particle detachment from the surface under any applied force. E.g., at electrostatic potential ~10 volts either particles <~0.1 μm or extremely loosely bound particles can be lofted.

Wilson T. L. Wilson K. B.
Regolith Sintering: A Solution to Lunar Dust Mitigation? **[#1422]**
A concept for lunar dust mitigation is presented that supports early deployment of large telescopes on the Moon. The technology involves plasma spraying and epoxy developed from a study using JSC simulant, and is compared with regolith sintering.

Stubbs T. J. Vondrak R. R. Farrell W. M.
Impact of Lunar Dust on the Exploration Initiative **[#2277]**
Apollo astronauts encountered many problems on the Moon caused by lunar dust. Advances in space physics should now permit a better understanding of lunar surface charging and dust transport, thus allowing us to better tackle dust-related issues.

Pike W. T. Standley I. M. Banerdt W. B.
A High-Sensitivity Broad-Band Seismic Sensor for Shallow Seismic Sounding of the Lunar Regolith **[#2002]**
There is a renewed interest in techniques for characterizing the surface and shallow subsurface (0–10s of meters depth) of the Moon. Seismic techniques are ideal for determining geomechanical properties. We present a seismic sensor which is optimized for lunar exploration requirements.

Lunar Surface Remote Sensing

Okada T. Arai T. Hosono K. Shirai K. Yamamoto Y. Ogawa K. Kato M.
First X-Ray Observation of Lunar Farside from Hayabusa X-Ray Spectrometer **[#1175]**
The X-ray fluorescence spectrometer or XRS on-board Hayabusa has observed the first X-ray emission off the surface of lunar farside on May 17 in 2004, just before the Earth swing-by. The data indicates that the overall average composition of lunar farside is consistent with anorthositic crust.

Garrick-Bethell I. Zuber M. T.
An Indigenous Origin for the South Pole-Aitken Basin Thorium Anomaly **[#2372]**
Based on analysis of a combination of datasets we propose that the thorium anomaly in the northwest corner of the South Pole-Aitken basin most likely reflects an indigenous process.

Thompson T. W. Campbell B. A.
Unusual Radar Backscatter Properties Along the Northern Rim of Imbrium Basin **[#1535]**
The terra along the northern rim of Imbrium has unusually low radar backscatter, which is 2–4 times lower than other terra. This may be attributed to a mantle of pyroclastics in this area.

Campbell B. A. Campbell D. B. Chandler J.
New 70-cm Radar Mapping of the Moon **[#1385]**
We are collecting a new high-resolution 70-cm radar map of the lunar nearside.

Saito M. Takata T. Matsushita M. Chishima T. Ikeda Y. Hirao N. Iijima Y.
Ground-based Observation of Lunar Surface by Lunar VIS/NIR Spectral Imager **[#1513]**
Ground-based Lunar VIS/NIR Spectral Imager is developed in order to obtain 3 dimensional spectral and spatial images of the nearside of the moon. Preliminary imaging and data reduction were conducted in Mare Serenitatis and Tranquillitatis.

Giguere T. A. Hawke B. R. Gaddis L. R. Blewett D. T. Lucey P. G. Peterson C. A. Smith G. A. Spudis P. D. Taylor G. J.
Remote Sensing Studies of the Dionysius Region of the Moon **[#1092]**
The dark rays of Dionysius crater are dominated by mare debris, not by glassy impact melt. The mafic debris was derived from a dark layer exposed high on the inner crater wall.

Lawrence S. J. Hawke B. R. Lawrence D. J. Gillis J. J. Lucey P. G. Smith G. A. Taylor G. J.
The Composition and Origin of the Dewar Geochemical Anomaly **[#1549]**
We report the results of a remote sensing investigation of the thorium anomaly located northeast of Dewar crater on the lunar farside. The elevated thorium values correlate with FeO and TiO_2 enhancements. Possible origin mechanisms are discussed.

Kodama S.   Yamaguchi Y.
Mare Volcanism on the Moon Inferred from Clementine UVVIS Data **[#1641]**
The mare basalts in Oceanus Procellarum and Mare Imbrium were mapped, and their stratigraphy was established using the Clementine UVVIS data in order to understand the temporal and spatial variations of the lunar mare volcanism.

Gillis J. J.   Lucey P. G.   Campbell B. A.   Hawke B. R.
Clementine 2.7 μm Data and 70-cm Earth-based Radar Data Provide Additional Constraints for UVVIS-based Estimates of TiO_2 *Content for Lunar Mare Basalts* **[#2254]**
Looking to improve the accuracy of your UVVIS derived TiO_2 compositions for lunar basalts? Look no further, 2.7-μm and 70-cm radar data sets provide complementary information to the UVVIS ratio that may improve your estimates of TiO_2 composition.

Holsclaw G. M.   McClintock W. E.   Robinson M. S.
Comparison of Newly Acquired Lunar Spectra with the Titanium Abundance Maps Derived from Clementine **[#2376]**
Spectra of several locations on the Moon has been acquired. The correlation of the 360/450-nm color ratio with titanium abundance is examined.

Hackwill T.   Guest J. E.   Spudis P.
Basalts in Mare Serenitatis, Lacus Somniorum, Lacus Mortis and Part of Mare Tranquillitatis **[#1654]**
We have used Clementine data to investigate the spatial distribution of FeO and TiO_2 wt% in the Mare Serenitatis region. We suggest there is a correlation between FeO/TiO_2 wt% and basalt depth.

Kramer G. Y.   Jolliff B. L.   Neal C. R.   Kirkland L. E.   Fessler B.
Distinguishing High-Al Mare Basalt Units Using High Resolution Clementine Data **[#2256]**
High resolution Clementine FeO and TiO_2 are used to search for high-Al mare basalts exposures. Small impacts into a region, which are large enough to penetrate the regolith but do not excavate below the maria, act as windows revealing the composition of the fresh basalt.

Bussey D. B. J.   Schenk P. M.
Galileo's View of the Lunar North Pole **[#1219]**
Analysis of Galileo SSI images have provided new topography information for the north polar region. In addition these images represent a unique snapshot of the polar illumination conditions.

Hagerty J. J.   Lawrence D. J.   Elphic R. C.   Feldman W. C.   Vaniman D. T.   Hawke B. R.
Revised Thorium Abundances for Lunar Red Spots **[#1746]**
We use Lunar Prospector gamma-ray data and Clementine spectral reflectance data to revisit the interpretation of thorium abundances at the Gruithuisen red spot, with implications for other lunar red spots.

Wilcox B. B.   Lucey P. G.   Cahill J. T.
Space Weathering and Thermal Properties of Fresh Craters on the Moon **[#2293]**
We examine correlations between space weathering as determined from Clementine UV-VIS images and rock abundance as determined from thermal images taken during lunar eclipse, and present implications for the state of the regolith and its evolution.

Lunar Geophysics

Wilson T. L.
Moonshine Versus Earthshine: Physics Makes a Difference **[#1201]**
The Moon is treated as a calorimeter for measuring its cosmic-ray (CR) albedo produced by energetic CRs striking its surface. Monte Carlo results are used to predict this albedo as a component of lunar luminescence. The dark of the Moon is redefined.

Petrova N.   Gusev A.
Modeling of the Free Lunar Libration **[#1448]**
Results of modeling of free lunar rotation modes in dependence on a size, ellipticity, densitiy and state of aggregation of a lunar core, effects of dissipation are considered for the two- and three-layer Moon.

Gusev A. Kawano N. Petrov N.
Fine Phenomena of the Lunar Libration **[#1447]**
The geophysical evolution processes for formation of a fluid outer/solid inner core in the Moon are considered. In a case of free rotation of a three-layer Moon four modes in its polar motion might be observed.

Kikuchi F. Ping J. Hong X. Aili Y. Liu Q. Matsumoto K. Asari K. Tsuruta S. Kono Y. Hanada H. Kawano N.
VLBI Observation of Narrow Bandwidth Signals from the Spacecraft **[#1551]**
We carried out a VLBI observation of GEOTAIL by using a narrow bandwidth system. A few carrier waves with frequency interval of 1.5 MHz were correlated by software. As a result, the group delay was estimated within an error of less than 1 ns.

Bulow R. C. Johnson C. L. Shearer P. M.
Detection of New Deep Moonquakes in the Apollo Lunar Seismic Data: Implications for Temporal and Spatial Distribution **[#1581]**
New deep moonquakes found in the Apollo seismic data create a complete event catalog and larger numbers of stackable waveforms for a given deep cluster. These findings permit more robust analyses of tidal periodicities and source locations.

Khan A. Mosegaard K. Williams J. G. Lognonné P.
The Core of the Moon — Molten or Solid? **[#1122]**
We have inverted the second degree tidal love number, tidal quality factor, mass and moment of inertia to obtain information on the lunar core. Our results show that a small core of radius 350 km, density of 7 g/ccm and shear wave velocity around 0 km/s is the most likely outcome.

Barkin Yu. V. Ferrandiz J. M. Garcia Ferrandez M.
Earth, Moon, Mercury and Titan Seismicity: Observed and Expected Phenomena **[#1076]**
Using a dynamical analogy in translatory-rotary motions of the Moon and others synchronous satellites and Mercury we have obtained evaluations of periods of variations of the seismic activity of the Titan and Mercury.

Koyama J.
Chaotic Occurrence of Some Deep Moonquakes **[#1077]**
By a nonlinear method of Poincare map to time distribution in the newly-revised Apollo seismic event catalogue, we have revealed previously undetected features of hidden periodic components on the deep moonquake activity.

Nakamura Y.
Spatial Extent of a Deep Moonquake Nest — A Preliminary Report of Reexamination **[#1168]**
Spatial extent of A1 deep moonquake nest was reexamined with a recently expanded list of events. Contrary to expectation, the spread of hypocenters remained about the same — less than a km. A question remains why the nest is so compact.

Williams J. G. Boggs D. H. Ratcliff J. T.
Lunar Fluid Core and Solid-Body Tides **[#1503]**
Solutions for lunar science parameters continue to improve. A fluid core and strong tidal dissipation are inferred from the effect of dissipation on rotation. A second line of evidence for a fluid core, the core-mantle boundary flattening, appears significant.

Johnson C. L. Stixrude L. Lithgow-Bertelloni C. Bulow R. C. Shearer P. M.
Mineralogical and Seismological Models of the Lunar Mantle **[#1565]**
We construct self-consistent mineralogical models of the moon, calculating their associated physical properties, including seismic velocities. We assess models compatible with new and published travel times from lunar seismograms.

Beck A. R. Morgan Z. T. Liang Y. Hess P. C.
Dunite Dikes in the Lunar Mantle? **[#2220]**
We investigate mechanisms for melt migration through the lunar mantle with a series of harzburgite dissolution experiments. High-Ti magmas preferentially dissolve orthopyroxene and precipitate olivine forming dunite.

Seki K. Terada N. Shinagawa H. Ozima M.
Estimation of Ion Escape Rates from Non-Magnetic Earth: On Contribution of Terrestrial Ion Flows to Non-Solar Components Implantated in Lunar Soils **[#1200]**
Loss rates of heavy atmospheric constituents (e.g., N and Ar) from early non-magnetic Earth through the solar wind induced escape are estimated in order to access whether these escaping ions contribute to non-solar components implanted in lunar soils.

Lunar Isotopes

Moynier F.   Herzog G. F.   Albarède F. A.
Isotopic Fractionation of Copper and Zinc in Lunar Materials **[#1382]**
Cu and Zn isotope abundance measurements for lunar samples fall into three groups: Ti-rich basalt 74275 has near normal isotope abundances; orange glass 74220 is enriched in the lighter isotopes; ten soils are enriched in the heavier isotopes.

Farquhar J.   Wing B. A.
Sulfur Multiple Isotopes of the Moon: ^{33}S and ^{36}S Abundances Relative to Canon Diablo Troilite **[#2380]**
We are measuring sulfur multiple isotope abundances in 10 lunar basalts, a suite of terrestrial igneous rocks, and samples of Canon Diablo Troilite (CDT). Ongoing measurements suggest that the acid volatile sulfur (AVS) in lunar basalts is only slightly enriched in ^{34}S relative to CDT.

Ranen M. C.   Jacobsen S. B.
Isotopic Composition of Lunar Soils and the Early Differentiation of the Moon **[#2023]**
This study will measure Hf-W, Rb-Sr, Lu-Hf, and ^{147,146}Sm-^{143,142}Nd isotopes of Apollo 14 and 16 soils to estimate the average isotopic composition of the lunar crust in order to constrain timescales and magnitude of magma ocean crystallization.

Nemchin A. A.   Whitehouse M. J.   Pidgeon R. T.   Meyer C.
Isotopic Composition of Oxygen in Lunar Zircons **[#1274]**
Oxygen isotope analyses are reported for zircons from three lunar samples. They fall on the δ^{17}O vs. δ^{18}O terrestrial fractionation line. All samples with an exception of one show a restricted range of δ^{18}O, similar to that reported for lunar rocks.

Pidgeon R. T.   Nemchin A. A.   Meyer C.
A Further Investigation of the Exceptional Zircon Aggregate in Lunar Thin Section 73235,82 **[#1275]**
The exceptional zircon aggregate is interpreted as fragments of an original large zircon set within a matrix of secondary zircon formed during a major impact. The two U-Pb ages in this zircon register the primary zircon age and the age of impact.

Impacts and Their Effects on Earth and Above

Carmona J. A.   Cook M.   Cooper M.   Schmoke J.   Reay J.   Matthews L.   Hyde T. W.
Construction of a PZT Sensor Network for Low and Hypervelocity Impact Detection **[#1127]**
This paper will discuss a multiple PZT sensor network capable of determining both impactor momentum and location currently in development within CASPER.

Welten K. C.   Hillegonds D. J.   Jull A. J. T.   Kring D. A.
Atmospheric Fragmentation of the Gold Basin Meteoroid as Constrained from Cosmogenic Nuclides **[#2352]**
We studied the atmospheric fragmentation of the large Gold Basin meteoroid (R = 3–5 m) by evaluating a possible relationship between shielding depth (derived from cosmogenic nuclides in 40 Gold Basin samples) and the location of find in the strewnfield.

Chapman M. G.
Newly Discovered Meteor Crater Metallic Impact Spherules: Report and Implications **[#1907]**
This report documents the discovery and implications of large (3 mm to 1.5 cm), nonvesicular metallic spherules 82 km from Meteor (Barringer) impact crater.

Herzog G. F.   Alexander C. M. O'D.   Glass B. P.   Berger E. L.   Delaney J. S.
Potassium Isotope Fractionation in Australasian Microtektites: Evidence for Evaporation and Re-Condensation in a Vapor Plume **[#1167]**
Values of δ^{41}K (‰) for 13 Australasian microtektites range from -10.2 ± 0.5 to $+14.1\pm0.5$; no such large effects are seen in tektites. We propose that the isotopic fractionation took place in a plume, initially hot but rapidly cooling, associated with microtektite formation.

Serefiddin F.   Herzog G. F.   Koeberl C.
Beryllium-10 in Ivory Coast Tektites **[#1466]**
^{10}Be concentrations in Ivory Coast tektites are consistent with formation from near surface terrestrial soils. Concentrations 77% lower than in Australasian tektites reflect differences in source materials, longer decay and environmental factors.

Lee S. R. Horton J. W. Jr. Walker R. J.
Osmium-Isotope and Platinum-Group-Element Systematics of Impact-Melt Rocks, Chesapeake Bay Impact Structure, Virginia, USA **[#1700]**
Low $^{187}Os/^{188}Os$ ratios and enriched PGE concentrations in impact-melt rocks from the late Eocene Chesapeake Bay impact structure clearly confirm the presence of as much as 0.1 to 0.2% of an extraterrestrial component in the structure.

Sklute E. C. Dyar M. D. Minitti M. E. Leshin L. A. Guan Y. Luo S. Ahrens T. J.
Mössbauer Spectroscopy of Shocked Amphiboles **[#2040]**
Room temperature Mössbauer data from unshocked and shocked amphiboles are used to understand the oxidation/reduction effects of simulated impact on hydrous minerals.

McHone J. F. Fries M. Steele A.
Raman Imaging of Natural Coesite in Archived Petrographic Thin Sections: Vredefort Impact Structure **[#2315]**
Using a confocal Raman imager, natural coesite from the Vredefort Dome, South Africa has been nondestructively detected and mapped in petrographic thin sections.

Langenhorst F. Kyte F. T. Retallack G. J.
Reexamination of Quartz Grains from the Permian-Triassic Boundary Section at Graphite Peak, Antarctica **[#2358]**
A reexamination of quartz grains from the P/T boundary at Graphite Peak, Antarctica shows no evidence of planar deformation features characteristic of shock metamorphism.

Huson S. A. Pope M. C. Watkinson A. J. Foit F. F.
Possible Planar Elements in Zircon as Indicator of Peak Impact Pressures from the Sierra Madera Impact Crater, West Texas **[#2048]**
Shock features in zircon grains to tentatively place an upper limit on pressure during the Sierra Madera impact event.

Öhman T. Raitala J.
Geochemistry of the Dark Veinlets in the Granitoids from the Söderfjärden Impact Structure, Finland: Preliminary Results **[#1738]**
Peculiar dark veinlets in the granitoids on the rim of Söderfjärden impact crater haven't yet revealed any petrographic or geochemical evidence of friction melting or shock metamorphism. Thus their genetic connection to the impact remains unresolved.

Harris R. S. Schultz P. H. Bunch T. E.
Evidence for Shocked Feldspars and Ballen Quartz in 450,000 Year Old Argentine Impact Melt Breccias **[#1966]**
Shocked feldspars (containing PDFs and diaplectic glass) and ballen quartz identified in Centinela del Mar (450 ka) melt breccias support the impact origin of these glasses and provide insights into the shock deformation of porous sediments.

Sakamoto M. Gucsik A. Ninagawa K. Nishido H. Shichi R. Toyoda S. Bidló A. Brezsnyánszky K.
Mt. Oikeyama Structure: First Impact Structure in Japan? **[#1242]**
The pillaring texture of the microdeformations and PDFs of the quartz from Oikeyama, Japan, suggest that this structure was formed by an impact event.

Di Achille G.
A New Candidate Impact Site in Northeastern Sudan Detected from Remote Sensing **[#1606]**
A new possible impact structure has been observed in the northeastern Sudan. Using remote sensing analysis, geomorphologic and topographic evidence had been inferred to propose the impact site candidature for the study structure.

Belhai D. Merle O. Vincent P. Afalfiz A. Devouard B.
Are the Complex Algerian Meteoritic Craters Potential Hydrocarbon Traps? **[#1023]**
The geological analysis of the meteoritic craters of Tin Bider and Ouarkziz (Sahara, Algeria) reveals identical characters to those of Ava and Viewfield. Their detailed study will make it possible to slice as for the presence or not of hydrocarbons.

Heggy E. Paillou P. Mills D. Clifford S. M.
Mapping Buried Impacts Craters Using Ground-penetrating Radar: Mapping Some Structural Elements of the Largest Impact Field in the Western Egyptian Desert **[#2375]**
We present ground penetrating profiles of a number of relatively small buried craters of 30 to 100 m diameters and 3 to 10 m deep located in the largest impact crater field recently discovered in Southwest of the Egyptian by Paillou et al. in early 2004.

Earl J. Chicarro A. F. Koeberl C. Marchetti P. G. Milnes M.
Automatic Recognition of Crater-like Structures in Terrestrial and Planetary Images **[#1319]**
We describe new efforts regarding recognition and detection of impact craters on Earth and Mars by using remote sensing images. In particular, approaches based on the Hough Transform and on the Radial Consistency measure are considered and compared.

Milam K. A. Deane B.
Petrogenesis of Central Uplifts in Complex Terrestrial Impact Craters **[#2161]**
An examination of the petrogenesis of central uplifts in complex terrestrial craters and the common paragenetic sequence that deformation features display.

Horton J. W. Jr. Gohn G. S. Jackson J. C. Aleinikoff J. N. Sanford W. E. Edwards L. E. Powars D. S.
Results from a Scientific Test Hole in the Central Uplift, Chesapeake Bay Impact Structure, Virginia, USA **[#2003]**
A test hole in the Chesapeake Bay impact structure provides the first cores from the central uplift; reveals previously unknown suevites, melt rocks, shock-metamorphic features, and hydrothermal alteration; and serves as a pilot for future drilling.

King D. T. Jr. Petruny L. W.
Sedimentology of Impactoclastic Breccias, Cretaceous-Tertiary Boundary, Belize **[#1045]**
Impactoclastic breccias related to Chicxulub impact structure were analyzed using standard sedimentologic techniques in an attempt to better understand their origin and mode(s) of emplacement.

Zurcher L. Lounejeva-Baturina E. Kring D. A.
Preliminary Analysis of Relative Abundances of Hydrothermal Alteration Products in the C1-N10, Y6-N19, and Yax-1_863.51 Impact Melt Samples, Chicxulub Structure, Mexico **[#1983]**
Impact melt rocks from the C-1, Y-6, and Yax-1 boreholes in the Chicxulub structure sampled what may be a continuous crater-sized hydrothermal system. The purpose of this study is to estimate mineral modes to review possible alteration zonation patterns at the scale of the impact structure.

Kalleson E. Dypvik H. Naterstad J.
Sedimentary Infill of the Gardnos Impact Crater — A Field Report **[#1182]**
Recent field and core studies of the late Precambrian Gardnos impact structure have resulted in an updated and redrawn geological map, and a proposed sediment infill history, describing the sedimentary processes acting in the fresh crater.

Lindgren P. Parnell J.
Liquid Immiscibility in Suevite Melt, Gardnos Impact Crater **[#1629]**
Suevite melt from Gardnos impact crater show textures of liquid immiscibility between two silicate phases. These textures include intermingling tunnels, budding structures, flow of one phase within the other and curved menisci between the two phases.

Ormö J. Lindström M. M.
New Drill-Core Data from the Lockne Crater, Sweden: The Marine Excavation and Ejection Processes, and Post-Impact Environment **[#1124]**
Three short core drillings were performed in August 2004. They give information on the post-impact, geochemical environment, and the excavation process when strongly influenced by a thick layer of water in the upper part of the target.

Tsikalas F. Faleide J. I.
Post-Impact Deformation of Impact Craters: Towards a Better Understanding Through the Study of Mjølnir Crater **[#1022]**
The study of Mjølnir Crater has clearly shown the great importance of long-term deformation processes operating after impact. It appears that the establishment of a "post-impact modification correction factor" is prerequisite for several structures.

Glimsdal S. Pedersen G. Shuvalov V. Dypvik H. Langtangen H. P. Kristiansen O.
Tsunami Generated by the Mjølnir Impact **[#1287]**
The tsunami generated by the Mjølnir impact is described. Due to shallow water, we have found that the tsunami formed undular bores resulting in trains of solitary waves with amplitudes up to 300 m.

Dypvik H. Wolbach W. S. Shuvalov V. Weaver S. L. W.
Did the Mjølnir Asteroid Impact Ignite the Barents Sea Hydrocarbon Source Rocks? **[#1020]**
The soot particles most likely came from pyrolysis and combustion heating of the organic rich, partly volatile, dark clays of the sea bed (Hekkingen Formation). This heating occurred during shock wave propagation through the target sediments with fire lasting the 20 minutes dry sea bed period.

Graham R. A. Wilson W. F.
Reinvestigation of the Bee Bluff Structure South of Uvalde, Texas, 'The Uvalde Crater.' **[#1086]**
Investigation of the Bee Bluff Structure provides new evidence for an impact crater origin. A 300 kg rock preserving numerous impactite features called the 'Uvalde Crater Rosetta Stone,' promises to provide detail on the first billion nanoseconds of the impact events.

Sandberg C. A. Poole F. G. Morrow J. R.
Milk Spring Channels Provide Further Evidence of Oceanic, >1.7-km-Deep Late Devonian Alamo Crater, Southern Nevada **[#1538]**
New conodont microfossil and stratigraphic data on a deep-water, offshore breccia channel deposit of the marine, early Late Devonian Alamo Impact, Nevada, provide further evidence of its crater depth and off-platform impact site.

Dulin S. A. Elmore R. D. Gardner K. G.
Impacts in Carbonate Target Rocks: A Paleomagnetic Study of the Weaubleau-Osceola and Alamo Breccia Impact Structures **[#1371]**
The objective of this paleomagnetic study is to investigate two impact features in carbonate rocks to develop a model that can be used to constrain the age of impacts and provide insights on the sedimentary processes involved during deposition of bolide related units.

Glass B. J. Domville S. Lee P.
Further Geophysical Studies of the Haughton Impact Structure **[#2398]**
The investigation discussed here examines and surveys the Haughton Impact Structure, characterizing it and the surrounding regional area with newly-added gravity survey data.

MER and MOC Results

Golombek M. P. Arvidson R. E. Bell J. F. III Christensen P. R. Crisp J. Ehlmann B. L. Fergason R. L. Grant J. A. Haldemann A. F. C. Parker T. J. Squyres S. W. Athena Science Team
Assessment of Mars Exploration Rover Landing Site Predictions **[#1542]**
Assessment of Mars Exploration Rover landing site predictions made in the evaluation of remote sensing data during selection indicates most of the important surface characteristics were correctly predicted.

Schwochert M. A. Maki J. N.
The Mars Exploration Rover Cameras: A Status Report **[#1793]**
With more than 68,000 images returned from the surface of Mars, the Mars Exploration Rover camera suite continues to perform extremely well. Image SNRs are greater than 200:1, flat fields remain stable, and single-pixel degradation is negligible.

Fergason R. L. Christensen P. R.
Thermophysics at the MER Spirit and Opportunity Landing Sites: Perspectives from the Surface and from Orbit **[#1265]**
Understanding thermophysical properties of MER landing site surfaces is important for identifying recent processes effecting these regions. We developed a technique to calculate thermal inertia values from Mini-TES spectra and present our results.

Bertelsen P. Bell J. F. III Goetz W. Gunnlaugsson H. P. Herkenhoff K. E. Hviid S. F. Johnson J. R. Kinch K. M. Knudsen J. M. Madsen M. B. McCartney E. Merrison J. Ming D. M. Morris R. V. Olsen M. Proton J. B. Sims M. Squyres S. W. Yen A. S.
Dynamic Dust Accumulation and Dust Removal Observed on the Mars Exploration Rover Magnets **[#2250]**
The Mars Exploration Rovers carry a set of Magnetic Properties Experiments designed to investigate the properties of the airborne dust in the Martian atmosphere. This abstract will focus on dust deposition and dust removal on some of the magnets.

Li R. Squyres S. W. Arvidson R. E. Bell J. F. III Crumpler L. S. Des Marais D. J. Di K. Golombek M. P. Grant J. Guinn J. Greeley R. Kirk R. L. Maimone M. Matthies L. H. Malin M. C. Parker T. Sims M. Soderblom L. A. Wang J. Watters W. A. Whelley P. Xu F. Athena Science Team
Results of Rover Localization and Topographic Mapping for the 2003 Mars Exploration Rover Mission **[#1349]**
This paper presents the results of rover localization and topographic mapping for the 2003 MER mission. Topographic maps, rover traverse maps, and updated rover locations have been routinely produced to support tactical and strategic operations.

Seelos F. P. Arvidson R. E. Guinness E. A. Wolff M. J.
Radiative Transfer Photometric Analyses at the Mars Exploration Rover Landing Sites **[#2054]**
MER Pancam radiance data is inverted to optimize bidirectional reflectance model parameters for the Martian surface.

Blaney D. L. Bell J. F. III Cabrol N. A. Christensen P. R. Farand W. Ming D. W. Moersch J. E. Ruff S. Athena Science Team
Spectral Divsersity at Gusev Crater from Coordinated Mini-TES and Pancam Observations **[#2064]**
Spirit has explored Gusev crater with Pancam and Mini-TES. Coordinated and targeted observations were used to determine the spectral diversity. Three classes of rocks were identified spectrally. Natural and brushed surfaces can be spectrally similar.

Ruff S. W. Christensen P. R. Blaney D. L. Athena Science Team
The Rocks of Gusev Crater as Viewed by Mini-TES **[#2155]**
Mini-TES on the Spirit rover has documented three different classes of rocks in Gusev Crater that represent a diverse geological history.

Cabrol N. A. Greeley R. Athena Science Team
Characterization of Non-Organized Soils at Gusev Crater with the Spirit Rover Data **[#2328]**
We surveyed the characteristic of non-organized soils at Gusev crater at microscale and macroscale in four main traverse regions: (1) Landing site to Bonneville crater; (2) Bonneville to West Spur; (3) the West Spur region; and (4) the Columbia Hills up to sol 363.

Wang A. Haskin L. A. Korotev R. L. Jolliff B. L. de Souza P. A. Jr. Kusack A. G. Athena Team
Evidence of Phyllosilicate in Wooly Patch — an Altered Rock Encountered on the Spirit Rover Traverse **[#2327]**
Rock Wooly Patch on West Spur has several specific physical and chemical features. Based on our analyses, phyllosilicates of kaolinite, serpentine, and chlorite types, plus some feldspar and pyroxene are prime candidates to constitute this rock.

Metzger S. M.
Evidence of Dust Devil Scour at the MER Spirit Gusev Site **[#2397]**
Using MOC and MER, this report examines at broadly different scales the effects of dust devil vortices on the surface in Gusev crater. Results include a rare occurrence of proper meteorological and geological formation conditions, and the removal of substantial volumes of dust from the surface.

Edgett K. S. Malin M. C.
The Sedimentary Rocks of Meridiani Planum, in Context **[#1171]**
Sedimentary rocks at the MER-B site are part of a stratigraphic section more than 1 km thick. The rocks are not superimposed on heavily cratered terrain, they are part of it, and they record a rich, diverse history.

Weitz C. M. Anderson R. C. Bell J. F. III Cabrol N. A. Calvin W. M. Ehlmann B. L. Farrand W. H. Greeley R. Herkenhoff K. E. Johnson J. R. Jolliff B. L. Morris R. V. Soderblom L. A. Squyres S. W. Sullivan R. J.
Seeing the Soils of Meridiani Planum Through the Eyes of Pancam and Microscopic Imager **[#1362]**
We are using data from the Pancam and Microscopic Imager (MI) on the Opportunity rover to characterize soil grains at Meridiani Planum greater than 0.3 mm in size. In general, the size of most grains within Eagle crater falls between 1.5–3.5 mm, and they are very circular in cross section.

King P. L. Lescinsky D. T. Nesbitt H. W.
Comparison of Predicted Salt Precipitation Sequences with Mars Exploration Rover Data **[#2300]**
We compare predicted salt precipitation sequences with Mars Exploration Rover data.

Kargel J. S.
Aqueous Chemistry, Physical Chemistry, and Sedimentology of Rocks at the Mars Rover Landing Sites **[#2149]**
Observations at Meridiani Planum indicate layer-by-layer aqueous deposition in a highly acidic and hypersaline sea that was very cold, but not as cold as current prevalent conditions. A huge debris flow is likely at Gusev Crater.

Schaefer M. W. Dyar M. D. Agresti D. G. Schaefer B. E.
Error Analysis of Remotely-Acquired Mössbauer Spectra **[#2047]**
Mössbauer spectroscopy is being used to assist in mineral identification on Mars. We discuss the major sources of error associated with peak positions in remotely-acquired spectra, and speculate on their magnitude and influence on interpretation.

Seda T. Irving A. J.
Thin Wafer Transmission Mössbauer Spectra of Four Shergottites: Implications for Mineralogy of Rocks at Mars Exploration Rover Sites **[#2204]**
Mössbauer spectra were obtained on thin wafers of four shergottite meteorites for comparison with data for rocks at the Spirit and Opportunity sites.

Bérczi Sz.
Possibility of Karst Morphology on the Martian Surface at the Meridiani Landing Site from Comparison with Terrestrial Analogs **[#1051]**
On Opportunity images of the 70–74 sols chains of pits forming a trench pattern can be interpreted as dolines, the whole trench pattern as a solution groove, both belonging to counterpart terrestrial karst morphology.

Jolliff B. L. Athena Science Team
Composition of Meridiani Hematite-rich Spherules: A Mass-Balance Mixing-Model Approach **[#2269]**
A mass-balance model using APXS data and microscopic images indicates that the composition of spherules ("blueberries"), found at the Meridiani site by the Mars Exploration Rover Opportunity and thought to be concretions, contain ~45–60 wt% hematite.

Gánti T. Pocs T. Bérczi Sz. Ditroi-Pukas Z. Gal-Solymos K. Horváth A. Nagy M. Kubovics I.
Morphological Investigations of Martian Spherules, Comparisons to Collected Terrestrial Counterparts **[#2026]**
We studied the morphology of the Martian spherules and compared them with their terrestrial counterparts with hematite crust, collected in Venezuela and West Australian deserts, and discussed their possible formation processes.

Stein T. C. Arvidson R. E.
MER Analyst's Notebook: Integrating Data and Documentation for Mission Playback **[#1246]**
The MER Analyst's Notebook provides access to the MER mission data archives by integrating sequence information, engineering and science data, and documentation into Web-accessible pages to facilitate mission "replay."

Malin M. C. Edgett K. S.
MGS MOC: First Views of Mars at Sub-Meter Resolution from Orbit **[#1172]**
Since 2003, MGS MOC has been acquiring images of Mars at sub-meter resolution, revealing new details and testing hypotheses regarding the planet's geology and geomorphology.

Mars Geochemistry

Stafford K. W. Boston P. J.
Theoretical Evaporite Karst Development on Mars **[#2291]**
Recent evidence of stratified sulfate rich rocks on Mars implies possible evaporite deposits. This suggests that evaporite karst and cave development similar to that observed on Earth may be present.

Chipera S. J. Vaniman D. T. Bish D. L. Carey J. W. Feldman W. C.
Experimental Stability and Transformation Kinetics of Magnesium Sulfate Hydrates that may be Present on Mars **[#1497]**
The stability and kinetics of various Mg-sulfate hydrates were investigated at variable RH and temperature for extrapolation to Mars conditions. Epsomite, hexahydrite, starkeyite and kieserite show the largest stabilities but other hydrates persist.

Lane M. D. Bishop J. L. Dyar M. D. Cloutis E. A. Forray F. L. Hiroi T.
Integrated Spectroscopic Studies of Anhydrous Sulfate Minerals **[#1442]**
A suite of anhydrous sulfates were studied using visible/near-infrared reflectance, midinfrared emittance, and Mössbauer spectroscopies.

Rothstein Y. Dyar M. D. Schaefer M. W. Lane M. D. Bishop J. L.
Fundamental Mössbauer Parameters of Hydrous Iron Sulfates **[#2108]**
Mössbauer data acquired at variable temperatures are presented. Results are used to determine the temperature dependence and recoil-free fraction of hydrous iron sulfates.

Sutter B. Dalton J. B. Ewing S. A. Amundson R. McKay C. P.
Infrared Spectroscopic Analyses of Sulfate, Nitrate, and Carbonate-bearing Atacama Desert Soils: Analogs for the Interpretation of Infrared Spectra from the Martian Surface **[#2182]**
The infrared spectroscopic characteristics of Atacama Desert soils containing sulfates, nitrates, and carbonates are examined as potential analogs to Mars soils.

Hasenmueller E. A. Bish D. L.
The Hydration and Dehydration of Hydrous Ferric Iron Sulfates **[#1164]**
The dehydration/hydration behavior of jarosite and of the hydrated ferric sulfates kornelite, botryogen, and coquimbite, was analyzed by X-ray diffraction methods up to 300°C in vacuum. All three hydrous sulfates began to break down at ~50°C.

Jänchen J. Bish D. L. Möhlmann D. T. F. Stach H.
Experimental Studies of the Water Sorption Properties of Mars-Relevant Porous Minerals and Sulfates **[#1263]**
We evaluated experimentally water sorption properties of minerals identified by OMEGA in martian soil. Our results show up to 20% water in zeolites, clays, sulfates at martian surfaces conditions for equatorial latitudes as shown by Mars Odyssey.

Michalski J. R. Kraft M. D. Sharp T. G. Christensen P. R.
Palagonite-like Alteration Products on the Earth and Mars I: Spectroscopy (0.4–25 microns) of Weathered Basalts and Silicate Alteration Products **[#1188]**
Poorly crystalline silicate alteration products may be widespread on Mars. We discuss spectral evidence for these materials in weathered terrestrial basalts, similarities to spectra of Mars, and the implications for chemical alteration on Mars.

McAdam A. C. Leshin L. A. Sharp T. G. Harvey R. P. Hoffman E. J.
Investigation of Weathering Products of Martian Meteorite Analog Materials and Implications for the Formation of Martian Surface Fines **[#2041]**
We report on the mineralogy of an Antarctic Mars analog material. The mineral assemblage suggests that significant chemical weathering has occurred and that acid fog style weathering contributed to the production of chemical weathering products.

Kraft M. D. Michalski J. R. Sharp T. G.
Palagonite-like Alteration Products on the Earth and Mars 2: Secondary Mineralogy of Crystalline Basalts Weathered Under Semi-Arid Conditions **[#1376]**
In weathering rinds of crystalline basalts, we find poorly crystalline secondary silicates, similar to palagonites. Small volumes of these products cause rinds to have "glassy" thermal-IR spectra. Similar spectral surfaces on Mars may be altered.

Arlauckas S. A. McLennan S. M.
Dissolution Rates and Weathering Products of Iron-Titanium Oxides: pH and Temperature Dependence **[#2011]**
Experiments show that Fe-Ti oxides dissolve readily at low pH and temperature on short timescales. After dissolution in H_2SO_4, Fe-bearing sulfate minerals precipitate from the fluid. Dissolution rates and evaporite mineralogy will be discussed.

Hurowitz J. A. Tosca N. J. McLennan S. M. Athena Science Team
Experimental Basalt Alteration at Low-pH: Implications for Weathering Relationships on Mars **[#2025]**
in situ analyses of Martian rocks and soils to experimental data from alteration of synthetic Martian basalt at low-pH are compared. Results indicate that dissolution of olivine at low-water to rock ratio is an important weathering process on Mars.

Marion G. M. Kargel J. S.
Stability of Magnesium Sulfate Minerals in Martian Environments **[#2290]**
We will explore the thermodynamics of $MgSO_4$ minerals on the surface of Mars.

Socki R. A. Gibson E. K. Jr. Bissada K. K.
Contribution of Organic Material to the Stable Isotope Composition of Some Terrestrial Carbonates as Analogs for Martian Processes **[#1703]**
A more through understanding of the effects of aqueous weathering and the potential contribution of organic compounds on the isotopic composition of Martian carbonate minerals can be gained by studying some terrestrial occurrences of carbonate rocks.

Wet Mars: Oceans, Gullies, and More

Barnhart C. J. Tulaczyk S. Asphaug E. Kraal E. R. Moore J. M.
Ice-Ridge PileUup and the Genesis of Martian "Shorelines" **[#1560]**
The geomorphology of crater "shoreline" features is a key to the Martian past, yet the interpretation of surface morphology lacks the definition of a quantitative model. We model geomorphic systems that posit ice plugs as the formation mechanism.

Salamuniććar G.
New Insight into Valleys-Ocean Boundary on Mars Using 128 Pixels Per Degree MOLA Data: Implication for Martian Ocean and Global Climate Change **[#1455]**
This work investigates new insight into the relationship between morphology and elevation of Martian valleys termini and hypothetical Martian ocean including their implication for global climate change using 128 pixels per degree MOLA data.

Santiago D. L. Colaprete A. Haberle R. M. Sloan L. C. Asphaug E.
Outflow Channels Influencing Martian Climate: Global Circulation Model Simulations with Emplaced Water **[#1787]**
We are using the NASA Ames Mars General Circulation Model to examine the climatic consequences of the sudden burst of water from outflow channels on Mars, represented here by incrementally emplacing water on the surface.

Crown D. A. Bleamaster L. F. III Mest S. C. Teneva L. T.
Styles and Timing of Volatile-driven Activity in the Eastern Hellas Region of Mars **[#2097]**
Current research integrates geologic studies of the basin floor and east rim using Viking Orbiter, Mars Global Surveyor, and Mars Odyssey datasets to provide a synthesis of the history of volatiles in the region.

Rodriguez J. A. P. Sasaki S. Tanaka K. L. Skinner J. A. Jr. Dohm J. M. Miyamoto H. Fairén A. G. Kuzmin R. O. Schulze-Makuch D. Baker V. R.
Outflow Channel Floor Collapse and the Formation of the Simud and Tiu Valles, Mars **[#1786]**
We investigate the geologic history of the Simud and Tiu Valles. Based on geologic mapping and geomorphic assessment using Viking-, Mars Global Surveyor-, and Mars Odyssey-based information we discuss significant surface collapse in the region.

Sato H. Kurita K.
Circular Collapsed Features Related to the Chaotic Terrain Formation on Mars **[#2248]**
we examined distribution and morphologies of the circular collapses around the Xanthe terra region, Mars. We explored a model of its formation and give suggestions how the chaotic terrains were formed and discharged a huge amount of water.

Bargery A. S. Wilson L. Mitchell K. L.
Modelling Catastrophic Floods on the Surface of Mars **[#1961]**
We investigate evaporation, freezing and sublimation of water flowing on the surface of Mars. Rheological changes due to ice crystal growth in water are discussed, and we attempt to relate water volume flux and maximum run-out distance.

Mitchell K. L. Leesch F. Wilson L.
Uncertainties in Water Discharge Rates at the Athabasca Valles Paleochannel System, Mars **[#1930]**
We use Darcy-Weisbach flow modelling, considering all quantifiable uncertainties, in order to recalculate the volumetric flux of the floods that formed Athabasca Valles, and find uncertainties of three to four orders of magnitude.

Marinangeli L. Rossi A. P. Pondrelli M. Baliva A. Di Lorenzo S. Ori G. G. Hauber E. Neukum G. HRSC Team
Paleoenviromental Evolution of the Holden-Uzboi Area **[#1702]**
A variety of younger fluvio-lacustrine environments and glacial morphologies have been recognized in the Holden-Uzboi area, suggesting variations of the water cycle trough time.

Leverington D. W.
Evaluation of Candidate Crater-Lake Sites on Mars **[#1522]**
There is a direct association on Mars between candidate crater-lake sites and ridged plains that mark both the source regions and basins of accumulation of massive effusive volcanic events.

Williams R. M. E. Edgett K. S.
Valleys in the Martian Rock Record **[#1099]**
Martian valley systems are part of the layered upper crust and exhibit a variety of preservation states including partial or discontinuous exposure and inverted relief.

Harrison K. P. Grimm R. E.
Evolution of Martian Valley Network Formation: Surface Runoff to Groundwater Discharge **[#1218]**
The morphological differences between densely dissecting, degraded martian valley networks and sparsely dissecting, pristine networks, are proposed to result from a temporal evolution away from surface runoff erosion toward groundwater processes.

Gulick V. C.
Revisiting Valley Development on Martian Volcanoes Using MGS and Odyssey Data **[#2345]**
The valley networks found on the slopes of Martian volcanoes represent an interesting subset of the Martian valley networks. Here I consider what new constraints can be applied to the formation of these valleys utilizing MGS and Odyssey data.

Kereszturi A.
Cross Profile and Volume Analysis of Bahram Valles on Mars **[#1609]**
We analysed cross section profiles of Bahram Valles on Mars and the connection between its shape, the surrounding terrain and the probable erosional processes, and estimated the volume of transported material during its formation.

Heldmann J. L. Johansson H. Carlsson E. Mellon M. T.
Northern Hemisphere Gullies on Mars: Analysis of Spacecraft Data and Implications for Formation Mechanisms **[#1271]**
We test the validity of gully formation mechanisms by analyzing data from the Mars Global Surveyor and Mars Odyssey spacecrafts to uncover trends in the dimensional and physical properties of the gullies and their surrounding terrain.

Dickson J. L. Head J. W. III
Detection of Gullies on Central Peaks and Crater Rims on Mars: Implications for the Origin of Gullies **[#1097]**
We present evidence in MOC narrow-angle image data for gully landforms on isolated surfaces, such as central peaks and crater rims. We use this data to argue that surface accumulation and melting of snowpacks is the likely candidate for formation.

Craig J. Sears D.
Albedo Study of the Depositional Fans Associated with Martian Gullies **[#1198]**
This work is a two-part investigation of the albedo of the depositional aprons or fans associated with Martian gully features. Using Adobe Systems Photoshop 5.0 software we analyzed numerous Mars Global Surveyor MOC and Mars Odyssey THEMIS images.

Travis B. J.
On Modeling the Seepage of Water into the Martian Subsurface **[#2338]**
Numerical simulations of water infiltration into the Martian regolith from surface sources of water indicate that infiltration can occur rapidly and that only a partially saturated condition is likely to develop in the subsurface.

Howard A. D. Moore J. M. Irwin R. P. III Craddock R. A.
A Sedimentary Platform in Margaritifer Sinus, Meridiani Terra, and Arabia? **[#1545]**
A topographic bench between –1000 m to –1700 m is postulated to be a constructional fluvial platform.

Bourke M. C. Brearley A. J. Haas R. Viles H. A.
The Surface Features of 'Pristine' Flood-transported Boulders **[#2253]**
Surface features on basalt boulders that are unique to fluvial transport have been identified and can be used to identify similar features on planetary surfaces.

Salamuniććar G.
Recursive Topography Based Surface Age Computations for Mars: New Insight into Surficial Processes that Influenced Craters Distribution as a Step Toward the Formal Proof of Martian Ocean Recession, Timing and Probability **[#1451]**
This work investigates new algorithm how to measure influence on craters distribution, providing new insight into the processes that caused this influence (probably lava flows and polar caps), the amount of resurfacing and the ocean hypothesis.

Nguyen D. Romero K. Cassiani N. Rogers J. Lee J. Saribudak E.
Thermal Analysis of Aqueous Features on Mars **[#2036]**
An investigation of the relationship between sinuous, dendritic features on Mars, believed to be aqueous, and the temperature of the land's surfaces. THEMIS IR images were compared to the known aqueous features of the Kasei Valles.

Horváth A. Kereszturi A. Bérczi Sz. Sik A. Pócs T. Gesztesi A. Gánti T. Szathmáry E.
Annual Change of Martian DDS-Seepages **[#1128]**
Dark Dune Spots (DDSs) are sources of slope streaks that we explain as seepages flowing down-slope from the defrosting dark regions. This water-related interpretation gives stronger evidence for the biological model of DDS formation.

Möhlmann D. T. F.
The Importance of Adsorption Water in the Upper Martian Surface **[#1120]**
There is adsorption water in and above the upper martian surface at mid- and low latitudes. This "unfrozen" adsorption water behaves liquid-like. Related physical, chemical and possible biological consequences are discussed.

Mars Global Units and Composition

Haldemann A. F. C. Larsen K. W. Jurgens R. F. Slade M. A.
Comparing Goldstone Solar System Radar Earth-based Observations of Mars with Orbital Datasets **[#2347]**
Radar data, requires significant data processing to extract elevation, reflectivity and roughness. This presentation summarizes how to compare GSSR delay-Doppler data to other Mars datasets, including some ideosyncracies of the radar data.

Dohm J. M. Kerry K. Keller J. Baker V. R. Boynton W. V. Maruyama S. Anderson R. C.
Mars Geological Province Designations for the Interpretation of GRS Data **[#1567]**
Based on a synthesis of published geologic, paleohydrologic, topographic, and geophysical information, we have defined geologic provinces that represent significant windows into the geologic evolution of Mars, consistent with the GEOMARS theory and supported by GRS data.

Hahn B. C.   McLennan S. M.   Taylor G. J.   Boynton W. V.
Integrating Global-scale Mission Datasets — Understanding the Martian Crust **[#1853]**
Individual chemical datasets such as TES and GRS must be cross-correlated with other datasets, such as surface age, in order to understand Martian crust/mantle evolution.

Taylor G. J.   Stopar J.   Boynton W. V.   Brückner J.   Wänke H.
Assessing Aqueous Alteration on Mars Using Global Distributions of K and Th **[#1540]**
K/Th shows modest variations on Mars that could be caused by igneous processes or aqueous alteration. The extent of aqueous alteration might be muted by the time it takes to dissolve the host minerals for K and Th, and the relative immobility for Th.

Gasnault O.   Maurice S.   d'Uston C.   Feldman W. C.   Boynton W. V.
Comparison of Three Hydrogen Distributions at the Equator of Mars **[#2318]**
Three maps of hydrogen in the Martian surface were derived from the gamma/neutron experiments. We compare them in the equatorial band to show their interrelation that varies with H- and Fe-abundances, and burial depths.

Clark C. S.
The Martian Watershed, Geology, Dichotomy and Paleohydrology on Two World Maps with Constant Scale Natural Boundaries **[#2189]**
An overview with novel map projections of martian paleohydrology and crustal dichotomy, focused on the planetary watershed and underlying geology.

Clevy J. R.   Kattenhorn S. A.
Possible Fault Control of Hydrogen Ion Concentrations Near Schiaparelli Crater, Mars **[#1052]**
Linear hydrogen concentrations, which are potential water indicators, mimic the width and trend of graben between Scylla and Charybdis Scopulus, Mars, suggesting structural control of potential subsurface water locations.

Heggy E.
Loss Tangent Map of the Martian Surface: A Frequency Dependent Model for the Near Equatorial Regions **[#2109]**
Using laboratory dielectric characterization of basaltic Mars-like soils and soil density distribution extracted from TES data, we suggest a frequency dependent loss tangent and complex dielectric map of the Martian surface in the frequency range from 1 MHz to 3 GHz.

Mars Infrared Spectroscopy

Stockstill K. R.   Moersch J. E.   McSween H. Y. Jr.   Christensen P. R.
THEMIS Multipsectral Analysis of Proposed Paleolake Basins in the Aeolis Quadrangle of Mars **[#2107]**
We use THEMIS data to search for small-scale aqueous deposits within proposed paleolake basins in the Aeolis quadrangle of Mars.

Whisner S. C.   Moersch J. E.
Correlating Remotely-sensed Nighttime Thermal Radiance Images with Field-mapped Geologic Units: A Terrestrial Case Study with Applications to Mars **[#2103]**
Dust (Mars) and vegetation (Earth) spectral features overwhelm compositional spectral features in SWIR. Nighttime TIR reveals deeper structural and lithologic complexities, confirmed by surface mapping in SE TN due to the greater sensing depth associated with diurnal thermal propagation.

Archinal B. A.   Sides S.   Weller L.   Cushing G.   Titus T.   Kirk R. L.   Soderblom L. A.   Duxbury T. C.
Model Development and Testing for THEMIS Controlled Mars Mosaics **[#2052]**
We describe our algorithm for making controlled mosaics of Mars using THEMIS IR images. Also discussed are issues regarding making large area or global mosaics, such as automatic tiepointing, rejection of outliers, and block adjustment solutions.

Lane M. D.
Evidence for Aqueously Precipitated Sulfates in Northeast Meridiani Using THEMIS and TES Data **[#2180]**
An investigation using THEMIS and TES midinfrared spectral data has revealed a channel to the northeast of the Meridiani plains that contains aqueously precipitated sulfates. Sulfates are also identified in the surrounding plains.

Moersch J. E.   Crumpler L. S.   Arvidson R. E.   Blaney D. L.   Christensen P. R.   Fergason R.   Golombek M. P.   Knudson A.   Piatek J.   Ruff S.   Squyres S.   Tornabene L. L.   Wyatt M.   Athena Science Team
Comparison of Orbital Infrared Observations and Surface Measurements by the Mars Exploration Rover Spirit at Gusev Crater **[#2020]**
Thermal inertias derived from THEMIS night infrared images are correlated with rock population measurements made by the Mars Exploration Rover Spirit while traversing the plains between Bonneville crater and the Columbia Hills.

Dunn T. L.   McSween H. Y. Jr.   Milam K. A.
Using Thermal Emission Spectra to Model Modal Mineralogies of Alkalic Rocks: Applications for Mars **[#1776]**
Modal mineralogies of a suite of terrestrial alkalic rocks were determined by both electron microprobe mapping and deconvolution of thermal emission spectra. Modeled modes were then compared to laboratory measured modes to access their accuracy.

Murphy N. W.   Jakosky B. M.   Rafkin S. C. R.   Larsen K.   Putzig N. E.   Mellon M. T.
Thermophysical Properties of the Surface of Isidis Basin, Mars **[#2218]**
We investigated the properties of the high thermal inertia surface in Isidis basin by comparing thermal data from TES and THEMIS, visible data from THEMIS and MOC, ground-based radar data, and results of mesoscale atmospheric modeling.

Anderson F. S.   Drake J. S.   Hamilton V. E.
Extracting Compositional Variation from THEMIS Data for Features with Large Topography on Mars Via Atmospheric Equalization **[#1852]**
We present an atmospheric equalization for THEMIS IR data. This equalization permits analysis of composition in regions that are difficult to study because of differences in atmospheric path length resulting from large changes in surface elevation.

Rogers A. D.   Bandfield J. L.   Christensen P. R.
Global Spectral Classification of Martian Low-Albedo Regions with MGS-TES **[#2131]**
TES data are used to re-examine low-albedo surfaces for region-to-region differences in spectral response. Regional variations are present; the differences in spectral shapes indicate that they may differ in primary mineralogy or alteration history.

Rodricks N.   Greenhagen B.   Kirkland L. E.   Herr K. C.
Composition Determined by Linear Mixture Modeling Varies with the Lab Spectra Used **[#2388]**
Composition determined by linear mixture modeling varies with the lab spectra used.

Gaddis L. R.   Soderblom L.   Kirk R. L.   Titus T.
High-Resolution Topography of Layers in the Valles Marineris Via 'Thermoclinometry' **[#2001]**
This study addresses the use of high-resolution topographic data and morphologic analyses to study the origin of interior layered deposits in the Valles Marineris.

Sohl-Dickstein J.   Johnson J. R.   Grundy W. M.   Guinness E. A.   Graff T.   Shepard M. K.   Arvidson R. E.   Bell J. F. III   Christensen P. R.   Morris R.
Modeling Visible/Near-Infrared Photometric Properties of Dustfall on a Known Substrate **[#2235]**
We present a comprehensive visible/near-infrared two-layer radiative transfer modeling study using laboratory spectrogoniometry of variable dust thicknesses deposited on substrates with known photometric parameters.

Kirkland L. E.   Herr K. C.   Adams P. M.   Prothro L. B.   Allen B. M.
The Search for Underground Hydrothermal Activity Using Small Craters: An Example from the Nevada Test Site **[#2185]**
This is an airborne (satellite analog) study of mineral indicators of hydrothermal activity exposed by manmade explosion craters in basalt at the Nevada Test Site. This draws mainly on non-NASA expertise, and develops discovery routes for Mars.

Wilcox B. B.   Hamilton V. E.
THEMIS Observations of Compositional Variation in Elysium Planitia **[#1557]**
We identified a region in Elysium Planitia where dust is thin enough in local areas and certain Ls for the surface below to contribute to the emissivity spectrum. Initial analysis suggests it is olivine-rich and resembles neither Surface Type 1 or 2.

Byrnes J. M.   King P. L.   Ramsey M. S.   Lee R. J.
Synthesis and Analysis of Silicate Glasses: Applications to Remote Sensing of Volcanic Surface Units on Earth and Mars **[#2089]**
A suite of glasses have been synthesized that represent end-member feldspars and volcanic glass analogs. Compositional and structural analyses of the glass samples have implications for thermal infrared remote sensing of volcanoes on Earth and Mars.

Witter J. B.   Hamilton V. E.   Houghton B. F.
Thermal Infrared Spectroscopy of Explosively Erupted Terrestrial Basalts: Potential Analogues for Surface Compositions on Mars **[#1114]**
We have acquired tephra samples from explosive (Plinian) basaltic eruptions of Etna (Italy), Tarawera (New Zealand), and Masaya (Nicaragua) volcanoes for spectral analysis and comparison to Martian infrared surface spectra.

Eluszkiewicz J.   Cady-Pereira K.   Uymin G.   Moncet J.-L.
Martian Radiative Transfer Modeling Using the Optimal Spectral Sampling Method **[#2181]**
A new radiative transfer model for a wide range of Mars remote sensing applications will be described.

Mars Climate/Atmosphere

Wilson R. J. Smith M. D.
The Effects of Atmospheric Opacity on the Seasonal Variation of Martian Surface Temperature **[#1947]**
We have identified nighttime TES surface temperature anomalies in the Tharsis region of Mars during the NH summer solstice season that we attribute to the presence of optically thick water ice clouds.

Deo S. Kalchgruber R. Mayer B.
Radiative Transfer Calculations for the Atmosphere of Mars in the 200–900 nm Range **[#1029]**
We used the libRadtran software package for radiative transfer calculations for the atmosphere of Mars in the 200–900 nm range. The libRadtran software package and the input parameters are presented and the results of the simulations will be compared to spectra on Earth.

Hale A. S. Tamppari L. K. Christensen P. R. Smith M. D. Bass D. Qu Z. Pearl J. C.
Water Ice Clouds in the Martian Atmosphere: A View from MGS TES **[#1083]**
We use the technique of *Tamppari et al.*, 2000 to map water ice clouds in the Martian atmosphere using the MGS TES data and compare that to the work done by *Tamppari et al.*, 2000 on the Viking data. This provides the most direct "apples-to-apples" comparison.

Kanak K. M.
Large Eddy Simulation of Coherent Structures and Dust Devil-like Vortices in the Martian Boundary Layer **[#2158]**
A Large Eddy Simulation of the Martian Boundary Layer is carried out for the purpose of simulating dust devil-like vortices. Support is added for the application of LES to the Martian atmosphere and provides a tool for further investigation of the role of dust devils.

Boettger H. M. Foing B. H. Read P. L. Lewis S. R.
Diurnal Variability in Martian Atmospheric Water Vapour: Near Surface Ice Out of Equilibrium as a Source **[#1647]**
We attempt to reconcile model and observationsal data from GRS and atmospheric probes, in reference to the diurnal behaviour of atmospheric water vapour.

Sugita S. Schultz P. H.
An Efficient Methane Producing Mechanism Due to Iron Meteorite Impacts **[#1621]**
If a large amount of methane existed, Mars may have been kept warm due to its strong greenhouse effect. In this study, we propose a mechanism to produce a large amount of methane from iron meteorites impacting H_2O under a CO_2-rich atmosphere.

Lyons J. R. Manning C. E. Nimmo F.
Formation of Methane on Mars by Fluid-Rock Interaction in the Crust **[#2332]**
We show that a single dike ~10 km in size can drive methane production on Mars.

Forget F. Haberle R. M. Montmessin F.
Spatial Variation of Methane and Other Trace Gases Detected on Mars: Interpretation with a General Circulation Model **[#1597]**
The recent detection of methane on Mars and especially its large spatial variations is surprising. We performed gas transport simulations in a GCM to assess in which conditions (sources, liftetime, sinks) such a gas can exhibit such variations.

Mars: Marscellaneous

Lillis R. J. Brain D. A. Halekas J. S. Mitchell D. L. Lin R. P.
December 27th Magnetar Event Observations by Mars Global Surveyor **[#2313]**
The largest recorded gamma ray burst was seen at Earth on December 27, 2004. This event was recorded by the electron instrument on Mars Global Surveyor, lasted less than one second, and prompted an unusual ionospheric response 10–20 minutes later.

Litvak M. L. Mitrofanov I. G. Kozyrev A. S. Sanin A. B. Tretyakov V. I. Boynton W. V. Hamara D. Shinohara C. Saunders R. S.
Two Successive Martian Years on the Orbit: Similarities and Differences of CO_2 Seasonal Cycle from HEND/ODYSSEY Data **[#1653]**
The main goal of the study is comparison between similarities and differences of two successive CO_2 cycles observed during several years by orbital neutron spectrometer HEND installed onboard Mars Odyssey mission.

Instruments II: Rovers, Robotics, IR, and More

Bell M. S. Allen C. C.
Cleanroom Robotics — Appropriate Technology for a Sample Receiving Facility? **[#1395]**
Robotic processing has been recommended for use in a Receiving Facility supporting a Mars Sample Return Mission. Inorganic, organic and biological contamination can be controlled and minimized using current robot technology in a curation environment.

Mimoun D. Lognonné P. Banerdt W. B. Schibler P. Giardini D. Pont G.
The Mars SEIS Experiment: A Mars Seismic Package **[#1685]**
For the incoming Mars missions, IPGP has developed the SEIS experiment. It includes seismic sensors to measure seismic activity and Martian tides. This paper presents a review of the SEIS design and development, and preliminary breadboard performances.

Sykulska H. Vijendran S. Pike W. T.
Patterned Substrates for the Phoenix Microscopy Station **[#2166]**
This work aims to develop patterned substrates for the microscopy station on the 2007 Phoenix lander. Experiments show that careful sample preparation will be essential to maximise the scientific return from the optical and atomic force microscopes.

Blake D. F. Sarrazin P. Bish D. L. Chipera S. J. Vaniman D. T. Feldman S. Collins S. A.
CheMin: A Definitive Mineralogy Instrument in the Analytical Laboratory of the Mars Science Laboratory (MSL '09) **[#1608]**
CheMin is a miniature X-ray diffraction/X-ray fluorescence instrument that has been chosen for the analytical laboratory of MSL. CheMin will unequivocally determine the mineralogy of complex rocks and soils during the two-year duration of the MSL '09 mission.

Dyar M. D. Lane M. D. Bishop J. L. O'Connor V. Cloutis E. A. Hiroi T.
Integrated Spectroscopic Studies of Hydrous Sulfate Minerals **[#1622]**
Hydrous sulfate minerals are the focus of integrated XRD, compositional, VNIR, IR, emissivity, and Mössbauer studies.

French L. C. Anderson F. S. McMurtry G. Pilger E. Stopar J.
A Rugged Miniature Mass-Spectrometer for Measuring Aqueous Geochemistry on Mars **[#2138]**
This project is to miniaturize and shock-harden a rotating field mass spectrometer (RFMS) for high precision measurements of aqueous geochemistry on Mars.

Urgiles E. Wilcox J. Z. Toda R. Crisp J. George T.
Atmospheric Electron-induced X-Ray Spectrometer (AEXS) Instrument Development **[#1438]**
This paper describes the progress in data acquisition and establishing the observational capability of the AEXS instrument. The AEXS enables non-destructive evaluation of sample surfaces in planetary ambient atmospheres.

Wilcox J. Z. Urgiles E. Toda R. George T. Crisp J.
Atmospheric Electron-induced X-Ray Spectrometer (AEXS) Instrument Development **[#1059]**
The progress in the development of the AEXS instrument for *in situ* excitation of XRF spectra *in situ* using a focused electron beam transmitted through the encapsulation membrane from samples in planetary ambient atmosphere. We describe the development status of the miniature stand-alone instrument.

Jernsletten J. A.
Fast-Turnoff Transient Electromagnetic (TEM) Field Study at the Mars Analog Site of Rio Tinto, Spain **[#1014]**
This report describes a Fast-Turnoff Transient Electromagnetic (TEM) study at the Peña de Hierro ("Berg of Iron") field area of the Mars Analog Research and Technology Experiment (MARTE), near the towns Rio Tinto and Nerva, Andalucia region, Spain.

Jernsletten J. A.
Time Domain Electromagnetics for Mapping Mineralized and Deep Groundwater in Mars Analog Environments **[#1013]**
This study evaluates Transient Electromagnetics (TEM) for sounding of groundwater in Mars analog environments. Data from two field studies are shown: 1) TEM data from Pima County, Arizona; and 2) Fast-Turnoff TEM data from Rio Tinto, Spain.

Nelson R. M. Hapke B. W. Smythe W. D. Manatt K. S. Eddy J.
An Improved Instrument for Investigating Planetary Regolith Microstructure **[#1521]**
We renovated the JPL Long Arm Goniometer permitting measurements at phase angles as small as 0.05 degrees to 20 degrees. We can study the reflectance scattering behavior of regolith materials at phase angles at which important changes occur. We report the first results from the instrument.

Ravine M. A. Bell J. F. III Malin M. C. Miller D.
Semi-Autonomous Rover Operations: A Mars Technology Program Demonstration **[#1592]**
A 25 kg testbed rover will be used to demonstrate autonomous long range (~10 km) operation at three Mars analog field sites. This capability would enable investigation of localized high value science targets on Mars with Mars Scout-class missions.

Castaño R. Estlin T. Gaines D. Castano A. Bornstein B. Anderson R. C. Judd M. Stough T. Wagstaff K.
Science Alert Demonstration with a Rover Traverse Science Data Analysis System **[#2260]**
The Onboard Autonomous Science Investigation System (OASIS) evaluates geologic data gathered by a planetary rover. We describe results for the system in detecting and reacting to a science alert, as well as the reliability of the rock finder and run time performance.

Wilson G. R. Andringa J. M. Beegle L. W. Jordan J. F. Mungus G. S. Muliere D. A. Vozoff J. Wilson T. J.
Mars Suface Mobility: Comparison of Past, Present, and Future Rover Systems **[#2219]**
The objective of this study was to explore past, present, and future Mars rover concepts and compare their cost, size, and performance metrics in the context of the goals and objectives of the Mars Exploration Program.

Brown A. J.
Hydrothermal Mars "Through the CRISM": Which Hydroxyl Band and Why **[#1091]**
The spectral region covered by CRISM contains several OH absorption bands. The subject of this report is: Which of the available OH absorption bands should be targeted during CRISM preliminary mapping?

Mena-Fernandez S. Xie H.
Understanding the Olympus Mons and Valles Marineris Using THEMIS Imagery **[#1056]**
This study aims at developing methods to assess Mars' mineral composition through THEMIS images. All analyses will be based temperature, radiance, and emissivity. Initial results indicate a difference in temperatures between the Olympus Mons and the Valles Marineris.

Klima R. L. Pieters C. M.
Capabilities and Limitations of Infrared Reflectance Microspectroscopy **[#1459]**
Spectral analysis of planetary materials in the laboratory is fundamentally limited by the character of samples and system optics. We present experimental results defining general constraints for planetary science applications with microspectroscopy.

Hamilton V. E. Lucey P. G.
One Spectrometer, Two Spectra: Complementary Hemispherical Reflectance and Thermal Emission Spectroscopy Using a Single FTIR Instrument **[#1272]**
We are introducing a new IR instrument at UH that is capable of both hemispherical reflectance and thermal emission measurements; it enables truly comparable E & R studies of undisturbed particulate samples as well as cross-calibration opportunities.

Roush T. L.
Near-Infrared (0.67–4.7 μm) Optical Constants Estimated for Montmorillonite **[#1210]**
Procedures to estimate the wavelength dependence of both the real and imaginary indices of refraction from reflectance spectra are described. Resulting absorption coefficients compare favorably with those previously reported for montmorillonite.

Kirkland L. E. Herr K. C. Adams P. M. Prothro L. B. Allen B. M.
MarsLab at the Nevada Test Site: Rover Search for Subsurface Hydrothermal Activity Exposed by Small Craters **[#2199]**
This is a ground-based (rover analog), thermal-infrared spectral study of mineral exposed by manmade explosion craters in basalt at the Nevada Test Site. One goal is to determine which minerals present exhibit identifiable spectral signatures.

Milam K. A. McSween H. Y. Jr. Moersch J. E. Christensen P. R.
Accuracy of Derived Plagioclase Compositions from Thermal Emissivity Spectra of Multi-Component Mixtures of Pure Plagioclase **[#1863]**
This study determines the accuracy to which plagioclase compositions can be derived in multi-component mixtures of (pure) plagioclase, the most abundant mineral phase at the martian surface.

Gilmore M. S. Bornstein B. Merrill M. D. Castaño R. Greenwood J. P.
Generation and Performance of Automated Jarosite Mineral Detectors for Vis/NIR Spectrometers at Mars **[#1155]**
We have developed an algorithm that identifies jarosite in Vis/NIR spectra autonomously.

Greenhagen B. T. Kirkland L. E. Adams P. M. Grabowski T. K.
MarsLab Investigation of the Spectral Signature of Gypsum Bearing Rocks of Differing Composition and Formation Environment **[#2117]**
In this study, we used field based infrared spectroscopy to compare gypsum bearing rocks of differing composition and formation environment to enhance our knowledge of the role of several mineralogical and textural factors that cloud high fidelity compositional identification.

Heavens N. G. Kirkland L. E. Adams P. M.
Mars Analog Field Infrared Spectroscopy at Alunite, Clark County, NV: Comparison with EDXS **[#1936]**
In this study, we compare the results of Mini-TES-like field measurements of an outcrop with EDXS, BSE, and XRD analyses of samples of weathered surfaces from the same site.

Mitrofanov I. G. Litvak M. L. Kozyrev A. S. Mokrousov M. I. Sanin A. B. Tretyakov V. I.
Dynamic Albedo of Neutrons (DAN): Active Nuclear Experiment Onboard NASA Mars Science Laboratory **[#1635]**
In our presentation we describe instrument DAN based on neutron activation technique and selected for NASA/MSL mission. The main task of this experiment is local measurments of water distribution in martian subsurface around MSL rover.

Exploration: The Future

Kminek G. Exploration Team
The ESA Exploration Programme — Exomars and Beyond **[#2408]**
An update of the ESA Exploration Programme, with opportunities for international participation and identification of exploration technology developments.

Stevens C. M. Stocky J. F. Nelson R. M.
NASA's New Millennium ST-9 Project **[#1526]**
The ST-9 mission will validate one of five technology capabilities. NASA has prepared a NASA Research Announcement (NRA) soliciting proposals for Solar Sail capability, Large Space Telescopes, Formation Flying, Aerocapture, and Pinpoint Landing.

Chmielewski A. B. Nelson R. M. Stevens C. M. Chien S. Davies A. G. Sherwood R. L. Wyman W.
NASA's New Millennium ST6 Project **[#1523]**
The New Millennium ST6 project developed the Autonomous Sciencecraft Experiment (ASE)and the Inertial Stellar Compass (ISC). ASE improves a spacecraft's ability to make intelligent decisions on what information to gather and downlink. ISC determines a spacecraft's attitude and adjusts its pointing.

Davies A. G. Chien S. Baker V. R. Castaño R. Cichy B. Doggett T. Dohm J. M. Greeley R. Ip F. Rabideau G. Sherwood R. Tran D.
Maximizing Mission Science Return Through Use of Spacecraft Autonomy: Active Volcanism and the Autonomous Sciencecraft Experiment **[#1445]**
The Autonomous Sciencecraft Experiment has demonstrated how science return from missions is increased through use of autonomy. Applications aimed towards planetary volcanism on Io, Mars and icy bodies are discussed.

Ip F. Dohm J. M. Baker V. R. Castano B. Chien S. Cichy B. Davies A. G. Doggett T. Greeley R. Sherwood R.
Monitoring Floods with NASA's ST6 Autonomous Sciencecraft Experiment: Implications on Planetary Exploration **[#2263]**
Space autonomy technology together with floodwater classifiers developed as part of NASA's Autonomous Sciencecraft Experiment (ASE) creates the new capability to autonomously detect, assess, react to, and monitor dynamic events such as flooding.

Fink W. Dohm J. M. Tarbell M. Hare T. M. Baker V. R.
Next-Generation Robotic Planetary Surface/Subsurface Reconnaissance Missions: A Paradigm Shift **[#1977]**
A fundamentally new scientific mission concept for remote planetary surface/subsurface reconnaissance will soon replace engineering and safety constrained mission designs, allowing for optimal acquisition of information from extraterrestrial targets.

Levine J. S. ARES Science Team ARES Engineering Team
The Aerial Regional-scale Environmental Survey (ARES) Mission to Mars **[#1258]**
We describe an exploration mission concept for ARES, an Aerial Regional-scale Environmental Survey of Mars designed to fly an instrumented platform over the surface Mars at very low altitudes (1–3 km) for significant distances.

Coltrane J. J. Arena A. S.
CFD Modeling of NASA's ARES Platform **[#1042]**
NASA has designed a plane for aerial exploration of Mars. This project seeks to explore the aerodynamics of the plane through computational fluid dynamics and share some interesting facts about this proposed Mars Scout platform with the geologic community.

Carsey F. D. Beegle L. W. Nakagawa R. Elliott J. O. Matthews J. B. Coleman M. L. Hecht M. H. Ivanov A. B. Head J. W. III Milkovich S. M. Paige D. A. Hock A. N. Poston D. I. Fensin M. Lipinski R. J. Schriener T. M.
Palmer Quest: A Feasible Nuclear Fission "Vision Mission" to the Mars Polar Caps **[#1844]**
We will describe results of a "vision Mission" study called Palmer Quest, a mission to the deep subsurface of the North Polar Cap of Mars to assess the basal habitat and search for life, using a nuclear powered thermal probe, a surface flux station, and a robotic vehicle.

Banerdt W. B. Christensen U. Crisp D. Dehant V. Delory G. T. Lognonné P. Sotin C. Spohn T.
A Network of Geophysical Observatories for Mars **[#2074]**
We review the scientific rationale and technical requirements for a Mars geophysical network mission to investigate its interior and atmosphere and contribute to Mars exploration. We then discuss current activities aimed toward the implementation of such a mission.

Thompson J. Wiens R. C. Bernardin J.
Mars Atmospheric Sample Return Instrument Development **[#1136]**
This work focuses on the development of the atmospheric collection experiment instrument (ACE). A benchtop prototype system was built and tested to determine the suitability of the design to collect gas samples under Mars atmospheric pressure conditions.

Sollitt L. Arenberg J. W.
A Novel Approach to the Detection of Bouguer Anomalies and Mass Concentrations **[#1235]**
A novel detection approach is presented to detect Bouguer anomalies and associated mass concentrations (mascons) beneath the surfaces of planetary bodies.

Hare T. M. Kirk R. L. Archinal B. A. Tanaka K. L.
Working with Planetary Coordinate Reference Systems **[#2213]**
While planetary coordinate reference systems are well defined, when mixing map projections, datasets, and software packages, there are many potential pitfalls. Accurate documentation and standards will help software to interface more successfully.

Herrick R. R.
Stereo Matching Tool, a Freeware Program for Viewing Stereo Imagery and Editing Match Points **[#1984]**
A variety of missions are producing stereo image pairs (e.g., Galileo, MOC, HRSC). Stereo Matching Tool (SMT), is freeware that allows stereo pairs to be viewed and match points for photogrammetry to be manually edited.

Gibbens M. J. Cook A. C.
Evaluating Automated Feature Extraction Using Expert Opinion **[#1716]**
We apply automated cartographic feature detection algorithms to planetary images and compare with human expert opinion.

Meteorite Characterization Techniques

Kohout T. Kletetschka G. Pesonen L. J. Wasilewski P. J.
Determination of Meteorite Porosity Using Liquid Nitrogen **[#1743]**
We introduce a new harmless method for porosity measurement suitable for meteorite samples. The method is a modification of the Archimedean method based on immersion of the samples in a liquid medium like water or organic liquids. We used liquid nitrogen for its chemically inert characteristics.

Strait M. M. Consolmagno G. J.
Validation of Methods Used to Determine Microcrack Porosity in Meteorites **[#2073]**
Porosity measurements of meteorites were evaluated, and inconsistencies between hand sample and thin section methods were investigated and can be ascribed to weathering effects, experimental uncertainties and image quality.

Smith D. L. Ernst R. E. Samson C. Herd R. K.
Magnetic Susceptibility of Stony Meteorites: Evaluation of Anisotropy and Frequency Dependence **[#1408]**
Evaluation of four magnetic parameters that show promise as meteorite classification tools and discriminants: bulk magnetic susceptibility and its frequency dependence, and the degree and shape of the anisotropy of magnetic susceptibility.

Macke R. J. Consolmagno G. J. Rochette P. Britt D. T.
A Fast, Non-Destructive Method for Classifying Ordinary Chondrite Falls Using Density and Magnetic Susceptibility **[#1550]**
We describe a fast, non-destructive method for classification of H, L, and LL chondrites using grain density and magnetic susceptibility measurements.

Smith D. L. Samson C. Herd R. K. Christie I. Sink J.-E. DesLauriers A. Ernst R. E.
Measuring the Bulk Density of Meteorites and Rock Samples Non-Destructively Using 3D Laser Imaging **[#1372]**
Initial results are presented of a new non-destructive technique for determining the bulk density of meteorites and other solid objects using a Laser Camera System.

Nettles J. W. McSween H. Y. Jr.
Size and Shape Distributions of Chondrules and Metal Grains Revealed by X-Ray Computed Tomography Data **[#2018]**
X-ray CT data were used to measure size and shape distributions of chondrules and metal grains in three ordinary chondrites. Comparisons of these distributions has implications for potential nebular sorting processes.

Fries M. Steele A.
Inclusions Within Chondrule Mineral Grains as Characterized Using Confocal Raman Imaging **[#2238]**
Rounded, randomly emplaced inclusions within chondrule mineral grains have been characterized by confocal Raman imaging and found to contain mixtures of carbon, metal sulfides, mineral grains, and other components. Initial characterization of inclusions from Allende and EET 96188 are described.

Moroz L. V. Schmidt M. Schade U. Hiroi T. Ivanova M. A.
Synchrotron-based Infrared Microspectroscopy as a Useful Tool to Study Hydration States of Meteorite Constituents **[#1357]**
We show that synchrotron-based IR microspectroscopy is a useful tool to study hydration states of meteorites *in situ*.
We show that Dho225 and Dho735 are metamorphosed carbonaceous chondrites whose matrices are dehydrated compared to CM2 chondrites.

Hoffman E. J. Schade U. Moroz L.
Anomalous Spectra of High-Ca Pyroxenes: Further Correlations Between NIR and Mössbauer Patterns **[#2096]**
As for previously reported high-Ca pyroxenes, Mössbauer spectra of the infrared spectral Type B ("anomalous") samples in this study also present an anomaly, indication of more Fe-III than shown by chemical analysis. Minor phases may be responsible.

Schwandt C. S.
Evolution of Meteorite Chip Samples During Typical Storage Methods: A Seven and a Half Year ALH 84001 Case Study **[#1910]**
Examination of a meteorite chip intermittently over more than seven years reveals the mobilization and re-crystallization of halite and sulfates on the surface of the sample.

Lyon I. C. Matsuda Y. Strasser P.
Analysis of Extra-Terrestrial Materials by Muon Capture — Developing a New Technique for the Armory **[#1636]**
We are developing a new analytical technique for elemental and isotopic analysis of extra-terrestrial materials using muon capture. The technique is in its early stages but offers new possibilities such as non-destructive and thin-film analysis.

Enstatite Chondrites

Park J. Okazaki R. Nagao K. Bartoschewitz R.
Noble Gas Study of New Enstatite SaU 290 with High Solar Gases **[#1632]**
SaU 290 was found in Adam County, Oman, by R. and C. Bartoschewitz, 2004. It is classified as an E3. Noble gas analysis was performed at University of Tokyo. SaU 290 shows very high solar noble gas concentrations, which suggest brecciated structure.

Nakashima D. Nakamura T.
Trapped Noble Gas Components and Exposure History of the Enstatite Chondrite ALH84206 **[#1187]**
We measured noble gases in the enstatite chondrite ALH84206, and discuss trapped noble gas components and exposure history.

Mullane E. Russell S. S. Gounelle M.
Enstatite Chondrites: An Iron and Zinc Isotope Study **[#1250]**
We examine the fractionation systematics of iron and zinc isotopes in enstatite chondrites.

Organics in Meteorites

Ashley J. W. Huss G. R. Garvie L. A. J. Guan Y. Buseck P. R. Williams L. B.
Nitrogen and Carbon Isotopic Measurements of Carbon Nanoglobules from the Tagish Lake Meteorite by Secondary Ion Mass Spectrometry **[#2205]**
We report on a method for identifying carbon-rich nanoglobule targets in carbonaceous chondrites for C and N isotope analysis by SIMS, together with the results of that analysis.

Remusat L. Palhol F. Robert F. Derenne S.
Hydrogen Isotopic Composition of Aliphatic Linkages in Carbonaceous Chondrites Insoluble Organic Matter **[#1350]**
Ruthenium tetroxide oxidation allowed us to study the aliphatic linkages in Orgueil and Murchison Insoluble Organic Matter. The recovered products were analysed by GC-irMS to determine their D/H isotopic ratio.

Wang Y. Huang Y. Alexander C. M. O'D. Fogel M. Cody G.
Molecular and Compound-Specific Hydrogen Isotope Analysis of Insoluble Organic Matter from Different Carbonaceous Chondrite Groups **[#1010]**
We have conducted the first systematic analyses of molecular distribution and δD values of individual compounds in pyrolysates of insoluble organic matter from different carbonaceous chondrite groups, using flash pyrolysis coupled to compound-specific D/H analysis.

Yabuta H. Williams L. Cody G. Pizzarello S.
The Insoluble Carbonaceous Material of CM Chondrites as Possible Source of Discrete Organics During the Asteroidal Aqueous Phase **[#1367]**
The hydrothermal treatment of Murray insoluble organic material may release water and solvent soluble organic compounds.

Wirick S. Cody G. Flynn G. J. Jacobsen C. Keller L. P. Nakamura K. Zolensky M.
Detection of a Water Soluble Component of the Tagish Lake Meteorite **[#1662]**
A soluble component was detected in a pristine sample of the Tagish Lake meteorite using X-ray absorption spectromicroscopy and spectra collected from the soluble component matched spectra collected from a microtomed thin section.

Watson J. S. Pearson V. K. Gilmour I. Pillinger C. T. Turner D. Perkins R. Morgan G. H.
Pyrolysis-GC×GC-TOFMS to Characterize Carbonaceous Chondrites **[#1842]**
Using pyrolysis-GC×GC-TOFMS to analyze organic carbon in carbonaceous chondrites gives a massive increase in both sensitivity and structural information from samples when compared to traditional Py-GC-MS.

Watson J. S. Sephton M. A. Gilmour I.
Macromolecular Organic Acids in the Murchison Meteorite **[#1829]**
This study has detected bound organic acids within the Murchison meteorite organic macromolecule. Benzoic acid was the most abundant compound; other abundant compounds include C1 and C2 benzoic acids. Their origin and significance will be discussed.

Cooper G. Dugas A. Byrd A. Chang P. M. Washington N.
Keto-Acids in Carbonaceous Meteorites **[#2381]**
Keto-acids (pyruvic acid homologs) have been identified in carbonaceous chondrites by GC-MS. All compounds were identified as their trimethylsilyl (TMS), isopropyl ester (ISP), and tert-butyldimethylsilyl (tBDMS) derivatives.

Garvie L. A. J. Buseck P. R.
Structure and Bonding of Carbon in Clays from CI Carbonaceous Chondrites **[#1515]**
TEM and EELS reveal two C-clay associations in the CI CCs. Carbon occurs with fine- grained clays and in coarse-grained phyllosilicates. The data show the nanometer-scale chemical heterogeneity and structural diversity of the C materials with clays.

Busemann H. Alexander C. M. O'D. Fries M. Nittler L. Steele A.
Scanning Micro-Raman Spectroscopy on Carbon-rich Residues of Primitive Chondrites: A Tool for Chondrite Classification and Stardust Analysis **[#1975]**
We present results obtained by Raman spectroscopy of various organic residues of primitive chondrites in order to better characterize the microstructural state of the organic matter. These results will be correlated with the petographic classification of the chondrites.

Carbonaceous Chondrites

Chizmadia L. J.
Fine-grained Rims of Y-791198 are Texturally, Mineralogically and Compostionally Similar to GEMS-type IDPs **[#2229]**
The fine-grained rims of Y-791198 are texturally, mineralogically and compositionally similar to the primitive chondrites, ALH77307 and Acfer094, and to GEMS. This has implications for a connection between comets and asteroids.

Nakamura T. M. Sugiura N. Kimura M. Miyazaki A. Krot A. N.
Corundum and Corundum-Hibonite Grains Discovered by Cathodoluminescence in the Matrix of Acfer 094 Meteorite **[#1249]**
We found 43 corundum and 3 corundum-hibonite grains in the matrix of the Acfer 094 meteorite by cathodoluminescence imaging. We report textural observations, chemical compositions, and oxygen isotopic compositions of some of these grains.

Watt L. E. Bland P. A. Prior D. J. Russell S. S.
Fayalitic Olivine in Allende Matrix: Evidence for a Secondary Origin **[#1305]**
Electron backscatter diffraction (EBSD) has been used to determine the crystal morphology for olivines in the matrix and chondrule margins of Allende (CV3 chondrite), in dehydrated serpentinite and in the unique carbonaceous chondrite Acfer 094.

Komatsu M. Krot A. N. Miyamoto M. Keil K.
EBSD Study of Amoeboid Olivine Aggregates with Low-Ca Pyroxenes in the Y-81020 CO3.0 Chondrite **[#1573]**
We performed the mineralogical and structural study of AOAs. Although low-Ca pyroxenes in AOA are chemically similar to those in Type I chondrules, they are much finer-grained than in chondrules and probably formed by gas-solid condensation.

Velbel M. A. Tonui E. K. Zolensky M. E.
Compositions of Partly Altered Olivine and Replacement Serpentine in the CM2 Chondrite QUE93005 **[#1840]**
Serpentine replacing olivine in QUE93005 has a narrow range of compositions, regardless of the reactant olivine's composition. Homogeneity of replacement serpentines in QUE93005 and ALH81002 favors homogeneity of aqueous solutions on >cm scales.

Bullock E. S. Grady M. M. Russell S. S. Gounelle M.
Fe-Ni Sulphides Within a CM1 Clast in Tagish Lake **[#1883]**
The composition, abundance and mineral associations of Fe-Ni sulphides within a CM1 clast in Tagish Lake are described, and compared with Fe-Ni sulphides in the carbonate-rich and carbonate-poor lithology of Tagish Lake, as well as Fe-Ni sulphides from CI and CM chondrites.

Morris A. A Baker L Franchi I. A Wright I. P
Evolved Gas Analysis of Hydrated Phases in Murchison and Orgueil **[#1925]**
To better characterise the hydrated minerals in chondrites Evolved Gas Analysis of Murchison, Orgueil and selected minerals has been carried out. Meteorite water release profiles show significant differences to expected reference minerals.

Hezel D. C. Palme H. Burkhardt C.
3-Dimensional Chemical Analyses of Components in the Carbonaceous Chondrites Acfer 209 (CR) and Allende (CV) **[#2330]**
We perform 3-D chemical characterizations of meteoritic volumes (Acfer 209 and Allende). The results allow statements about the chondrule-matrix relationship, the chondrule, CAI, etc. bulk compositions, problems when analyzing 2-D thin sections, etc.

Anic A. Twelker E. Blattnig P. Whitby J. A. Benz W.
Origin of the Metal Spherules in Gujba **[#1775]**
An attempt is made to constrain the conditions that led to the formation of the metal spherules in the Gujba meteorite. Homogenous nucleation theory is coupled to an SPH impact code.

Bunch T. E. Irving A. J. Larson T. E. Longstaffe F. J. Rumble D. III Wittke J. H.
"Primitive" and Igneous Achondrites Related to the Large and Differentiated CR Parent Body **[#2308]**
Granular-textured achondrite NWA 3100 has oxygen isotopic compositions identical to those of CR chondrites, as do the paired igneous achondrites NWA 011 and NWA 2400. Core-mantle separation and partial melting probably occurred in the CR parent body.

Zolensky M. E. Abell P. A. Tonui E.
Metamorphosed CM and CI Carbonaceous Chondrites Could be from the Breakup of the Same Earth-crossing Asteroid **[#2084]**
We suggest that metamorphosed CM and CI chondrites derive from the same, recently disrupted, Earth-crossing asteroid.

Hiroi T. Tonui E. Pieters C. M. Zolensky M. E. Ueda Y. Miyamoto M. Sasaki S.
Meteorite WIS91600: A New Sample Related to a D- or T-type Asteroid **[#1564]**
We have newly identified WIS91600 as another possible sample from a D- or T-type asteroid based on reflectance spectroscopy. WIS91600 and Tagish Lake may represent a variety in composition and/or acqueous alteration among D- and T-type asteroids.

Ordinary Chondrites

Yasuda S. Nakamoto T.
Inhomogeneous Temperature Distribution in Chondrules in Shock-Wave Heating Model **[#1252]**
Temperature in a dust particle was examined using 3-D heat conduction calculations. It was found that all the chondrule forming particles have inhomogeneous distribution, and there were two types of distribution depending on the rotation rate.

Bonal L. Bourot-Denise M. Boronkay A. Montagnac G. Quirico E.
CO3 Chondrites: Metamorphic Sequence and Interclassification with Ordinary Chondrites **[#1699]**
Metamorphic grade of 7 CO chondrites is determined based on structural order of the Organic Matter. Petrographic types are attempted by interclassification with ordinary chondrites and are confronted with petrographic tracers.

Gattacceca J. Rochette P. Denise M. Consolmagno G. J. Folco L.
An Impact Origin for the Foliation of Ordinary Chondrites **[#1309]**
We present a large dataset of AMS measurements in order to elucidate the origin of chondrite foliation. Deformation resulting from dynamic uniaxial compaction of an originally loose porous material during impacts is the most plausible mechanism for the formation of foliation in chondrites.

Grimm R. E. Bottke W. F. Durda D. D. Enke B. Scott E. R. D. Asphaug E. Richardson D.
Joint Thermal and Collisional Modeling of the H-Chondrite Parent Body **[#1798]**
Disruption and reassembly of parent bodies while still hot may explain both "onion-shell" and random trends in cooling rates.

Welzenbach L. C. McCoy T. J. Grimberg A. Wieler R.
Petrology and Noble Gases of the Regolith Breccia MAC 87302 and Implications for the Classification of Antarctic Meteorites **[#1425]**
The MAC 87302 ordinary chondrite regolith breccia contains diverse clast types, including foreign impact melts, similar to the range of ordinary chondrite meteorites seen at MacAlpine Hills, Antarctica.

Bleacher L. V. Huss G. R. Leshin L. A. Miller M. Garcia R. Clary S. Jr. Gwilliam J. Sloan L.
Meteorites from the Franconia, Arizona Area: Observations and Summary of Petrographic Characteristics **[#1807]**
Meteorites from the Franconia, AZ area are predominantly H chondrites. Although most appear to pair with Franconia, the variability observed for others may be sufficiently distinct to assign some chondrites to separate falls.

Kelley M. S. Asher P. M. Welten K. C. Jull A. J. T. Shultz L. Roden M. Mertzman S. A. Albin E. F.
Analysis of the Statesboro, Georgia Shock-darkened L5 Chondrite **[#1483]**
We summarize results from various analytical techniques used to study the Statesboro L5 chondrite. The specimen is not scientifically unique, but it provides an interesting story and adds to the database of meteorites found in the state of Georgia.

Gildea K. J. Burgess R. Lyon I. C. Sears D. W.
Iron Isotope Geochemistry of Metal Grains in Ordinary Chondrites **[#1668]**
Iron isotopic measurements of metallic iron separated from ordinary chondrites of different petrologic types are presented to understand isotopic fractionation caused by nebula, parent body and terrestrial weathering processes.

Ebisawa N. Nagao K.
Noble Gases and I-Xe Ages of the Zag Meteorite **[#1718]**
Noble gases for clast and matrix materials from Zag meteorite indicate high concentrations of halogens in matrix but in clast. Late closure time for I-Xe system (about 20 Ma later than Bjurböle) indicate complex history for the Zag parent body.

Heck Ph. R. Schmitz B. Baur H. Wieler R.
Determination of Production Rates of Cosmogenic He and Ne in Meteoritic Chromite Grains **[#1712]**
Chromites are used to obtain exposure ages of fossil meteorites. Production rates for cosmogenic He and Ne had to be based on modeling. We present directly determined production rates in chromites by comparing to bulk meteorite data.

Mikouchi T. Makishima J. Koizumi E. Zolensky M. E.
Porphyritic Olivine-Pyroxene Clast in Kaidun: First Discovery of an Ordinary Chondrite Clast? **[#1956]**
We report mineralogy and petrology of an interesting clast in Kaidun, showing close affinities to type II POP chondrules in UOCs. This may be the first ordinary chondrite clast in this enigmatic brecciated meteorite.

Mironenko M. V. Zolotov M. Yu.
Thermodynamic Models for Aqueous Alteration Coupled with Volume and Pressure Changes in Asteroids **[#2207]**
New codes are developed to model pressure, volumes, and compositions as functions of alteration progress, initial rock composition, ice/rock ratio and initial porosity of an asteroid. Case study calculations for Semarkona are presented.

Herd R. K. Hunt P. A. Venance K. E.
On the Need for an Atlas of Chondrule Textures **[#2241]**
Chondritic meteorites are complex groups of extraterrestrial rocks. Detailed textural and mineralogical examination of chondrules can yield important information on their origins. A community effort to produce an atlas of chondrule textures is proposed.

Lukács B. Józsa S. Kovács Zs. Szakmány Gy. Bérczi Sz.
How We Used the Antarctic Meteorite Thin Section Set of NIPR to a Synthesis of the Thermal Evolution of a Chondritic Body **[#1300]**
We interpreted an evolutionary synthesis of regions (belts) in the chondritic parent body by arranging the NIPR set members according to 1) chondritic thermal metamorphism and 2) the differentiated crust, mantle and core regions.

Oxygen in the Solar System

Colson R. O. Malum K. M.
Dependence of Ru_2O_3 Activity on Composition of Silicate Melts: Using Statistical Correlations to Infer Thermo-Dynamic Behavior in the Melt **[#1190]**
Variations in the activity of Ru_2O_3 with melt composition arise due to contributions from both $a_{Ru}{}^{3+}$ and $a_O{}^{2-}$ in the melt. $a_{Ru}{}^{3+}$ can be understood as depending on the mixing between Ru^{3+} and Al^{3+}, Mg^{2+}, and Fe^{2+}. $a_O{}^{2-}$ can be modeled by a buffering reaction with bridging and non-bridging oxygens.

Aléon J. Hutcheon I. D. Weber P. K. Duprat J.
Magnesium Isotope Mapping of Silica-rich Grains Having Extreme Oxygen Isotope Anomalies **[#1901]**
Mg isotope mapping of SiO_2-rich grains from Murchison with extreme ^{17}O and ^{18}O excesses are consistent with a solar system origin of these O isotope anomalies upon irradiation by the young Sun.

Ushikubo T. Hiyagon H. Sugiura N.
Oxygen, Ca, and Ti Isotopic Compositions of Hibonite-bearing Inclusions **[#1283]**
Oxygen, Ca, and Ti isotopic compositions of hibonite-bearing inclusions were measured. Oxygen isotopes of the samples tend to fall along the CCAM line, and notable correlation was not found between O isotopes and isotopic anomalies of Ca and Ti.

Karner J. M. Shearer C. K. Papike J. J. Righter K.
Comparative Planetary Mineralogy: Co, Ni Systematics in Chromite from Planetary Basalts **[#1004]**
Cobalt and nickel partitioning are explored in chromite grains from the Earth, Moon, and Mars.

Early Solar System Processes and Planet Formation

Bureau H. Menez B. Malavergne V. Simogyi A. Munoz M. Simionovici A. Massare D. Burchard M. Kubsky S. Shaw C.
In Situ Determination of the Partitioning of Lead, Strontium and Rubidium Between Hydrous Melts and Aqueous Fluids at High Pressure and Temperature **[#1847]**
We have performed *in situ* high pressure and high temperature experiments in order to determine the partition coefficients of Pb, Sr, Rb between magmas and aqueous fluids.

Zhang L. Fei Y.
The Effect of Ni on Fe-FeS Phase Relations: Implications for the Chemistry of the Martian Core **[#2049]**
We have determined the solubility of Ni in the Fe_3S phase and the effect of Ni on the melting relations. The data will be used to understand the distribution of Ni and S in the Martian core if the core solidifies through the history.

Keshav S. Corgne A. McDonough W. F. Fei Y.
Potassium-bearing Iron-Nickel Sulfides in Nature and High-Pressure Experiments: Geochemical Consequences of Potassium in the Earth's Core **[#2016]**
In this contribution, we assess the effect of sequestering K in the core, as it is perhaps an element that is a key to reconciling geochemistry, paleomagnetism, accretion, and thermal evolution models for the planet.

Singletary S. J. Domanik K. J. Drake M. J.
Influence of Silicate Melt Composition on Metal/Silicate Partitioning of W, Ge, Ga and Ni **[#1945]**
We present new data for W, Ge, Ga and Ni that provide insight on the control of silicate melt composition on the partitioning of these elements between metal and silicate.

Malavergne V. Tarrida M. Combes R. Bureau H.
Uranium and Lead in the Early Planetary Core Formation: New Insights Given by High Pressure and Temperature Experiments **[#1823]**
We have performed high pressure (up to 15 GPa) and high temperature (1900°C) experiments in order to quantify possible fractionation of U and Pb into a metallic core during the first stage of planetary accretion.

Roskosz M. Mysen B. O.
Spectroscopic Study of Interactions Between Nitrogen and Silicate Melts Under High Pressure and Temperature: Insights into the Evolution of Geochemical Reservoirs **[#1965]**
Preliminary results on the possible interactions between nitrogen and silicate liquids under high-pressure and temperature.

Roskosz M. Luais B. Toplis M. J.
Experimental Determination of Iron Isotope Fractionation During High Temperature Segregation of Metal from Silicate Liquids: Evaporation or Diffusion? **[#1959]**
We present preliminary experimental results of iron isotopes fractionation during the segregation of metal iron from a silicate melt at high-temperature and 1-bar pressure.

Gardner K. G. Ferguson F. T. Nuth J. A.
The Vapor Pressure of Palladium at Temperatures up to 1973K **[#2240]**
Work includes measurement of Pd at high temperatures to confirm the accuracy of the Thermo-Cahn Thermogravimetric system up to 1973K and validation of two correction factors concerning the Knudsen effusion cell used in the experiments.

Marrocchi Y. Robert F. Binet L. Marty B.
Trapping of Xenon Upon Evaporation-Condensation of Organic Matter Under UV Irradiation: Isotopic Fractionation and Electron Paramagnetic Resonance Analysis **[#1792]**
Condensation experiment performed under UV irradiation reproduces Xe-P1 isotopic fractionation observed relative to solar end-member. In contrast, this process cannot account for the electron paramagnetic resonance signal observed in primitive meteorites.

Thomen A. Pack A.
Simulating Micro-Gravity in the Laboratory **[#1666]**
We present preliminary results from our high-T aerodynamic levitation experiments. We will discuss application of this method (containerless melting of liquds) to chondrule formation and partitioning experiments.

Mostefaoui S. Lugmair G. W. Hoppe P.
The Search for Extinct Iron-60 in Iron Meteorites **[#1611]**
We report NanoSIMS study of the Fe-Ni system in troilite from two iron meteorites. No ^{60}Ni excesses are found suggesting no evidence for life ^{60}Fe in these meteorites. We suggest a time span of ~6 Mys between core formation and troilite closure.

Moynier F. Blichert-Toft J. Telouk P. Albarède F. A.
Excesses of ^{60}Ni in Chondrites and Iron Meteorites **[#1593]**
Initial ^{60}Fe /^{56}Fe of 3×10^{-6} in metal and 7×10^{-6} in silicate are inferred from ^{60}Ni excesses in meteorites. These values indicate that ^{60}Fe was the major heat source in planetesimals.The time interval between silicate and metal condensation is ~5 My.

Cook D. L. Wadhwa M. Clayton R. N. Janney P. E. Dauphas N. David A. M.
Nickel Isotopic Composition of Fe-Ni Metal from Iron Meteorites and the Brenham Pallasite **[#1779]**
Measurement of the Ni isotopic composition of Fe-Ni metal from 8 iron meteorites and the Brenham pallasite revealed no resolvable excesses of radiogenic ^{60}Ni. Furthermore, no anomalies were found in ^{61}Ni or ^{64}Ni within the analytical uncertainties.

Pack A. Schönbeck T. Shelley J. M. Deloule É. Rollin-Bard C.
Experimental Study of Fe-, Co- and Ni-partitioning Between Forsterite and low-Co Fe,Ni-Alloys: Implications for Formation of Olivine Condensates in Equilibrium with Primitive Metal **[#1782]**
We combine experimental results with condensation calculations to model the composition (Fe, Co, Ni) of olivine condensates; results are compared with forsterite compositions from chondrites.

Dauphas N. Foley C. N. Wadhwa M. Davis A. M. Janney P. E. Qin L. Göpel C. Birck J.-L.
Protracted Core Differentiation in Asteroids from ^{182}Hf-^{182}W Systematics in the Eagle Station Pallasite **[#1100]**
The presence of radiogenic ^{182}W in the Eagle Station pallasite indicates that the metal in this meteorite differentiated late, possibly 10 My after Vesta.

Markowski A. Quitté G. Kleine T. Halliday A. N.
Tungsten Isotopic Constraints on the Formation and Evolution of Iron Meteorite Parent Bodies **[#1308]**
High-precision W isotope data measured in this study reveal small but resolvable differences within and between iron meteorite groups. We will discuss the possible explanations and implications for the formation and evolution of their parent bodies.

Kleine T. Mezger K. Palme H. Scherer E.
Tungsten Isotopes Provide Evidence That Core Formation in Some Asteroids Predates the Accretion of Chondrite Parent Bodies **[#1431]**
W isotope data for CAIs and iron meteorites show that core formation in some asteroids predates the formation of chondrules. We conclude that magmatic irons derive from the oldest (i.e., first-generation) planetesimals and that chondrites derive from second-generation asteroids.

Chen J. H. Papanastassiou D. A.
The Palladium Isotopic Composition in Iron Meteorites **[#1495]**
We report on the Pd isotope composition in iron meteorites and in a pallasite, and provide correlations with Ru and Mo endemic isotope effects.

Trinquier A.   Birck J.-L.   Allègre C. J.
Reevaluation of the ^{53}Mn-^{53}Cr Systematic in the Basaltic Achondrites **[#1946]**
The ^{53}Mn-^{53}Cr isotopic evolution of basaltic achondrites is reevaluated. The initial $^{53}Cr/^{52}Cr$ is lower than previously thought. It follows that the source of the HED meteorites is volatile depleted with lower than solar Mn/Cr ratio.

Trinquier A.   Birck J.-L.   Allègre C. J.
^{54}Cr Anomalies in the Solar System: Their Extent and Origin **[#1259]**
High precision ^{54}Cr runs (12 ppm) show a systematic and common deficit in basaltic achondrites the reverse to the excess in C-chondrites. It is the first ^{54}Cr deficit at the planetary scale. ^{54}Cr is an isotopic tool to constrain planetary formation.

Bouvier A.   Blichert-Toft J.   Vervoort J. D.   Albarède F. A.
Pb-Pb Isotope Dating of Ordinary Chondrites **[#2028]**
Pb-Pb ages of whole-rocks and chondrule separates from ordinary chondrites yield precise cooling ages. Type H closed earlier and shows also a faster cooling rate than types LL and L.

Busfield A.   Gilmour J. D.
I-Xe Dating of Mineral Separates and Integration with the Mn-Cr Timescale **[#1752]**
Mineral separates from four enstatite meteorites and a eucrite have been dated by the I-Xe technique. The data are incorporated into a combined I-Xe and Mn-Cr timescale.

Edwards S.   Ballentine C. J.   Gilmour J.
Constraints on the Role of Curium 247 as a Source of Fission Xenon in the Early Solar System **[#1739]**
Curium 247 as a source of fission xenon in the early solar system — a review of fission branching ratio and abundance constraints.

Djouadi Z.   d'Hendecourt L.   Leroux H.   Borg J.   Jones A. P.   Deboffle D.   Chauvin N.
Laboratory Study of the Irradiation and Thermal Processing of Silicate Dust Analogs **[#1185]**
Laboratory study of irradiation and thermal processing of silicate dust analogs has shown that crystallization is independent of the history of dust and other processes are needed to explain the presence of crystalline silicates in cold environments.

Dalla Stella A.   Marzari F.   Barbieri M.   Vanzani V.   Ortolani S.
Dynamical Evolution of Planets in Open Clusters **[#1253]**
We will show preliminary statistical results of a numerical investigation of planetary evolution in open clusters due to stellar encounters.

Genda H.   Abe Y.
Effects of Oceans on Atmospheric Loss During the Stage of Giant Impacts **[#2265]**
We numerically simulate the atmospheric blow-off by a Mars-sized giant impact. Here, we focus on the effect of an ocean on a planet. We show how the presence of an ocean enhances the atmospheric loss by a giant impact.

Sisterson J. M.
Measurement of Recoil Losses and Ranges for Spallation Products Produced in Proton Interactions with Al, Si, Mg at 200 and 500 MeV **[#1311]**
Recoil losses of ^{22}Na and ^{24}Na were measured in Al, Mg and Si targets. These losses were generally small and similar for the three target materials studied. These results are relevant to the study of radionuclides produced in presolar grains.

Asteroids, Comets, and Small Bodies

Clark P. E.   Clark C. S.
Constant Scale Natural Boundary Mapping as Tool for Characterizing Asteroids **[#1432]**
We are exploring the Constant Scale Natural Boundary (CSNB) approach to mapping and modeling asteroids in terms of morphological insight that can be gained in the context of traditional flat (2D) map projections and regular plate (3D) models.

Wilson L.   Head J. W. III
Dynamics of Groove Formation on Phobos by Ejecta from Stickney Crater: Predictions and Tests **[#1186]**
We examine the dynamics of groove formation on Phobos by ejecta from Stickney Crater, and make predictions and formulate tests of this hypothesis.

Benna M.   Mahaffy P. R.
Three Dimensional Multi-Fluid Simulation of Comet Halley **[#2257]**
We present some results of the 3D multi-fluid simulations generated by our MHD code CASIM for the atmosphere of a Halley-type comet with an outgassing dominated by water molecules.

Kadish J.
Implications of Internal Fragmentation on the Structure of Comets **[#1788]**
It is shown that a monolith can become internally fractured due to a perturbation in its stress field. The resulting breakup produces the same pattern of fragmentation as that observed during the splitting of comets.

Rivkin A. S. Pierazzo E.
Investigating the Impact Evolution of Hydrated Asteroids **[#2014]**
We use hydrocode simulation to investigate shock dehydration in low-velocity impacts to evaluate the relative proportions of dehydrated and still hydrated material in the impact ejecta.

Kirk R. L. Duxbury T. C. Hörz F. Brownlee D. E. Newburn R. L. Tsou P. Stardust Team
Topography of the 81/P Wild 2 Nucleus Derived from Stardust Stereoimages **[#2244]**
A detailed, stereo-derived topographic model of the visible half of the Wild 2 nucleus reveals a remarkably ellipsoidal overall shape with rugged topography dominated by craters having depth/diameter ratios near 0.2. Photometric modeling is next.

Vilas F.
Negative Searches for Evidence of Aqueous Alteration on Asteroid Surfaces **[#2033]**
ECAS NEA photometry, and the SDSS Moving Object Catalog, were searched for the 0.7-μm absorption feature due to oxidized iron in phyllosilicates. The feature is absent in the ECAS photometry; the SDSS search was inconclusive.

Flynn G. J. Durda D. D.
Catastrophic Disruption of Hydrated Targets: Implications for the Hydrated Asteroids and for the Production of Interplanetary Dust Particles **[#1152]**
Impact experiments were performed on three hydrated, metamorphic rock targets. It required less specific energy to disrupt the hydrated targets than anhydrous targets of similar mass, and the hydrated targets produced more fine-grained debris.

Durda D. D. Bottke W. F. Nesvorny D. Asphaug E. Richardson D. C.
Size-Frequency Distribution of Fragments from SPH/N-Body Simulations: Comparison with Observed Asteroid Families **[#1876]**
We investigate the morphology of size-frequency distributions (SFDs) resulting from impacts into 100-km diameter parent asteroids, represented by a suite of 160 SPH/N-body simulations, and compare with SFDs of observed main-belt asteroid families.

Cintala M. J. Durda D. D. Housen K. R.
Large-Scale Experimental Planetary Science Meets Planetary Defense: Deorbiting an Asteroidal Satellite **[#2160]**
Intentionally deorbiting an asteroidal satellite and monitoring the resulting collision between it and the primary asteroid, a capability that is well within the limitations of current technology, would provide data valuable to asteroid science and to planetary-defense missions.

Nazzario R. C. Hyde T. W.
Numerical Investigations of Kuiper Belt Binaries **[#1254]**
Observations of the Kuiper Belt indicate that a larger than expected percentage of KBO's (approximately 8 out of 500) are in binary pairs. This paper investigates the stability, development and lifetimes for Kuiper Belt binaries by tracking their orbital dynamics and subsequent evolution.

Moroz L. V.
Flat Spectral Curves of Low-Albedo Asteroids: Thermal Metamorphism or Space Weathering? **[#2056]**
Possible reasons for spectral mismatch between primitive carbonaceous meteorites and dark asteroids are discussed. Recent laboratory experiments suggest that space weathering could have produced flat spectral curves of C-, B-, F-, and G-type asteroids.

Mayne R. G. McCoy T. J. McSween H. Y. Jr.
Unbrecciated Eucrite MAC 02522: Petrology of a "Typical" Eucrite and Implications for Spectroscopy **[#1791]**
MAC 02522, is in many respects a "typical" eucrite, however when considering factors that may contribute to spectral features, its petrology may offer some interesting implications.

Sasaki T. Sasaki S. Watanabe J. Sekiguchi T. Yoshida F. Ito T. Kawakita H. Fuse T. Takato N. Dermawan B.
Difference in Degree of Space Weathering on the Newborn Asteroid Karin **[#1590]**
Here we report a near-infrared spectroscopy of the newborn asteroid Karin. For different rotational phases, we derived different spectra such as reddened spectrum like that of S- type asteroid and un-reddened spectrum like that of ordinary chondrite.

Neumann G. A. Barnouin-Jha O. S.
Joint Crossover Solutions of Altimetry and Image Data on 433 Eros **[#2267]**
Improved solutions both for asteroid-wide topography and NEAR's orbit locations will enhance our current views on the geodesy and thereby the internal properties of the asteroid 433 Eros as well as reveal much about the surface processes acting on small airless bodies.

Lim L. F. Nittler L. R. Starr R. D. McClanahan T. P.
Elemental Composition of 433 Eros: New Calibration of the NEAR-Shoemaker XRS Data **[#2031]**
Relative elemental abundances for six elements (Mg, Al, Si, S, Ca, Fe) in the surface layer of 433 Eros have been derived from a new calibration of the solar-induced fluorescence measured by the NEAR-Shoemaker X-ray Spectrometer (XRS).

Binzel R. P. Rivkin A. S. Thomas C. A. DeMeo F. E. Tokunaga A. Bus S. J.
The MIT-Hawaii-IRTF Joint Campaign for NEO Spectral Reconnaissance **[#1817]**
We announce a joint observing program for obtaining near-Earth object spectra. All data are being made available immediately via http://smass.mit.edu. We welcome broad community participation in target selection, observing, and data utilization.

Abe S. Borovicka J. Maeda K. Ebizuka 0. Watanabe J. I.
First Results of Quadrantid Meteor Spectrum **[#1536]**
The Quadrantid meteor shower is one of the most intense annual meteor showers. However, the parent body of Quadrantids is still in controversy. In this paper, we shall focus on the physical properties of the Quadrantid meteoroids and its parent body by means of Quadrantid meteor spectra.

Fauerbach M. Bennett T.
Photometric Lightcurve Measurements of Asteroids **[#1095]**
Photometric measurements of asteroids provide a great opportunity for small telescopes to collaborate with researchers at larger telescope facilities in astronomical research. Lightcurve data from our fall/winter observing campaign will be presented.

Haack H. Bidstrup P. R. Michelsen R. Andersen A. C. Jørgensen J. L.
Why Small is Beautiful — and How to Detect Another 10 Billion Small Main Belt Asteroids **[#1302]**
Estimates of the size distribution of main belt asteroids suggest that there is a population of approximately 10 billion objects in the meter to km range. We have explored the possibilities to build a fully autonomous spacecraft that can detect and study these objects from within the main belt.

Venechuk E. M. Franzen M. A. Sears D. W. G.
Radiation Resistance of a Silicone Polymer Grease Based Regolith Collector for the HERA Near-Earth Asteroid Sample Return Mission **[#1492]**
We investigated the effects of solar and galactic radiation on a silicone polymer grease's ability to collect imitation regolith for the HERA near-Earth asteroid sample return mission's proposed touch-and-go impregnable pad collector.

Franzen M. A. Roe L. A. Buffington J. A. Sears D. W. G.
Sample Collection from Small Airless Bodies: Examination of Temperature Constraints for the TGIP Sample Collector for the Hera Near-Earth Asteroid Sample Return Mission **[#1467]**
Here we describe experiments used to determine the temperature constraints for the TGIP collector designed for the Hera Near-Earth Asteroid Sample Return Mission. Equilibrium temperatures were calculated for potential target asteroids.

Buffington J. A. Franzen M. A. Azouggagh-McBride S. Roe L. A. Sears D. W. G.
Simulation of Extraterrestrial Sample Acquisition **[#1452]**
Here we describe a sampling mechanism intended to acquire surface samples from a near Earth asteroid. This device, named TGIP, was conceived and built to satisfy the science demands (within the engineering constraints) of the Hera Mission.

Azouggagh-McBride S. Roe L. A. Franzen M. A. Buffington J. A. Sears D. W. G.
Simulation of Recovery Impacts for the Prototype Hera Asteroid Sample Collector **[#1464]**
A series of experimental tests has demonstrated that asteroid surface samples collected by the proposed Hera Mission sample collector could survive a parachute-less Earth entry and subsequent impact.

Franzen M. A. Kracher A. Sears D. W. G. Cassidy W. Hapke B. W.
Space Weathering: A Proposed Laboratory Approach to Explaining the Sulfur Depletion on Eros **[#1461]**
The Near Shoemaker mission showed sulfur depletion on asteroid Eros. Potential mechanisms for sulfur loss are discussed as well as a proposed space weathering sputtering experiment that may contribute to the explanation of sulfur depletion on Eros.

Nishihara S. Abe M. Hasegawa S. Ishiguro M. Kitazato K. Miura N. Nonaka H. Ohba Y. Okyudo M. Ozawa T. Sarugaku Y. Ueno M.
Ground-based Lightcurve Observation of (25143) Itokawa, 2001–2004 **[#1833]**
The asteroid of 25143 Itokawa is a target of the Japanese sample return mission, Hayabusa. The optical observation of Itokawa had performed from March 2001 until October 2004. We report its absolute magnitude, slope parameter, and rotational period.

Kobayashi S. Demura H. Asada N. Furuya M. Hashimoto T. Kubota T. Saito J.
Shape Modeling for the Asteroid (25143) Itokawa, AMICA of Hayabusa Mission **[#1982]**
We report current status of shape modeling of (25143) Itokawa that is target asteroid of Hayabusa mission. Our method is adopted image-based modeling with multiview epipolar geometry.

Yoshimitsu T. Sasaki S. Yanagisawa M.
Current Status and Readiness on In-Situ Exploration of Asteroid Surface by MINERVA Rover in Hayabusa Mission **[#2289]**
This paper describes the current status of the MINERVA rover boarded on the Japanese asteroid explorer Hayabusa. Also the plan and the strategy to acquire surface images of the asteroid are presented.

Abe M. Takagi Y. Kitazato K. Hiroi T. Abe S. Vilas F. Clark B. E. Fujiwara A.
Observations with Near Infrared Spectrometer for Hayabusa Mission in the Cruising Phase **[#1604]**
NIRS is a near infrared spectrometer on-board the spacecraft Hayabusa. After the launch, we performed the observations of some bright stars and planets in the cruising phase toward the asteroid. We report the results of these observations.

Nemoto E. Asada N. Demura H. Kobayashi S. Furuya M. Kubota T. Hashimoto T. Saito J.
Preliminary Design of Visualization Tool for Hayabusa Operation **[#2050]**
When the tool for visualization asteroid is finished and implemented, it will be possible to project data acquired by some equipments to irregular shape polygon model. As a result, the tool will contribute to Hayabusa sample-return mission.

Teramoto K. Yano H.
Measurements of Sound Speed in Granular Materials Simulated Regolith **[#1856]**
We have measured sound speeds in regolith simulants in the 40–220 μm range. These results suggest the possibility of using velocity measurement of elastic waves in order to investigate major regolith size near asteroidal surfaces.

Byrne C. J.
Gravity Focusing of Swarms of Potential Impactors **[#1262]**
This abstract describes the effect on a swarm of potential impactors (debris from a comet for instance), as it passes by a large body such as Earth. The gravity field of the target body deflects the incoming swarm through a line of focus.

Cassini at Saturn: Titan, Saturn, Rings, Icy Satellites

Fussner S. McEwen A. S. Perry J. Turtle E. Dawson D. D. Porco C. West R. Cassini ISS Team
Dependence of Surface Contrast on Emission Angle in Cassini ISS 938-nm Images of Titan **[#2278]**
In 938-nm images of Titan obtained by Cassini ISS, contrast is seen to depend strongly on emission angle. This dependence is explored and quantified.

Perry J. McEwen A. S. Fussner S. Turtle E. West R. Porco C. Knowles B. Dawson D. D. Cassini ISS Team
Processing ISS Images of Titan's Surface **[#2312]**
Procedure for bringing out surface details in ISS images of Titan.

Kirk R. L. Callahan P. Seu R. Lorenz R. D. Paganelli F. Lopes R. M. Elachi C. Cassini RADAR Team
RADAR Reveals Titan Topography **[#2227]**
The first Cassini RADAR images and altimetry of Titan contain evidence for several relatively subdued topographic features including hills and possible flows with amplitudes of one to several hundred meters.

Schaller E. L. Brown M. E. Roe H. G. Bouchez A. H. Trujillo C. A.
Cloud Activity on Titan During the Cassini Mission **[#1989]**
Nightly small telescope photometry combined with numerous Keck and Gemini adaptive optics images of Titan allow us to provide context for the interpretation of high resolution images of Titan's clouds taken during Cassini flybys.

Lunine J. Artemieva N. A. Lorenz R. D. Flamini E.
Numerical Modeling of Impact Cratering on Titan with Implications for the Age of Titan's Surface **[#1504]**
Results reported from the first two Cassini flybys of Titan reveal few if any impact craters, suggesting that geological or atmospheric processes, or both, have worked to prevent the formation of craters or to hide or erase them after formation. Here we quantify some of these processes.

Garry J. R. C. Shettle T.
Experiments on the Acoustic Properties of Titan-like Atmospheres **[#1924]**
A laboratory apparatus has been built to examine the post-flight data of the Huygens' probes acoustic sensors, as well as to provide more data on attenuation in cryogenic gas mixes.

Estrada P. R. Mosqueira I.
A Gas-poor Planetesimal Feeding Model for the Formation of Giant Planet Satellite Systems: Consequences for the Atmosphere of Titan **[#2053]**
We develop a gas-poor planetesimal collisional capture which may be consistent with the mass and angular momentum of the Galilean satellites and Titan. We investigate this model's implications for the origin of Titan's atmosphere.

Fortes A. D. Stofan E. R.
Clathrate Formation in the Near-Surface Environment of Titan **[#1123]**
We discuss the possible formation of sinks for atmospheric and surface volatiles through the formation of clathrate hydrates in the upper crust of Titan.

Burr D. M. Emery J. P. Lorenz R. D.
Theoretical Calculations on Sediment Transport on Titan, and the Possible Production of Streamlined Forms **[#2044]**
We present theoretical calculations to assess the possibility of various types of sediment transport for likely conditions on Titan.

Bernard J.-M. Quirico E. Montagnac G. Reynard B. Mc Millan P. Bonal L. Rouzaud J.-N. Coll P. Schmitt B.
Which Tholins for Simulating Titan's Aerosols? **[#2183]**
The exploration of Titan by the Cassini-Huygens mission includes different spectrometers covering the visible and infrared ranges which will probe the atmosphere and the surface (DISR/CIRS).

Sekine Y. Imanaka H. Khare B. N. Bakes E. L. O. McKay C. P. Sugita S. Matsui T.
Experimental Study on Interactions Between H Atoms and Organic Haze **[#1414]**
Our experimental results indicate that interactions between H atoms and Titan tholin occur and form H_2 molecules. This may result in low concentration of reactive H atoms and high concentration of unsaturated hydrocarbons in Titan's stratosphere.

Moses J. I. Greathouse T. K.
The Variation of Hydrocarbon Abundances with Latitude and Season in Saturn's Stratosphere **[#1342]**
We will present results from a time-variable, 1-D model for stratospheric photochemistry on Saturn that accounts for variations in UV flux due to orbital position, solar-cycle variations, and ring-shadowing effects.

Greathouse T. K. Roe H. G. Richter M. J.
Changes in the Temperature of Saturn's Stratosphere from 2002 to 2004 and Direct Evidence of a Mesopause **[#1365]**
We have inferred the temporal and latitudinal variations of temperature in Saturn's stratosphere due to seasonal processes from data taken in 2002 and 2004. The 2004 data show distinct self-absorption cores indicative of a mesopause in Saturn's atmosphere.

Willis M. J. Ahrens T. J. Heinrich M. Beauchamp J. L.
Mass Spectrometer Calibration of the Cassini Cosmic Dust Analyzer for H_2O and D_2O Ices Via Laser Ablation **[#2228]**
We present results of experiments in which time of flight mass spectrometry of H_2O and D_2O ices was performed via laser ablation of ice layers generated on a cryogenically cooled Cu target to simulate ice impacts on the Cassini Cosmic Dust Analyzer.

Leisner J. S. Russell C. T. Dougherty M. K. Blanco-Cano X. Smith E. J. Tsurutani B. T.
Loss of Water from Saturn's E-Ring Through Ion Pick-Up **[#1935]**
With recent Cassini data, we study loss from Saturn's E-ring through ion pick-up by the ion cyclotron waves produced. Using Pioneer 11 and Voyager 1 observations, we map the variations due to latitude, local time, and ring inclination to the Sun.

Denk T. Neukum G. Helfenstein P. Thomas P. C. Turtle E. P. McEwen A. S. Roatsch T. Veverka J. Johnson T. V. Perry J. E. Owen W. M. Wagner R. J. Porco C. C. Cassini ISS Team
The First Six Months of Iapetus Observations by the Cassini ISS Camera **[#2262]**
Since arrival at Saturn, Iapetus has been studied intensively by the Cassini ISS camera. The results of the first half year of observations until before the New Year's Eve flyby are described.

Hendrix A. R. Hansen C. J.
An Overview of Cassini UVIS Icy Satellite Results So Far **[#2384]**
We present Cassini Ultraviolet Imaging Spectrograph results from Phoebe, Tethys, Dione, Iapetus, Mimas, Rhea and Enceladus.

Castillo J. C.
Expected Constraints on Rhea's Interior from Cassini **[#2243]**
We present degree-two gravity field computed for models of Rhea's interior in order to assess which properties of the interior are likely to be inferred from Cassini radio science measurements scheduled on November 26, 2005.

Mosqueira I. Estrada P. R.
On the Origin of the Saturnian Satellite System: Did Iapetus Form In-Situ? **[#1951]**
We construct two end-member models of regular satellite formation that are not dependent on specific choices for the turbulence parameter α. We find that the origin for the icy satellite Iapetus may serve to discriminate between the two.

Prentice A. J. R.
Saturn's Icy Moons: A Model for Their Origin and Bulk Chemical Composition **[#2378]**
Preliminary results of a new model for the formation of Saturn's family of mid-sized icy moons, namely Mimas, Enceladus, Tethys, Dione, Rhea and Iapetus, are reported. Predictions are made for the bulk chemical composition and mean uncompressed density of each satellite.

Outer Solar System

Becker T. Geissler P. E.
Galileo Global Color Mosaics of Io **[#1862]**
Late in the mission, the Galileo SSI experiment at Io accomplished a goal by acquiring global color coverage at a consistent phase angle. An accurate color mosaic of Io will be useful for scientific and education purposes. U.S.G.S. Astrogeology plans to construct global color mosaic products.

Hargitai H. Schenk P. M.
The Io Mountain Online Database **[#2102]**
We describe the complete database of the Mountains of Io, which is available online at http://planetologia.elte.hu/io.

Rathbun J. A. Block M. G. Spencer J. R.
Io from High-Resolution Galileo PPR Data Taken Simultaneously with SSI or NIMS Observations **[#1990]**
Io is the most volcanically active body in the solar system. Here, we present high-resolution Galileo PPR data taken simultaneously with NIMS and SSI. The data are used to examine volcano temperatures at Emakong, Pele, Zamama, Amirani, and other locations.

Thorsos I. E. Davies A. G.
An Impact Genesis for Loki Patera? **[#1950]**
We consider an impact-caused genesis for Loki Patera on Io. Loki may be an example of impact-triggered volcanism. Rapid resurfacing may have obscured original crater morphological features. An impact genesis may explain Loki's thermal excess.

Rainey E. S. G. Stevenson D. J.
Grain Size-dependent Viscosity and Oceans in Icy Satellites **[#2100]**
Scaling laws for grain size in a convective icy satellite are derived, and with scaling laws for non-Newtonian stagnant lid convection, are applied to the question of whether subsurface oceans can exist in large icy satellites.

Lee S. Pappalardo R. T. Makris N. C.
Europa's Porous Ice Rheology and Implications for Ice-penetrating Radar Scattering Loss **[#2346]**
We show that there is no compelling reason to expect large scattering loss for Europa's ice-penetrating radar missions, unlike previous studies. Scattering by inhomogeneities and rough surfaces is investigated at roughly 3-m radar wavelength.

Schenk P.
Landing Site Characteristics for Europa 1: Topography **[#2321]**
Europa's surface is significantly steeper than sites selected for Mars landers. Most terrains slope between 5 and 25 degrees. The smoothest features over 10–50 meter length scales are grey bands.

Fairén A. G. Amils R.
Evidence for Variable Thickness in Europa's Icy Shell: Implications for Astrobiology Mission Design **[#1087]**
Europa's crust is a dynamic non-uniform icy shell, which displays regional and temporal heterogeneity in thickness, originated in spatial variations in tidal heating and/or warm water upwellings from the silicate interior.

Földi T. Hargitai H. Hegyi S. Hudoba Gy. Kovács Zs. Roskó F. Tóth Sz. Pintér A. Bérczi Sz.
Europa Analog Ice-splitting Measurements and Experiments with Ice-Hunveyor on the Frozen Balaton-Lake, Hungary **[#1147]**
To observe Europa-analogous ice cover splitting, on the top of the stable icy surface of Balaton-Lake, Hungary, four new measurements were prepared with Ice-Hunveyor university lander model.

Vetter J. C. Kattenhorn S. A.
Quantifying Exact Motions Along Lineaments on Europa **[#1053]**
Identifying precise motions (combinations of sliding and opening/closing) is critical to the accurate characterization and interpretation of Europan lineaments. We present a technique for accurately determining these motions.

Gleeson D. Crawford Z. Barr A. C. Mullen M. Pappalardo R. T. Prockter L. M. Stempel M. M. Wahr J.
Wavy and Cycloidal Lineament Formation on Europa from Combined Diurnal and Nonsynchronous Stresses **[#2364]**
We consider the parameter space in which cycloidal, wavy, and arcuate structures on Europa can form, and explore the effects on cycloids of adding nonsynchronous rotation and diurnal stresses.

Patterson G. W. Head J. W. III Pappalardo R. T.
A Quantitative Analysis of Plate Motion on Europa: Implications for the Role of Rigid vs. Nonrigid Behavior of the Lithosphere **[#1069]**
We have developed a quantitative technique for determining the Euler pole of rotation between two rigid plates and use it here to help clarify the nature of deformation of Europa's lithosphere (rigid or nonrigid).

Patterson G. W. Head J. W. III Collins G. C. Pappalardo R. T. Prockter L. M. Lucchitta B. K.
Geological Mapping of Ganymede **[#1068]**
We are compiling a global geologic map of Ganymede (at the 1:15M scale) that will represent the most recent understanding of the satellite on the basis of Galileo Mission data. Our progress thus far is presented here.

Bedle H. Jurdy D. M.
Ganymede's Sulci on Global and Regional Scales **[#1161]**
Characteristics of Ganymede's sulci are analyzed based on terrain and global locale, in order to better understand stress regimes of sulcus formation.

Bland M. T. Showman A. P.
Numerical Modeling of Extensional Necking Instabilities: Application to Ganymede's Grooved Terrain **[#2137]**
We present numerical models of extensional necking instabilities under conditions that are appropriate to the formation of Ganymede's grooved terrain. The models produce surface morphologies that are broadly consistent with Ganymede's grooves.

Sasaki T. Kanno A. Ishiguro M. Kinoshita D. Nakamura R.
Presence of Nonmethane Hydrocarbons on Pluto **[#1591]**
Here we report an infrared spectroscopy of Pluto observed by Subaru telescope. Comparing the spectrum with model calculations, we suggest that some absorption features could be an indication of nonmethane hydrocarbons on Pluto's uppermost surface.

Kim K. J. Reedy R. C. Masarik J.
Effects of Cutoffs on Galactic Cosmic-Ray Interactions in Solar-System Matter **[#1397]**
The effects of cutoffs caused by magnetic fields on GCR interactions in the Earth's atmosphere and in the surface of Europa were studied using numerical-simulation codes. Locations of peaks and slopes of rates versus depth vary with cutoff.

De Young R. J. Bergstralh J. T.
New Active Remote-sensing Capabilities: Laser Ablation Spectrometer and Lidar Atmospheric Species Profile Measurements **[#1196]**
A follow on JIMO mission is proposed. A high energy laser is used for both laser ablation surface science and also for lidar measurements of atmospheric species profiles.

Arenberg J. W. Chou M. S. Sollitt L.
Laser Induced Desorption of Cryogenic Water Ice **[#1233]**
We report on continuing efforts to characterize a laser desorption and thermal emission spectroscopic technique that could be used to detect and analyze the abundances of organic and inorganic compounds in the surfaces of Jupiter's icy moons.

Whiddon W. B. Christensen A. Landecker P. Reuter J. Sollitt L.
Landing on Europa **[#1157]**
This paper will look at potential capabilities of a lander payload for the JIMO spacecraft. It will examine science opportunities at Europa that a lander could provide, as well as different classes of landers that could be deployed.

Christensen A. Leavitt K. Johnson T. Reuter J. M.
Unique Science Features of the JIMO Vehicle **[#1463]**
A conceptional design of the JIMO vehicle will be presented describing the entire system from the power source to the mission module, highlighting science features of the design.

Reuter J. Christensen A. Landecker P. Whiddon W. B. Sollitt L.
Nuclear Powered Spacecraft Enables New Science Capabilities for Future Space Science Missions **[#1158]**
This paper examines the use of the Prometheus One technology being developed for use in future space science missions. The paper will focus on mission design and science. Missions examined will include: Neptune/Triton Orbiter, Titan Orbiter, and Kuiper Belt Orbiter.

Spilker T. R. Spilker L. J. Ingersoll A. P.
Outstanding Science in the Neptune System from an Aerocaptured NASA "Vision Mission" **[#1928]**
NASA-funded studies at JPL and Caltech indicate aerocapture at Neptune would allow a Cassini-like mission to the Neptune system, including delivery of multiple Neptune entry probes and many close flybys of Triton, for intensive study of Neptune and its rings, satellites, and magnetosphere.

Weinwurm G. Weber R.
Planetary Gravity Fields and Their Impact on a Spacecraft Trajectory **[#1279]**
Implementation of complex ellipsoidal coordinates for the calculation of gravity field models of small irregular planetary bodies and the impact of the bodies' gravity fields on a spacecraft trajectory for future space mission flyby planning.

Friday, March 18, 2005
EUROPA (AND TRITON)
8:30 a.m. Salon A

Chairs: A. C. Barr
S. A. Kattenhorn

8:30 a.m. Prockter L. M. * Nimmo F. Pappalardo R. T.
A Shear Heating Origin for Ridges on Triton **[#1722]**
Morphologically similar ridges are present on the geologically young surfaces of Triton and Europa. We show that a plausible mechanism for Triton ridge formation is shear heating, driven by diurnal stresses occurring soon after Triton's capture.

8:45 a.m. Schenk P. *
The Crop Circles of Europa **[#2081]**
Giant Circles on Europa Astound and Amaze! Two antipodal sets of concentric troughs, at least 1500 km in diameter, are 500–1500 m deep and may be related to tidal or rotational stresses.

9:00 a.m. Nimmo F. * Schenk P. M.
Normal Faulting on Europa: Implications for Ice Shell Properties **[#1264]**
We use stereo topography to identify two normal faults on Europa, with D/L ratios similar to Earth. Modelling suggests the ice shell has a low shear modulus and elastic thickness of 0.2–1.2 km.

9:15 a.m. Lee S. * Pappalardo R. T. Makris N. C.
Surface Generated Cracks on Europa **[#2368]**
Conditions are derived for surface cracks to penetrate through Europa's ice shell based on fracture mechanics. It is shown that the cracks may reach the bottom of the shell under diurnal tensile stress if the shell is several kilometers thick.

9:30 a.m. Crawford Z. Pappalardo R. T. * Barr A. C. Gleeson D. Mullen M. Nimmo F. Stempel M. M. Wahr J.
Wavy Lineaments on Europa: Fracture Propagation into Combined Nonsynchronous and Diurnal Stress Fields **[#2042]**
The variety of Europa's observed lineament planforms from cycloidal, to wavy, to arcuate can be produced by propagation of fractures into a combined static nonsynchronous rotation stress and time-varying diurnal stress field.

9:45 a.m. Kattenhorn S. A. *
Compressive Anti-Cracks at the Tips of Strike-Slip Faults on Europa and Implications for Fault Mechanics **[#1144]**
Compressive quadrants at the tips of strike-slip faults on Europa show evidence of convergent structures, or anti-cracks, that partly accommodate the effects of the creation of new surface area by plate-spreading mechanisms.

10:00 a.m. Miyamoto H. * Mitri G. Dohm J. M. Showman A. P.
Flow-like Features on Europa: Geometric Patterns and Relation to Topography Collectively Constrain Material Properties and Effusion Rates **[#1616]**
We present numerical simulations of surface-ice flows on Europa to illuminate whether putative flow-like features actually resulted from flows. We provide theoretical support for the view that many of these features are not cryovolcanismic in origin.

10:15 a.m. Riley J. * Greenberg R. J. Sarid A. R.
Europa's South Polar Region: Reconstruction of the Sequential Resurfacing History **[#1516]**
Reconstruction of several generations of resurfacing and crust displacement near Europa's south pole shows that much of the surface was modified in the time between two separate chaos-formation events. The process of chaos formation seems unchanged over much of the history of the surface.

10:30 a.m. Mitri G. * Showman A. P.
Conductive-Convective Switches of the Ice Shell of Europa: Implications for the Surfaces Structures **[#1872]**
Modest variation in the heat flux in Europa's interior can produce repeated switches from a conductive to a convective configuration of the ice shell, with rapid and large variations in thickness. The rapidity of these switches implies that stress buildup, hence extensive fracture, would occur.

10:45 a.m. Han L. * Showman A. P.
Thermo-Chemical Convection in Europa's Icy Shell with Salinity **[#1465]**
We present numerical simulations of thermo-chemical convection to test the hypothesis that convection with salinity can produce Europa's pits and domes. Our simulations show that domes (200–300 m) and pits (300–400 m) can be produced under appropriate conditions.

11:00 a.m. Barr A. C. * Pappalardo R. T.
Convection in Ice I with Composite Newtonian/Non-Newtonian Rheology: Application to the Icy Galilean Satellites **[#2146]**
We use numerical models to determine the conditions required to trigger convection in the ice I shells of the icy Galilean satellites with a stress- temperature- and grain-size dependent rheology for ice I.

11:15 a.m. McKinnon W. B. *
On Convection in Ice I Shells of Outer Solar System Bodies — Application to Callisto and Titan **[#2387]**
Convection in Callisto's floating ice I shell is possible for reasonable grain sizes. Diffusion creep is the key. Not only possible, but probably required throughout much of Solar System history. For Titan, it depends on grain size and composition.

11:30 a.m. Vance S. * Brown J. M.
Double-Diffusive Convection and Other Modes of Salinity-modulated Heat and Material Transport in Europa's Ocean **[#2264]**
We assess the affect of salinity on dynamics and heat transport from floor to ceiling in Europa's ocean. We discuss a fluid-dynamical analysis of plume properties and possible connections with surface features.

Friday, March 18, 2005
MARS: FROM HYDROGEN TO ICE AND IMPLICATIONS FOR CLIMATE CHANGE
8:30 a.m. Salon B

Chairs: J. L. Fastook
J. S. Levy

8:30 a.m. Feldman W. C. * Prettyman T. H. Maurice S. Elphic R. C. Funsten H. O. Gasnault O. Lawrence D. J. Murphy J. R. Nelli S. Tokar R. L. Vaniman D. T.
Topographic Control of Hydrogen Deposits at Mid- to Low Latitudes of Mars **[#1328]**
A close study of the correspondence between relative maxima in water-equivalent hydrogen abundances with relative maxima in the topography at mid- to low latitudes of Mars suggest that weather patterns control the deposition onto, and/or vapor diffusion into surface soils from the atmosphere.

8:45 a.m. Murray J. B. * Muller J.-P. Neukum G. Werner S. C. Hauber E. Markiewicz W. J. Head J. W. III Foing B. H. Page D. Mitchell K. L. Portyankina G. HRSC Investigator Team
Evidence from HRSC Mars Express for a Frozen Sea Close to Mars' Equator **[#1741]**
We present evidence for a presently-existing frozen sea, with surface pack-ice, at 5°N, 150°E, age ca. 5 million years. It measures ca. 800 × 900 km and averages ca. 45 m deep. It has probably been protected from complete sublimation by ash and a sublimation lag of exposed sediment.

9:00 a.m. McBride S. A. * Allen C. C. Bell M. S.
Prospecting for Martian Ice **[#1090]**
Relations between craters and ice-wedge polygons were examined on MGS images to constrain the thickness and age of a possible ice-rich mantle in the northern mid-latitudes. Results indicate the mantle is about 40 m thick and dates from before 5 Ma.

9:15 a.m. Fishbaugh K. E. * Hvidberg C. S.
Effect of Flow on the Internal Structure of the Martian North Polar Layered Deposits **[#1331]**
We investigate the effect of flow on the internal layer structure of the cap and compare the results to the actual structure observed in image data. The results have implications for interpretation of the climate record preserved in the layers.

9:30 a.m. Marchant D. R. * Head J. W. III
Equilibrium Landforms in the Dry Valleys of Antarctica: Implications for Landscape Evolution and Climate Change on Mars **[#1421]**
An understanding of the origin and evolution of equilibrium landforms in the Antarctic Dry Valleys may be helpful in elucidating the origin of some enigmatic landforms on Mars and in interpreting recent changes in the Martian climate.

9:45 a.m. Levy J. S. * Head J. W. III Marchant D. R. Kreslavsky M. A.
Evidence for Remnants of Late Hesperian Ice-rich Deposits in the Mangala Valles Outflow Channel **[#1329]**
We assess several possible origins for a smooth unit on the floor of Mangala Valles, interpreting it as an ice-rich remnant created by ponding and ice-cover deflation during the waning stages of the outflow channel flood emplacement.

10:00 a.m. Head J. W. III* Marchant D. R. Agnew M. C. Fassett C. I. Kreslavsky M. A.
Regional Mid-Latitude Late Amazonian Valley Glaciers on Mars: Origin of Lineated Valley Fill and Implications for Recent Climate Change **[#1208]**
Evidence is presented that lineated valley fill in the Deuteronilus mid-latitude region of Mars originated from snow and ice accumulation and glacial flow during periods of high obliquity in the Amazonian.

10:15 a.m. Helbert J. * Benkhoff J.
Beyond the Equilibrium Paradigm — Glacial Deposits in the Equatorial Regions of Mars **[#1352]**
We will show, that even in the equatorial regions of Mars ground ice deposits can be stable over long periods of time. The main assumption we have to do is, that the near surface layer of Mars is not in an equilibrium state.

10:30 a.m. Elphic R. C. * Feldman W. C. Prettyman T. H. Tokar R. L. Lawrence D. J. Head J. W. III Maurice S.
Mars Odyssey Neutron Spectrometer Water-Equivalent Hydrogen: Comparison with Glacial Landforms on Tharsis **[#1805]**
Mars Odyssey neutron spectrometer measurements indicate enhanced water-equivalent hydrogen abundances on the western slopes of the Tharsis Montes, possibly in association with relict buried ice.

10:45 a.m. Fastook J. L. * Head J. W. III Marchant D. R. Shean D. E.
Ice Sheet Modeling: Mass Balance Relationships for Map-Plane Ice Sheet Reconstruction: Application to Tharsis Montes Glaciation **[#1212]**
We apply the properties of the Mars atmosphere to models of mass balance and spatial distribution on the flanks of Tharsis Montes; these lead to patterns that are strikingly similar to the geological evidence for ice accumulation and glacial flow.

11:00 a.m. Ishii T. * Miyamoto H. Sasaki S.
Viscous Flows from Poleward-facing Walls of Impact Craters in Middle Latitudes of the Alba Patera Area **[#2172]**
Inclinations of poleward-facing crater walls are smaller than those of equatorward-facing walls in middle latitudes of the Alba Patera area, which suggests that viscous flows of ice-rich materials would occur preferentially on poleward-facing slopes.

11:15 a.m. Shean D. E. * Head J. W. III Marchant D. R.
Debris-covered Glaciers Within the Arsia Mons Fan-shaped Deposit: Implications for Glaciation, Deglaciation and the Origin of Lineated Valley Fill **[#1339]**
We interpret flow-like features at Arsia Mons as debris-covered glaciers representing the most recent phases of glaciation in this region, providing insight into processes of glaciation and deglaciation on Mars. We discuss applications to other areas containing candidate glacial deposits.

11:30 a.m. Sakimoto S. E. H. *
Central Mounds in Martian Impact Craters: Assessment as Possible Perennial Permafrost Mounds (Pingos) **[#2099]**
We characterize topography for and model martian polar region impact crater central mounds as potential perennial permafrost mounds (pingos).

Friday, March 18, 2005
DIFFERENTIATED METEORITES
8:30 a.m. Salon C

Chairs: G. K. Benedix
C. M. Corrigan

8:30 a.m. Walker R. J. * McCoy T. J. Schulte R. F. McDonough W. F. Ash R. D.
^{187}Re-^{187}Os, ^{190}Pt-^{186}Os Isotopic and Highly Siderophile Element Systematics of Group IVA Irons **[#1313]**
High precision analysis of highly siderophile elements in group IVA irons are generally suggestive of simple crystal-liquid fractination. Fuzzy Creek is not consistent with this interpretation. Ungrouped irons Nedagolla and EET 83230 have some chemical characteristic consistent with IVA.

8:45 a.m. Honesto J. * McDonough W. F. Walker R. J. McCoy T. J. Ash R. D.
^{187}Re-^{187}Os Isotopic and Highly Siderophile Element Systematics of Group IVB Irons **[#1929]**
IVB irons were analyzed for highly siderophile element abundances and ^{187}Re-^{187}Os isotopic systematics. The results require a bulk core with very high refractory HSE abundances and low Re/Os.

9:00 a.m. Corrigan C. M. * Rumble D. III McCoy T. J. Ash R. D. McDonough W. F. Honesto J. Walker R. J.
The Tishomingo Iron: Relationship to IVB Irons, CR Clan Chondrites, and Angrites and Implications for the Origin of Volatile-depleted Iron Meteorites **[#2062]**
The oxygen isotopic and siderophile element composition of Tishomingo suggest formation through melting of a CR-like precursor through processes similar to IVB irons, but on a separate parent body. A direct link with angrites is possible.

9:15 a.m. Goodrich C. A. * Wlotzka F. Ross D. K. Spettel B. Dreibus G. Bartoschewitz R.
Northwest Africa 1500: A Plagioclase-bearing Monomict Ureilite **[#1073]**
NWA 1500 is an olivine-rich meteorite, with significant augite and plagioclase. We interpret it to be a cumulate ureilite, formed from a melt produced in a deep, oxidized source region. Its plagioclase represents the "missing basaltic component" from the UPB.

9:30 a.m. Nakamuta Y. *
Modal Abundances of Carbon in Ureilites: Implications for the Petrogenesis of Ureilites **[#1089]**
Modal abundances of carbon in ureilites were measured. The modal abundance and mg# of olivine were found to inversely relate and confirm the smelting reactions in the parent body and suggest that subgroups I and III came from different parent bodies.

9:45 a.m. Rankenburg K. * Brandon A. D. Humayun M.
Highly Siderophile Elements and Osmium Isotope Systematics in Ureilites: Are the Carbonaceous Veins Primary Components? **[#1224]**
An unsolved problem of ureilite research is the question of whether their carbon and associated metal are primary phases. We present Os isotope data for 18 bulk ureilites and compare HSE patterns to unravel the history of the ureilite parent body.

10:00 a.m. Kallemeyn G. W. * Warren P. H.
Siderophile Geochemistry of Ureilites: Reading the Record of Early Stages of Planetesimal Core Formation **[#2165]**
We present much new data for ureilites. The average ureilite composition can be modeled by assuming that the major yet not exhaustive siderophile depletions of typical ureilites formed by down-seepage of small proportions of S-rich metallic melt.

10:15 a.m. Mittlefehldt D. W. * Hudon P. Galindo C. Jr.
Petrology, Geochemistry and Genesis of Ureilites **[#1040]**
Ureilites are enigmatic achondrites that have some characteristics resulting from high temperature igneous processing, yet retain other characteristics inherited from the solar nebula.

10:30 a.m. Lee D.-C. * Halliday A. N. Singletary S. J. Grove T. L.
^{182}Hf-^{182}W Chronometry and an Early Differentiation in the Parent Body of Ureilites **[#1638]**
Ureilite parent body must have differentiated early, and melting events that can simultaneously remove Hf and W (e.g., smelting) are necessary to explain the observed Hf-W data.

10:45 a.m. Yamaguchi A. * Mikouchi T.
Heating Experiments of the HaH 262 Eucrite and Implication for the Metamorphic History of Highly Metamorphosed Eucrites **[#1574]**
We performed heating experiments of a eucrite near the solidus to understand mineralogical and chemical changes during high temperature metamorphism. Partial melts formed at 1050°–1100°C are rich in P and Ti, suggesting preferential melting of mesostasis phases.

11:00 a.m. Benedix G. K. * McCoy T. J. Lauretta D. S.
Iron Reduction During Metamorphism on the Winonaite/IAB Iron Meteorite Parent Body **[#1749]**
We show temperature and oxygen fugacity estimates that indicate, while some reduction did take place during cooling of the Winonaite-IAB parent body, it cannot account for the reduced mineral compositions. It is the intrinsic nature of the parent body.

11:15 a.m. Gounelle M. * Engrand C. Chaussidon M. Zolensky M. E. Maurette M.
An Achondritic Micrometeorite from Antarctica: Expanding the Solar System Inventory of Basaltic Asteroids **[#1655]**
We report on the texture, mineralogy, REEs abundance and oxygen istopopic composition of an Antarctic achondritic micrometeorite. This is the first basaltic micrometeorite. It is different from any other known planetary basalt.

11:30 a.m. Rai V. K. * Jackson T. L. Thiemens M. H.
Mass Independent Sulfur in Achondrites: Possible Evidence of Photochemistry in the Solar Nebula **[#1231]**
Sulfur isotopic composition of several achondritic meteorites has been measured. Though small but resolvable excesses of ^{33}S has been found in HED, Acapulcoite-Lodranites group of achondrites.

Friday, March 18, 2005
EARLY SOLAR SYSTEM EVOLUTION
8:30 a.m. Marina Plaza Ballroom

Chairs: A. P. Boss
F. A. Albarède

8:30 a.m. Boss A. P. *
Mixing and Transport of Chondrules and CAIs in the Solar Nebula **[#1024]**
The solar nebula was able to transport rapidly solids from the innermost regions to the asteroidal region, where chondrules, CAIs, and matrix grains were assembled in the chondritic meteorites, and beyond, possibly explaining crystalline silicates in comets.

8:45 a.m. Jacobsen S. B. * Ranen M. C. Petaev M. I. Smoliar M. I. Adams E. R.
The Problem of Incomplete Mixing of Interstellar Components in the Solar Nebula: Very High Precision Isotopic Measurements with Isoprobes P and T **[#2276]**
We discuss new chemical and isotopic data obtained with new generation mass spectrometers for bulk carbonaceous chondrites and CAIs. The data point to incomplete mixing of presolar materials in the solar nebula.

9:00 a.m. Simon J. I. * Russell S. S. Tonui E. Dyl K. A. Manning C. E. Young E. D.
Wark-Lovering Rims Record a Short Timescale for Changing Conditions in the Early Solar Nebula **[#2068]**
We present Mg isotope data that, when coupled with oxygen barometry data, show that Wark-Lovering rims formed by condensation in places resembling chondrite-forming regions of the solar nebula within ~300 k.y. after initial CAI formation.

9:15 a.m. Kita N. T. * Tomomura S. Tachibana S. Nagahara H. Mostefaoui S. Morishita Y.
Correlation Between Aluminum-26 Ages and Bulk Si/Mg Ratios for Chondrules from LL3.0–3.1 Chondrites **[#1750]**
We present new and re-measured data set for high precision ion microprobe ^{26}Al ages of chondrules from Bishunpur and Krymka (LL3.1). Correlation between ^{26}Al ages and their bulk Si/Mg ratios is examined and discussed.

9:30 a.m. Desch S. J. * Ouellette N.
The Meaning of Iron 60: A Nearby Supernova Injected Short-lived Radionuclides into Our Protoplanetary Disk **[#1327]**
We explain why the presence of short-lived radionuclides like ^{60}Fe in the early solar system demands a nearby supernova. Observations suggest the solar system disk had already formed and was < 1 pc from the supernova. We discuss the consequences.

9:45 a.m. Yin Q.-Z. *
Extinct Radioactivities in the Early Solar System and the Mean Age of the Galaxy **[#2091]**
I derived the mean age of the galaxy to be 12.3±3.6 Ga from the meteoritic records of extinct radioactivities at the beginning of the solar system. Unlike the U/Th cosmochronometer, this age constraints is independent of production ratios of nucleosynthetic models.

10:00 a.m. Albarède F. A. * Rosing M. Simionovici A. Blichert-Toft J. Bizzarro M. Scherer E. E.
Gamma-Ray Irradiation in the Early Solar System and the Conundrum of the ^{176}Lu Decay Constant **[#1528]**
The ^{176}Lu decay constants inferred from well-dated terrestrial rocks and meteorites are inconsistent by 3%. Excitation of the isomeric state (T1/2 = 3.7 h) in nebular gas and dust by gamma-rays from the nascent Sun accounts for this discrepancy.

10:15 a.m. Hood L. L. * Ciesla F. J.
The Planetesimal Bow Shock Model for Chondrule Formation: More Detailed Simulations in the Near Vicinity of the Planetesimal **[#1964]**
For plausible nebula gas densities, strong planetesimal bow shocks will lead to low-velocity impacts (and therefore accretion) of formed chondrules with sizes comparable to observed chondrule sizes.

10:30 a.m. Quitté G. * Latkoczy C. Halliday A. N. Schönbächler M. Günther D.
Iron-60 in the Eucrite Parent Body and the Initial ^{60}Fe/^{56}Fe of the Solar System **[#1827]**
We show that the ^{60}Fe-^{60}Ni chronometer dates both the crystallization and a later thermal metamorphic event in eucrites. A new estimate of 4.4×10^{-6} for the initial ^{60}Fe/^{56}Fe of the solar system, higher than generally assumed, is also proposed.

10:45 a.m. Ciesla F. J. * Cuzzi J. N.
The Distribution of Water in a Viscous Protoplanetary Disk **[#1479]**
We will present a new model to track the distribution of water in a viscously evolving protoplanetary disk and compare results to the inferred distribution of water vapor and ice in our own solar nebula.

11:00 a.m. Ebel D. S. * Alexander C. M. O'D.
Condensation from Cluster-IDP Enriched Vapor Inside the Snow Line: Implications for Mercury, Asteroids, and Enstatite Chondrites **[#1797]**
Cluster-IDPs are a better protoplanetary dust analog than chondritic CI dust. Condensation with C-IDP enrichments yields silicates with FeO ~0, plus CaS + MgS above 1000 K. Enstatite chondrites formed inside the snow line near a C-enriched midplane.

11:15 a.m. Kortenkamp S. J. *
The Fate of Neptune's Primordial Trojan Companions Lost During Planetary Migration **[#2242]**
Trojan-type companions of Neptune can be lost during primordial migration of the giant planets. These lost Neptune Trojans suffer many interesting fates including impact with Neptune and scattering into Neptune's outer mean motion resonances.

11:30 a.m. Bogard D. D. *
Characterizing the Early Impact Bombardment **[#1131]**
Different experimental approaches help characterize the nature and chronology of the enhanced impact bombardment of the inner solar system in the first billion years.

Friday, March 18, 2005
GALILEAN SATELLITES
1:30 p.m. Salon A

Chairs: J. A. Rathbun
J. B. Dalton

1:30 p.m. Geissler P. E. *
Volcanic Plumes and Plume Deposits on Io **[#1875]**
Observations from the Galileo and Cassini missions help explain the complex relationship between the venting of gases during volcanic eruptions, the dust carried aloft by the gases, and the surface changes produced by these episodes of violent volcanism.

1:45 p.m. Milazzo M. P. * Keszthelyi L. P. Radebaugh J. Davies A. G. Turtle E. P. Geissler P. E. Klaasen K. P. McEwen A. S.
Galileo SSI Observations of Volcanic Activity at Tvashtar Catena, Io **[#2335]**
We report on the analysis of Galileo SSI's observations of volcanic activity at Tvashtar Catena, Io November 1999 and October 2001.

2:00 p.m. Davies A. G. * Keszthelyi L. P.
Classification of Volcanic Eruptions on Io and Earth Using Low-Resolution Remote Sensing Data **[#1963]**
The ratio of 2- to 5-μm thermal fluxes is used to constrain volcanic eruption mode for low-spatial resolution data of volcanism on Io and Earth. This is a useful diagnostic tool for constraining future observations of Io's volcanism.

2:15 p.m. Rathbun J. A. * Spencer J. R.
Loki, Io: Groundbased Observations and a Model for Periodic Overturn **[#1981]**
Loki is the most powerful volcano on Io. Here we present groundbased data examining the time variabilty of Loki's 3.5-μm brightness. We also model these brightnesses based on Loki as a periodically overturning lava lake.

2:30 p.m. Keszthelyi L. P. * Milazzo M. P. Jaeger W. L. Wilson L. Mitchell K. L.
Reconciling Lava Temperatures and Interior Models for Io **[#1902]**
The very high temperatures reported for Ionian lavas imply an unrealistic degree of melting of the interior. Improved analysis of the Galileo SSI data and superheating of the ascending magma help resolve this problem.

2:45 p.m. Williams D. A. * Greeley R. Keszthelyi L. P. Crown D. A.
Strategies for the Global Geologic Mapping of Io **[#1150]**
In this presentation we discuss strategies for the global geologic mapping of Io using combined Galileo and Voyager data, based on lessons learned from regional mapping.

3:00 p.m. Radebaugh J. *
A Model for the Formation of Paterae on Io **[#1501]**
A model for patera formation is presented that uses our collective observations of Io's paterae and current understanding of Io's interior as the basis for the steps in the model.

3:15 p.m. Kirchoff M. R. * McKinnon W. B.
Mountain Building on Io: An Unsteady Relationship Between Volcanism and Tectonism **[#2245]**
We summarize thermoelastic stress modeling in Io's crust, results from statistical analysis of mountain and volcano distributions, and analysis/modeling of mountain strike orientations (they exist!). The implications for Io-oro-genesis are discussed.

3:30 p.m. Montési L. G. J. * Collins G. C.
On the Mechanical Origin of Two-Wavelength Tectonics on Ganymede **[#2093]**
The two wavelengths of tectonics observed on Ganymede can be explained by short- and long-range fault interaction in a single brittle ice layer.

3:45 p.m. Petford N. *
Rheology and Multiphase Flow in Congested Ammonia-Water-Ice Slurries **[#1043]**
Cryomagmas are natural examples of complex multiphase fluids. Some preliminary statements are made about the rheology of densely packed suspensions that have important bearing on their flow rates and eruptive style.

4:00 p.m. Dalton J. B. * Jamieson C. S. Quinn R. C. Prieto-Ballesteros O. Kargel J. S.
Cryogenic Reflectance Spectroscopy of Highly Hydrated Sulfur-bearing Salts **[#2280]**
Cryogenic reflectance spectroscopy of heavily hydrated sulfur compounds at temperatures relevant to Europa reveals fine structure which can be used to differentiate between them in studies of surface composition from spacecraft observations.

4:15 p.m. Prieto-Ballesteros O. * Kargel J. S. Selsis F. Fernández-Sampedro M. Sebastían Martínez E. Hogenboom D. L.
Searching for Clathrate Hydrates in the Europa Satellite **[#1353]**
We have studied the possibility to detect some hydrate clathrates in the Europa satellite using the current available data, such as some spectroscopic signatures and the geomorphology derived from the dissociation of these phases.

4:30 p.m. Hogenboom D. L. * Dougherty A. J. Kargel J. S. Mushi S. E.
Volumetric and Optical Studies of High-Pressure Phases of $MgSO_4$-H_2O with Applications to Europa and Mars **[#1825]**
Optical imaging of high-pressure phases of the $MgSO_4$-H_2O system while measuring the volume change of the sample near the eutectic transition provides new insight into the metastability of this system with consequences for modeling Europa's ocean.

Friday, March 18, 2005
MARS GEOCHEMISTRY AND WEATHERING
1:30 p.m. Salon B

Chairs: J. P. Greenwood
D. T. Vaniman

1:30 p.m. Newsom H. E. * Nelson M. J. Shearer C. K. Draper D. S.
The Martian Soil as a Geochemical Sink for Hydrothermally Altered Crustal Rocks and Mobile Elements: Implications of Early MER Results **[#1142]**
An altered rock geochemical sink model can explain the new data for the martian soil. The altered rock component could have formed by hydrothermal processes at any time in Mars history before erosion to form part of the soil.

1:45 p.m. Tosca N. J. * McLennan S. M. Clark B. C. Grotzinger J. P. Hurowitz J. A. Jolliff B. L. Knoll A. H. Schröder C. Squyres S. W. Athena Science Team
Geochemical Modeling of Evaporites on Mars: Insight from Meridiani Planum **[#1724]**
A model predicting mineral solubility in evaporating basaltic weathering solutions is constructed and tested. Calculations modeling evaporation and diagenesis at Meridiani are consistent with much available data returned by the Opportunity rover.

2:00 p.m. Wänke H. Boynton W. V. Brückner J. * Dreibus G. Taylor G. J. Evans L. James B. Keller J. Kerry K. Starr R. GRS Team
Sulfuric Acid All Over Early Mars? **[#1389]**
The Gamma-Ray Spectrometer of the 2001 Mars Odyssey mission yielded concentration maps for several elements in the mid-latitude regions of Mars. The role of sulfur and other elements on the surface are discussed.

2:15 p.m. Vaniman D. T. * Chipera S. J. Bish D. L. Carey J. W. Feldman W. C.
Martian Relevance of Dehydration and Rehydration in the Mg-Sulfate System **[#1486]**
Mg-sulfate salts may cycle between desiccated amorphous and more hydrated crystalline forms in near-surface equatorial deposits on Mars.

2:30 p.m. Minitti M. E. * Weitz C. M. Lane M. D. Bishop J. L.
Rock Coatings from Vulcano, a Martian Analog Environment **[#1835]**
We studied the chemistry, mineralogy and spectral character of rock coatings from an analog Mars weathering environment, Vulcano (Italy). The samples illustrate that substrate chemistry and weathering conditions influence coating formation.

2:45 p.m. Quinn R. C. * Zent A. P. Ehrenfreund P. Taylor C. L. McKay C. P. Garry J. R. C. Grunthaner F. J.
Dry Acid Deposition and Accumulation on the Surface of Mars and in the Atacama Desert, Chile **[#2282]**
Soil pH and Mars Oxidant Instrument tests are consistent with oxidative reactions triggered by dust and transient wetting in the Atacama. These responses are consistent with Viking LR observations and can be explained by the solvation of soil acids.

3:00 p.m. Greenwood J. P. * Gilmore M. S. Merrill M. D. Blake R. E. Martini A. M. Varekamp J.
Jarosite Mineralization in St. Lucia, W.I.: Preliminary Geochemical, Spectral, and Biological Investigations of a Martian Analogue **[#2348]**
Jarosite mineralization at the St. Lucia volcano is described.

3:15 p.m. Hamilton V. E. * Schneider R. D.
Alteration Phases Associated with High Concentrations of Orthopyroxene and Olivine on Mars **[#2212]**
Based on new deconvolution analyses using mineral end members, we are able to place quantitative constraints on the abundances of alteration phases associated with high concentrations of orthopyroxene and olivine on Mars.

3:30 p.m. Moore J. M. * Bullock M. A. Sharp T. G. Quinn R.
Mars-Analog Evaporite Experiment: Initial Results **[#2246]**
We rapidly evaporated Mars-analog brine under modern Martian conditions. We found that the predominant phase is gypsum, which occurs with a mixture of hydrous sulfates such as hexahydrite, and possibly mirabilite, and starkeyite.

3:45 p.m. Bullock M. A. * Moore J. M.
Aqueous Alteration of Basaltic Glass Under a Simulated Mars Atmosphere **[#2203]**
We have been performing experiments at NASA Ames that incubate volcanic glass in liquid water under Mars-simulated conditions. We find high levels of C, Fe, Ca, Mg, and Na in solution and a pH of 6.5 after 6 months.

4:00 p.m. Hausrath E. M. * Brantley S. L. AMASE
Basalt Weathering Rates in a Mars Analog Environment: Clues to the Duration of Water on Mars? **[#2339]**
Basalt samples were collected from Spitsbergen, Norway, a Mars analog site, and analyzed for chemical and physical weathering. A preliminary weathering estimation was then made, which may help constrain the duration of weathering on Mars.

4:15 p.m. Chevrier V. * Mathé P.-E. Rochette P.
Experimental Evidence of Martian Weathering **[#1784]**
Experimental weathering of primary iron phases in a CO_2 rich Martian atmosphere shows that the main neoformed iron (oxy)hydroxide under past conditions is goethite, associated to various phases (jarosite and siderite) depending on the substrate.

4:30 p.m. Parsons R. L. * Head J. W. III Marchant D. R.
Weathering Pits in the Antarctic Dry Valleys: Insolation-induced Heating and Melting, and Applications to Mars **[#1138]**
A preliminary assessment of data collected from the Antarctic Dry Valleys in 2004 highlights two end-members of weathering pit development, and offers support for pit formation resulting from mineral breakdown by insolation-derived snowmelt.

Friday, March 18, 2005
REMOTE SENSING, MARE BASALTS, AND LUNAR RESOURCE DEPOSITS
1:30 p.m. Salon C

Chairs: D. T. Blewett
R. C. Elphic

1:30 p.m. Blewett D. T. * Hawke B. R. Lucey P. G. Robinson M. S.
Two-Color Studies of the Mercurian and Lunar Surfaces **[#1245]**
We are using Mariner 10 color image data (UV and orange) to examine spectral trends associated with surface features on Mercury. Images of the Moon and lunar sample laboratory spectra provide a framework for interpreting the mercurian data.

1:45 p.m. Gillis J. J. * Lucey P. G.
Evidence that UVVIS Ratio is not a Simple Linear Function of TiO_2 Content for Lunar Mare Basalts **[#2252]**
Comparison of Clementine UVVIS ratio and Lunar Prospector neutron TiO_2 data reveal a less than optimal correlation for estimating TiO_2. We find that effects such as ilmenite grain size and bulk soil FeO content may be the cause of the poor correlation.

2:00 p.m. Pieters C. M. * Tompkins S.
Remote Sensing of Lunar Mineralogy: The Glass Conundrum **[#1346]**
New laboratory measurements of lunar pyroclastic samples are used to constrain requirements for remote mineral analyses. The extensive pyroclastic deposits at Aristarchus are shown to be Fe-rich, but Ti-poor, quench glasses.

2:15 p.m. Nicholis M. G. * Rutherford M. J.
Pressure Dependence of Graphite-C-O Phase Equilibria and Its Role in Lunar Mare Volcanism **[#1726]**
We present new constraints on graphite-C-O phase equilibria, and the depth of gas production in the Moon and other small planetary bodies.

2:30 p.m. Zeigler R. A. * Korotev R. L. Jolliff B. L. Haskin L. A.
Petrography of Lunar Meteorite MET 01210, A New Basaltic Regolith Breccia **[#2385]**
MET 01210 is a new lunar meteorite collected in Antarctica during the 2001 ANSMET field season. It is a basaltic regolith breccia composed predominantly of VLT basaltic material.

2:45 p.m. Arai T. * Misawa K. Kojima H
A New Lunar Meteorite MET 01210: Mare Breccia with a Low-Ti Ferrobasalt **[#2361]**
A new lunar meteorite is a mare breccia with low-Ti mare basalt. The pyroxene crystallization trend and estimated bulk-rock TiO_2 of the basalt is remarkably similar to A881757 basalt. The pyroxene compositions are also very similar to those of Luna 24 ferrobasalt.

3:00 p.m. Basu A. * McKay D. S.
A New Model of Size-graded Soil Veneer on the Lunar Surface **[#1321]**
The top ~ two millimeters of the lunar surface soil is size-sorted but perturbed by gardening and agglutination. This leads to higher irradiation of and vapor deposition on the smaller grains because they exist on top of others with a gradual decrease in irradiation of larger grains below.

3:15 p.m. Bentley M. S. * Ball A. J. Dyar M. D. Pieters C. M. Wright I. P. Zarnecki J. C.
Space Weathering: Laboratory Analyses and In-Situ Instrumentation **[#2255]**
Simulations of space weathering using laser irradiation are exploited to study the formation of sub-microscopic iron. A variety of magnetic techniques are evaluated to characterise this iron and are considered for *in situ* instrumentation.

3:30 p.m. Garrick-Bethell I. * Byrne S. Hoffman J. A. Zuber M. T.
Areas of Favorable Illumination at the Lunar Poles Calculated from Topography **[#2006]**
Using digital elevation models from Arecibo radar interferometry we present integrated illumination conditions at the poles over two lunations during winter and summer.

3:45 p.m. Elphic R. C. * Lawrence D. J. Feldman W. C. Prettyman T. H. Maurice S. Bussey D. B. J. Spudis P. D. Lucey P. G.
Using Models of Permanent Shadow to Constrain Lunar Polar Water Ice Abundances **[#2297]**
We use models of permanent shadow to constrain the locations of enhanced water- equivalent hydrogen at the Moon's poles, deconvolve Lunar Prospector neutron data subject to these constraints and find numerous locations of >1 wt% H_2O equivalent.

4:00 p.m. Neubert J. R. * Lucey P. G. Taylor G. J.
Properties of Permanently Shadowed Regolith **[#1613]**
Permanently shadowed areas at the lunar poles are unique. Regolith properties might be different from regolith elsewhere, gases might be trapped in amorphous ice, and chemical reactions might have formed organic compounds and phyllosilicates.

4:15 p.m. Stubbs T. J. * Vondrak R. R. Farrell W. M.
A Dynamic Fountain Model for Lunar Dust **[#1899]**
A dynamic fountain model is presented which describes how sub-micron dust is lofted up to ~100 km above the lunar surface. Sunlight scattered by this dust causes horizon glow and streamers above the terminator, as observed during the Apollo era.

4:30 p.m. Taylor L. A. * Taylor D. S.
Unique Properties of Lunar Soil for In Situ Resource Utilization on the Moon **[#1812]**
"In-Situ Resource Utilization" (ISRU) of the materials on the lunar surface, uniqueness of lunar soil, dust abatement, microwave principles and processing, and microwave products are discussed.

Friday, March 18, 2005
CHRONOLOGY OF A PROTOPLANETARY DISK
1:30 p.m. Marina Plaza Ballroom

Chairs: A. M. Davis
M. Wadhwa

1:30 p.m. Davis A. M. * Richter F. M. Mendybaev R. A. Janney P. E. Wadhwa M. McKeegan K. D.
Isotopic Mass Fractionation Laws and the Initial Solar System $^{26}Al/^{27}Al$ Ratio **[#2334]**
A variety of mass fractionation laws have been used to correct Mg isotopic data for natural mass fractionation effects. Using evaporation experiments, we have determined the proper law to use and we explore effects on ^{26}Al-^{26}Mg systematics.

1:45 p.m. Liu M.-C. * Iizuka Y. McKeegan K. D. Tonui E. Young E. D.
Supra-Canonical $^{26}Al/^{27}Al$ Ratios in an Unaltered Allende CAI **[#2079]**
Mg isotope distributions provide clues for CAI formations. However, due to isotopic disturbance, the original isotopic signals and $^{26}Al/^{27}Al$ are not necessary preserved. Here we present data for two inclusions from Allende that exhibit contrasting levels of preservation of initial $^{26}Al/^{27}Al$ signals.

2:00 p.m. Young E. D. * Simon J. I. Galy A. Russell S. S. Tonui E. Lovera O.
Supra-Canonical Initial $^{26}Al/^{27}Al$ Indicate a 10^5 Year Residence Time for CAIs in the Solar Proto-Planetary Disk **[#1525]**
We present new UV laser ablation and acid digestion MC-ICPMS analyses of 8 CAIs showing that there was more ^{26}Al in the early solar system than previously thought, and that the canonical initial $^{26}Al/^{27}Al$ represents a ~300,000 yr residence time for CAIs in the protoplanetary disk.

2:15 p.m. Tonui E. K. * Russell S. S. Simon J. I. Young E. D.
Canonical Anorthite in a Grosnaja Forsterite-bearing CAI **[#1530]**
Anorthite in a Grosnaja forsterite-bearing inclusion with canonical initial $^{26}Al/^{27}Al$ supports a new model for CAI evolution by Young et al. (this meeting) in igneous objects that show evidence for supercanonical initial $^{26}Al/^{27}Al$ of at least 6.0×10^{-5}.

2:30 p.m. Krot A. N. * Yurimoto H. Hutcheon I. D. MacPherson G. J.
Relative Chronology of CAI and Chondrule Formation: Evidence from Chondrule-bearing Igneous CAIs **[#1482]**
Type C CAIs ABC, TS26, and 93 from Allende experienced remelting with addition of chondrule Fe-Mg-silicates and incomplete O-isotopic exchange in an ^{16}O-poor gaseous reservoir ~2 Myr after formation of CAIs with the canonical $^{26}Al/^{27}Al$ ratio.

2:45 p.m. Ito M. * Ganguly J.
Closure Temperatures of the Short-lived Decay Systems, Be-B in Melilite and Al-Mg in Anorthite: Implications for the Chronology of CAIs and Early Solar System Events **[#1552]**
We have determined the closure temperatures of the decay systems to evaluate their effectiveness for the chronology of early solar system events.

3:00 p.m. Fagan T. J. * Guan Y. MacPherson G. J. Huss G. R.
Al-Mg Isotopic Evidence for Separate Nebular and Parent-Body Alteration Events in Two Allende CAIs **[#1820]**
Most secondary phases in two CAIs from Allende have no detectable radiogenic ^{26}Mg, but grossular in one Type A CAI has canonical radiogenic ^{26}Mg. The data indicate two discrete alteration events: possibly one nebular and one asteroidal.

3:15 p.m. Papanastassiou D. A. * Wasserburg G. J. Bogdanovski O.
The ^{53}Mn-^{53}Cr System in CAIs: An Update **[#2198]**
New high precision and high sensitivity techniques for Cr have been developed and applied to refractory inclusions. The usefulness of the Mn-Cr chronometer will depend on finding pristine inclusions, because, at present, the Al-Mg and Mn-Cr chronometers appear at variance with each other.

3:30 p.m. Pravdivtseva O. V. * Hohenberg C. M. Meshik A.
I-Xe Dating: The Time Line of Chondrule Formation and Metamorphism in LL Chondrites **[#2354]**
I-Xe ages of chondrules from LL chondrites of various metamorphic grades are considered relative to the revised absolute age of the Shallowater reference (4563.5 ± 1 Ma). They suggest long-lasting alteration on the parent body. The oldest I-Xe ages may reflect the time of chondrule formation.

3:45 p.m. Bizzarro M. * Baker J. A. Haack H.
Timing of Crust Formation on Differentiated Asteroids Inferred from Al-Mg Chronometry **[#1312]**
We report ^{26}Al-^{26}Mg data for basaltic meteorites from the angrite, eucrite and mesosiderite parent bodies, suggesting differentiation < 3 Myr of CAI formation. These planetesimals thus accreted while ^{26}Al was sufficiently abundant to drive melting.

4:00 p.m. Wadhwa M. * Amelin Y. Bogdanovski O. Shukolyukov A. Lugmair G. W.
High Precision Relative and Absolute Ages for Asuka 881394, a Unique and Ancient Basalt **[#2126]**
We present high precision Mg, Cr and Pb isotopic systematics in Asuka 881394. Our results demonstrate that Asuka 881394 formed within, at most, ~3 My of the formation of CAIs and that the Al-Mg, Mn-Cr and Pb-Pb chronometers are concordant in this sample.

4:15 p.m. Whitby J. A. * Crowther S. Busfield A. Gilmour J. D.
Inhomogeneity on the Lodranite Parent Body Inferred from I-Xe Systematics **[#1658]**
Measured model I-Xe ages for lodranite meteorites vary widely. It is suggested that this is due in part to migration of iodine in a fluid phase on the parent body whilst ^{129}I was still active.

4:30 p.m. Busemann H. * Busfield A. Gilmour J. D.
Ancient Volcanic Xenon in Single Glass Grains from the D'Orbigny Angrite **[#2299]**
We present high-sensitivity xenon data for single glass grains from the D'Orbigny angrite. These grains contain the first sample of volcanic gas from a planetary body other than the Earth and excess ^{129}Xe detected for the first time in angrites.

PRINT-ONLY PRESENTATIONS

Impacts

Hoffman N.
Origin of the Northern Lowlands of Mars in a Single String-of-Pearls Impact **[#1237]**
A String-of-Pearls impact on early Mars is a novel way to form the complex northern lowlands in essentially a single event, over a few days of real time. The impact fragments create overlapping basins which merge to form the northern plains.

Kashkarov L. L. Badjukov D. D. Ivliev A. I. Kalinina G. V. Nazarov M. A.
The Smerdyacheye Lake: New Evidence for Impact Origin and Formation Age **[#1822]**
Fission track and thermoluminescence studies of a glass beard found near the Smerdyacheye Lake crater support the possible impact origin of the structure.

Krivosheya K. V. Badyukov G. D. Badjukov D. D. Raitala J.
The Gagarin Ring Structure, Russia: A Possible Meteorite Crater **[#1688]**
Morphological, geophysical and mineralogical data strongly support the idea of impact origin of the 1.4 km Gagarin ring structure, the Smolensk district, Russia.

Marusek J. A.
The Cosmic Clock, the Cycle of Terrestrial Mass Extinctions **[#1009]**
Oort cloud comet impacts and nearby supernova events are believed to be the root cause for the greatest terrestrial mass extinctions during the past 500 million years. A dual cycle of extinctions is observed and well ordered in geological time.

Sazonova L. V. Fel'dman V. I. Miljavskij V. V. Borodina T. I. Sokolov S. N.
Some Peculiarities of Quartz, Biotite and Garnet Transformation in Conditions of Step-like Shock Compression of Crystal Slate **[#1037]**
A character investigated of changes of the crystal slate, which consists of a garnet, biotite, quartz and plagioclase has been studied using of recovery assemblies of planar geometry.

Svetsov V. V.
Impact Erosion of Atmosphere: Some Results of Numerical Simulations for Vertical Impacts **[#1675]**
Numerical simulations of vertical impacts have been made for impactor diameters from 75 m to 10 km and velocities from 15 to 70 km/s. The losses of air and retained masses of impactors were calculated for a 1 bar atmosphere on the Earth and Mars.

Vishnevsky S. A. Gibsher N. A. Raitala J. Öhman T. Palchik N. A.
The Popigai Fluidizites: Dense Water Inclusions in Lechatelierite; Evidence for Shock-generated Carbonate and Hydrous Silicate Melts **[#1145]**
New data (dense water inclusions in lechatelierite; evidences for carbonate and hydrous silicate melts) are presented for the Popigai impact fluidizites which are the first impactites of so kind described in terrestrial astroblemes.

Moon and Mercury

Berezhnoy A. A. Kozlova E. A. Shevchenko V. V.
The Cold Traps Near the South Pole of the Moon **[#1061]**
We have allocated a number of craters which can be considered as "cold traps " in the south pole region of the Moon. Some from these craters has properties similar to those of the echo coming from icy satellites of Jupiter and from the southern polar cap of Mars.

Chikmachev V. I. Pugacheva S. G. Shevchenko V. V.
General Structure of the Lunar South Pole — Aitken Basin and Possible Genesis of It **[#1078]**
We revised topographical data obtained for the region to construct a generalized structure of the SPA basin. We have used a cartographic method to analyze properties of the system of concentric depressions inside the ring structure.

Demidova S. I. Nazarov M. A. Kurat G. Brandstätter F. Ntaflos T.
New Lunar Meteorites from Oman: Dhofar 925, 960 and 961 **[#1607]**
New lunar meteorites Dhofar 925, 960 and 961 are the first Dhofar lunar meteorites, which contain both highland and mare material as well as a KREEP component. Here we report first data on petrography, mineralogy and chemistry of the new meteorites.

Domingue D. Vilas F.
Spectral Photometric Properties of the Moon **[#1978]**
Affects of photometry on spectral properties of solid surfaces as applied to the Moon.

Korokhin V. V. Velikodsky Yu. I.
Studying the Phase Dependence of Lunar Surface Brightness Using Data of Integral Observations **[#1437]**
On the base of integral photometry of the Moon, it is shown that the phase dependence of lunar surface brightness at relatively small phase angles (18–43°) is formed substantially by microrelief and at great ones 41°–120° by mesorelief.

Leontieva E. M. Matukov D. I. Nazarov M. A. Sergeev S. A. Shukolyukov Yu. A.
The First Isotopic Dating of the Dhofar 025 Lunar Meteorite by U-Pb Method Using Accessory Zircon **[#2013]**
For the first time Dhofar 025 meteorite is dated by U-Pb method using the accessory zircon. Acquired ages of zircon grain and breccia are 4, 5 and 2 Ga respectively. Our results suggest that Dhofar 025 is a unique rock ejected from the lunar farside.

Nazarov M. A. Demidova S. I. Brandstätter F. Ntaflos Th. Kurat G.
Deep-seated Crustal Material in Dhofar Lunar Meteorites: Evidence from Pyroxene Chemistry **[#1063]**
Al-rich, Ca-poor orthopyroxene fragments are present in Dhofar lunar highland meteorites. It suggests that the meteorites contain a certain portion of deep-seated lunar crustal material.

Ozima M. Seki K. Terada N. Miura Y. N. Podosek F. A. Shinagawa H.
Terrestrial Atmospheric Components in Lunar Soils: Record of Early Earth Evolution **[#1118]**
Lunar soils can be used to trace early earth evolution, since they contain non-solar components transported from the ancient Earth atmosphere.

Stooke P. J.
Lunar Laser Ranging and the Location of Lunokhod 1 **[#1194]**
Lunokhod 1's laser retroreflector cannot be used. If this is due only to uncertainty over its location there may be hope to recover it. A new location 5 km west of the usual cited location is suggested on the basis of comparison of surface and orbital images.

Velikodsky Yu. I. Korokhin V. V.
Model of Light Scattering by Lunar Regolith at Moderate Phase Angles: New Results **[#1917]**
New CCD-observations at phase angles 145°–153° and data of absolute photometry of the Moon confirm that our model can simultaneously describe observational phase dependences of brightness and polarization degree in wide range of phase angles.

Wood C. A. Higgins W. Pau K. C. Mengoli G.
The Lamont-Gardner Megadome Alignment: A Lunar Volcano-Tectonic Structure? **[#1116]**
The Lamont-Gardner Megadome Alignment is a 500 km alignment of volcanic, possible volcanic, and tectonic landforms crossing Mare Tranquillitatis. It has no control by local impact structures and may be a lunar volcano-tectonic feature.

Astrobiology

Steele A. Amundsen H. E. F. Fries M. Vicenzi E. Benning L. Maule J. Mysen B. Toporski J. Schweizer M. Fogel M.
A Morphological and Chemical Study of Carbonate Globules Contained Within Mantle Xenoliths of the Sverrefjell Volcano Spitsbergen — Implications for ALH84001 **[#2173]**
We describe Raman and elemental composition of globules similar to those found in ALH84001. We appear to see direct evidence of zonation of carbonate, carbon and silicon phases within terrestrial olivine mantle xenoliths.

Ghail R. C.
Geological Constraints on Extrasolar Earth-like Planets **[#1870]**
I examine the effects of variable chemical composition on Earth-mass planets and discuss the implications for the search for extrasolar life.

Strapoc D. Beard B. L. Schieber J.
How Can a Fingerprint of Primitive Bacteria Look Like? A Carbon and Iron Stable Isotopic Study of an Iron-oxidizing Bacterial Community **[#2232]**
We investigate what kind of C and Fe stable isotopic signatures may have left behind primitive iron-oxidizing bacteria as well on Earth as on Mars in the rock record, since there was high probability of interplanetary material exchange in early solar system history.

OMEGA@Mars

Cruikshank D. P.
Vassili Ivanovich Moroz — An Appreciation **[#1979]**
Vassili Moroz (b. 1931, d. 2004) was a key scientist and organizer in Soviet (Russian) and international programs of planetary exploration. He was a pioneer in infrared astronomy and in the study of the surfaces and atmospheres of Mars and Venus.

Forni O. Poulet F. Bibring J.-P. Erard S. Gomez C. Langevin Y. Gondet B. OMEGA Science Team
Component Separation of OMEGA Spectra with ICA **[#1623]**
The ICA component analysis applied to the OMEGA spectra is a fast and efficient tool that has proven to detect in hyperspectral data spatially independent component whose spectra can be automatically retrieved without any *a priori* knowledge of the composition.

Surficial Processes

Coleman N. M. Dinwiddie C. L.
Groundwater Depth, Cryosphere Thickness, and Crustal Heat Flux in the Epoch of Ravi Vallis, Mars **[#2163]**
We propose a method to estimate the cryosphere and groundwater depth via analysis of chaotes that formed in outflow channels. We derive a range of 700 to 1000 m for Iamuna Chaos in Ravi Vallis, and estimate the local Hesperian crustal heat flux was 30 to 50 mW m^2.

de Pablo M. A. Márquez A. Centeno J. D.
Geomorphologic Map of the Atlantis Basin, Terra Sirenum, Mars **[#1297]**
Here is shown the first geomorphologic cartography of the Atlantis basin region and the brief description of the mapped units.

Kuzmin R. O. Zabalueva E. V. Mitrofanov I. G. Litvak M. L. Parshukov A. V. Grin'kov V. Y. Boynton W. V. Saunders R. S.
Seasonal Redistribution of Water in the Surficial Martian Regolith: Results of the HEND Data Analysis **[#1634]**
We report results of the global mapping of the neutrons albedo on Mars and show the evidences for seasonal redistribution of the water in the surface regolith, based on HEND data.

Kuznetsov I. V. Kuzmin R. O. Greeley R.
Wind-related Erosion Depressions Within a Small Impact Craters in Chryse and Elysium Planitiae on Mars **[#1810]**
We report results of morphological and statistical analysis of the blowout hollows within a small impact craters in Chryse and Elysium Planitiae.

Luiro K. Raitala J. Hauber E. Neukum G. HRSC Co-Investigator Science Team
Landslides and the Tectonic Scarp in Coprates Chasma — Examples Studied from HRSC Data **[#1618]**
Eastern Valles Marineris landslides revisited with HRSC data.

Martinez-Alonso S. Mellon M. T. Jakosky B. M. Kindel B. C.
Mapping Compositional Diversity on Mars: Spatial Distribution and Geological Implications **[#1292]**
The Spectral Variance Index (SVI) identifies, from statistical analysis of MGS-TES data, regions of large surface materials diversity. We present a global SVI map and discuss its significance by comparison to landers data and to other global maps.

Thomson B. J. Schultz P. H.
The Geology of the Viking 2 Lander Site Revisited **[#1800]**
Crater densities near the Viking 2 Lander indicate an extreme loss of small craters, consistent with a recently active, deflated eolian mantle. This mantle was emplaced before the Late Hesperian's end, indicating a long dominance of eolian activity.

Tribbett K. L. McAdoo B. G.
A Reevaluation of Mass Movements Within the Valles Marineris Region of Mars Using MOLA and MOC Data **[#1151]**
Our research indicates that forces initiating Martian slumps may be higher in potential energy than those initiating Martian landslides. Our comparison of Martian slides to submarine landslides suggests that fluid or acoustic fluidization may be driving long runouts on Mars.

Vid'machenko A. P. Morozhenko A. V.
Mapping of the Physical Characteristics and Mineral Composition of a Superficial Layer of the Moon or Mars and Ultra-Violet Polarimetry from the Orbital Station **[#1015]**
We suggest using observational data on measurements of UV light's degree of linear polarization at phase angles in limits from 80 up to 120 degrees, that is, in those limits in which values of Brewster's angles are practical for all ground materials.

Zeltsman A.
Measuring the Surfaces on Mars **[#1502]**
Some images from Mars Rovers contain apparently flat surfaces. We measure how flat they actually are. The digital experiments are used to answer the question what would happen to offset value, if the point set observed was in slightly different position.

Mars: Volcanism and Tectonics

Arkani-Hamed J.
The Magnetic Crust of Mars **[#1994]**
This paper determines the thickness of the potentially magnetic layer of Mars in the Cimmeria and Sirenum Terrae, on the basis of thermal evolution models of Mars and the demagnetization of the uppermost crust by shock waves produced by impacts that have created craters of 100 km diameter or less.

Bazilevskaya E. A.
Thickness of the Olympus Mons Lava Flows as Measured from the MGS MOC and MOLA Data: Volcano Caldera and Flanks **[#1082]**
Thicknesses of the Olympus Mons lava flows have been measured: 4 to 11 m (mean ~ 6 m) for the volcano flanks and 4 to 26 m (mean ~ 10 m) for the caldera scarps, being similar to typical thicknesses of terrestrial basaltic flows.

Bruno B. C.   Fagents S. A.   Pilger E.   Rowland S.   Garbeil H.
Lava Flows on Olympus Mons, Mars: Estimates of Flow Speeds and Volume Fluxes from MOC, THEMIS and MOLA Data **[#2012]**
Lava flow velocities on Olympus Mons are estimated using *Jeffreys* (1925) based on dimensional data and assumed input parameters. Relationships among flow dimensions, slope, emplacement style and location on the edifice are also explored.

Martín-González F.   de Pablo M. A.   Márquez A.
Folded Structure in Terra Sirenum. Mars **[#1430]**
Located in Terra Sirenum, Mars, an elongated relief is surrounded by bedding surfaces. The asymmetric shape (cuesta) and the slope calculated from MOLA data, and also the images have been used to propose a folded structure. This folded structure is an upright fold.

Watters T. R.   McGovern P. J.
Flexure and the Topography of the Dichotomy Boundary on Mars **[#1874]**
We model lithospheric flexure of the southern highlands and compare deflection profiles for both a weakened and a continuous plate to the long wavelength topography of the dichotomy boundary in the eastern hemisphere of Mars.

Mars: Marscellaneous

Becker K. J.   Gaddis L. R.   Soderblom L. A.   Kirk R. L.   Archinal B. A.   Johnson J. R.   Anderson J. A.   Bowman-Cisneros E.   LaVoie S.   McAuley M.
Unified Planetary Coordinates System: A Searchable Database of Geodetic Information **[#1369]**
The Unified Planetary Coordinates system is a uniform geometric database for all Mars orbital remote sensing data using the IAU/IAG 2000 east planetocentric coordinate system that we will provide to the scientific community in a variety of forms.

Kostrikov A.
The Martian North Polar Cap Spirals are the Traces of an Ancient Ice Sheet Collapse **[#1018]**
Radial tension amplification came to the ice sheet cracking. Being influenced by Coriolis force, crack trajectories deviated, forming spirals. Accublation smoothing transformed the helical structure of crevasses to the helical structure of troughs.

Max M. D.   Clifford S. M.
Crustal Sources of Atmospheric Methane on Mars: The Association with Ground Ice and the Potential Role of Local Thermal Anomalies **[#2303]**
Potential crustal sources and pathways of atmospheric methane on Mars are discussed.

Maxe L. P.
An Earth Sedimentary Deposit as Analogue to Martian: The Comparison of IR-Spectra **[#1386]**
IR-spectra of the sedimentary deposit is used for the comparative analysis with Martian spectra. At the processing secondary minerals are synthesized. On Mars can be formed similar end products: silicates and aluminates of magnesium, calcium, iron, etc.

Michael G. G.   Reiss D.   Hauber E.   Scholten F.   Jaumann R.   Neukum G.   HRSC Co-Investigator Team
Rampart Ejecta Volume Measurements in Xanthe Terra, Mars, Using MOLA: Relation to HRSC-Camera Derived Age Measurements **[#1709]**
We studied 32 craters with fluidized ejecta ramparts in Xanthe Terra, making measurements of their ages using crater-counts on the ejecta in HRSC images [1], and of the thickness and volume of the ejecta using MOLA data.

Ozorovich Yu. A Lukomsky A. K.
Geoelectrical Markers and Oreols of Subsurface Frozen Structures on Mars for Long-Term Monitoring of Spatial and Temporal Variations and Changes of Martian Cryolitozone Structure on the Base Ground and Satellite Low-Frequency Radar Measurements **[#1332]**
Possibilities of long-term monitoring spatial and temporal variations and changes of subsurface geoelectrical section on the base geoelectrical markers and oreols of cryolitozone.

Ruiz J.
On Ancient Shorelines and Heat Flows on Mars **[#1135]**
The elevation range of putative paleoshorelines may inform about the thermal evolution of Mars, but lateral continuity of these features is poorly known, and diverse division and mixing of the originally proposed paleoshorelines could be required.

Sprenke K. F.
Evidence for Polar Wander in the Gravity and Magnetic Fields of Mars **[#1269]**
Evidence for polar wander on Mars can be found in the gravitational and magnetic fields of the planet. The consistency between the gravity and magnetic results in so far as the location of paleopoles is striking.

Williams A. F.
Chronology of Syrtis Major Quadrangle **[#1441]**
A chronology of the Syrtis Major Quadrangle on Mars has been devised using geologic, topographic, gravimetric, and magnetic data along with recent narrow-angle images from the Mars Orbiter Camera.

Meteorites

Alexeev V. A. Ustinova G. K.
Meteorite Data on the Solar Modulation of Galactic Cosmic Rays and an Inference on the Solar Activity Influence on Climate of the Earth **[#1012]**
Meteorite data on the galactic cosmic rays, the solar activity, and temperature variations in the Earth's atmosphere lead to the conclusion that the solar activity may be important factor exerting the influence upon the climate of the Earth.

Badjukov D. D. Brandstätter F. Kurat G. Libowitzky E. Raitala J.
Ringwoodite-Olivine Assemblages in Dhofar 922 L6 Melt Veins **[#1684]**
Melt veins in the L6 chondrite Dhofar 922 contain olivine-ringwoodite assemblages. Compositions of these co-existing olivine and ringwoodite correspond to the formation of the assemblages at 1200°C and 12.7 GPa.

Moggi-Cecchi V. Pratesi G. Mancini L.
NWA 1052 and NWA 1054: Two New Primitive Achondrites from North West Africa **[#1808]**
NWA 1052 and 1054 are two meteorites containing olivine, low- and high-Ca pyroxene, plagioclase, Fe-Ni, troilite, Cl-apatite and chromite. The texture and EMPA data on olivine and low- and high-Ca pyroxene suggest a classification as acapulcoites.

Fogel R. A.
An Analysis of the Solvus in the CaS-MnS System **[#2395]**
Solution modeling of experimental datasets for the CaS-MnS system indicate serious inter- and intra-dataset inconsistencies. This calls into question the use of MnS in CaS and CaS in MnS as geothermometers with current datasets. New experimental data for this system are presented for 1100°C.

Hua X. Wang Y. Hsu W. Sharp T. G.
Fremdlinge in Chondrules and Matrix of the Ningqiang Carbonaceous Chondrite **[#1762]**
A large number of Fremdlinge are found in chondrules and matrix of Ningqiang. Their mineral assemblages are similar to those in Allende CAIs. Their formation was a common phenomenon, closely associated with formation of CAIs and chondrules.

Ivanova M. A. Nazarov M. A. Brandstätter F. Moroz L. V. Ntaflos Th. Kurat G.
Mineralogical Differences Between Metamorphosed and Non-Metamorphosed CM Chondrites **[#1054]**
As compared to normal CM chondrite, Dhofar 955, the metamorphosed CM chondrites, Dhofar 225 and Dhofar 735 are characterized by a lack of tochilinite, and a lack of P-rich sulfides. These features could be due to thermal metamorphism.

Ivliev A. I. Kuyunko N. S. Skripnik A. Ya. Nazarov M. A.
Thermoluminescence Studies of Carbonaceous Chondrites **[#1065]**
The purpose of the present paper was to study carbonaceous chondrite metamorphism using the TL-device of the Vernadsky Institute.

Kurat G. Varela M. E. Zinner E.
Silicate Inclusions in the Kodaikanal IIE Iron Meteorite **[#1814]**
II-E iron meteorites are particularly interesting because they contain an exotic zoo of silicate inclusions including some chemically strongly fractionated ones. Here we present preliminary findings in our study of Kodaikanal silicate inclusions.

Lavrentjeva Z. A. Lyul A. Yu. Shubina N. A. Kolesov G. M.
REE and Some Other Trace Elements Distributions of Mineral Separates in Atlanta (EL6) **[#1011]**
REE and some other trace element distributions of mineral separates in Atlanta (EL6) are presented.

Lorenz C. A. Ivanova M. A. Kurat G. Brandstätter F.
FeO-rich Xenoliths in the Staroye Pesyanoe Aubrite **[#1612]**
The nine FeO-rich mineral and lithic clasts, corresponding to H- and carbonaceous chondrites, were found in the Staroye Pesyanoe aubrite. It indicates that flux of interplanetary dust onto aubrite parent body was different from that of Earth and HED.

Miyamoto M. Jones R. H. Koizumi E. Mikouchi T.
Verification of a Model to Calculate Cooling Rates in Olivine by Consideration of Fe-Mg Diffusion and Olivine Crystal Growth **[#1610]**
We developed a model to analyze chemical zoning in olivine based on Fe-Mg diffusion during olivine crystal growth to obtain the cooling rate. We verify this model by using Fe-Mg zoning in olivine produced by dynamic crystallization experiments.

Okazaki R. Nakamura T.
Origin and Thermal History of Lithic Materials in the Begaa LL3 Chondrite **[#1533]**
Origin and thermal history of unusually large lithic materials found in the Begaa LL3 chondrite is discussed based on the major/minor element abundances, oxygen isotopic ratios, and rare earth element abundances.

Pletchov P. Yu. Zinovieva N. G. Latyshev N. P. Granovsky L. B.
Evaluation of the Crystallization Temperatures and Pressures for Clinopyroxene in the Parental Bodies of Ordinary Chondrites **[#1041]**
Thermo- and barometry of clinopyroxene in ordinary chondrites indicates that, regardless of the chemical groups and petrological types of chondrites, they crystallized from chondritic melts at pressures of >0 kbar.

Skála R. Císařová I.
Crystal Structure of Troilite from Chondrites Etter and Georgetown **[#1284]**
Crystal structure of troilites from chondrites Etter and Georgetown is consistent with that reported earlier for troilite or its synthetic analogues. Studied troilites are slightly cation-deficient. The crystals represent the inversion twins.

Takeda H. Yamaguchi A. Otsuki M. Ishii T.
New Achondrites with High-Calcium Pyroxene and Its Implication for Igneous Differentiation of Asteroids **[#1298]**
We report two new achondrites, which contain more augite than previously described. Combined with data of silicate inclusions in IAB and IIE irons, we propose that augites are important component in partial melts of chondritic source materials.

Wasson J. T. Matsunami Y. Rubin A. E.
Possible Formation of IVA Irons by Impact Melting and Reduction of L-LL Chondrite Materials **[#1511]**
The oxygen-isotope composition of silicates in IVA irons indicates an origin from L-LL chondritic materials. This requires appreciable reduction. We suggest that melting and reduction resulted from an impact onto a porous primitive chondritic body.

Zinovieva N. G. Pletchov P. Yu. Latyshev N. P. Granovsky L. B.
Physicochemical Conditions of Clinopyroxene Crystallization in the Parental Bodies of Ordinary Chondrites **[#1038]**
Thermobarometry of pyroxenes in ordinary chondrites indicates that they crystallized from chondritic melts, first, under significant pressures in large parental bodies and then continued to crystallize in much smaller bodies (~9 kbar, R~750–850 km).

Oxygen in the Solar System

Papike J. J. Karner J. M. Shearer C. K.
Comparative Planetary Mineralogy: Valence State Partitioning of Cr, Fe, Ti, and V Among Crystallographic Sites in Olivine, Pyroxene, and Spinel from Planetary Basalts **[#1005]**
Valence state partitioning of Cr, Ti, V, and Fe into olivine, spinel, and pryoxene are explored in basalts from the Earth, Moon, and Mars.

Cassini at Saturn

Mousis O. Alibert Y. Benz W.
Volatiles Enrichments in Saturn — Predictions for Cassini **[#1180]**
We use the giant planets extended core-accretion model of *Alibert et al.* (2004, 2005) and the clathrate hydrate trapping theory to calculate the enrichments in O, C, N, S, Xe, Ar and Kr with respect to their solar abundances in Saturn's atmosphere.

Outer Planets and Satellites

Alibert Y. Mousis O. Benz W.
Volatiles Enrichments and Composition of Jupiter **[#1181]**
We use the giant planets extended core-accretion model of *Alibert et al.* (2004, 2005) and the clathrate hydrate trapping theory to calculate the enrichments in O, C, N, S, Xe, Ar and Kr with respect to their solar abundances in Jupiter's atmosphere.

Cox R. Ong L. C. F. Arakawa M.
Is Chaos on Europa Caused by Crust-penetrating Impacts? **[#2101]**
Some chaos areas on Europa may be sites of full-crustal penetration by impacts. Experimental evidence indicates that impact penetration can produce the features associated with chaos areas.

Ennis M. E. Davies A. G.
Thermal Emission Variability of Zamama, Culann and Tupan on Io Using Galileo Near-Infrared Mapping Spectrometer (NIMS) Data **[#1474]**
Galileo NIMS data of volcanic activity at Zamama, Culann and Tupan on Io are analysed to determine thermal output, style of activity, and volumes and rates of effusion. Individual eruption episodes are identified at each location.

Kuskov O. L. Kronrod V. A.
Chemical Differentiation and Internal Structure of Europa and Callisto **[#1036]**
Models of the internal structure of Europa and Callisto based on Galileo gravity measurements and constraints on the composition of chondrites are constructed. The results support the hypothesis that Callisto may have a liquid-water ocean.

Rosaev A. E.
The Effect of Parametric Resonance on the Structure of Planetary Rings **[#1016]**
The resonance perturbation of planetary ring by distant satellite is considered. The gravity interaction between ring particles is taken into account. The shift between simple mean motion resonances and parametric resonance zones is detected. This shift depends on ring properties.

Stephan K. Jaumann R. Hibbitts C. A. Hansen G. B.
Relationships Between Depths of Water Ice Absorption Bands — Indicator of Changes in Particle Size of Water Ice on the Surface of Ganymede **[#2061]**
Ratios of different band depths of water ice absorptions give indications for changes in particle sizes of water ice across the surface of Ganymede.

Veeder G. J. Matson D. L. Rathbun J. A. Davies A. G. Johnson T. V.
Loki Patera: A Magma Sea Story **[#1587]**
Our magma sea story considers Loki Patera on Io as the surface expression of a large uniform body of magma. At "sea" the state of the dark region within Loki is controlled by relatively local processes. When the sea crust founders, plates sink and are replaced by fresh, liquid lava.

Stardust

Koscheev A. P. Zaripov N. V. Ott U.
Diamond Nanograins in Carbon Soot: Does the Chemistry of Extracted Diamonds Depend on the Properties of Pristine Soot? **[#1406]**
Explosively produced nanodiamond-containing soot as well as extracted nanodiamonds were investigated by thermal desorption mass spectrometry. The surface chemistry of the nanodiamonds is shown to retain a memory of the synthesis conditions.

Tsou P. Brownlee D. E. Glesias R. Grigoropoulos C. P. Weschler M.
Cutting Silica Aerogel for Particle Extraction **[#2307]**
We report the current findings on three basic techniques of cutting silica aerogel for extracting the embedded samples: mechanical cutting, lasers cutting and ion beam milling.

Asteroids and Small Bodies

Golubeva L. Shestopalov D. McFadden L. A.
Searching for Faint Absorption Bands in Vestoid Reflectance Spectra by Means of Optimal Smoothing Algorithm **[#1206]**
The faint absorption bands near 480–490, 505, 530, 550 nm were found in the spectra of some vestoids from SMASS1 by using the optimal smoothing algorithm. According to the spectral data for the terrestrial pyroxenes and the HED these bands are associated with Fe^{2+} in asteroid surface pyroxenes.

Housen K. R.
Nudging an Asteroid with Explosives or Impacts **[#2249]**
Estimates and experimental results are summarized that describe the velocity increment that can be applied to an asteroid via impacts or near-surface explosions.

Busarev V. V. Dorofeeva V. A. Makalkin A. B.
Possibility of Separating Silicates and Organics in Large Kuiper Belt Objects **[#1074]**
We investigate a possibility of separating silicates and organics, phyllosilicate formation and layering matter in large Kuiper Belt Objects (from 200 km) on condition that water ocean forms in their interiors due to decay of ^{26}Al and/or collisions of the bodies.

Filonenko V. S. Churyumov K. I.
Photometrical Peculiarities and Outburst Activity of Two Target Comets **[#1656]**
The light curves of short-period comets 67P/Churyumov-Gerasimenko and 9P/Tempel 1 (which are targets for "ROSETTA" and "Deep Impact") have been constructed. Their photometrical behavior was studied. Photometrical parameters have been determined.

Michikami T. Moriguchi K. Nakamura R.
Application to Large Blocks on Asteroid 25143 Itokawa: Ejecta Mass Distribution with Low Velocity for Impact Cratering Experiment on Porous Target **[#1729]**
The impact cratering experiment was carried out in order to estimate the ejecta mass distribution with low velocity (<1 m/s). Based on this result, the number of large blocks (>1 m) on asteroid 25143 Itokawa can be estimated to be about 340.

Nakamura R. Ishiguro M. Nakamura A. M. Hirata N. Terazono J. Yamamoto A. Abe M. Hashimoto T. Saito J.
Inflight Calibration of Asteroid Multiband Imaging Camera Onboard Hayabusa: Preliminary Results **[#1602]**
Asteroid Multi-band Imaging CAmera (AMICA) is an imaging instrument onboard Hayabusa spacecraft to examine the surface topography and composition of the target S-type asteroid Itokawa. We report preliminary results of the inflight observations.

Perov N. I.
On Origin of Sedna **[#1049]**
In the frame of the space model of the binary problem of two-body: the Sun–Sedna and Sedna and Planet X a transition of Sedna, moving originally along heliocentric parabolic orbit, into elliptic orbit is under consideration. The parameters of Planet X are set up.

Shestopalov D. Golubeva L. McFadden L. A.
Optimal Smoothing of Asteroid Reflectance Spectra: The Search for Faint Absorption Bands **[#1165]**
We suggest the optimal smoothing algorithm for noisy reflectance spectra of the asteroids, which is intended for separating faint absorption bands from the noise.

Ward Wm. R.
Early Clearing of the Asteroid Belt **[#1491]**
The ensemble of embryos destined to become the Jovian core may have excited the primordial asteroid belt and initiated a fragmentation cascade there. Thus, the majority of the belt mass may have drifted via gas drag into the terrestrial zone prior to the formation of Jupiter.

Early Solar System Evolution

Asphaug E. Agnor C. Williams Q.
Tidal Forces as Drivers of Collisional Evolution **[#2393]**
At large scales, where the impact timescale is comparable to the gravitational timescale, planetary collisions can be dominated by unloading, torques and tides instead of shock.

Dauphas N.
Uranium-Thorium Cosmochronology **[#1126]**
Using the U/Th ratios measured in meteorites and low metallicity halo stars, the U/Th production ratio and the radiometric age of the Milky Way are estimated to be 0.571 (+0.037/–0.031) and 14.5 (+2.8/–2.2) Gy, respectively.

Leya I. Schönbächler M. Wiechert U. Halliday A. N.
Titanium Isotopic Composition of Solar System Objects **[#1338]**
We present the Ti isotopic composition for lunar whole rock samples and mineral separates and for terrestrial basalts measured via high resolution MC-ICPMS.

Marzari F. Scholl H. Tricarico P.
Stability of the 3:1 Resonance Locking in the 55 Cancri Planetary System **[#1289]**
The most crowded extrasolar planetary system discovered so far is the one around 55 Cancri with four planets. We applied Laskar's frequency map analysis which yields a quantitative measure for the stability of the system.

Sahijpal S. Soni P.
Planetary Differentiation of Accreting Planetesimals with ^{26}Al and ^{60}Fe as the Heat Sources **[#1296]**
Detailed numerical simulations involving linear accretional growth and planetary differentiation of planetesimals with ^{26}Al and ^{60}Fe as the heat sources have been attempted.

Ustinova G. K.
Phenomenological Excitation Functions of Xe Isotopes with Protons on Nuclei of Cs, La and Ce **[#1021]**
Using an elaborated phenomenological approach, the Xe isotope excitation functions on Cs, La and Ce are determined. The Xe isotope relations turned out to be strongly dependent on the proton energy, and practically independent of the target nuclei.

Vityazev A. V. Pechernikova G. V. Bashkirov A. G.
"Missing Xenon" Problem and Climate of the Early Earth **[#1719]**
The proposed solution for the problem of Xe deficit on the Earth and Mars is based on the fact of its enrichment in comparison to other noble gases in gas hydrates and models of impact erosion at final stage of the planet formation.

Genesis Mission

Manuel O. Myers W. A. Singh Y. Pleess M.
Solar Abundance of Elements from Neutron-Capture Cross Sections **[#1033]**
Excess light s-products in the photosphere (A = 25–207) confirm the solar mass separation recorded by excess light isotopes in the solar wind (A = 3–136). Both measurements show that major elements in the Sun and rocky planets are Fe, O, Ni, Si and S.

Venus

Kerzhanovich V. V. Yavrouian A. H. Hall J. L. Cutts J. A.
Dual Balloon Concept for Lifting Payloads from the Surface of Venus **[#1223]**
Two-balloon concept makes feasible Venus missions requiring lifting probes with surface sample to stratosphere. Metal bellow serves as low-atmosphere balloon to bring system to altitude where from polymer film balloon delivers the probe to upper atmosphere.

Krassilnikov A. S. Kostama V.-P. Aittola M. Guseva E. N. Cherkaschina O. S.
Relationship of Coronae, Regional Plains and Rift Zones on Venus **[#1831]**
We studied geology of 104 coronae of type 1 and 2 and their relationship with rift systems and regional plains on Venus. Global map of rift zones has been compiled. Majority of coronae has no association with rifts and predates regional plains.

Exploration

Landgraf M.
The Sun's Dust Disk — Discovery Potential of the New Horizons Mission During Interplanetary Cruise **[#1183]**
The dust disk detected by Pioneer at a heliocentric distance of 18 AU is a fraction of the dust generated by the Kuiper belt outside 30 AU. New Horizons will find a very high flux of more than 10 hits per day for each square meter of sensitive area.

Diaz A. Lodhi M. A. K. Wilson T. L.
A New Perspective on Trapped Radiation Belts in Planetary Atmospheres **[#1197]**
We show that trapped-belt proton spectra are actually bi-variant in energy E and atmospheric density ρ. As a paradigm shift, this helps clarify some of the historical difficulties associated with understanding planetary trapped radiation belts.

Education

Castilla G. de Pablo M. A. López C. Martín L.
Earth and Mars, Similar Features and Parallel Lives? Didactic Activities **[#1286]**
Here we present three didactic activities that allow a general view of the planet Mars compared with Earth. Each of these didactic activities are focused on one of these goals: geological history, geological processes and geomorphologic features, and finally the size of the reliefs.

Martín L. Castilla G. de Pablo M. A. López C.
Stability of Water on Mars. A Didactic Activity **[#1293]**
A didactic activity about the water of Mars using the pressure-temperature diagram of water stability and atmospheric data of the martian surface obtained by Viking spacecrafts that allow a discussion about the water existence on ancient and recent Mars with the students.

Program Author Index

** Denotes speaker*
FC = South Shore Harbour Fitness Center

Fisher T. A.	Instruments II Posters, Tue, p.m., FC
Fisk M. R.	Astrobiology Posters, Tue, p.m., FC
Flamini E.	Cassini at Saturn I, Wed, p.m., Salon B
Flamini E.	Cassini Posters, Thu, p.m., FC
Flasar F. M.*	Cassini at Saturn II, Thu, a.m., Salon B
Flasar F. M.	Cassini at Saturn III, Thu, p.m., Salon B
Fleischer I.	MER Results I, Wed, a.m., Salon B
Fletcher G.	Cassini at Saturn I, Wed, p.m., Salon B
Floss C.	Presolar Grains, Mon, a.m., Marina Plaza
Floss C.*	Interplanetary Dust, Tue, a.m., Marina Plaza
Floss C.	Presolar Grains Posters, Tue, p.m., FC
Floss C.	Chondrites, Wed, p.m., Salon C
Floyd S. R.	Lunar Missions Posters, Tue, p.m., FC
Flynn G. J.	Astrobiology II, Tue, a.m., Salon C
Flynn G. J.*	Interplanetary Dust, Tue, a.m., Marina Plaza
Flynn G. J.	Organics in Meteorites Posters, Thu, p.m., FC
Flynn G. J.	Asteroids, etc., Posters, Thu, p.m., FC
Fogel M.	Print Only: Astrobiology
Fogel M.	Organics in Meteorites Posters, Thu, p.m., FC
Fogel R. A.	Print Only: Meteorites
Fogel R. A.	Lunar Potpourri Posters, Thu, p.m., FC
Foing B. H.	Mars Express and HRSC I, Mon, a.m., Salon B
Foing B. H.	Lunar Missions Posters, Tue, p.m., FC
Foing B. H.	Mars Express Posters, Tue, p.m., FC
Foing B. H.	Mars Tectonics Posters, Tue, p.m., FC
Foing B. H.	Mars Instruments Posters, Tue, p.m., FC
Foing B. H.	Mars Climate Atmosphere Posters, Thu, p.m., FC
Foing B. H.	Mars: From Hydrogen to Ice, Fri, a.m., Salon B
Foit F. F.	Impacts: Effects on Earth Posters, Thu, p.m., FC
Folco L.	Micrometeorites and IDPs Posters, Tue, p.m., FC
Folco L.	Ordinary Chondrites Posters, Thu, p.m., FC
Földi T.	Lunar Potpourri Posters, Thu, p.m., FC
Földi T.	Outer Solar System Posters, Thu, p.m., FC
Foley C. N.	Achondrites Posters, Tue, p.m., FC
Foley C. N.*	Asteroid Spectroscopy, Wed, a.m., Salon A
Foley C. N.	Early Solar System Posters, Thu, p.m., FC
Foley D. J.	Dry (?) Mars Posters, Tue, p.m., FC
Fonti S.	Mercury Posters, Tue, p.m., FC
Ford P. G.	Venus Posters, Tue, p.m., FC
Forget F.	Mars Express and HRSC I, Mon, a.m., Salon B
Forget F.*	OMEGA@Mars Special Session, Tue, a.m., Salon B
Forget F.*	Mars Polar Atmosphere, Tue, p.m., Salon B
Forget F.	Mars Polar Posters, Tue, p.m., FC
Forget F.	Mars Climate Atmosphere Posters, Thu, p.m., FC
Formisano V.	Cassini at Saturn II, Thu, a.m., Salon B
Forni O.	Print Only: OMEGA@Mars
Forni O.	Asteroid Spectroscopy, Wed, a.m., Salon A
Forray F. L.	Mars Geochemistry Posters, Thu, p.m., FC
Fortes A. D.	Cassini at Saturn III, Thu, p.m., Salon B
Fortes A. D.	Cassini Posters, Thu, p.m., FC
Fortezzo C. M.	Mars Potpourri, Tue, p.m., Marina Plaza
Fouchet T.	OMEGA@Mars Special Session, Tue, a.m., Salon B
Francescetti G.	Cassini at Saturn I, Wed, p.m., Salon B
Franchi I. A	Carbonaceous Chondrites Posters, Thu, p.m., FC
Franchi I. A.	Nakhlites and Chassignites Posters, Tue, p.m., FC
Franke E. A.	Astrobiology Posters, Tue, p.m., FC
Franklin N. M.	Mars Tectonics Posters, Tue, p.m., FC
Franzen M. A.	Asteroids, etc., Posters, Thu, p.m., FC
Freeman J. J.	OMEGA@Mars Special Session, Tue, a.m., Salon B
Frei S.	Mars Express and HRSC I, Mon, a.m., Salon B
French L.	Instruments II Posters, Tue, p.m., FC
French L. C.	Instruments I Posters, Thu, p.m., FC
Freund F.	Lunar Impacts Posters, Thu, p.m., FC
Frew D.	Lunar Missions Posters, Tue, p.m., FC
Frey F.	Martian Meteorites Posters, Tue, p.m., FC
Frey F.	Martian Meteorites Posters, Tue, p.m., FC
Frey H. V.*	Mars Tectonism and Magnetism, Mon, p.m., Salon C
Frey H. V.	Mars Cratering Posters, Tue, p.m., FC
Frey H. V.	Mars Potpourri Posters, Tue, p.m., FC
Frey H. V.	E/PO Visualization Posters, Tue, p.m., FC
Friedrich J. M.	Refractory Inclusions Posters, Tue, p.m., FC
Friedrich J. M.*	Refractory Inclusions, Thu, a.m., Marina Plaza
Fries M.	Print Only: Astrobiology
Fries M.	Chondrites, Wed, p.m., Salon C
Fries M.	Impacts: Effects on Earth Posters, Thu, p.m., FC
Fries M.	Meteorite Characterization Posters, Thu, p.m., FC
Fries M.	Organics in Meteorites Posters, Thu, p.m., FC
Frost D.	Terrestrial Planet Formation, Mon, p.m., Salon A
Fueten F.	Mars Express and HRSC I, Mon, a.m., Salon B
Fueten F.	Mars Tectonics Posters, Tue, p.m., FC
Fujii M.	Mercury Posters, Tue, p.m., FC
Fujii M.	Lunar Missions Posters, Tue, p.m., FC
Fujimura A.	Lunar Missions Posters, Tue, p.m., FC
Fujimura A.	Lunar Potpourri Posters, Thu, p.m., FC
Fujiwara A.	Asteroids, etc., Posters, Thu, p.m., FC
Fulchignoni M.*	Cassini at Saturn I, Wed, p.m., Salon B
Funaki M.	Martian Meteorites Posters, Tue, p.m., FC
Funsten H. O.	Mars: From Hydrogen to Ice, Fri, a.m., Salon B
Furuya M.	Asteroids, etc., Posters, Thu, p.m., FC
Fuse T.	Asteroids, etc., Posters, Thu, p.m., FC
Fussner S.	Cassini at Saturn I, Wed, p.m., Salon B
Fussner S.	Cassini at Saturn II, Thu, a.m., Salon B
Fussner S.	Cassini Posters, Thu, p.m., FC
Gaddis L. R.	Print Only: Mars: Marscellaneous
Gaddis L. R.	Lunar Missions Posters, Tue, p.m., FC
Gaddis L. R.	MER Results I, Wed, a.m., Salon B
Gaddis L. R.	Lunar Potpourri Posters, Thu, p.m., FC
Gaddis L. R.	Lunar Remote Sensing Posters, Thu, p.m., FC
Gaddis L. R.	Mars Infrared Posters, Thu, p.m., FC
Gaffey M. J.*	Asteroid Spectroscopy, Wed, a.m., Salon A
Gaffney A. M.*	Lunar Basalts, Wed, p.m., Salon A
Gagnepain-Beyneix J.	Lunar Basalts, Wed, p.m., Salon A
Gaines D.	Instruments I Posters, Thu, p.m., FC
Galindo C. Jr.	Differentiated Meteorites, Fri, a.m., Salon C
Gallino R.	Presolar Grains, Mon, a.m., Marina Plaza
Galopeau P.	Cassini at Saturn II, Thu, a.m., Salon B
Gal-Solymos K.	MER and MOC Posters, Thu, p.m., FC
Galy A.	Disk Chronology, Fri, p.m., Marina Plaza
Ganguly J.	Disk Chronology, Fri, p.m., Marina Plaza
Gánti T.	MER and MOC Posters, Thu, p.m., FC
Gánti T.	Wet Mars Posters, Thu, p.m., FC
Garbeil H.	Print Only: Mars Volcanism
Garbeil H.	Mars Potpourri Posters, Tue, p.m., FC
Garcia R.	Venus Posters, Tue, p.m., FC
Garcia R.	Ordinary Chondrites Posters, Thu, p.m., FC
Garcia Ferrandez M.	Lunar Geophysics Posters, Thu, p.m., FC
Garcia-Comas N.	OMEGA@Mars Special Session, Tue, a.m., Salon B
Gardner K. G.	Impacts: Effects on Earth Posters, Thu, p.m., FC
Gardner K. G.	Early Solar System Posters, Thu, p.m., FC
Gardner T. G.	Lunar Missions Posters, Tue, p.m., FC
Garrick-Bethell I.	Lunar Remote Sensing Posters, Thu, p.m., FC
Garrick-Bethell I.*	Remote Sensing, Mare Basalts, etc., Fri, p.m., Salon C
Garrison D. H.	Nakhlites and Chassignites Posters, Tue, p.m., FC
Garrison D. H.	Irons and Stony-Irons Posters, Tue, p.m., FC
Garry J. R. C.	Cassini Posters, Thu, p.m., FC
Garry J. R. C.	Mars Geochemistry & Weathering, Fri, p.m., Salon B
Garry W. B.*	Mars Volcanism, Wed, a.m., Salon C
Garvie L. A. J.	Chondrites, Wed, p.m., Salon C
Garvie L. A. J.	Organics in Meteorites Posters, Thu, p.m., FC
Garza E.	Astrobiology Posters, Tue, p.m., FC
Gasnault O.	Mercury Posters, Tue, p.m., FC
Gasnault O.	Instruments II Posters, Tue, p.m., FC
Gasnault O.	Lunar Potpourri Posters, Thu, p.m., FC
Gasnault O.	Mars Global Posters, Thu, p.m., FC
Gasnault O.	Mars: From Hydrogen to Ice, Fri, a.m., Salon B
Gattacceca J.	Micrometeorites and IDPs Posters, Tue, p.m., FC
Gattacceca J.	Martian Meteorites Posters, Tue, p.m., FC
Gattacceca J.	Ordinary Chondrites Posters, Thu, p.m., FC
GCMS Exp. Team	Cassini at Saturn I, Wed, p.m., Salon B
Geissler P. E.	Dry (?) Mars Posters, Tue, p.m., FC
Geissler P. E.	Outer Solar System Posters, Thu, p.m., FC
Geissler P. E.*	Galilean Satellites, Fri, p.m., Salon A
Gell D.	Cassini at Saturn I, Wed, p.m., Salon B
Gellert R.	Mercury Posters, Tue, p.m., FC
Gellert R.*	MER Results I, Wed, a.m., Salon B
Gellert R.	MER Results II, Wed, p.m., Marina Plaza
Genda H.	Early Solar System Posters, Thu, p.m., FC
Gendrin A.*	OMEGA@Mars Special Session, Tue, a.m., Salon B
Gendrin A.	OMEGA@Mars Posters, Tue, p.m., FC
Genesis Recovery Team	Genesis Special Session, Mon, p.m., Salon B
Genge M. J.*	Interplanetary Dust, Tue, a.m., Marina Plaza
Genge M. J.	Astrobiology Posters, Tue, p.m., FC
George T.	Instruments I Posters, Thu, p.m., FC
Gerasimov M. V.	Astrobiology Posters, Tue, p.m., FC
Gerasimov M. V.	Lunar Impacts Posters, Thu, p.m., FC
Gersonde R.	Impacts: Ejecta, Tue, p.m., Salon A
Gesztesi A.	Wet Mars Posters, Thu, p.m., FC
Ghail R. C.	Print Only: Astrobiology
Ghanbaja J.	Interplanetary Dust, Tue, a.m., Marina Plaza
Ghatan G.	Martian Fluvial Processes, Thu, p.m., Marina Plaza

Kirk R. L.	Cassini at Saturn II, Thu, a.m., Salon B
Kirk R. L.	Cassini at Saturn III, Thu, p.m., Salon B
Kirk R. L.	MER and MOC Posters, Thu, p.m., FC
Kirk R. L.	Mars Infrared Posters, Thu, p.m., FC
Kirk R. L.	Exploration Posters, Thu, p.m., FC
Kirk R. L.	Asteroids, etc., Posters, Thu, p.m., FC
Kirk R. L.	Cassini Posters, Thu, p.m., FC
Kirkland L. E.	Instruments II Posters, Tue, p.m., FC
Kirkland L. E.	Lunar Remote Sensing Posters, Thu, p.m., FC
Kirkland L. E.	Mars Infrared Posters, Thu, p.m., FC
Kirkland L. E.	Instruments I Posters, Thu, p.m., FC
Kirschvink J. L.	Astrobiology I, Mon, a.m., Salon A
Kita N. T.	Chondrules & Chondrites, Wed, a.m., Marina Plaza
Kita N. T.*	Early Solar System Evolution, Fri, a.m., Marina Plaza
Kitazato K.	Asteroids, etc., Posters, Thu, p.m., FC
Klaasen K. P.	Galilean Satellites, Fri, p.m., Salon A
Kleine T.	Lunar Highlands, Thu, a.m., Salon C
Kleine T.	Early Solar System Posters, Thu, p.m., FC
Kletetschka G.	Mars Tectonism and Magnetism, Mon, p.m., Salon C
Kletetschka G.	Lunar Impacts Posters, Thu, p.m., FC
Kletetschka G.	Meteorite Characterization Posters, Thu, p.m., FC
Klima R. L.*	Asteroid Spectroscopy, Wed, a.m., Salon A
Klima R. L.	Instruments I Posters, Thu, p.m., FC
Klingelhöfer G.	Mercury Posters, Tue, p.m., FC
Klingelhöfer G.*	MER Results I, Wed, a.m., Salon B
Klingelhöfer G.	MER Results II, Wed, p.m., Marina Plaza
Klug S. L.	E/PO K-12 Posters, Tue, p.m., FC
Kminek G.	Exploration Posters, Thu, p.m., FC
Knauth L. P.	MER Results II, Wed, p.m., Marina Plaza
Knoll A. H.	Astrobiology I, Mon, a.m., Salon A
Knoll A. H.	MER Results I, Wed, a.m., Salon B
Knoll A. H.	MER Results II, Wed, p.m., Marina Plaza
Knoll A. H.	Mars Geochemistry & Weathering, Fri, p.m., Salon B
Knollenberg J.	Mercury Posters, Tue, p.m., FC
Knowles B.	Cassini at Saturn III, Thu, p.m., Salon B
Knowles B.	Cassini Posters, Thu, p.m., FC
Knudsen J. M.	MER Results I, Wed, a.m., Salon B
Knudsen J. M.	MER and MOC Posters, Thu, p.m., FC
Knudson A.	Mars Infrared Posters, Thu, p.m., FC
Knudson A. T.	MER Results I, Wed, a.m., Salon B
Kobayashi M.	Mercury Posters, Tue, p.m., FC
Kobayashi M.-N.	Lunar Missions Posters, Tue, p.m., FC
Kobayashi N.	Lunar Missions Posters, Tue, p.m., FC
Kobayashi S.*	Presolar Grains, Mon, a.m., Marina Plaza
Kobayashi S.	Lunar Missions Posters, Tue, p.m., FC
Kobayashi S.	Asteroids, etc., Posters, Thu, p.m., FC
Kobayashi T.	Mars Volcanism Posters, Tue, p.m., FC
Kodama S.	Lunar Remote Sensing Posters, Thu, p.m., FC
Koeberl C.*	Impacts: Shocks, Thu, p.m., Salon A
Koeberl C.	Impacts: Effects on Earth Posters, Thu, p.m., FC
Koehler M.	Micrometeorites and IDPs Posters, Tue, p.m., FC
Koehler U.	Mars Express Posters, Tue, p.m., FC
Koehn P.	Lunar Missions Posters, Tue, p.m., FC
Kohlstedt D. L.	Oxygen in the Solar System, Thu, p.m., Salon C
Kohout T.	Lunar Impacts Posters, Thu, p.m., FC
Kohout T.	Meteorite Characterization Posters, Thu, p.m., FC
Koizumi E.	Print Only: Meteorites
Koizumi E.	Nakhlites and Chassignites, Tue, p.m., Salon C
Koizumi E.	Martian Meteorites Posters, Tue, p.m., FC
Koizumi E.	Ordinary Chondrites Posters, Thu, p.m., FC
Kojima H.	Remote Sensing, Mare Basalts, etc., Fri, p.m., Salon C
Kolb E. J.	Mars Polar Posters, Tue, p.m., FC
Kolesov G. M.	Print Only: Meteorites
Komatsu G.	Astrobiology II, Tue, a.m., Salon C
Komatsu G.	Mars Express Posters, Tue, p.m., FC
Komatsu G.	Mars Volcanism Posters, Tue, p.m., FC
Komatsu G.	MER Results II, Wed, p.m., Marina Plaza
Komatsu M.	Carbonaceous Chondrites Posters, Thu, p.m., FC
Komura K.	Genesis Posters, Tue, p.m., FC
Kono Y.	Lunar Geophysics Posters, Thu, p.m., FC
Korokhin V. V.	Print Only: Moon and Mercury
Korotev R. L.	Lunar Meteorites Posters, Tue, p.m., FC
Korotev R. L.	Lunar Basalts, Wed, p.m., Salon A
Korotev R. L.	MER and MOC Posters, Thu, p.m., FC
Korotev R. L.	Remote Sensing, Mare Basalts, etc., Fri, p.m., Salon C
Korteniemi J.	Mars Express and HRSC I, Mon, a.m., Salon B
Korteniemi J.	Mars Express Posters, Tue, p.m., FC
Kortenkamp S. J.*	Early Solar System Evolution, Fri, a.m., Marina Plaza
Korycansky D. G.*	Small Bodies, Thu, a.m., Salon A
Korycansky D. G.*	Impacts: Shocks, Thu, p.m., Salon A
Koscheev A. P.	Print Only: Stardust
Koschny D.	Lunar Missions Posters, Tue, p.m., FC
Kostama V.-P.	Print Only: Venus
Kostama V.-P.*	Mars Express and HRSC I, Mon, a.m., Salon B
Kostama V.-P.	Martian Impacts Posters, Tue, p.m., FC
Kostama V.-P.	Mars Express Posters, Tue, p.m., FC
Kostama V.-P.	Venus Posters, Tue, p.m., FC
Kostrikov A.	Print Only: Mars: Marscellaneous
Kotula P. G.	Chondrites, Wed, p.m., Salon C
Kouach D.	Instruments II Posters, Tue, p.m., FC
Kovács Zs.	Ordinary Chondrites Posters, Thu, p.m., FC
Kovács Zs.	Outer Solar System Posters, Thu, p.m., FC
Koyama J.	Lunar Geophysics Posters, Thu, p.m., FC
Kozlova E. A.	Print Only: Moon and Mercury
Kozlowski R. W. H.	Mercury Posters, Tue, p.m., FC
Kozyrev A. S.	Mars Polar Atmosphere, Tue, p.m., Salon B
Kozyrev A. S.	Lunar Missions Posters, Tue, p.m., FC
Kozyrev A. S.	Mars: Marscellaneous Posters, Thu, p.m., FC
Kozyrev A. S.	Instruments I Posters, Thu, p.m., FC
Kraal E. R.*	Mars Potpourri, Tue, p.m., Marina Plaza
Kraal E. R.	Wet Mars Posters, Thu, p.m., FC
Kracher A.	Asteroids, etc., Posters, Thu, p.m., FC
Kraft M. D.	Mars Geochemistry Posters, Thu, p.m., FC
Kramer G. Y.	Lunar Meteorites Posters, Tue, p.m., FC
Kramer G. Y.*	Lunar Basalts, Wed, p.m., Salon A
Kramer G. Y.	Lunar Remote Sensing Posters, Thu, p.m., FC
Krassilnikov A. S.	Print Only: Venus
Kreslavsky M. A.	Mars Polar Posters, Tue, p.m., FC
Kreslavsky M. A.	Venus Posters, Tue, p.m., FC
Kreslavsky M. A.	Mars: From Hydrogen to Ice, Fri, a.m., Salon B
Krimigis S. M.*	Cassini at Saturn II, Thu, a.m., Salon B
Kring D. A.	Martian Impacts, Tue, a.m., Salon A
Kring D. A.*	Impacts: Ejecta, Tue, p.m., Salon A
Kring D. A.	Lunar Highlands, Thu, a.m., Salon C
Kring D. A.	Impacts: Effects on Earth Posters, Thu, p.m., FC
Kristiansen O.	Impacts: Effects on Earth Posters, Thu, p.m., FC
Krivosheya K. V.	Print Only: Impacts
Kronberg P.	Mars Express and HRSC I, Mon, a.m., Salon B
Kronrod V. A.	Print Only: Outer Planets
Krot A. N.	Presolar Grains, Mon, a.m., Marina Plaza
Krot A. N.	Chondrules & Chondrites, Wed, a.m., Marina Plaza
Krot A. N.	Chondrites, Wed, p.m., Salon C
Krot A. N.	Refractory Inclusions, Thu, a.m., Marina Plaza
Krot A. N.	Carbonaceous Chondrites Posters, Thu, p.m., FC
Krot A. N.*	Disk Chronology, Fri, p.m., Marina Plaza
Krupp N.	Cassini at Saturn II, Thu, a.m., Salon B
Kubota T.	Asteroids, etc., Posters, Thu, p.m., FC
Kubovics I.	MER and MOC Posters, Thu, p.m., FC
Kubsky S.	Early Solar System Posters, Thu, p.m., FC
Kucheyev S. O.	Micrometeorites and IDPs Posters, Tue, p.m., FC
Kuebler K.	Instruments II Posters, Tue, p.m., FC
Kuehner S. M.	Lunar Meteorites Posters, Tue, p.m., FC
Kuehner S. M.	Martian Meteorites Posters, Tue, p.m., FC
Kuehner S. M.	Achondrites Posters, Tue, p.m., FC
Kuhlman G.	Mars Instruments Posters, Tue, p.m., FC
Kuhlman G.	Lunar Potpourri Posters, Thu, p.m., FC
Kuhn G.	Impacts: Ejecta, Tue, p.m., Salon A
Kührt E.	Mercury Posters, Tue, p.m., FC
Kumagai I.	Martian Impacts, Tue, a.m., Salon A
Kunihiro T.	Genesis Posters, Tue, p.m., FC
Kuppers M.	Cassini at Saturn I, Wed, p.m., Salon B
Kurat G.	Print Only: Moon and Mercury
Kurat G.	Print Only: Meteorites
Kurat G.	Micrometeorites and IDPs Posters, Tue, p.m., FC
Kurat G.	Refractory Inclusions Posters, Tue, p.m., FC
Kurita K.	Martian Impacts, Tue, a.m., Salon A
Kurita K.	Wet Mars Posters, Thu, p.m., FC
Kurth W. S.	Cassini at Saturn II, Thu, a.m., Salon B
Kurtz M. J.	E/PO Visualization Posters, Tue, p.m., FC
Kusack A. G.	MER Results I, Wed, a.m., Salon B
Kusack A. G.	MER and MOC Posters, Thu, p.m., FC
Kuskov O. L.	Print Only: Outer Planets
Kutyrev A. S.	Micrometeorites and IDPs Posters, Tue, p.m., FC
Kuyunko N. S.	Print Only: Meteorites
Kuzmin R. O.	Print Only: Mars Surficial Processes
Kuzmin R. O.	Wet Mars Posters, Thu, p.m., FC
Kuznetsov I. V.	Print Only: Mars Surficial Processes
Kyte F. T.*	Impacts: Ejecta, Tue, p.m., Salon A
Kyte F. T.	Impacts: Effects on Earth Posters, Thu, p.m., FC
Labrosse S.	Mars: Interior Processes, Mon, a.m., Salon C

Markiewicz W. J.	Mars: From Hydrogen to Ice, Fri, a.m., Salon B
Markowski A.	Early Solar System Posters, Thu, p.m., FC
Marov M. Ya.	Micrometeorites and IDPs Posters, Tue, p.m., FC
Márquez A.	Print Only: Mars Surficial Processes
Márquez A.	Print Only: Mars Volcanism
Marrocchi Y.*	Terrestrial Planet Formation, Mon, p.m., Salon A
Marrocchi Y.	Early Solar System Posters, Thu, p.m., FC
MEx HRSC Co-I Team	Mars Express and HRSC I, Mon, a.m., Salon B
MEx HRSC Team	Mars Express and HRSC I, Mon, a.m., Salon B
MEx OMEGA Team	Mars Polar Atmosphere, Tue, p.m., Salon B
MEx OMEGA Team	OMEGA@Mars Posters, Tue, p.m., FC
Marshall J. G.	Mars Potpourri Posters, Tue, p.m., FC
Martin M. C.	Micrometeorites and IDPs Posters, Tue, p.m., FC
Martin P.*	Venus, Tue, p.m., Salon A
Martin P.	Mars Instruments Posters, Tue, p.m., FC
Martin P.	Venus Posters, Tue, p.m., FC
Martin P. D.	Mars Express Posters, Tue, p.m., FC
Martín L.	Print Only: Education
Martinez-Alonso S.	Print Only: Mars Surficial Processes
Martín-Gago J. A.	Astrobiology Posters, Tue, p.m., FC
Martín-González F.	Print Only: Mars Volcanism
Martini A. M.	Mars Geochemistry & Weathering, Fri, p.m., Salon B
Marty B.*	Terrestrial Planet Formation, Mon, p.m., Salon A
Marty B.	Genesis Posters, Tue, p.m., FC
Marty B.	Early Solar System Posters, Thu, p.m., FC
Maruoka T.	Presolar Grains Posters, Tue, p.m., FC
Marusek J. A.	Print Only: Impacts
Maruyama S.	Mars Global Posters, Thu, p.m., FC
Marzari F.	Print Only: Early Solar System Evolution
Marzari F.	Early Solar System Posters, Thu, p.m., FC
Masarik J.	Outer Solar System Posters, Thu, p.m., FC
Massare D.	Early Solar System Posters, Thu, p.m., FC
Masson P.	Mars Express and HRSC I, Mon, a.m., Salon B
Masson Ph.	Mars Express and HRSC I, Mon, a.m., Salon B
Masson Ph.	OMEGA@Mars Posters, Tue, p.m., FC
Masson Ph.	Mars Express Posters, Tue, p.m., FC
Masson Ph.	Mars Volcanism, Wed, a.m., Salon C
Masumoto K.	Mars Volcanism Posters, Tue, p.m., FC
Masuoka C. M.	E/PO Visualization Posters, Tue, p.m., FC
Mateo-Marti E.	Astrobiology Posters, Tue, p.m., FC
Mateo-Martí E.	Astrobiology Posters, Tue, p.m., FC
Mathé P. E.	Mars Potpourri Posters, Tue, p.m., FC
Mathé P.-E.	Mars Geochemistry & Weathering, Fri, p.m., Salon B
Mather J. C.	Micrometeorites and IDPs Posters, Tue, p.m., FC
Mathies R. A.	Astrobiology Posters, Tue, p.m., FC
Matias A.	Mars Cratering Posters, Tue, p.m., FC
Matrajt G.	Interplanetary Dust, Tue, a.m., Marina Plaza
Matrajt G.	Micrometeorites and IDPs Posters, Tue, p.m., FC
Matson D. L.	Print Only: Outer Planets
Matson D. L.*	Cassini at Saturn I, Wed, p.m., Salon B
Matson D. L.	Cassini at Saturn II, Thu, a.m., Salon B
Matsuda Y.	Meteorite Characterization Posters, Thu, p.m., FC
Matsui T.	Impacts: Ejecta, Tue, p.m., Salon A
Matsui T.	Impact Modeling Posters, Tue, p.m., FC
Matsui T.	Dry (?) Mars Posters, Tue, p.m., FC
Matsui T.	Cassini Posters, Thu, p.m., FC
Matsumoto K.	Lunar Geophysics Posters, Thu, p.m., FC
Matsumoto M.	Lunar Potpourri Posters, Thu, p.m., FC
Matsunami Y.	Print Only: Meteorites
Matsushita M.	Lunar Remote Sensing Posters, Thu, p.m., FC
Matsuyama I.	Mars Geophysics Posters, Tue, p.m., FC
Matthews J. B.	Exploration Posters, Thu, p.m., FC
Matthews L.	Impacts: Effects on Earth Posters, Thu, p.m., FC
Matthies L. H.	MER and MOC Posters, Thu, p.m., FC
Matukov D. I.	Print Only: Moon and Mercury
Maturilli A.	Mars Potpourri Posters, Tue, p.m., FC
Matz K.-D.	Mars Express and HRSC I, Mon, a.m., Salon B
Matz K.-D.	Mars Express Posters, Tue, p.m., FC
Mauchien P.	Instruments II Posters, Tue, p.m., FC
Mauk B. H.	Cassini at Saturn II, Thu, a.m., Salon B
Maul J.	Stardust Mission Posters, Tue, p.m., FC
Maule J.	Print Only: Astrobiology
Maule J.*	Astrobiology I, Mon, a.m., Salon A
Maurette M.	Micrometeorites and IDPs Posters, Tue, p.m., FC
Maurette M.	Differentiated Meteorites, Fri, a.m., Salon C
Maurice S.	Mercury Posters, Tue, p.m., FC
Maurice S.	Lunar Missions Posters, Tue, p.m., FC
Maurice S.	Instruments II Posters, Tue, p.m., FC
Maurice S.	Mars Global Posters, Thu, p.m., FC
Maurice S.	Mars: From Hydrogen to Ice, Fri, a.m., Salon B
Maurice S.	Remote Sensing, Mare Basalts, etc., Fri, p.m., Salon C
Max M. D.	Print Only: Mars: Marscellaneous
Maxe L. P.	Print Only: Mars: Marscellaneous
Maxwell T. A.	Mars Potpourri, Tue, p.m., Marina Plaza
Mayer B.	Mars Climate Atmosphere Posters, Thu, p.m., FC
Mayne R. G.	Asteroids, etc., Posters, Thu, p.m., FC
Mayo S. C.	Stardust Mission Posters, Tue, p.m., FC
Mazumder M. K.	Dry (?) Mars Posters, Tue, p.m., FC
Mc Millan P.	Cassini Posters, Thu, p.m., FC
McAdam A. C.	Mars Geochemistry Posters, Thu, p.m., FC
McAdoo B. G.	Print Only: Mars Surficial Processes
McAuley M.	Print Only: Mars: Marscellaneous
McBride K. M.	Nakhlites and Chassignites Posters, Tue, p.m., FC
McBride S. A.*	Mars: From Hydrogen to Ice, Fri, a.m., Salon B
McCanta M. C.	Nakhlites and Chassignites, Tue, p.m., Salon C
McCanta M. C.*	Oxygen in the Solar System, Thu, p.m., Salon C
McCartney E.	MER Results I, Wed, a.m., Salon B
McCartney E.	MER and MOC Posters, Thu, p.m., FC
McClanahan T. P.	Asteroids, etc., Posters, Thu, p.m., FC
McClintock W. E.	Cassini at Saturn II, Thu, a.m., Salon B
McClintock W. E.	Lunar Remote Sensing Posters, Thu, p.m., FC
McCloskey R.	Education Programs Demonstrations, Sun, p.m., LPI
McColley S. M.	Mars Express Posters, Tue, p.m., FC
McColley S. M.	Venus Posters, Tue, p.m., FC
McComas D. J.	Cassini at Saturn II, Thu, a.m., Salon B
McCord T. B.	Mars Express and HRSC I, Mon, a.m., Salon B
McCord T. B.	Mars Express Posters, Tue, p.m., FC
McCord T. B.	Cassini at Saturn II, Thu, a.m., Salon B
McCoy T. J.	Asteroid Spectroscopy, Wed, a.m., Salon A
McCoy T. J.*	Chondrites, Wed, p.m., Salon C
McCoy T. J.	Ordinary Chondrites Posters, Thu, p.m., FC
McCoy T. J.	Asteroids, etc., Posters, Thu, p.m., FC
McCoy T. J.	Differentiated Meteorites, Fri, a.m., Salon C
McCubbin F. M.	Martian Meteorites Posters, Tue, p.m., FC
McDaniel K.	Venus Posters, Tue, p.m., FC
McDaniel T.	Lunar Missions Posters, Tue, p.m., FC
McDonnell A.	Cassini at Saturn I, Wed, p.m., Salon B
McDonough W. F.	Irons and Stony-Irons Posters, Tue, p.m., FC
McDonough W. F.	Refractory Inclusions, Thu, a.m., Marina Plaza
McDonough W. F.	Early Solar System Posters, Thu, p.m., FC
McDonough W. F.	Differentiated Meteorites, Fri, a.m., Salon C
McDowell M. L.	Mars Potpourri Posters, Tue, p.m., FC
McEntire R. W.	Cassini at Saturn II, Thu, a.m., Salon B
McEwen A. S.*	Martian Impacts, Tue, a.m., Salon A
McEwen A. S.	Lunar Missions Posters, Tue, p.m., FC
McEwen A. S.	Martian Impacts Posters, Tue, p.m., FC
McEwen A. S.	Mars Tectonics Posters, Tue, p.m., FC
McEwen A. S.	Mars Volcanism Posters, Tue, p.m., FC
McEwen A. S.*	Cassini at Saturn I, Wed, p.m., Salon B
McEwen A. S.	Cassini at Saturn II, Thu, a.m., Salon B
McEwen A. S.	Cassini at Saturn III, Thu, p.m., Salon B
McEwen A. S.	Cassini Posters, Thu, p.m., FC
McEwen A. S.	Galilean Satellites, Fri, p.m., Salon A
McFadden L. A.	Print Only: Asteroids and Small Bodies
McFadden L. A.*	Asteroid Spectroscopy, Wed, a.m., Salon A
McFarlane L.	Cassini at Saturn I, Wed, p.m., Salon B
McGill G. E.	Mars Potpourri, Tue, p.m., Marina Plaza
McGill G. E.	Mars Cratering Posters, Tue, p.m., FC
McGovern P. J.	Print Only: Mars Volcanism
McGovern P. J.*	Mars Volcanism, Wed, a.m., Salon C
McGovern P. J.	Martian Fluvial Processes, Thu, p.m., Marina Plaza
McHone J. F.	Impacts: Effects on Earth Posters, Thu, p.m., FC
McKay C.	Cassini at Saturn I, Wed, p.m., Salon B
McKay C. P.	Mars Potpourri Posters, Tue, p.m., FC
McKay C. P.	Instruments II Posters, Tue, p.m., FC
McKay C. P.	Astrobiology Posters, Tue, p.m., FC
McKay C. P.	Martian Fluvial Processes, Thu, p.m., Marina Plaza
McKay C. P.	Mars Geochemistry Posters, Thu, p.m., FC
McKay C. P.	Cassini Posters, Thu, p.m., FC
McKay C. P.	Mars Geochemistry & Weathering, Fri, p.m., Salon B
McKay D. S.	Astrobiology I, Mon, a.m., Salon A
McKay D. S.	Astrobiology II, Tue, a.m., Salon C
McKay D. S.	Interplanetary Dust, Tue, a.m., Marina Plaza
McKay D. S.	Nakhlites and Chassignites, Tue, p.m., Salon C
McKay D. S.	Astrobiology Posters, Tue, p.m., FC
McKay D. S.	Lunar Regolith Posters, Thu, p.m., FC
McKay D. S.	Remote Sensing, Mare Basalts, etc., Fri, p.m., Salon C
McKay G.*	Nakhlites and Chassignites, Tue, p.m., Salon C
McKeegan K. D.	Genesis Posters, Tue, p.m., FC
McKeegan K. D.	Refractory Inclusions Posters, Tue, p.m., FC

Wood C. A.	Print Only: Moon and Mercury
Wood C. A.	Cassini at Saturn I, Wed, p.m., Salon B
Wood C. A.	Cassini at Saturn II, Thu, a.m., Salon B
Wood C. A.*	Cassini at Saturn III, Thu, p.m., Salon B
Wood J. A.	Refractory Inclusions, Thu, a.m., Marina Plaza
Wooden D. H.	Interplanetary Dust, Tue, a.m., Marina Plaza
Woolum D. S.	Genesis Special Session, Mon, p.m., Salon B
Woolum D. S.	Genesis Posters, Tue, p.m., FC
Wright I. P	Carbonaceous Chondrites Posters, Thu, p.m., FC
Wright I. P.	Nakhlites and Chassignites, Tue, p.m., Salon C
Wright I. P.	Presolar Grains Posters, Tue, p.m., FC
Wright I. P.	Remote Sensing, Mare Basalts, etc., Fri, p.m., Salon C
Wrobel K. E.	Mars Polar Posters, Tue, p.m., FC
Wünnemann K.	Impact Modeling Posters, Tue, p.m., FC
Wünnemann K.*	Small Bodies, Thu, a.m., Salon A
Wünnemann K.	Impacts: Shocks, Thu, p.m., Salon A
Wyatt M.	Astrobiology II, Tue, a.m., Salon C
Wyatt M.	Astrobiology Posters, Tue, p.m., FC
Wyatt M.	Mars Infrared Posters, Thu, p.m., FC
Wyatt M. B.	Mars: Interior Processes, Mon, a.m., Salon C
Wyatt M. B.	Astrobiology Posters, Tue, p.m., FC
Wyatt M. B.	MER Results I, Wed, a.m., Salon B
Wyatt M. B.	MER Results II, Wed, p.m., Marina Plaza
Wye L.	Cassini at Saturn I, Wed, p.m., Salon B
Wyman W.	Exploration Posters, Thu, p.m., FC
Wyrick D. Y.	Mars Tectonics Posters, Tue, p.m., FC
Xie H.	Instruments I Posters, Thu, p.m., FC
Xie Z.*	Impacts: Shock Effects, Thu, a.m., Salon A
Xu F.	MER and MOC Posters, Thu, p.m., FC
Xu H. F.*	Astrobiology II, Tue, a.m., Salon C
Xu J.	Cassini at Saturn I, Wed, p.m., Salon B
Yabuta H.	Organics in Meteorites Posters, Thu, p.m., FC
Yada T.*	Presolar Grains, Mon, a.m., Marina Plaza
Yakovlev O. I.	Lunar Impacts Posters, Thu, p.m., FC
Yamada I.	Lunar Missions Posters, Tue, p.m., FC
Yamada R.	Lunar Missions Posters, Tue, p.m., FC
Yamaguchi A.	Print Only: Meteorites
Yamaguchi A.	Lunar Highlands, Thu, a.m., Salon C
Yamaguchi A.*	Differentiated Meteorites, Fri, a.m., Salon C
Yamaguchi Y.	Lunar Remote Sensing Posters, Thu, p.m., FC
Yamamoto A.	Print Only: Asteroids and Small Bodies
Yamamoto S.*	Impacts: Ejecta, Tue, p.m., Salon A
Yamamoto S.	Impact Experiments Posters, Tue, p.m., FC
Yamamoto Y.	Lunar Missions Posters, Tue, p.m., FC
Yamamoto Y.	Lunar Remote Sensing Posters, Thu, p.m., FC
Yamashita N.	Lunar Missions Posters, Tue, p.m., FC
Yanagisawa M.	Asteroids, etc., Posters, Thu, p.m., FC
Yanai K.	Achondrites Posters, Tue, p.m., FC
Yang F.	Dry (?) Mars Posters, Tue, p.m., FC
Yang J.	Irons and Stony-Irons Posters, Tue, p.m., FC
Yano H.	Stardust Mission Posters, Tue, p.m., FC
Yano H.	Impact Experiments Posters, Tue, p.m., FC
Yano H.	Asteroids, etc., Posters, Thu, p.m., FC
Yasuda S.	Ordinary Chondrites Posters, Thu, p.m., FC
Yavrouian A. H.	Print Only: Venus
Yelle R. V.	Cassini at Saturn I, Wed, p.m., Salon B
Yen A. S.	Astrobiology I, Mon, a.m., Salon A
Yen A. S.	MER Results I, Wed, a.m., Salon B
Yen A. S.*	MER Results II, Wed, p.m., Marina Plaza
Yen A. S.	MER and MOC Posters, Thu, p.m., FC
Yin Q.-Z.*	Early Solar System Evolution, Fri, a.m., Marina Plaza
Yingst R. A.	Dry (?) Mars Posters, Tue, p.m., FC
Yingst R. A.	Instruments II Posters, Tue, p.m., FC
Yokochi R.	Terrestrial Planet Formation, Mon, p.m., Salon A
Yoshida F.	Asteroids, etc., Posters, Thu, p.m., FC
Yoshida T.	Presolar Grains Posters, Tue, p.m., FC
Yoshimitsu T.	Asteroids, etc., Posters, Thu, p.m., FC
Yoshitake M.*	Refractory Inclusions, Thu, a.m., Marina Plaza
Young D. T.	Instruments II Posters, Tue, p.m., FC
Young D. T.	Cassini at Saturn II, Thu, a.m., Salon B
Young E. D.	Lunar Highlands, Thu, a.m., Salon C
Young E. D.	Refractory Inclusions, Thu, a.m., Marina Plaza
Young E. D.	Early Solar System Evolution, Fri, a.m., Marina Plaza
Young E. D.*	Disk Chronology, Fri, p.m., Marina Plaza
Young E. F.	Asteroid Spectroscopy, Wed, a.m., Salon A
Yseboodt M.	Mercury Posters, Tue, p.m., FC
Yurimoto H.	Presolar Grains, Mon, a.m., Marina Plaza
Yurimoto H.	Presolar Grains Posters, Tue, p.m., FC
Yurimoto H.	Refractory Inclusions, Thu, a.m., Marina Plaza
Yurimoto H.	Disk Chronology, Fri, p.m., Marina Plaza
Zabalueva E. V.	Print Only: Mars Surficial Processes
Zamani P.	Mars Express Posters, Tue, p.m., FC
Zanda B.	Chondrules & Chondrites, Wed, a.m., Marina Plaza
Zaranek S. E.	Mars: Interior Processes, Mon, a.m., Salon C
Zaripov N. V.	Print Only: Stardust
Zarka P.	Cassini at Saturn II, Thu, a.m., Salon B
Zarnecki J. C.*	Cassini at Saturn I, Wed, p.m., Salon B
Zarnecki J. C.	Remote Sensing, Mare Basalts, etc., Fri, p.m., Salon C
Zasova L.	OMEGA@Mars Special Session, Tue, a.m., Salon B
Zavaleta J.	Astrobiology I, Mon, a.m., Salon A
Zavaleta J.	Astrobiology Posters, Tue, p.m., FC
Zebker H. A.	Cassini at Saturn I, Wed, p.m., Salon B
Zega T. J.*	Chondrites, Wed, p.m., Salon C
Zegers T. E.*	Mars Express and HRSC I, Mon, a.m., Salon B
Zegers T. E.	Mars Express Posters, Tue, p.m., FC
Zegers T. E.	Mars Tectonics Posters, Tue, p.m., FC
Zeigler R. A.	Lunar Basalts, Wed, p.m., Salon A
Zeigler R. A.*	Remote Sensing, Mare Basalts, etc., Fri, p.m., Salon C
Zellner N. E. B.	Lunar Highlands, Thu, a.m., Salon C
Zellner N. E. B.	Lunar Impacts Posters, Thu, p.m., FC
Zeltsman A.	Print Only: Mars Surficial Processes
Zender J.	Lunar Missions Posters, Tue, p.m., FC
Zender J.	Mars Express Posters, Tue, p.m., FC
Zent A. P.	Mars Polar Posters, Tue, p.m., FC
Zent A. P.	Mars Geochemistry & Weathering, Fri, p.m., Salon B
Zhang L.	Early Solar System Posters, Thu, p.m., FC
Zhong S.	Mars Tectonism and Magnetism, Mon, p.m., Salon C
Zhong S.	Mars Geophysics Posters, Tue, p.m., FC
Zimbelman J. R.	Mars Potpourri, Tue, p.m., Marina Plaza
Zimbelman J. R.	Mars Volcanism Posters, Tue, p.m., FC
Zimbelman J. R.*	Martian Fluvial Processes, Thu, p.m., Marina Plaza
Zimmerman W. F.	Astrobiology Posters, Tue, p.m., FC
Zimmermann L.	Genesis Posters, Tue, p.m., FC
Zinner E.	Print Only: Meteorites
Zinner E.	Presolar Grains Posters, Tue, p.m., FC
Zinner E.	Presolar Grains Posters, Tue, p.m., FC
Zinner E.	Refractory Inclusions Posters, Tue, p.m., FC
Zinovieva N. G.	Print Only: Meteorites
Zipfel J.	MER Results I, Wed, a.m., Salon B
Zipfel J.	MER Results II, Wed, p.m., Marina Plaza
Zolensky M. E.	Stardust Mission Posters, Tue, p.m., FC
Zolensky M. E.	Martian Meteorites ALH84001 Posters, Tue, p.m., FC
Zolensky M. E.	Astrobiology Posters, Tue, p.m., FC
Zolensky M. E.	Chondrules & Chondrites, Wed, a.m., Marina Plaza
Zolensky M. E.	Organics in Meteorites Posters, Thu, p.m., FC
Zolensky M. E.	Carbonaceous Chondrites Posters, Thu, p.m., FC
Zolensky M. E.	Ordinary Chondrites Posters, Thu, p.m., FC
Zolensky M. E.	Differentiated Meteorites, Fri, a.m., Salon C
Zolotov M. Yu.*	Chondrules & Chondrites, Wed, a.m., Marina Plaza
Zolotov M. Yu.	Ordinary Chondrites Posters, Thu, p.m., FC
Zuber M. T.	Mars: Interior Processes, Mon, a.m., Salon C
Zuber M. T.	Mercury Posters, Tue, p.m., FC
Zuber M. T.	Lunar Remote Sensing Posters, Thu, p.m., FC
Zuber M. T.	Remote Sensing, Mare Basalts, etc., Fri, p.m., Salon C
Zurbuchen T. H.	Genesis Special Session, Mon, p.m., Salon B
Zurbuchen T. H.	Lunar Missions Posters, Tue, p.m., FC
Zurcher L.	Impacts: Effects on Earth Posters, Thu, p.m., FC
Zuschneid W.	Mars Express and HRSC I, Mon, a.m., Salon B

Notes